MINIMALISTIC DESCRIPTIONS OF NONDYNAMICAL ELECTRON CORRELATION: FROM BOND-BREAKING TO TRANSITION-METAL CATALYSIS

A Thesis
Presented to
The Academic Faculty

by

John S. Sears

In Partial Fulfillment
of the Requirements for the Degree
DOCTORATE OF PHILOSOPHY in the
School of Chemistry and Biochemistry

Georgia Institute of Technology
December 2007

MINIMALISTIC DESCRIPTIONS OF NONDYNAMICAL ELECTRON CORRELATION: FROM BOND-BREAKING TO TRANSITION-METAL CATALYSIS

Approved by:

Dr. C. David Sherrill, Advisor
School of Chemistry and Biochemistry
Georgia Institute of Technology

Dr. Thomas Orlando
School of Chemistry and Biochemistry
Georgia Institute of Technology

Dr. Jean-Luc Brédas
School of Chemistry and Biochemistry
Georgia Institute of Technology

Dr. Peter J. Ludovice
School of Chemical and Biomolecular Engineering
Georgia Institute of Technology

Dr. Mostafa A. El-Sayed
School of Chemistry and Biochemistry
Georgia Institute of Technology

Date Approved: November 13, 2007

This thesis is dedicated to my son, Tyler. He has been the driving motivation in my life since the day he was born. I love you son, to infinity and back.

ACKNOWLEDGEMENTS

The Lord has blessed my life in so many ways and through encounters with so many wonderful people. I wish to thank my parents, whose love and guidance from childhood have helped to carry me this far. My interests in mathematics and science began at an early age and were certainly inspired by the many wonderful teachers I encountered as a youth. I would especially like to thank Mr. Limbaugh, Mrs. Smith, and Mrs. Popovich for the numerous hours spent with me in those days. I am forever grateful to all of the students and faculty at The University of the South. My times spent on the mountain in Sewanee were certainly the happiest in my life. The domain is a magnificent place of wonder and opportunity where "angels walk the streets" in what the great Southern author Peter Taylor called "the long green hinterland that is Tennessee" and in the place I will forever call "home." I would especially like to thank Dr. Emily Puckette and Dr. Clay C. Ross in the Mathematics Department and Dr. Ed. Kirven and Dr. John Shibata in the Chemistry Department. Their doors were always open, their advice well informed, and their friendships cherished forever. Lastly, I would like to thank my graduate advisor, Dr. Sherrill, and the entire Sherrill research group. My graduate career has coincided with many of the most challenging personal times of my life. Without the understanding of my research advisor I never could have persevered. I would especially like to thank Dr. Micah Abrams for his friendship and for the many hours of coffee and stimulating conversation we enjoyed together. He is a truly well respected colleague and a treasured friend.

TABLE OF CONTENTS

LIST OF TABLES

LIST OF FIGURES

SUMMARY

From a theoretical standpoint, the accurate description of potential energy surfaces for bond breaking and the equilibrium structures of metal-ligand catalysts are distinctly similar problems. Near degeneracies of the bonding and anti-bonding orbitals for the case of bond breaking and of the partially-filled d-orbitals for the case of metal-ligand catalyst systems lead to strong *non-dynamical correlation* effects. Standard methods of electronic structure theory, as a consequence of the *single-reference approximation*, are incapable of accurately describing the electronic structure of these seemingly different theoretical problems. The work within highlights the application of multi-reference methods, methods capable of accurately treating these near-degeneracies, for describing the bond-breaking potentials in several small molecular systems and the equilibrium structures of metal-salen catalysts. The central theme of this work is the ability of small, compact reference functions for accurately describing the strong non-dynamical correlation effects in these systems.

CHAPTER 1

INTRODUCTION

The ability to *a priori* calculate the properties of atoms and molecules has long been recognized to be of central importance in chemistry, in atomistic and molecular physics, and more recently in molecular biology and biophysics. Theoretical calculations enable the exploration of molecular properties for species that are difficult, quite often impossible, to study experimentally. Indeed, even for systems that afford experimental exploration, theoretical investigations are capable of providing atomic-level insight that may not be afforded by experimental means. The combination of experimental exploration and theoretical insight often provides the most highly detailed level of understanding for molecular systems and reaction mechanisms.

Computational chemistry, to a large degree, has piggybacked to the forefront of the research world as a consequence of the "Moore's Law" growth in computational power [1, 2]. Although a purely empirical observation that dates back to 1965, the accuracy of "Moores Law" and the rapid advances in computational abilities that it has so accurately predicted have made high-level calculations of chemically interesting systems readily available to most chemists [3]. These statements should, in no way, detract from the simultaneous advances that have taken place in the development and implementation of new and improved algorithms by the computational community [4-30]. No doubt future advances in both areas will continue to enhance the impact of computational methods in the chemical sciences.

The Born-Oppenheimer Approximation and the Independent-Particle Model

In quantum mechanics, our problem is the solution of the eigenvalue problem

$$\hat{H}\left|\Psi_i\right\rangle = E_i\left|\Psi_i\right\rangle \quad \left(\left|\Psi_i\right\rangle \in h\right) \tag{1.1}$$

where $\hat{H}$ is the molecular Hamiltonian operator, $\left|\Psi_i\right\rangle$ is a state vector in Hilbert space, and E_i is an allowed energy level. The total (non-relativistic) molecular Hamiltonian for a system of N electrons and M nuclei takes the form (in atomic units)

$$\hat{H} = -\sum_{A=1}^{M}\frac{1}{2M_A}\nabla_A^2 - \frac{1}{2}\sum_{i=1}^{N}\nabla_i^2 + \sum_{A>B}^{M}\frac{Z_A Z_B}{R_{AB}} + \sum_{i>j}^{N}\frac{1}{r_{ij}} - \sum_{i=1}^{N}\sum_{A=1}^{M}\frac{Z_A}{r_{iA}}. \tag{1.2}$$

The first two terms in (1.2) are the nuclear and electronic kinetic energy operators, $\hat{T}_N$ and $\hat{T}_e$ respectively. The second two terms are the nuclear-nuclear and electron-electron repulsion terms, $\hat{V}_N$ and $\hat{V}_e$ respectively. The final term in (1.2) is the electron-nucleus attraction term, $\hat{V}_{Ne}$. Equation (1.1) is formally a second-order differential equation in $3(N+M)$ variables that is closed-form solvable for only the simplest of systems. Certain approximations are required to obtain solutions (albeit approximate) to (1.1) for nontrivial chemical systems.

The first approximation routinely applied is the so-called Born-Oppenheimer approximation [31]. The disparity of the nuclear and electronic masses allows for the electronic motion to accommodate, almost instantaneously, the motion of the nuclei. This allows for a (almost exact) separation of nuclear and electronic motion, where the electrons move adiabatically on the potential created by the nuclei. This simplifies the problem in (1.1) to one of just the electronic motion;

$$\hat{H} = \hat{T}_N + \hat{V}_N + \hat{\mathcal{H}} \approx \hat{\mathcal{H}} + V_N \tag{1.3}$$

where the electronic Hamiltonian operator is given by

$$\hat{\mathcal{H}} = \hat{T}_e + \hat{V}_e + \hat{V}_{Ne}\,. \tag{1.4}$$

Note that, in (1.3), the nuclear kinetic energy under the Born-Oppenheimer approximation goes to zero while the nuclear-nuclear potential is constant. This greatly simplifies our problem to one of solving for the electronic wavefunction (state function), $\Phi_m(\mathbf{R})$, parameterized by the nuclear coordinates, $\mathbf{R}$;

$$\left(\hat{\mathcal{H}} + V_N\right)\left|\Phi_m(\mathbf{R})\right\rangle = E_m(\mathbf{R})\left|\Phi_m(\mathbf{R})\right\rangle\,. \tag{1.5}$$

Equation (1.5) is the electronic Schrödinger equation, the solutions of which accurately describe the structure and motions of the electrons in the vast majority of chemical systems. The research presented within this thesis details the problems with obtaining accurate solutions to (1.5) for systems where standard approaches of electronic structure theory often break down.

Although the Born-Oppenheimer approximation simplifies the solution of (1.1) to one for just the electronic motion, equation (1.5), further approximations are required to make the equations tractable for chemical systems. This is where the *independent-electron* models arise. The independent-electron models transform the problem in (1.5) from the solution of a full N-electron Hamiltonian to that of N 1-electron Hamiltonians. Of the independent-electron models, none has obtained the use and fruitfulness of the Hartree-Fock (HF) model. In HF theory, the wavefunction is represented as a single Slater determinant of spin orbitals, thus enforcing the antisymmetry properties of the electronic wavefunction. In restricted closed-shell HF theory (RHF) this results in wavefunctions of the form

$$\Phi = (N!)^{-1} \left| \psi_1(\mathbf{x}_1)\bar{\psi}_1(\mathbf{x}_2)\ldots\ldots\psi_n(\mathbf{x}_{N-1})\bar{\psi}_n(\mathbf{x}_N) \right\rangle$$
$$= (N!)^{-1} \begin{vmatrix} \psi_1(\mathbf{x}_1) & \bar{\psi}_1(\mathbf{x}_1) & \cdots & \psi_n(\mathbf{x}_1) & \bar{\psi}_n(\mathbf{x}_1) \\ \psi_1(\mathbf{x}_2) & \bar{\psi}_1(\mathbf{x}_2) & \cdots & \psi_n(\mathbf{x}_2) & \bar{\psi}_n(\mathbf{x}_2) \\ \vdots & \vdots & & \vdots & \vdots \\ \psi_1(\mathbf{x}_N) & \bar{\psi}_1(\mathbf{x}_N) & \cdots & \psi_n(\mathbf{x}_N) & \bar{\psi}_n(\mathbf{x}_N) \end{vmatrix}. \qquad (1.6)$$

The spin-orbitals, ψ_i, are defined in terms of the spatial orbitals, ϕ_i, as

$$\psi_i = \phi_i\alpha \quad \bar{\psi}_i = \phi_i\beta. \qquad (1.7)$$

The ϕ_i's are taken to form an orthonormal set of spatial molecular orbitals. For the closed-shell case, the expression for the energy of the system takes the form

$$E = 2\sum_i \langle\phi_i|h|\phi_i\rangle + \sum_{i>j}\left[2\langle\phi_i\phi_j|\phi_i\phi_j\rangle - \langle\phi_i\phi_j|\phi_j\phi_i\rangle\right]. \qquad (1.8)$$

The first term in (1.8) consists of matrix elements of the one-electron Hamiltonian,

$$h_i = \frac{1}{2}\nabla_i^2 - \sum_A \frac{Z_A}{r_{iA}}, \qquad (1.9)$$

including the electronic kinetic energy and the electron-nuclear potential energy terms. The second term contains the two-electron contributions,

$$\langle\phi_p\phi_q|\phi_r\phi_s\rangle = \langle\phi_p\phi_q|\frac{1}{r_{12}}|\phi_r\phi_s\rangle$$
$$= \int d\mathbf{x}_1 \int d\mathbf{x}_2 \psi_p^*(\mathbf{x}_1)\psi_q^*(\mathbf{x}_2) r_{12}^{-1} \psi_r(\mathbf{x}_1)\psi_s(\mathbf{x}_2), \qquad (1.10)$$

which are simply the two-electron repulsion terms in physicist's notation [32]. In typical applications, the spatial orbitals are expanded in term of some finite basis set of atom-centered Gaussian-type orbitals. In HF theory the orbitals (expansion coefficients) are optimized variationally to yield the lowest single-determinant energy subject to spatial and spin symmetry restrictions (and orbital orthonormallity conditions). As will be discussed below, HF theory is not capable of providing reliable energetics for chemically-relevant energy differences. However, HF theory is typically the starting point for the vast majority of *ab initio* chemical investigations.

Electron Correlation and Post-HF Methods

Clearly, $\hat{\mathcal{H}}$ (and subsequently the electronic Schrödinger equation) is not exactly separable into 1-electron Hamiltonians. The equations are coupled, which is to say that the motion of the electrons is correlated. The magnitude and nature of electron-correlation effects, being essentially the corrections to independent particle models, will be dependent to the choice of orbital model with respect to which such correlation effects are considered [33]. However, in this work we will adhere to the widely accepted definition of the correlation energy (more appropriately the basis-set correlation energy) as the difference between the HF energy and the exact non-relativistic energy in a given one-particle basis,

$$E_{corr} = \varepsilon - E_{HF}\,. \tag{1.11}$$

It is of use to note that, although it is a common misconception and the definition of E_{corr} as defined above implies that HF theory does not include any explicit electron correlation, the HF approach does indeed include some account of electron correlation effects. Through the use of a Slater determinant, which obeys the well-known antisymmetry (Pauli exclusion) principles for the exact electronic wavefunction, HF theory includes a small amount of correlation energy for same-spin electrons. Often referred to as *Fermi* correlation, this effect results in an over stabilization of high-spin states described by HF theory. Owing to the fact that HF theory is a variational method, E_{corr} will always be a negative quantity. Relative to the total energy, E_{corr} is a small quantity. HF theory is capable of recovering approximately 99% of the total energy for most molecular systems at their equilibrium geometries (98.5% for He_2, 98.9% for LiH, 99.04% for H_2O, 99.5% for N_2, and 99.5% for NH_3) [33]. It is unfortunate that the

magnitude of the error in HF theory, E_{corr}, is the same order of magnitude as the energies for chemically interesting phenomena.

Given that HF theory is capable of recovering such a large percentage of the total energy, one might assume that the HF wavefunction provides a reasonable starting point (reference function) from which to stage more advanced approaches. It is typically true that HF theory does provide a reasonable starting point for more advanced "correlated" methods of electronic structure. To a large extent, although not exclusively, standard methods of electronic structure theory are based upon HF reference functions. Such approaches are typically referred to as *post-HF* methods. The vast majority of post-HF methods can be classified into one of three categories or models of electron correlation: configuration interaction (CI), perturbation theory (PT), or coupled cluster theory (CC). As will be discussed below, each of these models, in actuality, defines a hierarchy of approximate methods that (in principle) can build in complexity to reach the exact solution to the Schrödinger equation.

The HF determinant, although the best (in a variational sense) single-determinant description of the electronic structure, is not the only determinant which can be formed from the ψ_i's. Given any set of $2K$ spin orbitals (such as those which would result from a HF calculation in a singe-particle basis of dimension K), we can construct a set of $\begin{pmatrix} 2K \\ N \end{pmatrix}$ different N-electron Slater determinants. The set of all N-particle states that can be formed from the $2K$ spin orbitals will be denoted as $F(2K,N)$. Such a set forms a abstract linear vector space which is just a subspace of the 2^{2K}-dimensional *Fock* space, $F(2K)$;

$$F(2K) = \bigcup_{g=0}^{2K} F(2K, g). \tag{1.12}$$

Each determinant in $F(2K, N)$ can be represented by an occupation-number vector $|\mathbf{k}\rangle$,

$$|\mathbf{k}\rangle = |k_1, k_2, \ldots, k_{2K}\rangle = \begin{cases} 1 & \psi_i \text{ occupied} \\ 0 & \psi_i \text{ unoccupied} \end{cases}. \tag{1.13}$$

The HF determinant in this notation, typically written as $|\Psi_0\rangle$ or $|0\rangle$, is thus

$$|\Psi_0\rangle = |1_1, 1_2, \ldots, 1_N, 0_{N+1}, \ldots, 0_{2K-1}, 0_{2K}\rangle. \tag{1.14}$$

It is often convenient to express "excited" or "substituted" determinants relative to $|\Psi_0\rangle$ using operators. Such operators are referred to as *second quantized* operators. In the standard formulation of quantum mechanics, observables are expressed as operators acting upon the states (functions). In second quantization, both the operators and the states they act upon are represented as operators. Although a detailed presentation of second quantization is beyond the scope and the needs of the work presented, a brief introduction to some of the key concepts will facilitate some of the later discussion. For the interested reader many of the intricacies and details of second quantization can be found elsewhere [34, 35].

In second quantization all states (and all operators) are constructed in terms of elementary creation and annihilation operators. Determinants other than $|\Psi_0\rangle$ are constructed by strings of these operators acting, typically, upon $|\Psi_0\rangle$. The creation operator $a_a^\dagger$ creates a particle in ψ_a;

$$a_a^\dagger |k_1, k_2, \ldots, 0_a, \ldots, k_{2K}\rangle = |k_1, k_2, \ldots, 1_a, \ldots, k_{2K}\rangle. \tag{1.15}$$

Unsurprisingly, the annihilation operator a_i deletes a particle in ψ_i;

$$a_i \left| k_1, k_2, \ldots, 1_i, \ldots, k_{2K} \right\rangle = \left| k_1, k_2, \ldots, 0_i, \ldots, k_{2K} \right\rangle . \tag{1.16}$$

Here, and throughout this thesis, the indices $i, j, k, \ldots$ will be used to represent spin-orbitals occupied in the reference, indices $a, b, c, \ldots$ correspond to virtual (unoccupied) orbitals, and the indices $p, q, r, s, \ldots$ for the general case of orbitals that can be either occupied or unoccupied. It suffices to say that any vector in $F(2K)$, and subsequently in $F(2K, N)$, can be expressed as a string of creation and annihilation operators acting upon the reference state $\left| \Psi_0 \right\rangle$. The exact N-particle solution of (1.5) for a fixed one-particle basis of dimension K can in principle be expressed exactly in terms of the vector space $F(2K, N)$.

The configuration interaction approaches [36] approximate the exact N-particle wavefunction as a linear combination of vectors in $F(2K, N)$;

$$\left| \Phi_0 \right\rangle = \left(c_0 + \sum_{\substack{a \\ i}} c_a^i a_a^\dagger a_i + \sum_{\substack{ab \\ ij}} c_{ab}^{ij} a_b^\dagger a_a^\dagger a_j a_i + \sum_{\substack{abc \\ ijk}} c_{abc}^{ijk} a_c^\dagger a_b^\dagger a_a^\dagger a_k a_j a_i + \cdots \right) \left| \Psi_0 \right\rangle . \tag{1.17}$$

If the expansion in (1.17) is not truncated (except when the number of creation and annihilation operators reaches N, the number of electrons) we arrive at the full configuration interaction (FCI) approach. FCI provides the exact solution to (1.5) in the given one-particle basis. Thus, from the definition in (1.11), we find that

$$E_{corr} = E_{FCI} - E_{HF} . \tag{1.18}$$

In typical applications, the FCI expansion grows far too rapidly to provide a tractable approach. However, the expansion in (1.17) provides several logical places for truncation. When restricted to the first two terms (all singly-excited determinants), we arrive at the CI singles (CIS) approach. [It should be noted that singles do not interact

with $|\Psi_0\rangle$ as a consequence of Brilluoin's theorem [37]; however they do provide an adequate zero-order representation of singly-excited electronic states] Inclusion of higher-order terms provides CI singles and doubles (CISD); CI singles, doubles, and triples (CISDT); and an entire hierarchy of higher-order CI approaches.

As $|\Psi_0\rangle$ is expected to be a very good approximation to $|\Phi_0\rangle$ for many molecular systems, the application of perturbation theory (PT) to systematically improve upon HF theory is indeed tempting. The most widely applied and successful post-HF method has been the PT approach of Møller and Plesset truncated at second-order (MP2) [32]. In Møller-Plesset PT, the Fock operator is taken as the zero-order potential and $|\Psi_0\rangle$ as the zero-order wavefunction. The HF energy is the sum of the zero- and first-order energies and the first-order wavefunction (second-order energy) is spanned by only the space of double excitations as a consequence of Brilliouin's theorem: [37]

$$
\begin{aligned}
E_{MP}^{(0)} &= \sum_i \varepsilon_i \\
E_{MP}^{(1)} &= -\frac{1}{2}\sum_{ij}\langle ij||ij\rangle \\
E_{MP}^{(2)} &= \frac{1}{4}\sum_{\substack{ab\\ij}}\frac{\left|\langle ij||ab\rangle\right|^2}{\varepsilon_i+\varepsilon_j-\varepsilon_a-\varepsilon_b} \\
E_{HF} &= E_{MP}^{(0)} + E_{MP}^{(1)} \qquad .
\end{aligned}
\tag{1.19}
$$

Although it is certainly possible to extend the perturbation expansion further down the hierarchical MPn series, it has been demonstrated that the perturbation series is slowly convergent (if convergent at all) [38-40] and typical applications seldom venture beyond MP2.

The coupled cluster ansatz has proven to be one of the most highly accurate post-HF methods. The success of the CC approaches is a consequence of the exponential expansion of the wavefunction:

$$\left|\Phi_0\right\rangle = e^{\hat{T}}\left|\Psi_0\right\rangle = \left(1 + \hat{T} + \frac{1}{2!}\hat{T}^2 + \frac{1}{3!}\hat{T}^3 + \ldots\right)\left|\Psi_0\right\rangle$$

$$\hat{T} = \hat{T}_1 + \hat{T}_2 + \hat{T}_3 + \hat{T}_4 + \ldots$$

$$\hat{T}_1 = \sum_{\substack{a \\ i}} t_i^a a_a^\dagger a_i \quad \hat{T}_2 = \sum_{\substack{ab \\ ij}} t_{ij}^{ab} a_b^\dagger a_a^\dagger a_i a_j \quad \hat{T}_3 = \sum_{\substack{abc \\ ijk}} t_{ijk}^{abc} a_c^\dagger a_b^\dagger a_a^\dagger a_i a_j a_k \,. \tag{1.20}$$

If all $\hat{T}_n$ are included in the expansion, one arrives at the FCI limit. However, the exponential expansion for a truncated CC model results in the inclusion of higher-order excitations as products of lower-order excitations (i.e. quadruple excitations as products of double excitations). Truncated CC methods (unlike truncated CI) are size extensive and size consistent. The term size-consistency refers to the additive separability of the energy in the limit of noninteracting fragments:

$$E_{AB} = E_A + E_B, \tag{1.21}$$

where E_{AB} is the energy of a system composed of two noninteracting fragments, **A** and **B**, at infinite separation; and E_A , E_B are energies of the corresponding fragments. Size extensivity is a property attributed to methods where the energy scales linearly with the size of the system. The accuracy of size-extensive methods will not degrade as the size of the system increases.

While the post-HF models presented above differ greatly in the manner by which they include corrections to the HF reference, the primary assumption of these (and all) post-HF methods is that $\left|\Psi_0\right\rangle$ is the leading contribution to $\left|\Phi_0\right\rangle$ and the contribution of other determinants is relatively small. When this is the case, the approaches presented

above (when truncated at reasonable order) provide highly accurate descriptions of the correlation energy.

Dynamical and Non-Dynamical Electron Correlation

The HF model separates the N-electron Schrödinger equation, equation (1.5), into N 1-electron equations by replacing the electron-electron repulsion term with the interaction of each electron with the average potential created by the remaining N-1 electrons. This is the so-called *mean field* approximation [32]. In reality each electron responds instantaneously to the positions of the remaining N-1 electrons and the post-HF methods discussed above attempt to recover these interactions, referred to as *dynamical correlation*. When the HF approach provides an adequate solution to the electronic structure problem, the corrections for dynamical correlation are small and the post-HF methods above provide highly accurate results. However, under certain circumstances discussed below the HF method fails to provide a reasonable description of the electronic structure of the system.

While the mean-field approximation is certainly the most highly discussed and well understood approximation inherent to HF theory, there is a second approximation intrinsic to the theory that causes the HF description of the electronic structure to break down under certain circumstances. The *single reference* approximation assumes that the electronic structure of the system can be well described (at least at zero order) by a single Slater determinant. This is typically the case for most well behaved systems at their equilibrium geometries. The variational nature of the self-consistent field (SCF) procedure attempts to arrive at the "best" single determinant description of the electronic structure for the given one-particle basis. However, for systems that exhibit near-

degeneracy of two or more electronic configurations the single-reference approximation breaks down. In such cases, the electronic structure can only be well described by a superposition of these degenerate or nearly-degenerate configurations. The effect of near-degeneracy in electronic configurations has been termed nondynamical correlation (also referred to as *static* correlation and *left-right* correlation).

Nondynamical correlation can be best understood by considering a specific example. Subsequent sections will address the role of nondynamical correlation in two important areas of chemistry; bond-breaking potentials and transition-metal catalysts. The model considered here has been used extensively to test the reliability of approximate methods of electronic structure for systems exhibiting large nondynamical correlation effects [41-47]. For now, consider the simple H_4 model system constructed by previous authors [48]. The H_4 model, depicted in Figure 1, consists of two stretched hydrogen molecules in an isosceles trapezoidal arrangement. All nearest-neighbor distances are fixed at 2 bohr and the model parameter $\alpha\left(0 \le \alpha \le 1/2\right)$ transforms the system from non-degenerate (single-reference) at $\alpha = 1/2$ to a fully degenerate case at $\alpha = 0$. At $\alpha = 1/2$ the system consists of two co-linear hydrogen molecules and the correlation energy is predominately dynamical. However, at $\alpha = 0$ the system consists of two degenerate electronic configurations, one describing bonding between 1 and 2 and 3 and 4 and one describing bonding between 1 and 4 and 2 and 3 [see Figure 1]. As α varies between these two values the mixing (or interaction) between these two distinctly different electronic configurations will vary; i.e. the strength of both the dynamical and nondynamical correlation effects will change. In the degenerate case, $\alpha = 0$, the sinlge-

reference approximation intrinsic to HF theory breaks down giving rise to large errors for HF and post-HF methods.

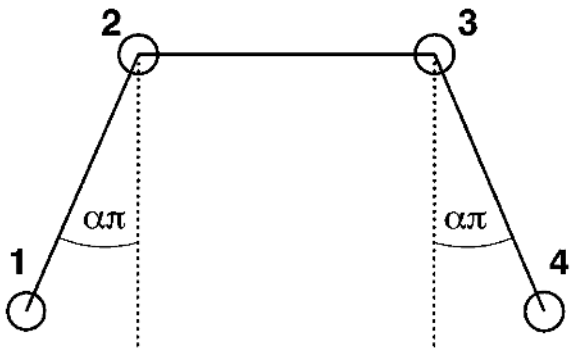

Figure 1. Nuclear configurations and definition of the model parameter α for the H_4 model. Figure reproduced from reference 48.

With the exception of a few specific examples, the correlation energy from (1.11) is not explicitly separable. For the H_2 molecule at infinite separation there is clearly not any dynamical correlation and the correlation energy is purely non-dynamical. Likewise, the uniform electron gas has no degeneracy and the correlation energy is thus considered to be entirely a dynamical effect [49]. While some authors have put forward definitions of the nondynamical (an thus the dynamical) correlation energy [49], such separations of the correlation energy are somewhat arbitrary and can lead to unphysical interpretations under certain circumstances. Nonetheless, the conceptual separation of the correlation energy into two distinctly separate effects (those arising from the instantaneous interaction of the electrons and those arising from near-degeneracy in electronic configurations) has proven extremely useful. Subsequent sections will highlight the importance of non-dynamical correlation for bond-breaking potentials and transition-metal catalysts, focusing on the fertility of minimalistic descriptions of such effects when combined with corrections for dynamical electron correlation.

CHAPTER 2

NON-DYNAMICAL CORRELATION AND BOND BREAKING

This section outlines the difficulties associated with nondynamical correlation effects as they pertain to the bond-breaking problem. While the post-HF methods described previously provide high-accuracy results for small chemical systems at their equilibrium geometry, the ability to understand most chemical processes of interest (i.e. reaction mechanisms) requires knowledge of the potential energy surface and the ability to accurately describe the making and breaking of chemical bonds. As bonds are stretched far from equilibrium near degeneracies arise among the electronic configurations. The problem is best understood by considering the dissociation of the H_2 molecule, which has been extensively discussed by other authors [32, 34].

For minimal-basis H_2 (a single atomic basis function on each center), the RHF molecular orbitals give rise to bonding (σ_g) and antibonding (σ_u) combinations that can be demonstrated to be

$$\begin{aligned}\sigma_g(\mathbf{r}) &= N_g\left[\phi_A(\mathbf{r})+\phi_B(\mathbf{r})\right]\\ \sigma_u(\mathbf{r}) &= N_u\left[\phi_A(\mathbf{r})-\phi_B(\mathbf{r})\right].\end{aligned} \tag{2.1}$$

The $\phi_{A/B}$'s are the atomic basis functions centered at nucleus A/B and the normalization constants are defined as

$$\begin{aligned}N_g &= \frac{1}{\sqrt{2(1+S)}}\\ N_u &= \frac{1}{\sqrt{2(1-S)}},\end{aligned} \tag{2.2}$$

where S is the overlap between the two atomic basis functions. In the limit of infinite separation the overlap goes to zero and the normalization constants both tend to $\sqrt{1/2}$. At infinite separation, the energy of the system should be the sum of the energies of two noninteracting hydrogen atoms. However, the RHF wavefunction ($|\Psi_0\rangle = |\sigma_g(\mathbf{r})^2\rangle$ for this system) severely overestimates the dissociation limit for even H_2. By requiring the electrons to occupy the same spatial molecular orbital they interact in HF theory even at infinite separation. Both electrons are forced to have the same spatial distribution, which is clearly not appropriate for infinitely separated hydrogen atoms. This results in terms that not only describe the dissociation to $H\bullet + H\bullet$ but also to $H^- + H^+$. The remaining determinant of appropriate (Σ_g^+) symmetry places both electrons in the antibonding orbital, i.e. $|\sigma_u(\mathbf{r})^2\rangle$. This describes a system where both of the electrons are out of phase. At the dissociation limit it no longer matters if the electrons are in phase or out of phase, and both $|\sigma_g(\mathbf{r})^2\rangle$ and $|\sigma_u(\mathbf{r})^2\rangle$ are degenerate electronic configurations. Thus, both determinants are required for an accurate description of the noninteracting hydrogen atoms. At infinite separation the resulting wavefunction is of the form

$$|\Psi\rangle = \frac{1}{\sqrt{2}}|\sigma_g(\mathbf{r})^2\rangle - \frac{1}{\sqrt{2}}|\sigma_u(\mathbf{r})^2\rangle. \tag{2.3}$$

As can be seen, the appropriate description of the hydrogen molecule at infinite separation requires the inclusion of two equally important determinants and the correlation is completely nondynamical. At intermediate distances the importance of the $|\sigma_u(\mathbf{r})^2\rangle$ configuration will vary from its value at infinite separation and the correlation energy will consist of a mixture of dynamical and nondynamical effects. The problem

presented here is not specific to bond breaking in H_2 and is not a consequence of the minimal one-particle basis set employed. Indeed, restricted HF theory is unable to describe the homolytic dissociation of a closed-shell system to noninteracting open-shell fragments due to the presence of the ionic terms in the closed-shell description. The problem can be somewhat helped by removing the requirement that the α and β spin-orbitals be constructed from the same spatial molecular orbitals, as is done in the unrestricted HF (UHF) formalism. However, while UHF can provide a qualitatively correct description of the dissociation process the resulting wavefunctions are heavily spin contaminated. This will lead to complications in the prediction of spin-dependent properties.

While post-HF methods based upon RHF reference functions, when truncated at an appropriate order, do include both of the dominant configurations necessary to describe the bond-breaking surface, the two nearly degenerate configurations ($\left|\cdots(\sigma)^2\right\rangle$ and $\left|\cdots(\sigma^*)^2\right\rangle$) are not treated on an equal footing. Consider the CISD approximation, configuration interaction truncated at single and double substitutions. While the $\left|\cdots(\sigma^*)^2\right\rangle$ determinant is included in the CI expansion ($\left|\cdots(\sigma^*)^2\right\rangle$ is a double excitation relative to $\left|\cdots(\sigma)^2\right\rangle$), the remaining singly- and doubly-excited determinants primarily describe dynamical correlation effects in the $\left|\cdots(\sigma)^2\right\rangle$ configuration. Thus, CISD tends to overestimate the dissociation energy due to a lack of dynamical correlation for the $\left|\cdots(\sigma^*)^2\right\rangle$ configuration. The MP2 energy (when based upon RHF reference functions) diverges due to the presence of small denominators in the second-order energy from

(1.19), a consequence of the degeneracy of the bonding and antibonding orbitals. Even one of the most robust post-HF methods CCSD(T), which includes all singles and doubles with a perturbative treatment of triple excitations, can provide unphysical potentials for simple molecular systems. The dissociation energy predicted by post-HF methods can be improved by employing a UHF reference function, although such approaches are often spin contaminated and have difficulty accurately describing the potential at intermediate bond lengths.

The accurate description of the dissociation process requires treating all nearly-degenerate configurations on an equal footing. The nature of the single-reference approximation makes this extremely challenging for post-HF methods to accomplish. Some authors have attempted to overcome the single-reference breakdown through the development of "dressed" single-reference methods that include limited numbers of higher-order excitations [50] and other authors have examined using orbitals other than the RHF or UHF orbitals as a starting-point for single-reference methods [44, 47, 48]. Ultimately, the only general way to treat nondynamical correlation effects accurately is to apply methods, generally referred to as multireference methods, capable of treating all nearly-degenerate configurations on an equal footing. However, as will be discussed in subsequent chapters, the use of true multireference methods provides a completely new set of challenges.

CHAPTER 3

THE SPIN-FLIP AND SPIN-COMPLETE SPIN-FLIP APPROACHES

As discussed above, the *ab initio* modeling of bond-breaking reactions remains a central challenge for standard theoretical methods. Conventional post-HF treatments are incapable of remedying the deficiencies of the single-reference formalism. While much effort has been applied by others to accurately treat the inherent multireference character of the molecular wavefunction within the reference space [51], an alternative approach pointed to by Krylov [52] attempts to reformulate the problem to remove the multireference character of the reference wavefunction. The spin-flip (SF) models [52-55] describe closed- and open-shell singlet states within a single-reference formalism as $\alpha \rightarrow \beta$, spin-flipping, excitations from a high-spin $\left(M_s = 1\right)$ triplet reference state. While the singlet state becomes highly multireference as bonds are stretched far from equilibrium, the triplet state remains strongly single-reference across the entirety of the bond-breaking coordinate. This results in significantly smaller corrections for dynamical and nondynamical electron correlation [52]. Formally an equation of motion (EOM) approach in which the target states are sought in the basis of determinants which conserves the number of electrons but flips the spin of one electron, numerous SF approaches have been developed for the description of bond breaking and diradicals [52-66].

The Spin-Flip Model

The simplest member of the SF hierarchy of methods, referred to both as SF-SCF and SF-CIS [52], treats the target states as single (spin-flipping) excitations from the SCF

description of the high-spin reference state. For the case of breaking a single bond, the SF-CIS wave function is:

$$\left|\Psi^{SF-CIS}\right\rangle = \hat{R}_1 \left|\Phi_0^{\alpha\alpha}\right\rangle \tag{3.1}$$

where $\Phi_0^{\alpha\alpha}$ is a single Slater determinant describing the high-spin reference state and $\hat{R}_1$ is the single excitation operator which flips the spin of a single electron,

$$\hat{R}_1 = \sum_{ia} r_i^a \hat{a}^+ \hat{i} \ . \tag{3.2}$$

The second-quantized operators $\hat{a}^+$ and $\hat{i}$ create a particle in spin-orbital a and a hole in spin-orbital i respectively. The amplitudes, r_i^a are determined by the diagonalization of the electronic Hamiltonian in the basis of the singly-excited SF determinants. As pointed out by Krylov, the spin-orbital formulation is identical to that of the conventional CIS model [59, 67].

The simplest model, SF-CIS, demonstrated a systematic improvement over both spin-restricted or spin-unrestricted HF models for breaking single bonds for several systems [52]. The SF-CIS wave function and corresponding energies are qualitatively correct and remain well balanced along the entirety of the bond-breaking coordinate. For the challenging case of F_2 ($D_e = 1.66$ eV), the SF-CIS approach provides a dissociation energy of 0.28 eV compared to a value of 10.69 eV from RHF [52]. When augmented with corrections for dynamical correlation either through perturbation theory via SF-CIS(D) or through optimized-orbitals coupled cluster doubles via SF-OD the values are 1.14 eV and 1.24 eV respectively [54]. The SF formulation extends previously-existing single-reference methods to regions away from equilibrium [52-55, 59, 63, 65]. The SF-CIS methods provides a superior starting point than the conventional RHF reference for

regions away from equilibrium. Furthermore, it has been demonstrated that the SF-CIS is size-consistent [52], as defined in (1.21). While the SF-SCF approach is size-consistent and does provide a dramatic improvement to the conventional HF reference for bond breaking, the SF-CIS formalism suffers from spin contamination effects addressed below.

The Spin-Complete Spin-Flip Model

Although the SF methods are capable of effectively describing the multireference nature of the wave function using a single-reference formalism, the SF solutions are not pure spin eigenfunctions. By arbitrarily choosing the $\alpha\alpha$ reference from the three degenerate components of the triplet state, a slight imbalance occurs in the treatment of degenerate spin configurations in the final wave function. Since all the leading determinants are present in the SF subspace together with their spin-coupled counterparts, the resulting spin contamination of target wave functions is rather small (although it can be large for excited states—see the following). In other words, the spin contamination of the SF wave functions is due to the spin polarization of the SF wave functions, rather than spin-symmetry breaking which single-reference methods often exhibit when a single-determinantal description is not appropriate [68]. Despite the above-mentioned imbalance, the simplest SF method, SF-CIS performed well on several test cases [52] and was greatly improved once augmented with perturbative corrections to include dynamical correlation as in SF-CIS(D) [54], or when all double excitations were explicitly included as in SF-CISD [55]. The success of the SF approach leads to questions concerning the improvement that might be obtained by using spin-complete wave functions. This work [69] presents a spin-complete variant of the SF-CIS model, denoted SC-SF-CIS. The following sections discuss the theoretical approach and implementation of the SC-SF-CIS model and presents results for excitation energies, equilibrium geometries, and potential energy curves for dissociation of a single bond in several small molecules.

Spin-completeness of the SF-CIS Wave Function: Theory and Implementation

For open-shell electron configurations, several determinants are required to form an eigenfunction of $\hat{S}^2$. For a simple example, consider the case of two electrons in two orbitals. Of the four $M_s = 0$ determinants, two are of a closed shell type, i.e., $|\phi_1\alpha\phi_1\beta\rangle$ and $|\phi_2\alpha\phi_2\beta\rangle$. When the same set of spatial orbitals is employed for the α and β spin-orbitals, the closed-shell determinants are spin pure, i.e., they are eigenfunctions of both the $\hat{S}$ and the $\hat{S}^2$ operators. The open-shell determinants, $|\phi_1\alpha\phi_2\beta\rangle$ and $|\phi_1\beta\phi_2\alpha\rangle$, are not eigenfunctions of $\hat{S}^2$. However, they do form what we will call a spin-coupled set, and singlet and triplet $\hat{S}^2$ eigenfunctions are obtained by the appropriate linear combination of these determinants, i.e., $2^{-1/2}\left(|\phi_1\alpha\phi_2\beta\rangle \pm |\phi_1\beta\phi_2\alpha\rangle\right)$. Thus, a CI wave function that includes one of these determinants must also include the other if the total wave function is to be a spin eigenfunction.

Turning back to the SF approach, consider the simple case of four electrons in four spatial orbitals, as in Figure 2. Configurations (b) through (j) result from single SF excitations from the reference (a). Configurations (b) and (c) are of a closed-shell type (i.e., contain no unpaired electrons) and are thus spin eigenfunctions. Open-shell configurations (d) and (e) include singly occupied spatial orbitals and are thus not spin eigenfunctions of the system, but do form a ‘‘spin-coupled’’ set and thus can be combined to obtain an eigenfunctions of $\hat{S}^2$. Configurations (f)–(j) are not spin eigenfunctions, and their ‘‘spin-complements’’ cannot be obtained by a single SF excitation from (a). Thus, a linear combination of (b)–(j), i.e., the SF-CIS wave function for this particular system, is not a spin eigenfunction. The missing spin-complements of (f)–(j) are shown in Figure 3. These nine determinants should be added to the nine SF-

CIS determinants from Figure 2 to achieve spin-completeness. For the case of six electrons in six spatial orbitals, the SF-CIS space consists of 16 determinants. To form the SC-SF-CIS wave function, 28 additional determinants are required.

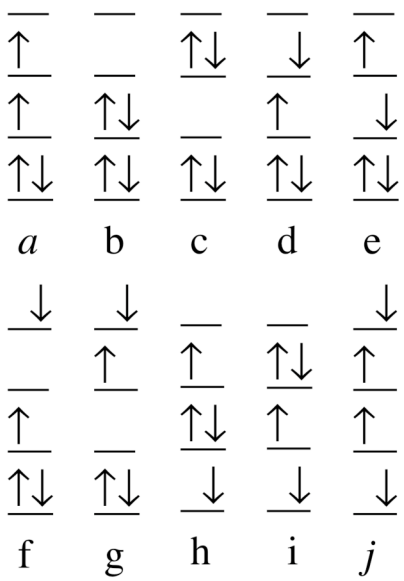

Figure 2. System consisting of four electrons in four orbitals. Configuration (a) is the triplet reference. Configurations (b)-(j) are produced by single spin-flipping electronic excitations. Note that (b) and (c) are spin eigenfunctions and that (d) and (e) form a "spin-coupled" set. However, configurations (f)-(j) are all missing one or more complementary spin configurations.

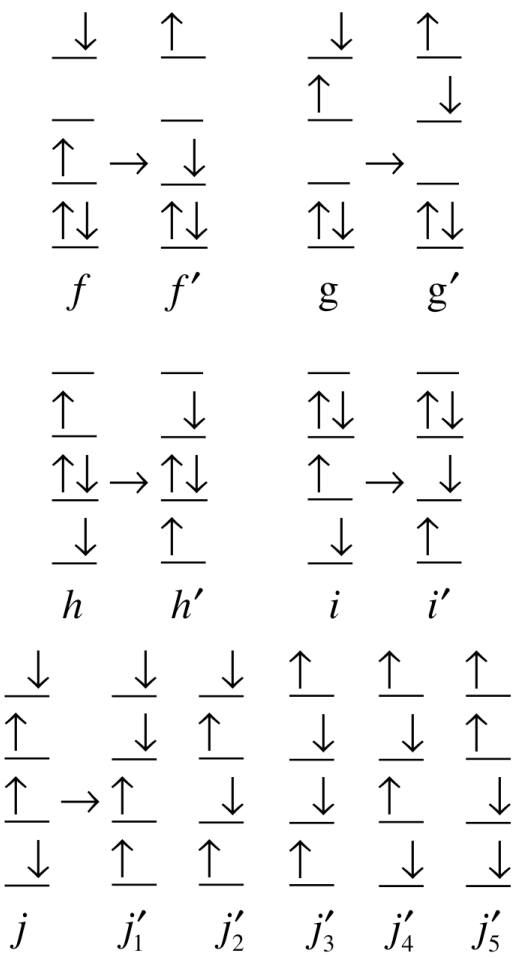

Figure 3. Determinants (f)-(j) from Figure 2 and the corresponding "spin-complements."

In order to estimate the total number of determinants in the SF-CIS and the SC-SF-CIS subspaces, let us partition the *molecular* orbital space into three subspaces; (i) a subspace of O doubly occupied orbitals denoted by $\mathbf{O}$; (ii) a subspace of X singly occupied orbitals denoted by $\mathbf{X}$ (for the triplet reference, $\mathbf{X}$ contains only two molecular orbitals); and (iii) a subspace of V unoccupied orbitals denoted by $\mathbf{V}$. The choice of the partitioning is defined by the appropriate high-spin reference. The total number of electrons is thus equal to $2O + X$. If there are no symmetry imposed restrictions, the target SF-CIS subspace contains $2(O + V + 2) + OV$ determinants: four $X \rightarrow X$ excitations [determinants (b)–(e) from Figure 2]; $2O$ and $2V$ excitations of the $O \rightarrow X$

and $X \rightarrow V$ types, respectively, since $X = 2$ for the SF reference [determinants (h), (i) and (f), (g)]; and OV determinants of the $O \rightarrow V$ type [determinant j]. The spin-complements from Figure 3 are formally a restricted subset of double and triple spin-orbital excitations relative to the high-spin triplet reference. The (f') and (g') type determinants are $X \rightarrow X$, $X \rightarrow V$ doubles (there are $2V$ of these). Likewise, the (h') and (i') type determinants are $X \rightarrow X$, $O \rightarrow X$ doubles (there are $2O$ of these). The (j_1'), (j_2'), (j_4'), and (j_5') type determinants are $X \rightarrow X$, $O \rightarrow V$ doubles ($4OV$ total). Finally, there are OV triple $X \rightarrow X$, $X \rightarrow X$, $O \rightarrow V$ excitations of the (j_3') type. To summarize, the total number of determinants in the SC-SF-CIS is $4(O+V+1)+6OV$. Thus, the number of determinants included in either method is $\mathrm{O}(OV)$. For a specific example, the HF molecule in a 6-31G basis, taking symmetry restrictions into account and with the 1*s* orbital on fluorine frozen, requires 17 determinants for SF-CIS and 50 determinants for SC-SF-CIS.

We have implemented the SC-SF-CIS model by modifying the restricted active space configuration interaction (RAS-CI) program, DETCI [36]. In the RAS-CI method, determinants are selected by partitioning of the molecular orbitals into several subspaces and then choosing determinants according to the number of electrons allowed in each subspace. As described by Sherrill and Schaefer [36, 70, 71], we divide the active (nonfrozen) orbitals into four subspaces, labeled I, II, III, and IV. The orbital partitioning is determined by the specific bond to be broken. The bonding orbital ϕ_B defines the RAS II subspace, and all other active occupied orbitals are placed in RAS I. RAS III contains the corresponding antibonding orbital ϕ_B^*, and all remaining virtual orbitals are placed in

RAS IV. In terms of the $\mathbf{O}$, $\mathbf{V}$, and $\mathbf{X}$ subspaces introduced earlier, RAS I and RAS IV correspond to the $\mathbf{O}$ and $\mathbf{V}$ subspaces, respectively, while RAS II and RAS III form together the $\mathbf{X}$ subspace.

Once the orbitals have been distributed among these RAS subspaces, the determinants for the SC-SF-CIS are chosen as follows. A maximum of one excitation is allowed from RAS I, a maximum of two electrons are allowed in RAS III (which contains only a single orbital anyway), and a maximum of one electron is allowed in RAS IV. A maximum of two electrons are allowed simultaneously in RAS III and RAS IV. Finally, if an electron is in RAS IV, then there must be at least one hole in RAS II. These rather complex rules are necessary to generate exactly the SC-SF-CIS determinantal subspace, and are different from the usual RAS-CI procedures [36, 71].

The above-mentioned scheme for selecting determinants can be used with any type of molecular orbitals, allowing us to investigate the effect of different orbital choices in addition to testing the importance of spin-completeness. The EOM formulation of the SF models suggests that one employ orbitals obtained for the high spin reference state [either unrestricted Hartree–Fock (UHF) or restricted open shell Hartree–Fock (ROHF) or Brueckner-type, as in spin-flip optimized orbital coupled-cluster doubles (SF-OD)]. Previous SF-CIS benchmarks employed UHF orbitals for the high-spin triplet of the appropriate symmetry. In the present work, we also use high-spin triplet Hartree–Fock orbitals, but they are obtained in the ROHF procedure (for rigorous spin-completeness, it is necessary to use the same spatial molecular orbitals for α and β spin-orbitals).We have also tested the performance of the restricted Hartree–Fock (RHF) orbitals obtained

for the closed-shell singlet wave function, as well as two-configuration self-consistent-field (TCSCF) orbitals.

Although our CI space is generated in the RAS-CI scheme as described earlier, for simplicity we will speak as though the space is generated from a triplet ‘‘reference’’ as in the original SF-CIS procedure. Results were generated using the lowest triplet state of the given symmetry as a reference. For the bond breaking examples, this reference becomes $\left|\Psi_D \phi_B \alpha \phi_B^* \alpha\right\rangle$ as the bond is stretched.

Size-Consistency of the SC-SF-CIS Method

In this section, we discuss the size-consistency of the SC-SF-CIS model, closely following the presentation from Ref. [55]. We adhere to the terminology used in Refs. [55] and [72]. Recall the definition of size consistency presented in (1.21). Here, we restrict ourselves to the case where **A** and **B** are closed-shell systems. In the following we will show that SC-SF-CIS, using an UHF triplet reference, is size-consistent in the sense that the total SF energy is equal to the sum of the SF energy of fragment **A** and the HF energy of fragment **B**. Therefore, the accuracy of the SF-CI description of the bond breaking localized at a reaction center in a large molecule would not be affected by molecular size. However, SF-CI would fail to describe simultaneous breaking of two bonds, even in case of noninteracting bonds.

For excited states described by the SF-CI or SF-CC models, the total energy of a target state consists of the reference energy and the corresponding transition energy. Thus, (1.21) is satisfied if (i) the reference energy of the composite system is the sum of the reference energies for fragments, and (ii) the transition energy is additive. Condition (i) is satisfied by any SF-CI model due to size-consistency of the Hartree–Fock model

given that the orbitals are obtained from the Hartree–Fock calculation for the SF reference determinant. In the following, we prove that the transition energy for the ‘‘excitation’’ localized on fragment **A** in the super-molecule is the same as the transition energy for the fragment **A**, i.e., that energies of target states on the fragment **A** are not affected by the presence (at infinite distance) of the fragment **B**. Thus, the quality of SF-CI description would not degrade with the increase of molecular size. However, the SF-CI correlation energy is not additive.

We start by dividing all the determinants into four groups; (i) the reference determinant, $|0_A \cdot 0_B\rangle$ or simply $|0\rangle$; (ii) determinants involving excitations localized on fragment **A**, $|\Phi_A \cdot 0_B\rangle$ or $|A\rangle$; (iii) determinants involving excitations localized on fragment **B**, $|0_A \cdot \Phi_B\rangle$ or $|B\rangle$; (iv) determinants that involve excitations of electrons on both fragments, $|\Phi_A \cdot \Phi_B\rangle$ or $|AB\rangle$ (i.e., those which describe simultaneous excitation of both subsystems or electron transfer between them).

In the SF implementation employing a triplet reference, the reference determinant is the Hartree–Fock determinant describing the $\alpha\alpha$ component of the reference triplet state. We assume that the two unpaired electrons are localized on fragment **A** [73]. Thus, $|0_A\rangle$ is the Hartree–Fock determinant for fragment **A** in the *triplet* state, and $|0_B\rangle$ is the Hartree–Fock determinant for fragment **B** in the *singlet* state. Later in the discussion, we use $|0\rangle$ and $|\mathbf{p}\rangle$ to refer to (i) and (ii)–(iv) determinants, respectively. While $|0\rangle$ is the $M_s = 1$ determinant, all $|\mathbf{p}\rangle$ have $M_s = 0$, since they are generated by spin-flipping excitations from $|0\rangle$.

In the separated limit, the Hamiltonian operator of the composite system is the sum of those for the individual fragments:

$$\hat{H} = \hat{H}_A + \hat{H}_B . \tag{3.3}$$

As pointed out by Koch *et al.* [74], the sufficient condition for size-consistency is a block-diagonal structure of the matrix of the Hamiltonian (3.3) in the above-described many-electron basis [75], which the rest of this section proves

First, all the $\langle 0|\hat{H}|\mathbf{p}\rangle$ and $\langle \mathbf{p}|\hat{H}|0\rangle$ blocks are zero, because the determinants $|0\rangle$ and $|\mathbf{p}\rangle$ describe states with different number of α and β electrons and, therefore, they do not interact across the (nonrelativistic) Hamiltonian. Using the shorthand notation $\hat{H}_{PQ} \equiv \langle P|\hat{H}|Q\rangle$, other nondiagonal blocks of the matrix of the Hamiltonian (3.3) are

$$\hat{H}_{AB} = \langle 0_B|\Phi_B\rangle \cdot \langle \Phi_A|\hat{H}_A|0_A\rangle + \langle 0_A|\Phi_A\rangle \cdot \langle \Phi_B|\hat{H}_B|0_B\rangle, \tag{3.4}$$

$$\hat{H}_{BA} = \langle 0_A|\Phi_A\rangle \cdot \langle \Phi_B|\hat{H}_B|0_B\rangle + \langle \Phi_B|0_B\rangle \cdot \langle 0_A|\hat{H}_A|\Phi_A\rangle, \tag{3.5}$$

$$\hat{H}_{B,AB} = \langle \Phi_B|\Phi'_B\rangle \cdot \langle 0_A|\hat{H}_A|\Phi_A\rangle + \langle 0_A|\Phi_A\rangle \cdot \langle \Phi_B|\hat{H}_B|\Phi'_B\rangle, \tag{3.6}$$

$$\hat{H}_{A,AB} = \langle 0_B|\Phi_B\rangle \cdot \langle \Phi_A|\hat{H}_A|\Phi'_A\rangle + \langle \Phi_A|\Phi'_A\rangle \cdot \langle 0_B|\hat{H}_B|\Phi_B\rangle . \tag{3.7}$$

Due to the orthogonality, all of the $\langle 0_A|\Phi_A\rangle$ and $\langle 0_B|\Phi_B\rangle$ terms are zero. Moreover, the $\langle 0_A|\hat{H}_A|\Phi_A\rangle$ matrix elements are also zero, since $|0_A\rangle$ and $|\Phi_A\rangle$ have different number of α and β electrons. However, $\langle 0_B|\hat{H}_B|\Phi_B\rangle$ is not necessarily zero, since the fragment **B** is in the singlet state. Thus, $\hat{H}_{AB}$, $\hat{H}_{BA}$, and $\hat{H}_{B,AB}$ blocks are always zero, regardless of the levels of excitation included in the CI expansion, molecular orbitals used, and the multiplicity of the reference (as long as $|0\rangle$ and $|\mathbf{p}\rangle$ are of different M_s). However, the $\hat{H}_{A,AB}$ term is zero only in the particular circumstances. This term reduces to

$\langle \Phi_A | \Phi'_A \rangle \cdot \langle 0_B | \hat{H}_B | \Phi_B \rangle$. In case of the SF-CI model employing a triplet reference and including up to *M*-tuple excited determinants, the CI expansion includes excitations which flip the spin of one electron. Thus, since the determinant Φ_A includes *at least* one electron excitation, the excitation level in the determinant Φ_B does not exceed *M*-1 substitutions. Therefore, term (3.7) does not exist for single excitations. Moreover, for any double excitations the term $\langle \Phi_B | \hat{H}_B | 0_B \rangle$ zeros out because of the Brillouin theorem (if one employs *unrestricted Hartree–Fock triplet orbitals* for the reference determinant). If the SF-CI expansion includes higher excitations, nonzero $\hat{H}_{A,AB}$ terms may appear and violate size-consistency.

As discussed in the previous section, spin-completeness of the SF-CIS method requires adding a selected subset of doubly and triply excited determinants. As shown earlier, for any double excitations, the $\hat{H}_{A,AB}$ terms are zero. Therefore, we should consider only triply excited determinants from the SC-SF-CIS determinantal subspace, i.e., the $X \to X$, $X \to X$, $O \to V$ excitations. Since such triple excitations include excitations of two electrons within the open-shell subspace $\mathbf{X}$, the corresponding Φ_A includes *at least* double electron excitation, and the excitation level in Φ_B is thus restricted to single substitutions. Thus, for the restricted triple excitations of the $X \to X$, $X \to X$, $O \to V$ type, the $\hat{H}_{A,AB}$ term is zero. Therefore, size-consistency of the SF-CIS model is not impacted by adding the selected subset of doubly and triply excited determinants as required by spin-completeness. However, all of the SF-CI models include terms violating size-consistency when the Brillouin theorem is not satisfied, i.e., in the case when *restricted* triplet or singlet orbitals are used. In the following, we present a

numerical example which demonstrates the effect of different orbital choices on the size-consistency of excitation energies.

Results and Discussion

We present SC-SF-CIS results for several benchmark molecules and compare the results to the spin-incomplete SF-CIS approach. Using ROHF triplet orbitals allows a clear comparison of the effects of obtaining spin eigenfunctions, while SC-SF-CIS results using other orbitals facilitate the analysis of the importance of triplet orbitals to the success of the method.

Be atom

A clear example of the advantages of using spin-complete wave functions is given by the excited states of Be atom, which have already been investigated using the SF-CIS and spin-flip configuration interaction singles and doubles (SF-CISD) methods [52, 54]. The total and excitation energies for low-lying states of Be calculated in a 6-31G basis by different SF models, traditional CISD, and full CI are presented in Table 1. If the SF-CIS method is based upon a $^3P\left(1s^2 2s 2p_z\right)$ reference, then the $\left(1s^2 2s 2p_x\right)$ or $\left(1s^2 2s 2p_y\right)$ components of excited ^3P or ^1P states cannot be described properly, because the $\left|1s^2 2s\beta 2p_{x,y}\alpha\right\rangle$ determinants are missing. The same holds for both the $\left(1s^2 2p_z 2p_x\right)$ and $\left(1s^2 2p_z 2p_y\right)$ components because the $\left|1s^2 2p_z\beta 2p_{x,y}\alpha\right\rangle$ determinants are missing. The SF-CIS roots corresponding to these states are heavily spin-contaminated and yield greatly overestimated excitation energies [52]. When all double excitations are explicitly present in the wave function (as in the SF-CISD model), the description of these states significantly improves: both spin-contamination and artificial energy splittings are

considerably reduced at the SF-CISD or SF-OD level. As expected, the perturbative account of doubles in the SF-CIS(D) method is not capable of restoring the balance. The SC-SF-CIS model explicitly includes the missing determinants and provides reasonable predictions of the excitation energies of these components of the lowest-lying ^3P and ^1P states, as demonstrated in Table 1. In fact, the artificial splittings in the SC-SF-CIS are smaller than those in a more expensive SF-CISD model. The errors against full CI are fairly large (about 0.7 eV) but are about what should be expected for a method containing primarily single excitations (errors of 1 eV or more are common for CIS). The $\left(1s^2 2s 2p_{x,y}\right)$ and $\left(1s^2 2s 2p_z\right)$ components of the lowest ^3P and ^1P states are not strictly degenerate, because even the spin-complete SC-SF-CIS approach fails to treat the three *p* orbitals on an equal footing when it singles out one of them (here, $2p_z$) to constitute RAS II. The SC-SF-CIS calculation with closed-shell singlet orbitals which have identical energies for all three of the 2*p* orbitals confirms that the failure to reproduce the exact degeneracy is due to the CI space, rather than the orbitals. In fact, singlet orbitals yield slightly larger splittings than triplet orbitals. Overall, the components that should be exactly degenerate are artificially split by no more than 0.05 and 0.004 eV with singlet and triplet orbitals, respectively. Similar to the lowest ^3P state, the description of the $\left(1s^2 2p_z 2p_{x,y}\right)$ components of the next-higher ^3P state is also considerably improved by the SC-SF-CIS method. To summarize, although the SC-SF-CIS approach is a considerable improvement in that it describes excited states that are not accessible by SF-CIS, unfortunately it does not significantly improve vertical excitation energies of the states present in SF-CIS.

Table 1. Ground state total energies (hartree) and excitation energies (eV) for Be atom using a 6-31G basis set.[a]

State	SC-SF-CIS (singlet orbs)	SC-SF-CIS (triplet orbs)	SF-CIS	SF-CIS(D)	SF-CISD	CISD	FCI
$^1S\left(1s^2 2s^2\right)$	-14.584 255	-14.584 904	-14.584 111	-14.597 209	-14.613 056	-14.613 493	-14.613 545
$^3P\left(1s^2 2s 2p_z\right)$	2.102	2.131	2.111	2.432	2.861	2.877	2.862
$^3P\left(1s^2 2s 2p_{x,y}\right)$	2.129	2.132	4.087	4.144	2.867	2.877	2.862
$^1P\left(1s^2 2s 2p_z\right)$	5.938	5.973	6.036	6.254	6.578	6.598	6.577
$^1P\left(1s^2 2s 2p_{x,y}\right)$	5.988	5.977	7.481	7.743	6.586	6.598	6.577
$^3P\left(1s^2 2p_z 2p_{x,y}\right)$	7.327	6.982			7.671	7.696	7.669
$^1D\left(1s^2 2p_z^2\right)$	8.815	8.925	8.94	9.038	8.624	8.637	8.624

[a]SF methods employ a $^3P\left(1s^2 2s 2p_z\right)$ reference.

As discussed earlier, the SC-SF-CIS excitation energies are rigorously size-consistent only when UHF triplet orbitals are employed, due to the applicability of Brillouin's theorem. In this case, the quality of SC-SF-CIS is independent of molecular size, i.e., excitation energies of Be would not be affected by a Ne atom located 100 Å away. We use this example to investigate the numerical consequences of using ROHF triplet or RHF singlet orbitals in the SC-SF-CIS calculations. The ground state and excitation energies for Be with a Ne atom 100 Å away calculated using the same 6-31G basis set are given in Table 2. Both RHF orbitals of the ground state, $\mathrm{Be}\left(^1S\right)\mathrm{Ne}\left(^1S\right)$, and ROHF orbitals of the lowest triplet state, $\mathrm{Be}\left(^3P\right)\mathrm{Ne}\left(^1S\right)$, have been tested. The excitation energies for Be–Ne are identical to those for Be in most cases. For the states where the Be–Ne excitation energy differs from that of Be, the difference is always less than 0.001 eV. These results imply that the size-consistency of the SC-SF-CIS model is not considerably affected by using orbitals other than triplet UHF ones. Therefore, the

quality of SC-SF-CIS should be only slightly impacted by molecular size when using the restricted orbitals. The use of the restricted orbitals is important to ensure that the final wave function is an eigenfunction of $\hat{S}^2$.

Table 2. SC-SF-CIS ground state total energies (hartree) and excitation energies (eV) for Be atom with and without a Ne atom 100 Å away, using a 6-31G basis set.[a]

State	Be (singlet orbs)	Be (triplet orbs)	Be-Ne (singlet orbs)	Be-Ne (triplet orbs)
$^1S\left(1s^2 2s^2\right)$	-14.584 255	-14.584 904	-143.058 132	-143.058 781
$^3P\left(1s^2 2s 2p_z\right)$	2.102	2.131	2.103	2.132
$^3P\left(1s^2 2s 2p_{x,y}\right)$	2.129	2.132	2.129	2.132
$^1P\left(1s^2 2s 2p_z\right)$	5.938	5.973	5.938	5.973
$^1P\left(1s^2 2s 2p_{x,y}\right)$	5.988	5.977	5.989	5.977
$^3P\left(1s^2 2p_z 2p_{x,y}\right)$	7.327	6.982	7.327	6.982
$^1D\left(1s^2 2p_z^2\right)$	8.815	8.925	8.815	8.926

[a]SF methods employ a $^3P\left(1s^2 2s 2p_z\right)$ reference.

H_2O

Although the spin-flip approach is designed for bond breaking problems, it is important to verify its performance for well-behaved molecules at their equilibrium geometries. Somewhat surprisingly, in previous work SF-CIS had difficulty in accurately predicting the equilibrium geometry of H_2O when the lowest-lying triplet state, $^3B_1$, was used as a reference [54], while SF calculations using a higher $^3B_2$ reference yielded accurate results. The origin of these problems has been attributed to near-instabilities found for the $^3B_1$ Hartree–Fock wave function. Table 3 presents our SC-SF-CIS values for H_2O using the standard Huzinaga–Dunning polarized double-ζ (DZP) basis set. We

have employed the $^3B_1$ reference (to compare to previous work) and a $^3A_1$ reference which would be more appropriate for breaking the O–H bonds.

Table 3. Total energies and equilibrium geometries for H2O using a DZP basis set.[a]

Method	Energy	r_e	θ_e
SC-SF-CIS(singlet orbs)/$\left(^3B_1\right)$	-76.055 171	0.9511	106.14
SC-SF-CIS(triplet orbs)/ $\left(^3B_1\right)$	-76.042 001	0.9572	106.56
SC-SF-CIS(singlet orbs)/ $\left(^3A_1\right)$	-76.059 521	0.9629	104.56
SC-SF-CIS(triplet orbs)/ $\left(^3A_1\right)$	-76.045 076	0.9799	103.92
SF-CIS/$\left(^3B_1\right)$	-76.005 093	0.9517	107.70
SF-CIS(D)/ $\left(^3B_1\right)$	-76.240 017	0.9564	105.58
SF-OD/$\left(^3B_1\right)$	-76.268 212	0.9610	104.95
SCF	-76.047 009	0.9437	106.63
MP2	-76.258 560	0.9616	104.48
CCSD	-76.267 869	0.9610	104.63
CCSD(T)	-76.270 965	0.9618	104.49
Expt		0.9578	104.5

[a]Total energies in hartree, bond lengths in angstroms, and bond angles in degrees.

SF-CIS using the $^3B_1$ reference greatly overestimates the bond angle (107.7° versus 104.5° experimentally). The SC-SF-CIS method reduces this error, giving bond angles of 106.1° and 106.6° using singlet and triplet orbitals, respectively. If one employs the $^3A_1$ reference, which is more appropriate for the type of bond breaking reactions targeted by the SF approach, then much more reasonable bond angles are obtained (104.6° and 103.9°), although now the bond length is somewhat overestimated (by 0.005 or 0.022 Å). The SC-SF-CIS wave function for this case requires 78 determinants, compared to 24 determinants for SF-CIS; both of these CI spaces are very small. More

complete SF models such as SF-CIS(D) and SF-OD yield results for the $^3B_1$ reference which are in good agreement with experiment or with conventional correlated single-reference methods such as second-order Møller–Plesset perturbation theory (MP2) or coupled-cluster singles and doubles (CCSD).

HF

The spin-flip approach seeks to address bond-breaking processes. We have considered bond breaking in the HF molecule using a 6-31G basis, for which an exact treatment of electron correlation is readily accessible via full CI and for which previous SF results have been reported [52]. Total electronic energies at various bond lengths are provided in Table 4, and potential energy curves are displayed in Figure 4. For HF, both the bonding and anti-bonding orbitals are of σ symmetry, so we have used a $^3\Sigma$ reference (in the SF language) as in previous SF studies. We note that this is the lowest-lying triplet state only at stretched geometries, and not at equilibrium, where the lowest triplet is of $^3\Pi$ symmetry.

Table 4. Total energies (hartree) for HF dissociation using a 6-31G basis set.[a]

R_{HF}(Å)	SC-SF-CIS (singlet orbs)	SC-SF-CIS (triplet orbs)	SF-CIS	FCI
0.7	-99.892 219	-99.869 146	-99.837 26	-100.005 489
0.8	-99.973 916	-99.960 823	-99.929 34	-100.087 139
0.9	-100.003 583	-99.999 269	-99.968 11	-100.114 251
0.95	-100.008 009	-100.006 798	-99.975 88	-100.116 698
1.0	-100.008 182	-100.009 077	-99.978 53	-100.114 621
1.1	-100.000 391	-100.003 006	-99.973 78	-100.102 115
1.2	-99.986 493	-99.988 806	-99.961 64	-100.083 938
1.2764	-99.973 972	-99.975 479	-99.950 30	-100.068 708
1.4	-99.952 807	-99.952 850	-99.931 42	-100.044 285
1.6	-99.921 562	-99.919 569	-99.904 71	-100.009 752
1.8	-99.897 433	-99.894 624	-99.885 55	-99.984 078
2.0	-99.881 084	-99.878 602	-99.873 48	-99.967 201
2.1	-99.875 386	-99.873 358	-99.869 48	-99.961 487
2.2	-99.870 987	-99.869 509	-99.866 50	-99.957 183
2.4	-99.865 079	-99.864 751	-99.862 71	-99.951 656
2.6	-99.861 685	-99.862 361	-99.860 74	-99.948 741
2.8	-99.859 712	-99.861 174	-99.859 79	-99.947 238
3.0	-99.858 528	-99.860 578	-99.859 39	-99.946 465
3.2	-99.857 792	-99.860 272	-99.859 23	-99.946 065
3.4	-99.857 331	-99.860 111	-99.859 16	-99.945 857

[a]SF models employ a $^3\sum$ reference .

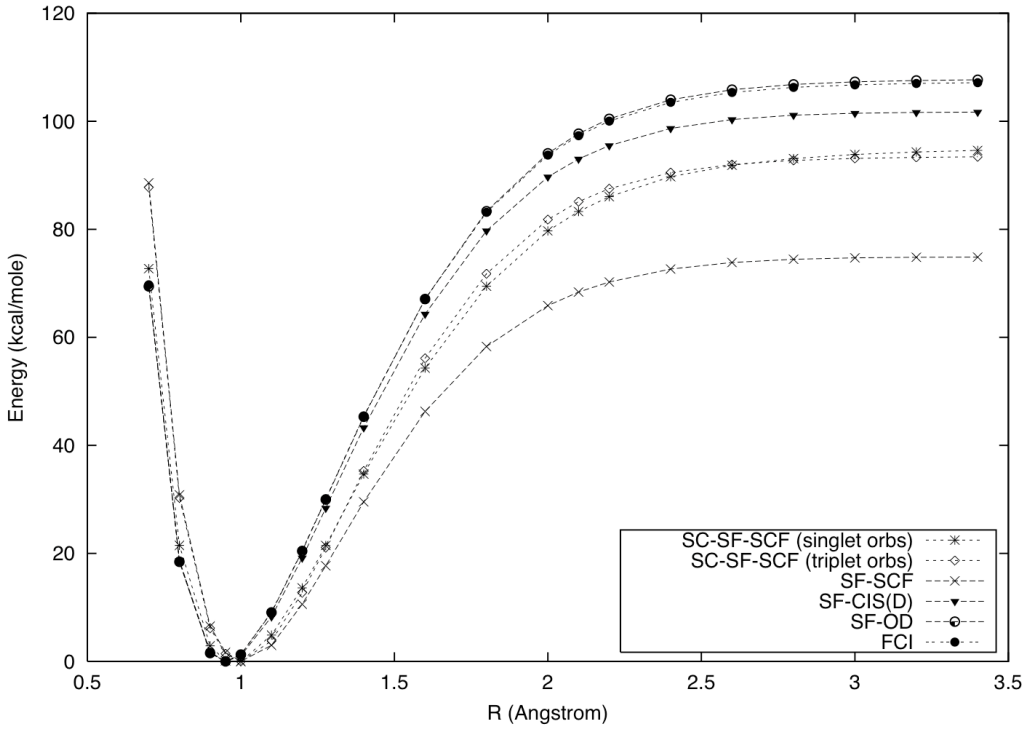

Figure 4. Potential energy curves for HF using a 6-31G basis set. The minimum energy at each level of theory has been set to zero.

Figure 4 makes it clear that the spin-complete SC-SF-CIS is a dramatic improvement over SF-CIS; the error in the well depth compared to full CI is reduced by more than $2/3$. Figure 5 displays errors versus full CI as a function of bond length. A perfectly flat error curve would indicate a potential energy curve parallel to the full CI curve, and molecular properties predicted from such a curve would be identical to the full CI results. The errors for SC-SF-CIS are generally flat past about 1.5 Å, but become larger at shorter distances. This reflects the increased importance of dynamical electron correlation - almost totally absent in SF-CIS or SC-SF-CIS - when the nuclei are closer

together. As expected, triplet orbitals yield slightly lower SC-SF-CIS energies at large distances, while singlet orbitals perform better around equilibrium. Overall, the singlet orbitals give a potential energy curve which is more parallel to full CI.

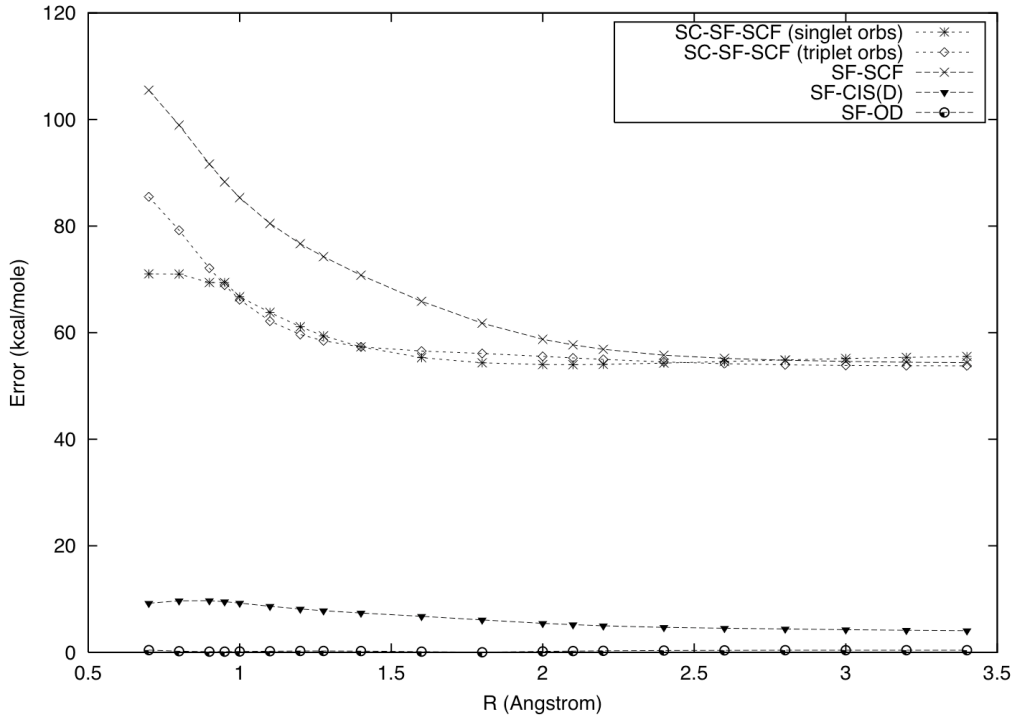

Figure 5. Error vs FCI for HF using a 6-31G basis set.

As seen in the figures, the SF-CIS(D) method eliminates the vast majority of the error in SF-CIS by including an approximate, perturbative treatment of dynamical correlation. The SF-CIS(D) error curve in Figure 5 is nearly flat. Since SC-SF-CIS is a much better wave function than SF-CIS, we anticipate that perturbative corrections for dynamical correlation as in SF-CIS(D) should provide excellent results across the entire potential energy surface at modest computational cost.

F_2

F_2 is a particularly challenging problem for electronic structure theory due to strong dynamical and nondynamical correlation effects. Indeed, it is unbound at the UHF level of theory. Here we examine bond breaking in F_2 using the DZP+ basis set of Ref. [76], which is the standard Huzinaga–Dunning [77, 78] double-ζ set with the most diffuse p function uncontracted and augmented by six Cartesian d functions $\left[\alpha_d(\mathrm{F}) = 1.580\right]$. Potential energy curves for SF-CIS and SC-SF-CIS are displayed in Figure 6 and compared to previously published curves using SF-CIS(D) [54], CASSCF [76] (which is identical to valence optimized orbital coupled-cluster doubles, or VOO-CCD, in this particular case), multireference CISD (MRCISD) [76], and VOO-CCD(2) [68]. Table 5 presents total energies, equilibrium geometries, dissociation energies, and harmonic vibrational frequencies for F_2 predicted by several theoretical methods.

Table 5. Equilibrium distances, dissociation energies, and harmonic vibrational frequencies for F_2 molecule using a DZP+ basis set.[a]

Method	R_e	D_e	ω_e	E_{tot}
SC-SF-CIS(singlet orbs)	1.469	1.29	826.44	-198.851 06
SC-SF-CIS(triplet orbs)	1.448	1.37	855.94	-198.858 07
SF-CIS	1.567	0.28	468	-198.801 57
SF-CIS(D)	1.429	1.14	824	-198.195 42
SF-OD	1.437	1.24	831	-199.223 16
RHF	1.332	10.69	1254	
RHF-CCSD	1.410	2.36	945	
UHF-CCSD	1.410	0.95	1006[b]	
VOO-CCD(2)	1.417	1.51	899[b]	-199.205 71
MR-CISD	1.435	1.22	821	
Expt.	1.412	1.66	916.64	

[a]SF models employ a $^3\Sigma_u$ reference. Total energies are in hartree, dissociation energies are in eV, bond lengths are in Å, and vibrational frequencies are in cm^{-1}. D_e was computed as the energy difference at R_e and R_{FF}=100 bohr.
[b]This work.

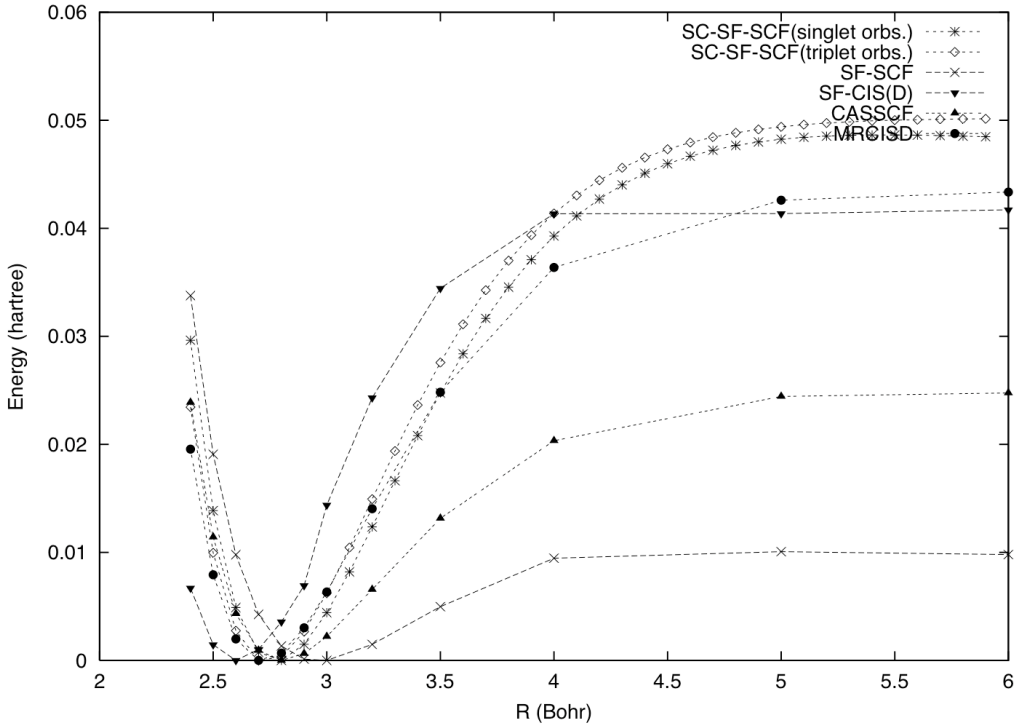

Figure 6. Potential energy curves for F_2 using a DZP+ basis set. The minimum energy at each level has been set to zero.

We observe that even the full valence CASSCF, which should properly describe nondynamical correlation, underestimates the more reliable VOO-CCD(2) dissociation energy by more than a factor of 2. Likewise, SF-CIS provides rather poor results for this case, obtaining just 17% of the experimental dissociation energy and just 19% of the VOOCCD(2) result, which is probably the most reliable of the theoretical values considered here. Just by adding the missing spin complements, SC-SF-CIS comes much closer to matching the VOO-CCD(2) curve and obtains 83% of the experimental dissociation energy and 91% of the VOO-CCD(2) predicted dissociation energy. Singlet and triplet orbitals perform similarly, the latter being slightly closer to VOO-CCD(2) at large distances. The SF-CIS(D) method, while greatly improving upon SF-CIS,

nevertheless gives a curve rather different than VOO-CCD(2). Given that SC-SF-CIS is a much better starting point, we expect that SC-SF-CIS(D) results would agree well with VOO-CCD(2).

The very large error in the SF-CIS bond length (more than 0.15 Å) is reduced to less than 0.06 Å in SC-SF-CIS. Likewise, the dissociation energy of 0.28 eV predicted by SF-CIS is greatly improved by SC-SF-CIS (1.3-1.4 eV depending on orbital choice) when compared to the VOO-CCD(2) result of 1.51 eV or the experimental value of 1.66 eV. Note that similar improvement is achieved in frequencies. The SF-CIS underestimates experimental frequencies [or accurate theoretical frequencies, such as the RHF-CCSD or VOO-CCD(2) ones] by almost a factor of 2. The SC-SF-CIS frequencies are much better, and are surprisingly close to the SF-CIS(D) and the SF-OD ones. It is also surprising that, when comparing to the experimental frequency, only the RHF-CCSD model outperforms the vibrational frequencies computed by the SC-SF-CIS model with triplet orbitals for this unusually challenging case. Furthermore, note that the simple SC-SF-CIS method gives better dissociation energies than even coupled-cluster singles and doubles, CCSD, using either a RHF or UHF reference. Only SF or multireference methods which include dynamical correlation [i.e., SFCIS(D), SF-OD, VOO-CCD(2), or MRCISD] approach the quality of the simple SC-SF-CIS predictions of the dissociation energy, and for this basis set only VOO-CCD(2) is closer to experiment.

C_2H_4

For a different type of bond breaking, we consider the rotation about the C–C bond in ethylene, which requires the breaking of a π bond. This is a challenging test case for theory, since traditional single-reference methods yield an unphysical cusp in the

torsional potential at 90°. The torsional potential has been calculated by freezing all degrees of freedom except the torsional angle, and the DZP basis and geometrical parameters used here match those in previous work [79]. Total energies are presented in Table 6, and Figure 7 plots the torsional potentials at each level of theory. Figure 8 displays these potentials near the barrier. We compare SC-SF-CIS with three different choices of orbitals (singlet, triplet, and TCSCF orbitals) to SF-CIS, CASSCF, SF-CIS(D), SF-OD, and TCSCF-CISD. The most reliable results currently available are from the TCSCF-CISD method, which generates all single and double excitations out of the two determinants [$(\pi)^2$ and $(\pi*)^2$] in the TCSCF reference. However, since SC-SF-CIS does not include substantial dynamical correlation, we cannot hope to match the TCSCF-CISD results. Instead, a more direct comparison is to a method with a reliable treatment of nondynamical correlation, such as CASSCF.

Table 6. Total energies (hartree) for the ethylene torsional potential using a DZP basis. Unoptimized barrier height, ΔE=E(90°)-E(0°), is also shown.[a]

Angle (deg)	SC-SF-CIS (singlet orbs)	SC-SF-CIS (triplet orbs)	SC-SF-CIS (TCSCF orbs)	SF-CIS	SF-CIS(D)	SF-OD	TCSCF-CISD
0	-78.097 12	-78.105 83	-78.113 87	-78.068 70	-78.346 37	-78.388 38	-78.365 89
15	-78.091 95	-78.100 87	-78.109 09	-78.064 26	-78.341 98	-78.383 93	-78.361 43
30	-78.077 25	-78.086 36	-78.094 85	-78.051 09	-78.328 77	-78.370 69	-78.348 12
45	-78.054 42	-78.063 22	-78.071 49	-78.029 85	-78.306 99	-78.349 08	-78.326 34
60	-78.025 26	-78.033 14	-78.039 95	-78.002 60	-78.277 90	-78.320 31	-78.297 24
75	-77.994 50	-78.000 65	-78.003 90	-77.974 93	-78.246 19	-78.288 27	-78.264 71
80	-77.986 11	-77.991 50	-77.993 22	-77.967 81	-78.237 41	-78.278 95	-78.255 22
85	-77.980 29	-77.984 99	-77.985 46	-77.963 01	-78.231 29	-78.272 18	-78.248 33
90	-77.978 21	-77.982 17	-77.982 55	-77.961 31	-78.229 07	-78.269 64	-78.245 74
ΔE(eV)	3.24	3.36	3.57	2.92	3.19	3.23	3.27

[a]Geometry used: r_{CC}=1.330 Å, r_{CH}=1.076 Å, α_{HCH}=116.6°. ΔE for RHF, OD, VOD(2), and CASSCF methods are 4.76, 3.91, 3.43, and 3.40 eV, respectively.

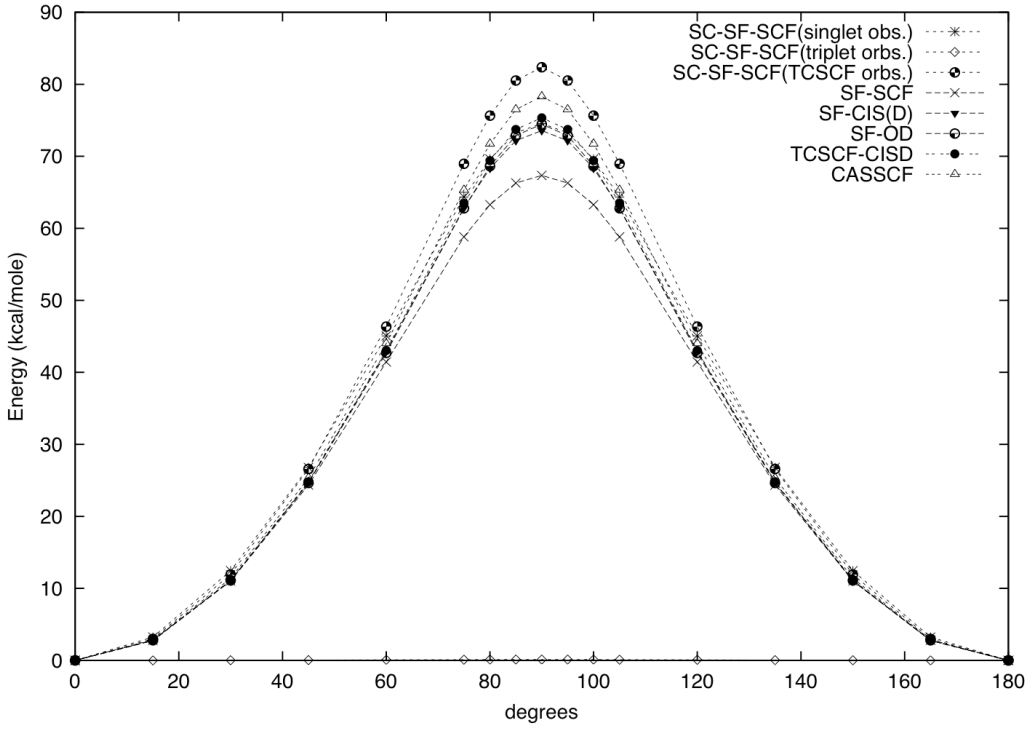

Figure 7. Potential energy curves for ethylene using a DZP basis set. The minimum energy at each level of theory has been set to zero.

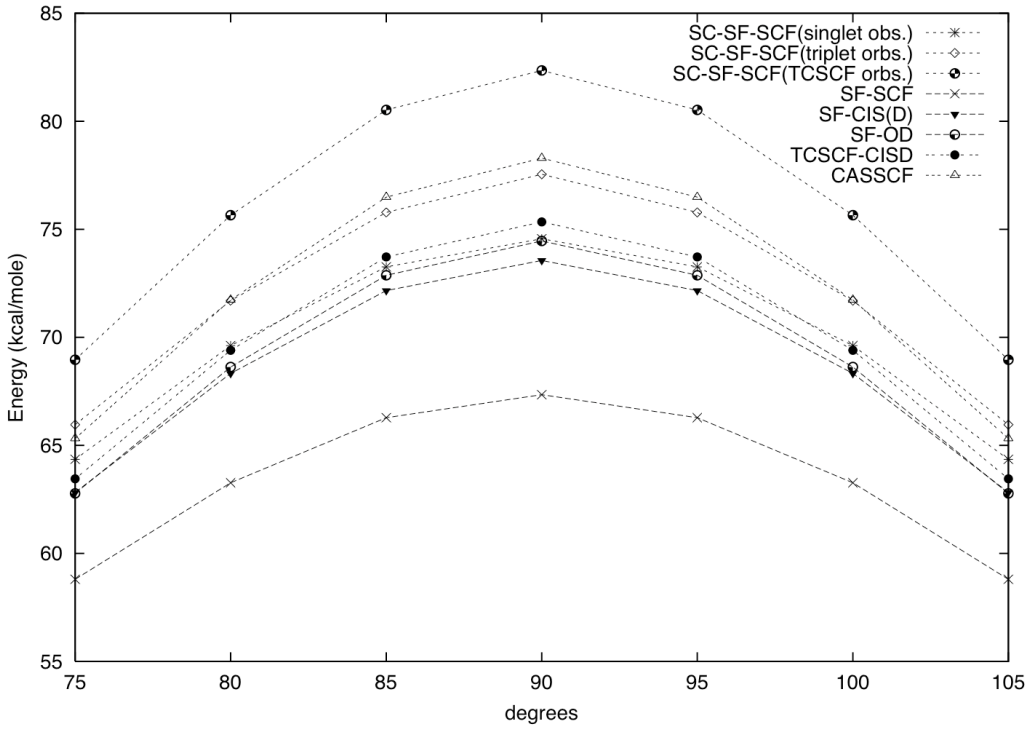

Figure 8. Potential energy curves for ethylene using a DZP basis set near 90°. The minimum energy at each level of theory has been set to zero.

The choice of orbitals in the SC-SF-CIS procedure is clearly important; we observe large differences (several kcal mol^{-1}) in energies depending on which orbitals are used. For mimicking the behavior of CASSCF, SC-SF-CIS with triplet orbitals is best, with very small differences from CASSCF (the difference in the barrier height is just 0.8 kcal mol^{-1}). SC-SF-CIS with singlet orbitals underestimates the CASSCF barrier height by about 3.7 kcal mol^{-1}, and SC-SF-CIS with TCSCF orbitals overestimates the barrier height by about the same amount (4.1 kcal mol^{-1}). The use of singlet orbitals makes SC-SF-CIS fortuitously close to the much more complete TCSCF-CISD treatment. It is perhaps surprising that the TCSCF orbitals, which are optimal for both of the important configurations at 90°, do not give better results. However, Table 6 makes it clear that the

overestimation of the barrier height is actually due to an improved treatment of the untwisted ethylene at 0°; it appears that the TCSCF orbitals allow SC-SF-CIS to recover a small part of the dynamic correlation near 0°, while they are about the same as triplet orbitals in describing the nondynamical correlation at 90°. Whether singlet, triplet, or TCSCF orbitals are used, the SC-SF-CIS results are significantly improved over SF-CIS in matching the CASSCF curve.

Trimethylenemethane (TMM)

A molecule with a broken bond has two unpaired electrons and can be loosely called a diradical [80]. More rigorously, Salem defines diradicals as molecules in which two electrons occupy two (near)-degenerate orbitals [80]. Due to large nondynamical correlation effects, this is a difficult situation that is well described by the SF approach due to the balanced treatment of the four nearly degenerate configurations needed to describe low-lying diradical states [56].

To investigate this application of the SF method, SC-SF-CIS has been used to predict the lowest energy levels of TMM. The planar ground state $\left({}^3A_2'\right)$ of TMM is of D_{3h} symmetry. The largest Abelian subgroup of $D_{3h}\left(C_{2v}\right)$ is used for computational purposes. The ${}^3B_2$ (C_{2v} symmetry label) reference is used in the conventional SF terminology. The SC-SF-CI ground state total energy and vertical excitation energies for the lowest excited states have been obtained in the same geometry and DZP basis set used in previous studies (see Table 7, which employs the C_{2v} symmetry labels for excited states). The SC-SF-CIS results are compared to a hierarchy of traditional SF methods.

Table 7. Ground state total energies (hartree) and excitation energies (eV) for TMM using a DZP basis set.[a]

Method	$^3A_2'$	$^1A_1$	$^1B_2$	$2\,^1A_1$	$^3A_1$	$^3B_2$	$^5B_2$
SC-SF-CIS (singlet orbs)	-154.937 82	1.951	1.529	5.651	6.475	5.899	7.750
SC-SF-CIS (triplet orbs)	-154.937 03	1.376	1.372	5.263	6.105	5.123	6.889
SF-CIS	-154.905 53	1.154	1.154	6.627	8.428	8.428	5.712
SF-CIS(D)	-155.435 85	1.160	1.160	3.821	6.018	6.018	6.729
SF-OD	-155.514 14	1.198	1.198	4.000	5.941	5.941	7.221

[a]SF-DFT/6-31G* optimized geometries.

The most accurate vertical excitation energies are those calculated by SF-OD. Unexpectedly, the SC-SF-CIS actually does worse than SF-CIS for the lowest singlet states. This is probably due to the surprisingly good performance of SF-CIS for these states. The SF-CIS error for these states is 0.044 eV. A maximum error of 0.753 eV is obtained for these states using the SC-SF method. As previously mentioned, errors of an electron volt or more are common for CIS. Thus, these results are surprisingly good for a method that contains primarily single excitations. The benefits of the SC-SF-CIS method become noticeable, however, when one considers the higher excited states of TMM. Errors in the vertical excitation energies range from 1.5 to 2.6 eV for conventional SF-CIS, while the errors in SC-SF-CIS never exceed 1.7 eV and are typically around 0.5 eV for all states except the second A_1 state. Apparently, the SC-SF approach offers a more balanced treatment of all of the low-lying excited states.

As for other test cases, the perturbative corrections to SF as in SF-CIS(D) greatly correct the errors of SF-CIS. Indeed, SF-CIS(D) reduces the errors in vertical excitation energies to less than 0.492 eV for TMM. We anticipate that SC-SF-CIS(D) will offer even better results for such systems.

Conclusions

Employing spin eigenfunctions significantly improves the quality of the SF-CIS results for the single bond breaking processes and excited states. Indeed, the SC-SF-CIS method eliminates spin-contamination and recovers over 50% of the error in the SF-CIS dissociation energies. Formally, spin-completeness is achieved by adding a selected subset of doubly and triply spin-orbital excited (with respect to the SF reference) determinants. Although the number of determinants increases, the scaling of the number of determinants comprising the SC-SF-CIS determinantal space is the same as in SF-CIS, i.e., $\mathrm{O}(OV)$ as opposed to the $\mathrm{O}\left(O^2V^2\right)$ scaling of the size of the SF-CISD subspace.

Results are not dramatically different for different choices of orbitals. This implies that the excellent performance of the SF approach is due to the determinants included in the wave function and not the orbital choice. The determinants that represent single SF excitations from the triplet reference, including their spin complements, are important in describing the changes that take place when bonds are stretched from equilibrium. Further investigations into the importance of various classes of determinants for describing stretched geometries are under way. In cases where the SF-CIS method works only qualitatively (e.g., F_2), the SF-CIS(D) approach was very close to the more computationally expensive benchmark results. It is anticipated that perturbative corrections to the improved zeroth-order reference will offer even better results than SF-CIS(D) at equivalent computational costs.

While the SF-CIS and SC-SF-CIS approaches do provide reliable starting points for addressing the bond-breaking problem, in as much as they both include the leading determinants necessary for a qualitatively correct description of the potential energy surface, such approaches have merely skirted around the inherent multireference nature

of the system. In doing so, much of the general applicability of these approaches is lost. For instance, the application of the SF- and SC-SF methods has been limited to breaking at most a single bond (as well as diradicals which can be considered as molecules with a single broken bond)[52-56, 59, 62-66, 69]. The problem is that, while the SF methodology can hypothetically be applied to breaking multiple bonds (this can be accomplished using a reference state of higher spin multiplicity [52]), the target states will require increasingly higher levels of excitation in the SF operator. For example, the description of the low-spin ($M_s = 0$) target state requires the inclusion of all singly-excited determinants, all singly- and doubly-excited determinants, and all singly-, doubly-, and triply-excited determinants to describe the breaking of single, double, and triple bonds respectively. Many of these determinants will contribute very little to the leading (zeroth order) description of the electronic structure. Thus, while the SF and SC-SF methodologies provide inexpensive approaches for the breaking of single bonds in large molecular systems, such approaches will not be applicable as the number of stretched bonds increases. The SF and SC-SF approaches scale exponentially in the number of bonds being broken, losing general applicability beyond the breaking of a single bond. Furthermore, the inclusion of greater than double excitations in SF- and SC-SF theories [as would be required to describe the breaking of a triple bond or the simultaneous dissociation of three single bonds] introduces terms that violate the size-consistency of the method. This loss of generality is true of many "dressed" single-reference methods and is not limited to the SF approaches [81].

CHAPTER 4

TRUE MULTI-REFERENCE APPROACHES FOR BOND BREAKING

As mentioned above, the HF model provides the "best" single-determinant description of the electronic structure problem. However, as has been addressed for bond breaking and will be subsequently discussed for transition-metal catalysts, the single-reference approximation can often give rise to large errors from HF theory. While the dressed single-reference approaches (such as the SF and SC-SF models) can provide a reasonable starting point for describing the dissociation of both single and (technically) multiple bonds, such approaches are not capable of general application and have merely evaded the inherent multi-reference nature of the electronic structure. This section outlines "true" multi-reference methods that are capable of treating (in the reference space) all of the strong correlation effects present in the system.

The Multi-Configurational Self-Consistent Field Method

It was seen that, for the case of stretched H_2, two nearly degenerate determinants are required to obtain a qualitatively correct description of the potential energy surface. If one takes the reference space as a linear (CI) expansion of these two determinants, i.e. $|\Psi\rangle = C_0 \left|\sigma_g(\mathbf{r})^2\right\rangle + C_1 \left|\sigma_u(\mathbf{r})^2\right\rangle$, and optimizes both the orbital and CI coefficients (in a variational sense) one arrives at the multiconfigurational self-consistent-field (MCSCF) approach [33, 82]. The MCSCF expansion is not limited to two configurations as in this simple example; although many important phenomena can be well described by such a simple expansion when combined with corrections for dynamical electron correlation.

Indeed, the TCSCF-CISD (two-configuration self-consistent-field with CI singles and doubles for dynamical correlation) results for the torsional potential of ethylene are still considered the benchmark calculations for this particular system [79]. In the most general sense the MCSCF expansion (at least at convergence) takes on the form:

$$\left|\Psi_{MCSCF}\right\rangle = \left|\mathbf{C}\right\rangle = \sum_{I} C_I \left|I\right\rangle, \tag{3.8}$$

where I runs over all determinants included in the MCSCF expansion. By abandoning the single-reference approximation the MCSCF expansion can, in principle, provide a correct description of the dissociation process as well as a number of electronic states across the entire potential energy surface [82-85]. The MCSCF method can be viewed as an extension of the HF equations of Roothaan in which the single-reference restriction has been removed. However, while the MCSCF approach is considerably more robust than HF and post-HF approaches for systems with strong static correlation effects, the problems that are occasionally observed in the optimization of HF wave functions are significantly compounded in the MCSCF approach [34].

The optimization of the MCSCF wave function represents an extremely difficult computational problem, a problem that is somewhat disguised by the simple expansion in (3.8). In formal development the MCSCF expansion is typically written, without any loss of generality, in the form

$$\left|\Psi_{MCSCF}\right\rangle = \left|\boldsymbol{\kappa},\ \mathbf{C}\right\rangle = \exp\left(-\hat{\kappa}\right)\sum_{I} C_I \left|I\right\rangle, \tag{3.9}$$

where the vector $\left|\mathbf{C}\right\rangle$ is consistent with the definition from (3.8) and the vector $\left|\boldsymbol{\kappa}\right\rangle$ consists of the parameters for the orbital-rotation operator, $\exp\left(-\hat{\kappa}\right)$, found in (3.9), where:

$$\hat{\kappa} = \sum_{p>q} \kappa_{pq} \left(a_p^\dagger a_q - a_q^\dagger a_p \right). \tag{3.10}$$

The optimization of the MCSCF wave function consists of variationally solving for the vectors $|\mathbf{C}\rangle$ and $|\boldsymbol{\kappa}\rangle$, describing the CI expansion and the orbital-rotation operator respectively [34]. It should be noted that, in a typical iterative MCSCF optimization, the orbitals are rotated following each iteration such that $|\boldsymbol{\kappa}\rangle$ becomes $\mathbf{0}$. While this certainly has an impact on the coefficients in $|\mathbf{C}\rangle$, the resulting wave function is unchanged. That such a transformation even exists is a consequence of the redundancy of the MCSCF equations. Under certain circumstances described below, it is possible to easily remove some (although not all) of the redundancies in the working MCSCF equations. The combination of these redundant orbital rotations and the nonlinear nature of the optimization procedure gives rise to many difficulties in the optimization of general MCSCF wave functions. This has severely limited the size of general MCSCF expansions. This is why, as Roos has pointed out, 'The CASSCF model [which is a specific example of MCSCF] has not been developed for treating dynamical correlation effects, but to provide a good starting point for such studies'[86]. The accurate treatment of dynamical correlation effects requires the inclusion of a large number of determinants with small individual contributions to the exact wave function. Furthermore, as discussed by other authors, the convergence difficulties inherent to MCSCF wavefunctions has severely limited the routine application of multi-reference methods by non-specialists [34]. The principle requirement as well as the central difficulty in the application of the MCSCF method remains the selection of the "important" determinants included in the MCSCF CI expansion. The guiding principle is that the determinants required for

describing all relevant non-dynamical correlation effects should be included in the MCSCF expansion of the reference space. Although the active-space MCSCF approaches described below simplify the selection of important determinants, the general application of MCSCF methods remains primarily confined to specialists in multi-reference approaches.

Active-Space MCSCF Approaches

Early applications of MCSCF wave functions relied heavily upon chemical insight in the selection of the determinants included in the MCSCF expansion [82]. A more general approach, termed complete active-space self-consistent field (CASSCF) [51], has proven very popular for bond-breaking problems. CASSCF transforms the ambiguity of selecting a set of appropriate determinants into a problem of choosing an important subset of the molecular orbitals. The CASSCF approach optimizes the orbitals so as to minimize the energy of the CI expansion that includes all possible determinants which can be formed in the space of active orbitals. If the active space is chosen appropriately, the CASSCF wave function will necessarily contain the most important determinants in the reference. However, the active-space full CI expansion scales factorially with the size of the space and thus it is limited to rather small active spaces. The active space approaches can be extended to larger spaces than those accessible to CASSCF expansions by placing dividing the "active" orbitals in to multiple subspaces and placing restrictions upon the number of electrons allowed in each subspace. Such an approach is referred to as the restricted active-space SCF (RASSCF) approach [34, 36]. There is no theoretical limit upon the number of subspaces that can be employed in the

definition of a RASSCF wave function, although typical applications have been limited to three or four subspaces. General RASSCF definitions have been employed to construct advanced wave functions for particular applications [69, 87, 88]. The active-space approaches tranfer the ambiguity in selecting the important electronic configurations for the MCSCF expansion to that of choosing the important subset of molecular orbitals. Furthermore, the CASSCF and RASSCF expansions are invariant to rotations of orbitals within any subspace (or within the active space for CASSCF). This greatly facilitates the removal of redundant variational parameters (orbital rotations) from the MCSCF wave-function optimization, leading to typically smoother convergence than for general MCSCF expansions. Such effects have been extensively discussed elsewhere [34].

In order for CASSCF, as well as MRCI, MRPT and MRCC approaches based on a CASSCF reference, to be considered as a 'model chemistry' in Pople's sense [89], the ambiguity must be removed in the definition of the active orbitals. The fully optimized reaction space (FORS) introduced by Ruedenberg and co-workers [90-92] is one prescription for such a selection process. The FORS method employs a set of active orbitals that is equivalent to the valence shell atomic orbitals, i.e. (1 s) for hydrogen, (2s, $2p_x$, $2p_y$, $2p_z$) for first row atoms, etc. That is to say that the valence active space consists of one active space orbital of a given symmetry for each molecular orbital that can be formed from the valence orbitals of the atoms in the molecule. Such an active space has been employed by numerous authors [51, 93], having taken on the obvious title of a 'full-valence' or 'valence' active space. A second approach introduced by Ruedenberg and co-workers [82] and termed the 'extended independent-particle model' (EIPM) allows the same number of active spatial orbitals as there are electrons. This approach, when

combined with a neglect of the core correlation, has been applied by other authors [51, 93-96], sometimes under the more descriptive label of a 'one-to-one' active space.

Recently, Abrams and Sherrill compared the use of the valence and one-to-one active spaces for breaking bonds to hydrogen in several small molecules to the exact full configuration interaction results [93]. The conclusion of this work was that the larger of the two active spaces gives the best results across the entire potential energy surface. This is a disappointing result because the length of the CI expansion scales factorially with the number of active orbitals and electrons, so that large active spaces lead to dramatic increases in the computational cost of obtaining a CASSCF wavefunction. In addition, Dunning has argued that the larger, one-to-one active space is perhaps too large because it can be biased toward equilibrium geometries in some cases [97]. Large active spaces may also give rise to multiple solutions in wavefunction space that give nearly indistinguishable energies. The CASSCF equations form a highly nonlinear problem where the orbitals and CI expansion are solved for in an iterative fashion [34, 51, 98]. Although very robust optimization methods have been developed [98-100], it is not completely clear what impact the factorial scaling of the CAS reference will have on possible optimization problems as one begins extending the applications to larger systems. At the same time, however, it would be very desirable to use smaller active spaces if this could be accomplished without a great loss in accuracy. Pulay and Hamilton have suggested that UHF natural orbital occupation numbers serve as a good diagnostic for selecting active orbitals [101], and this approach may make it easier to eliminate all but the most important orbitals from the active space. However, this still requires the definition of numerical cut-offs and Pulay and Hamilton have pointed out that 'with rigid

thresholds on the occupation numbers, the active space can change suddenly, resulting in steps on the energy surface' [101]. In the remainder of this chapter, we examine a priori, threshold-free definitions of minimalist active spaces, analogous to the valence and one-to-one active space definitions [87].

Minimal Reference Spaces for Bond Breaking

For reactions breaking a covalent single bond, the most obvious minimal active space would simply be the relevant bonding and antibonding orbitals. For a double bond, the minimum number of active orbitals would be four, and so on. We consider reference wavefunctions including all determinants that can be formed in the active space (CASSCF) as well as some with restrictions on the allowed determinants (RASSCF) [102]. Full configuration interaction benchmark curves for the symmetric dissociation of H_2O and the dissociation of N_2 by Olsen and co-workers [96, 103], as well as new curves for breaking single bonds in HF and CH_4 recently obtained for a dense set of points by our group [104], allow us to systematically evaluate the performance of minimalist reference functions by comparison to the exact results for the given one-particle basis set.

Theoretical Approach

CASSCF wavefunctions were determined using the various active space choices defined below, and these reference functions and orbitals were then used in multi-reference perturbation theory and multi-reference CI computations of bond-breaking reactions in HF, CH_4, H_2O (both bonds) and N_2. Here we use the same cc-pVDZ basis sets for H_2O and N_2 as used in the full CI studies by Olsen and co-workers [96, 103] and the 6-31G** and 6-31G*basis sets for HF and CH_4 used in our previous full CI study

[104]. The potential energy curve for methane was obtained by constraining the three C-H bonds to the equilibrium bond length (1.086 Å) [105] and the HCH angles to the tetrahedral value while stretching a single C-H bond. The H_2O potential energy surface was obtained at the same geometries as in the previous work [96] by fixing the HOH angle and simultaneously stretching both O-H bonds.

For multi-reference perturbation theory, we tested CASPT2 [106] and CASPT3 [107], as implemented in MOLPRO [28]. For multi-reference CI, we tested the first-order and second-order CI wavefunctions (FOCI and SOCI), which include all single or all single and double substitutions out of the CASSCF determinants, respectively [108, 109]. MRCI computations were performed using MOLPRO excepting the larger computations for N_2, where we used the DETCAS and DETCI modules of PSI 3.2 [8].

Three active spaces were examined here: 1:1, valence and minimal. Again, for each bond to be broken, the minimal active space considered here contains only one bonding and one anti-bonding orbital of the appropriate symmetries. More specifically, the active spaces for the molecules in this study are as follows: HF 1:1= ($8e^-$/4022), val=($8e^-$/3011) and min=($2e^-$/2000); CH_4 1:1=val= ($8e^-$/62) and min=($2e^-$/20); H_2O 1:1=($8e^-$/4022), val=($8e^-$/3012) and min=($4e^-$/2002); and N_2 1:1=($10e^-$/30110311), val=($10e^-$/20110211) and min=$6e^-$/10110111). Here the notation indicates (number of active electrons/number of active orbitals per irreducible representation of the largest Abelian subgroup). For HF, CH_4, and H_2O one core orbital is always restricted to remain doubly occupied, corresponding to the 1s core orbitals of F, C and O respectively. For N_2 the two N core orbitals are always restricted to remain doubly occupied. For calculations using the minimal active space, all of the valence lone pair orbitals and the other three C–

H bonding orbitals for CH_4 are restricted to remain doubly occupied in the CASSCF reference. The CASSCF orbital optimizations were with a 'restricted core' meaning that all non-redundant orbital rotations were allowed. Additional restrictions on the CI space in the reference wavefunctions were considered, as described below.

Results and Discussion

Breaking Single Bonds

The CASSCF and MRCI potential energy curves for HF are displayed in Figure 9 and Figure 10. All of the multi-reference methods give qualitatively correct potential energy curves for HF or for any of the other test cases considered in this study. For this reason, we omit any further plots of the potential energy curves (which are available upon request from the authors). More instructive are plots of the error versus full CI for these systems. Plots of the errors for CASSCF, MRPT and MRCI for HF are given in Figure 11, Figure 12, and Figure 13 and analogous error plots for CH_4 are given in Figure 14, Figure 15, and Figure 16. The maximum, minimum and non-parallelity errors (NPEs) for HF and CH_4 are reported in Table 8 and Table 9, respectively. The NPE is calculated as the difference between the maximum and minimum error across the surface, giving a measure of how well the method mimics the FCI curve; a NPE of zero would imply that the calculated potential is exactly parallel to the FCI potential curve. It should be noted that, due to the finite number of points sampled on the surface, any computed NPE will be a lower bound to the actual NPE for the method.

Table 8. Maximum, minimum, and non-parallelity error (kcal mol^{-1}) for HF with a 6-31G* basis.

Method	Max error	Min error	NPE
CASSCF(1:1)	44.96(2.80)	40.13(0.70)	4.83
CASSCF(val)	104.10(0.95)	86.14(4.00)	17.96
CASSCF(min)	104.80(0.95)	86.14(4.00)	18.66
CASPT2(1:1)	3.84(1.40)	3.35(0.70)	0.49
CASPT2(val)	7.48(0.70)	4.70(2.40)	2.78
CASPT2(min)	4.75(0.70)	4.28(1.20)	0.47
CASPT3(1:1)	1.31(1.40)	0.83(0.70)	0.47
CASPT3(val)	4.82(0.70)	1.96(3.60)	2.87
CASPT3(min)	3.63(1.60)	1.86(4.00)	1.77
FOCI(1:1)	35.92(0.70)	22.17(4.00)	13.76
FOCI(val)	76.91(0.70)	73.72(1.20)	3.19
FOCI(min)	80.98(3.40)	78.60(1.00)	2.39
SOCI(1:1)	0.48(1.40)	0.44(4.00)	0.04
SOCI(val)	5.77(0.70)	2.57(3.40)	3.20
SOCI(min)	3.54(1.20)	2.56(4.00)	0.98

Table 9. Maximum, minimum, and non-parallelity error (kcal mol^{-1}) for CH4 with a 6-31G* basis.

Method	Max error	Min error	NPE
CASSCF(1:1=val)	51.91(0.70)	45.57(2.00)	6.33
CASSCF(min)	93.66(0.70)	84.42(4.00)	9.25
CASPT2(1:1=val)	7.59(0.80)	6.02(4.00)	1.57
CASPT2(min)	13.46(0.70)	12.24(2.80)	1.22
CASPT3(1:1=val)	2.10(1.00)	1.67(4.00)	0.43
CASPT3(min)	4.22(1.60)	3.67(4.00)	0.56
FOCI(1:1=val)	36.64(0.70)	24.43(2.60)	12.21
FOCI(min)	88.04(0.70)	78.32(1.80)	9.72
SOCI(1:1=val)	0.97(0.80)	0.67(2.20)	0.31
SOCI(min)	4.71(0.70)	4.11(4.00)	0.60

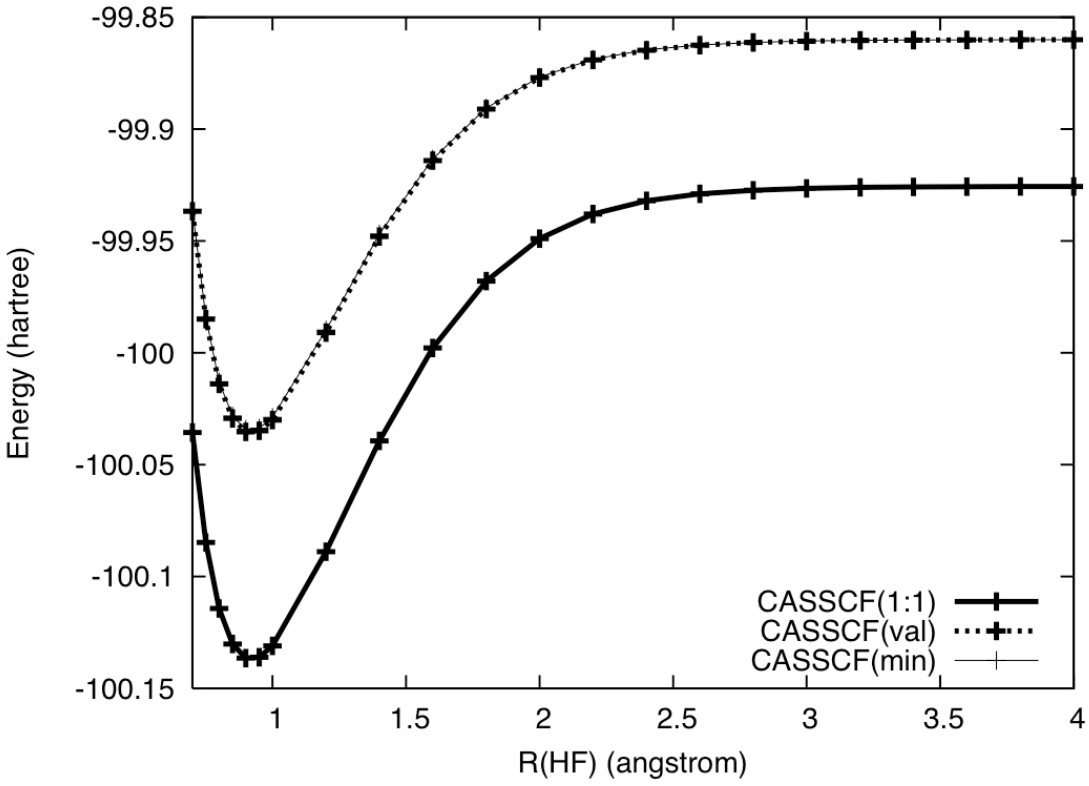

Figure 9. Total CASSCF energies for HF with a 6-31G*basis.

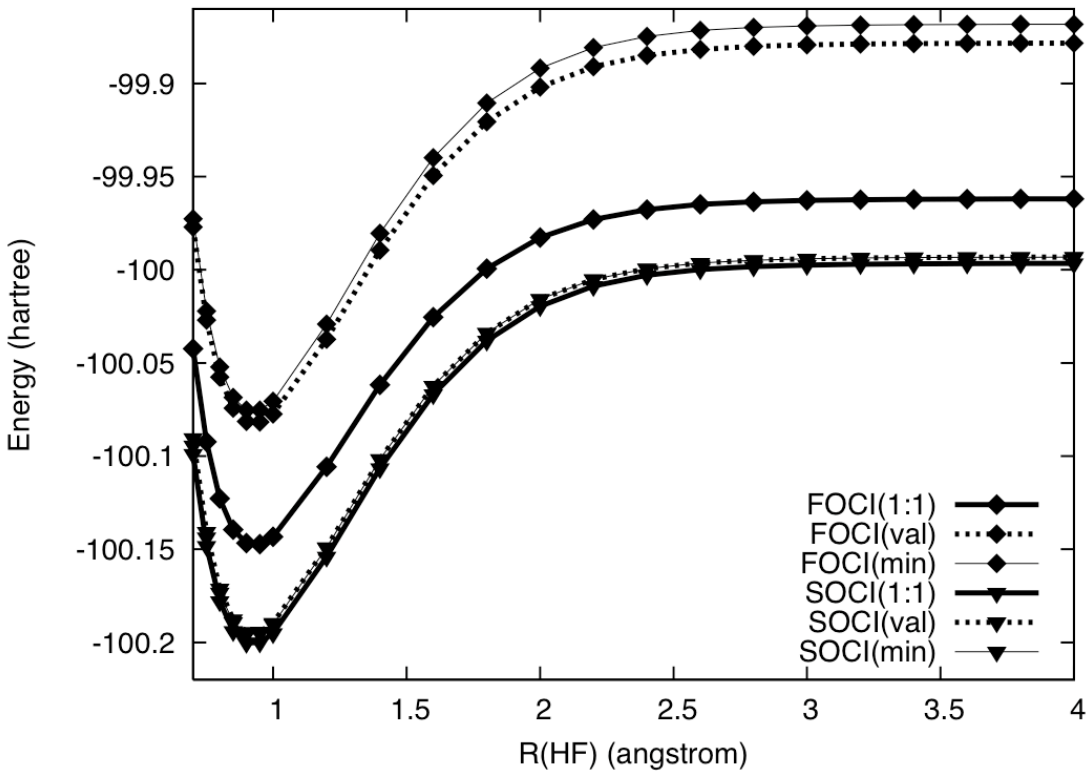

Figure 10. Total MRCI energies for HF with a 6-31G*basis.

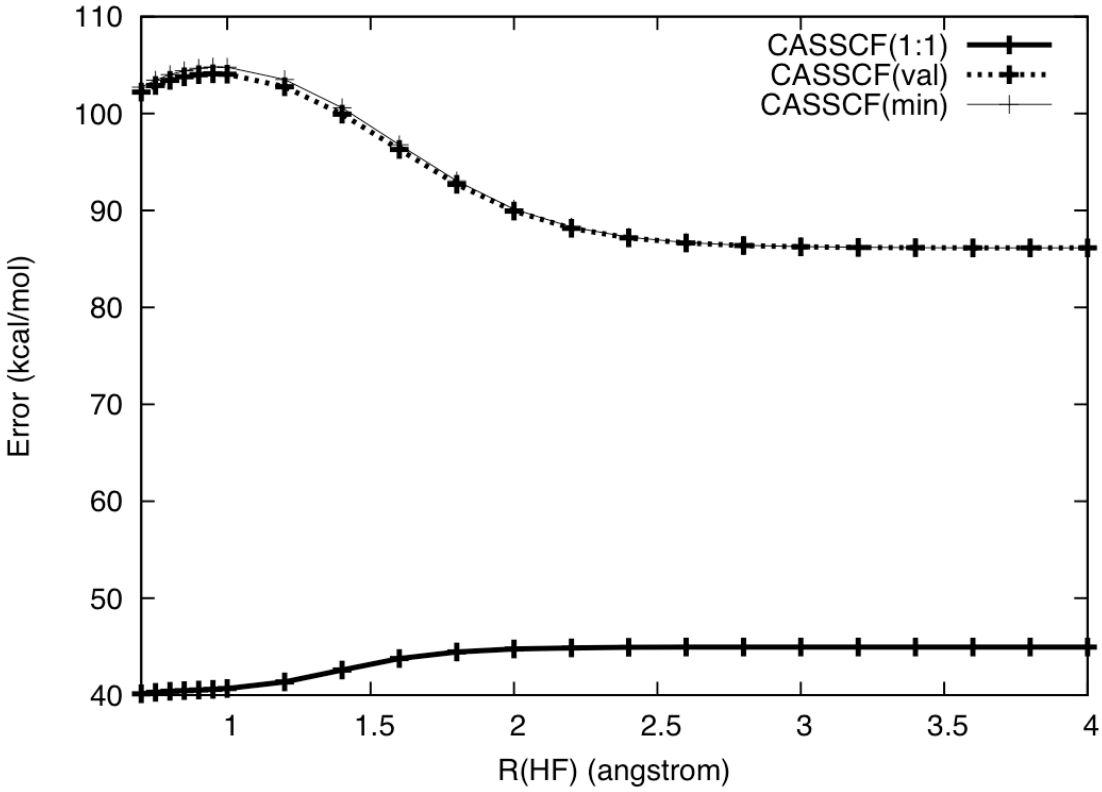

Figure 11. CASSCF errors vs. full CI for HF with a 6-31G*basis.

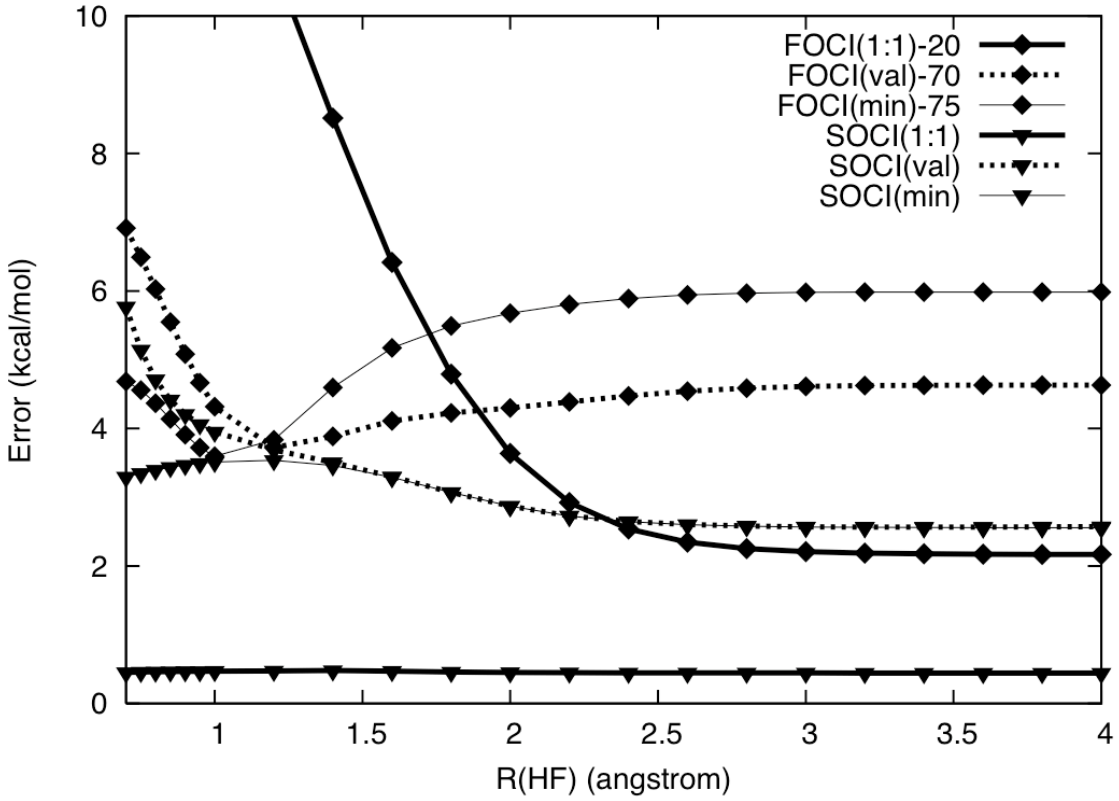

Figure 12. MRCI errors vs. full CI for HF with a 6-31G*basis.

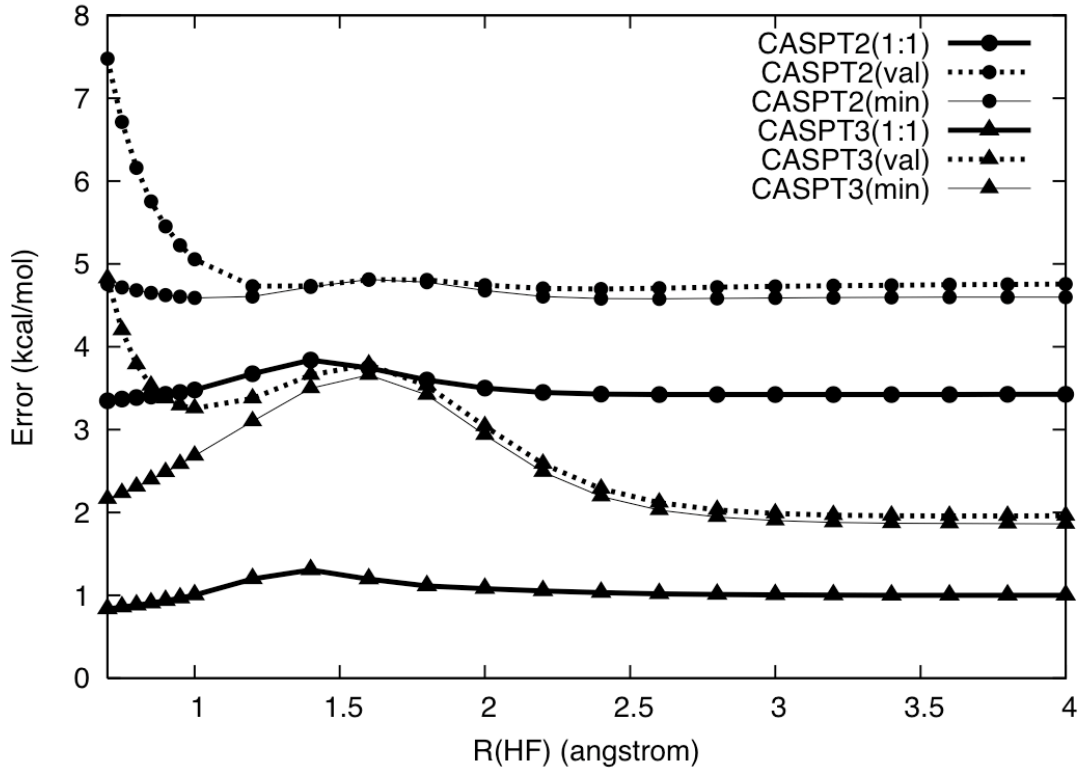

Figure 13. MRPT errors vs. full CI for HF with a 6-31G*basis.

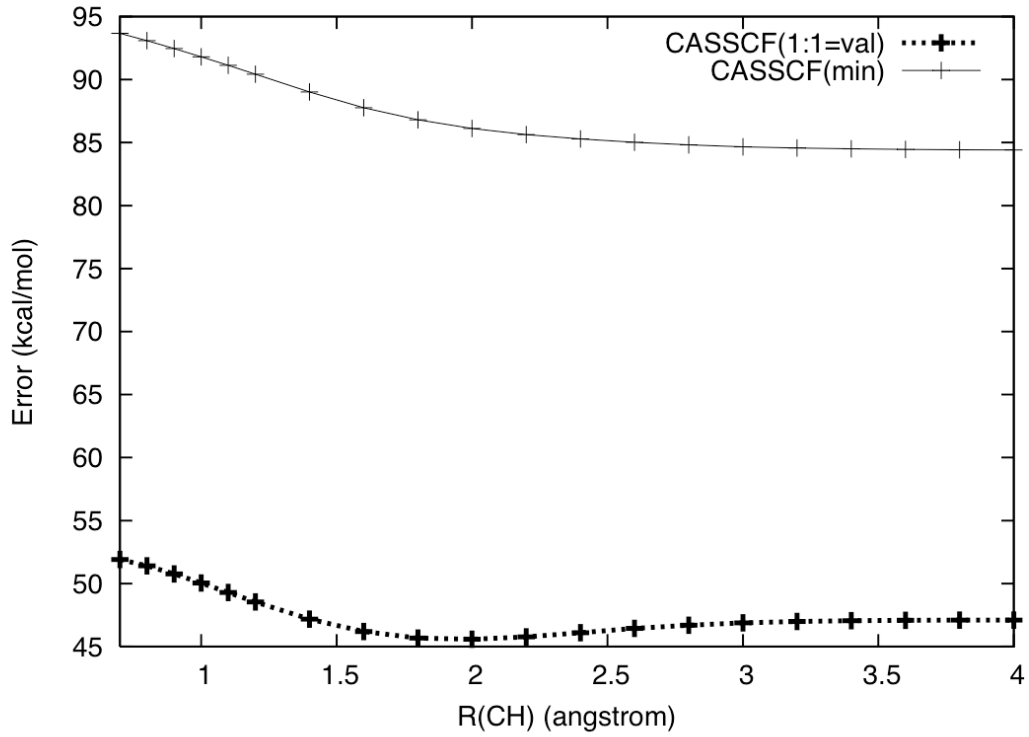

Figure 14. CASSCF errors vs. full CI for CH_4 with a 6-31G*basis.

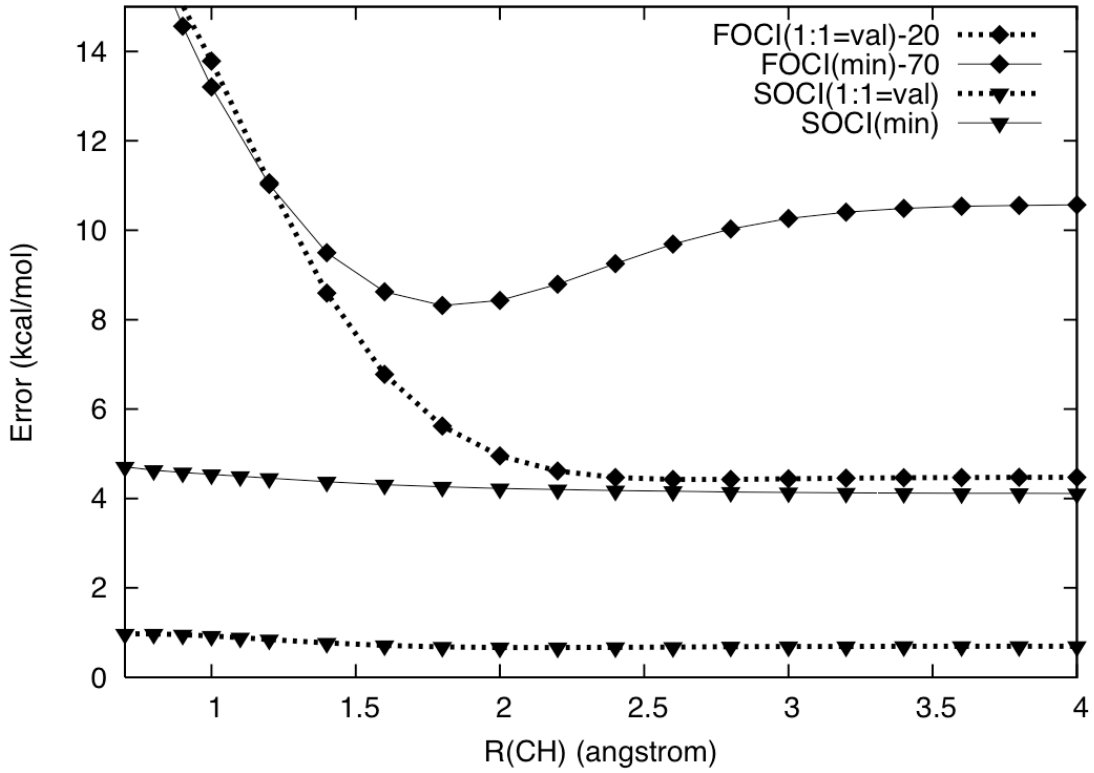

Figure 15. MRCI errors vs. full CI for CH_4 with a 6-31G*basis.

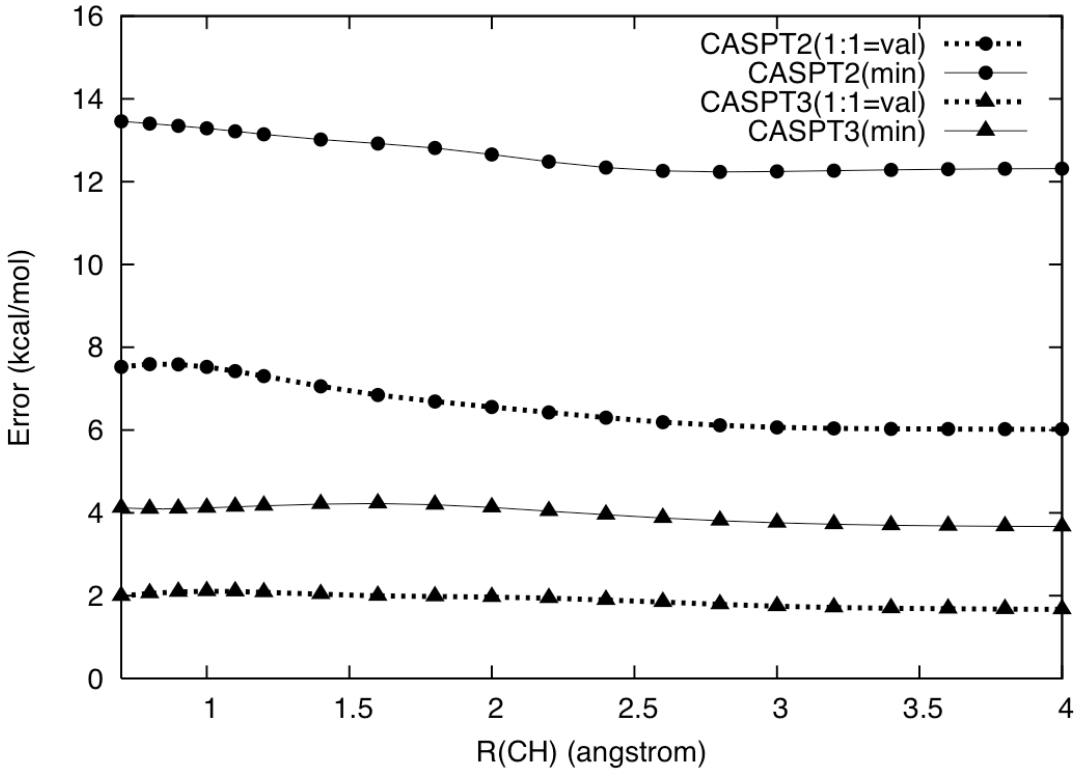

Figure 16. MRPT errors vs. full CI for CH_4 with a 6-31G*basis.

For HF, the valence active space and the minimal active space both have only one unoccupied active orbital, while the 1:1 active space is much larger. For CH_4, the valence and 1:1 active spaces are equivalent and both are significantly larger than the minimal active space. As seen in Figure 11 and Figure 14, CASSCF with the larger active spaces (1:1 for HF and valence/1:1 for CH_4) has much smaller errors than CASSCF with the smaller active spaces. For HF, the larger number of active occupied orbitals in the valence active space does not significantly improve over the minimal active space in CASSCF computations; the two CASSCF error curves are virtually identical in Figure 11. As indicated in Table 8 and Table 9, CASSCF non-parallelity errors are much smaller when the larger active spaces are used. We attribute the improved performance of larger active spaces at the CASSCF level to the partial inclusion of dynamical electron

correlation. Note that the largest errors for CASSCF tend to be at shorter distances, where dynamical electron correlation is the largest.

The first-order CI (FOCI) improves upon the CASSCF reference by adding single excitations into the virtual orbitals. This will add a very limited additional account of dynamical correlation through the inclusion of semi-internal double and higher-order excitations. As seen from Table 8 and Table 9, the absolute errors are significantly reduced from those of CASSCF, but they remain quite large. The error curves in Figure 12 and Figure 15 are shifted down to account for this. In both figures, the FOCI errors are rather flat for $R > 2.5\text{Å}$ for any of the three active spaces, but they rise rapidly as the distance is decreased, particularly for the 1:1 active space. This mimics the general trend for CASSCF; the lack of an explicit account of dynamical correlation leads to larger errors at shorter distances where the dynamical correlation is largest. It is perhaps surprising to note in Table 8 and Table 9 that the active spaces leading to the smallest errors for FOCI give the largest NPEs. Indeed, the FOCI NPEs are always bigger than the corresponding CASSCF NPEs, except in the case of the valence or minimal active spaces for HF, where the NPEs are quite small (3.19 and 2.39 kcal mol^{-1} respectively). The additional test cases of H_2O and N_2 below, indicate that FOCI gives NPEs somewhat improved or about the same as CASSCF except for large active spaces, when the NPEs can be larger than for CASSCF.

The remaining methods, CASPT2, CASPT3 and second-order CI (SOCI), all provide an explicit description of dynamical correlation by including at least double excitations in the virtual orbitals. With the exception of the minimal active space CASPT2

results for CH_4, all absolute errors are now below 10 kcal mol^{-1} and the NPEs are around 3 kcal mol^{-1} or less. The error curves for these methods, displayed in Figure 12, Figure 13, Figure 15, and Figure 16 are now quite flat with the exception of a rising error for decreasing *R* for HF with the valence active space. This anomalous behavior appears to be caused by an unphysical mixing between the fluorine core orbital and the fluorine lone pair of the same symmetry in the CASSCF; because the lone-pair orbital has an occupation number very close to 2, the CASSCF energy is nearly invariant to the mixing of this orbital with the core orbital. In subsequent frozen-core MRPT or MRCI computations, however, the energy is not invariant to such rotations. In support of this analysis, we find that MRCI NPEs are lower (and virtually identical) when: (1) the core orbital is frozen (not optimized) in the CASSCF procedure, or (2) the MRCI computation includes core correlation. For example, either of these changes drops the SOCI NPE from 3.20 to 0.90 kcal mol^{-1}. Further investigations of this effect in similar systems are underway. Excluding these valence active space results for HF, the NPEs for CASPT2, CASPT3 and SOCI are all below 2 kcal mol^{-1}.

It is very interesting to note that the minimal active space seems just as effective as the larger active spaces for the CASPT2 method, with NPEs for HF of 0.49 and 0.47 kcal mol^{-1} for the 1:1 and minimal active spaces, respectively. The corresponding values for CH_4 are 1.57 and 1.22 kcal mol^{-1}. For CASPT3, the larger active space is better, with NPEs for HF of 0.47 (1:1) and 1.77 kcal mol^{-1} (minimal) and for CH_4 of 0.43 (1:1=valence) and 0.56 kcal mol^{-1} (minimal). However, we also note that the CASPT3 method is not necessarily improved over CASPT2 for the HF molecule.

For the cases of HF and CH_4, SOCI with a minimal active space gives NPEs that are less than 0.98 kcal mol^{-1} as compared to 0.30 kcal mol^{-1} with the larger 1:1 active space. The smaller active space thus leads to only a modest increase in the error, but it affords great savings in computational cost. The final SOCI spaces for the minimal active space contain only about 3% of the determinants in the corresponding SOCI spaces employing the 1:1 reference. Additionally, the minimal CASSCF for HF and CH_4 respectively contain 33 and 75 variational parameters (CI coefficients plus non-redundant orbital rotations). In contrast, the 1:1 CASSCF for HF and CH_4 consist of 7142 and 2584 variational parameters. The minimal active space gives more than a 97% reduction in the number of variational parameters, which should significantly decrease the number of local minima in wavefunction space for this nonlinear optimization problem.

Breaking Multiple Bonds

The results from the previous section demonstrate the ability of a minimal active space reference to adequately recover the strong non-dynamical correlation effects for reactions breaking a single bond. However, one is often interested in describing multiple dissociation channels or the simultaneous breaking of multiple bonds. In these situations the non-dynamical correlation effects become much stronger, presenting an even greater challenge for the standard single-reference methods. Indeed, single-reference CCSD can suffer from non-variational collapse for reactions breaking multiple bonds. Here we consider the symmetric dissociation of H_2O and the dissociation of N_2, comparing results with the various active spaces to the exact FCI results of Olsen and co-workers [96, 103]. The multi-reference potential energy curves for H_2O and N_2, not included here, display

the correct general shape and are similar to those for HF presented in Figure 9 and Figure 10. Again, we present the more instructive plots of the error versus full CI, in Figure 17, Figure 18 , and Figure 19 for H_2O and Figure 20, Figure 21, and Figure 22 for N_2. Table 10 and Table 11 give the maximum errors, minimum errors and NPEs for H_2O and N_2, respectively.

Table 10. Maximum, minimum, and non-parallelity error (kcal mol^{-1}) for H_2O with a cc-pVDZ basis.

Method	Max error	Min error	NPE
CASSCF(1:1)	60.23(2.0R_e)	59.57(3.0R_e)	0.65
CASSCF(val)	102.94(1.0R_e)	78.16(3.0R_e)	24.78
CASSCF(min)	104.07(1.0R_e)	78.20(3.0R_e)	25.87
CASPT2(1:1)	7.11(1.5R_e)	5.28(3.0R_e)	1.83
CASPT2(val)	10.10(1.0R_e)	6.07(2.5R_e)	4.03
CASPT2(min)	9.81(1.0R_e)	6.27(2.0R_e)	3.55
CASPT3(1:1)	2.90(1.5R_e)	1.91(3.0R_e)	0.99
CASPT3(val)	4.14(1.0R_e)	1.85(3.0R_e)	2.30
CASPT3(min)	4.14(1.5R_e)	2.05(3.0R_e)	2.09
FOCI(1:1)	43.36(1.0R_e)	22.81(3.0R_e)	20.54
FOCI(val)	63.86(1.0R_e)	53.92(2.0R_e)	9.94
FOCI(min)	69.93(1.0R_e)	62.70(2.0R_e)	7.23
SOCI(1:1)	2.19(1.0R_e)	1.41(3.0R_e)	0.78
SOCI(val)	4.63(1.0R_e)	2.46(3.0R_e)	2.16
SOCI(min)	4.21(1.0R_e)	2.71(3.0R_e)	1.50

Table 11. Maximum, minimum, and non-parallelity error (kcal mol^{-1}) for N_2 with a cc-pVDZ basis.

Method	Max error	Min error	NPE
CASSCF(1:1)	104.39(1.9050)	81.46(0.7938)	22.93
CASSCF(val)	118.48(1.9050)	103.45(0.7938)	15.03
CASSCF(min)	124.05(1.5875)	109.46(0.7938)	14.59
CASPT2(1:1)	9.63(1.4288)	7.76(1.9050)	1.88
CASPT2(val)	11.76(0.9525)	8.20(1.9050)	3.56
CASPT2(min)	14.35(1.2700)	9.15(1.9050)	5.20
CASPT3(1:1)	4.69(1.7463)	2.46(0.7938)	2.23
CASPT3(val)	3.94(1.7463)	3.33(1.1113)	0.61
CASPT3(min)	4.88(1.5875)	3.33(0.7938)	1.55
FOCI(1:1)	44.40(0.9525)	35.89(1.7463)	8.51
FOCI(val)	62.57(0.7938)	54.21(1.7463)	8.36
FOCI(min)	75.92(0.9525)	60.94(1.9050)	14.98
SOCI(1:1)	2.50(1.9050)	1.75(0.7938)	0.75
SOCI(val)	4.18(0.7938)	3.47(1.2700)	0.72
SOCI(min)	4.54(1.7463)	3.68(0.7938)	0.86

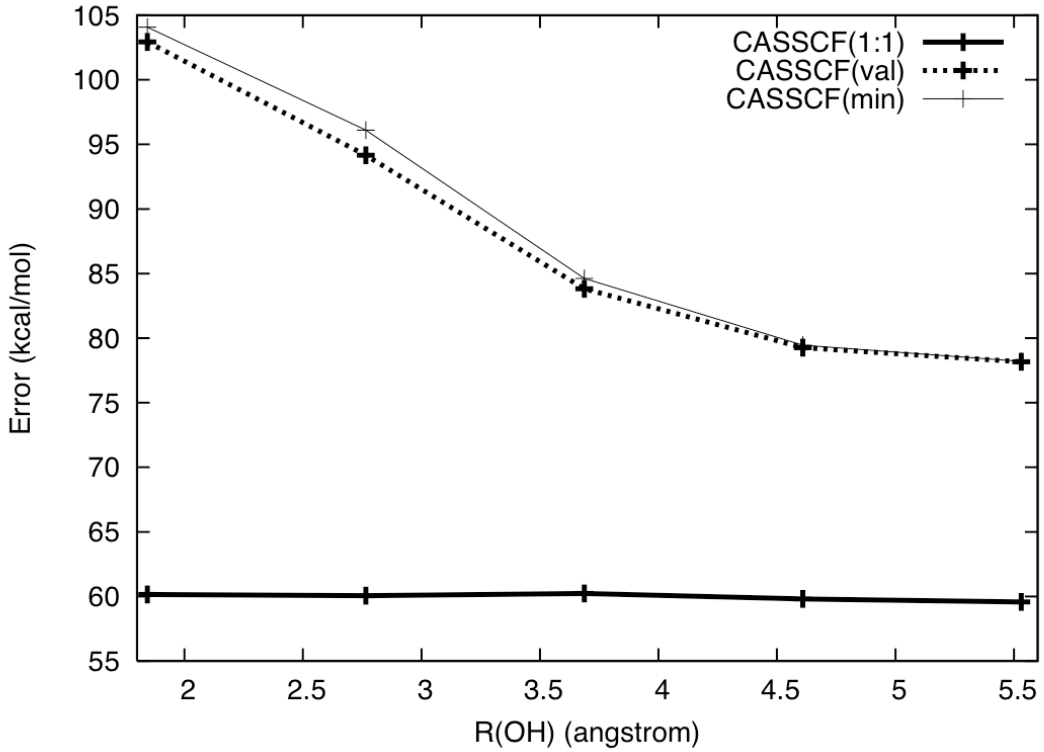

Figure 17. CASSCF errors vs. full CI for symmetric dissociation of H_2O with a cc-pVDZ basis.

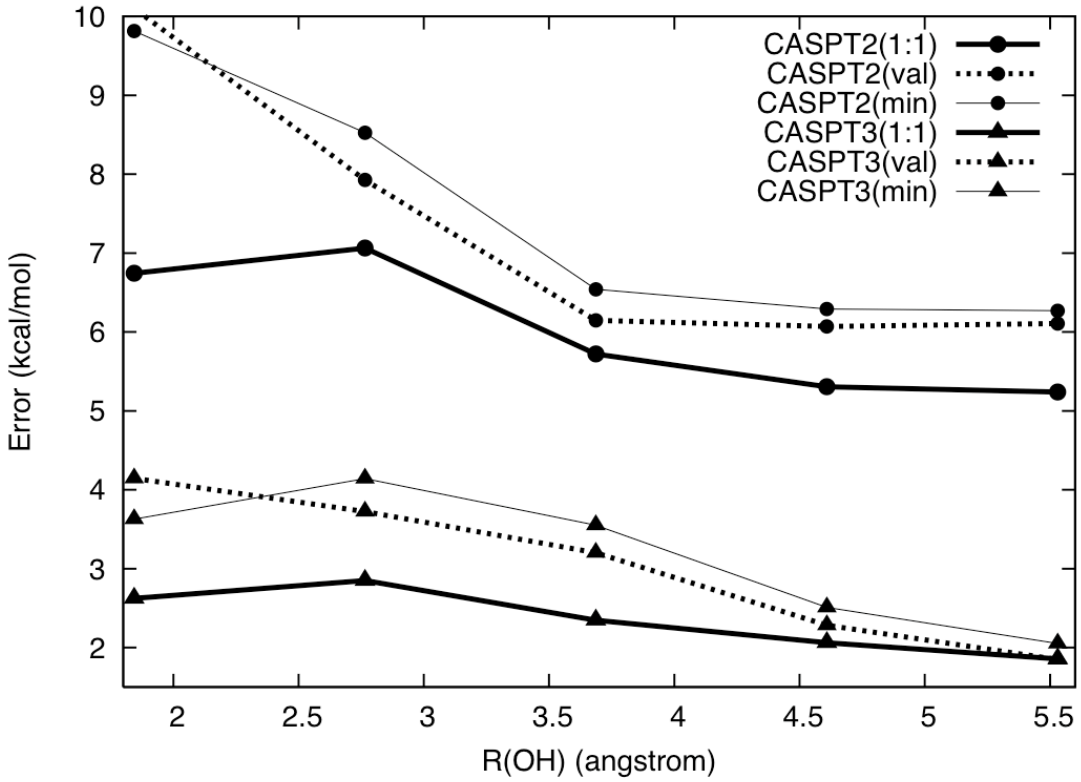

Figure 18. MRPT errors vs. full CI for symmetric dissociation of H_2O with a cc-pVDZ basis.

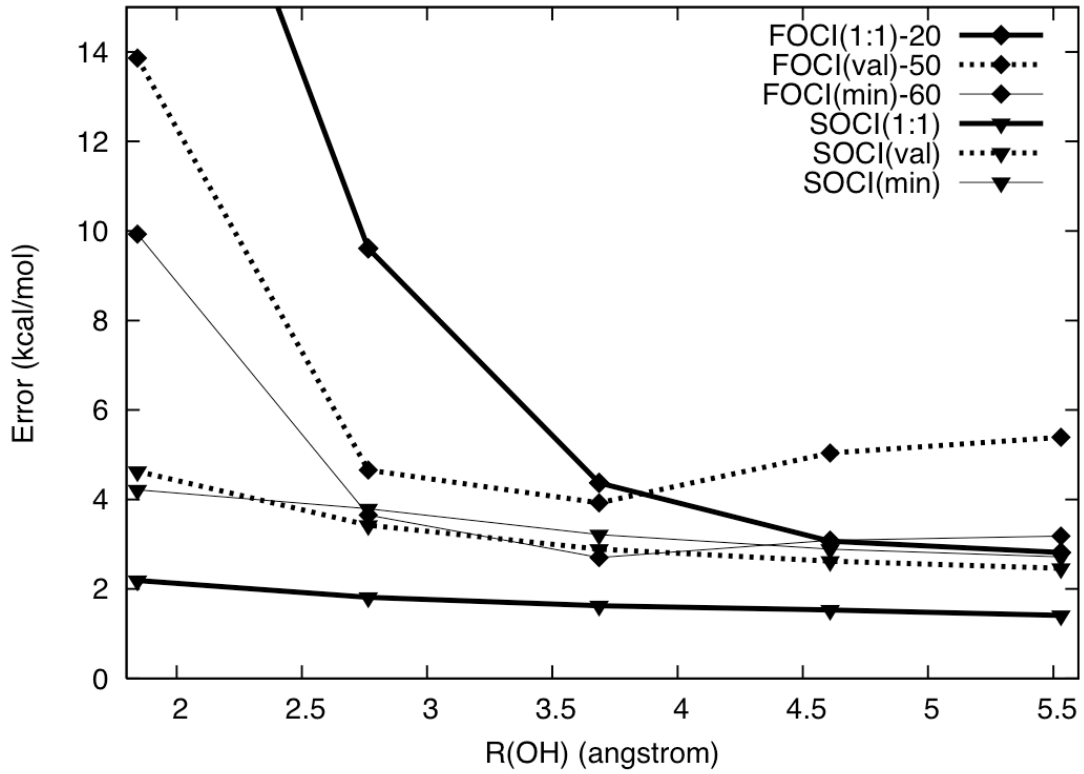

Figure 19. MRCI errors vs. full CI for symmetric dissociation of H_2O with a cc-pVDZ basis.

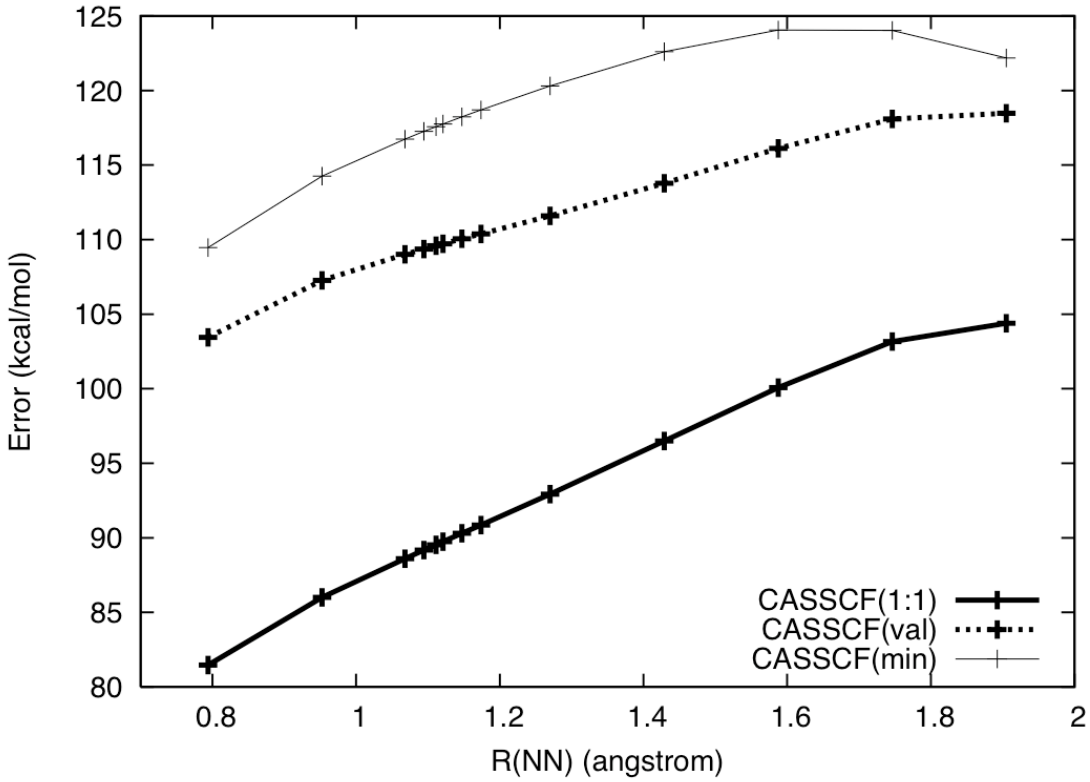

Figure 20. CASSCF errors vs. full CI for dissociation of N_2 with a cc-pVDZ basis.

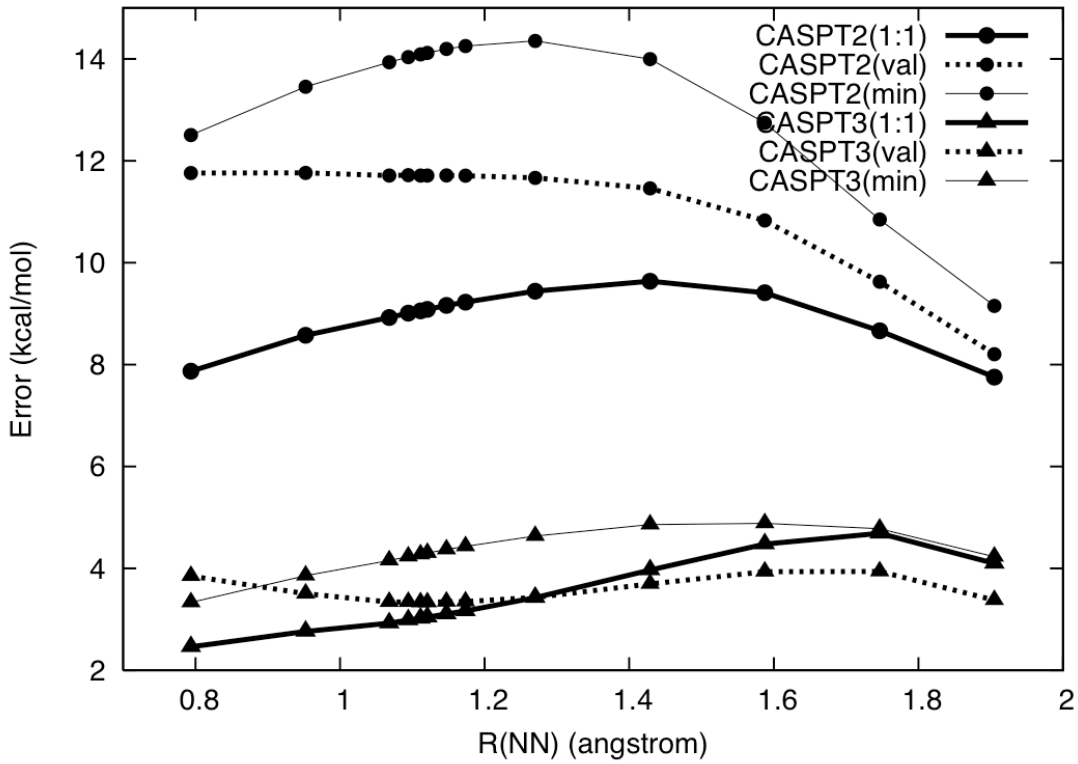

Figure 21. MRPT errors vs. full CI for dissociation of N_2 with a cc-pVDZ basis.

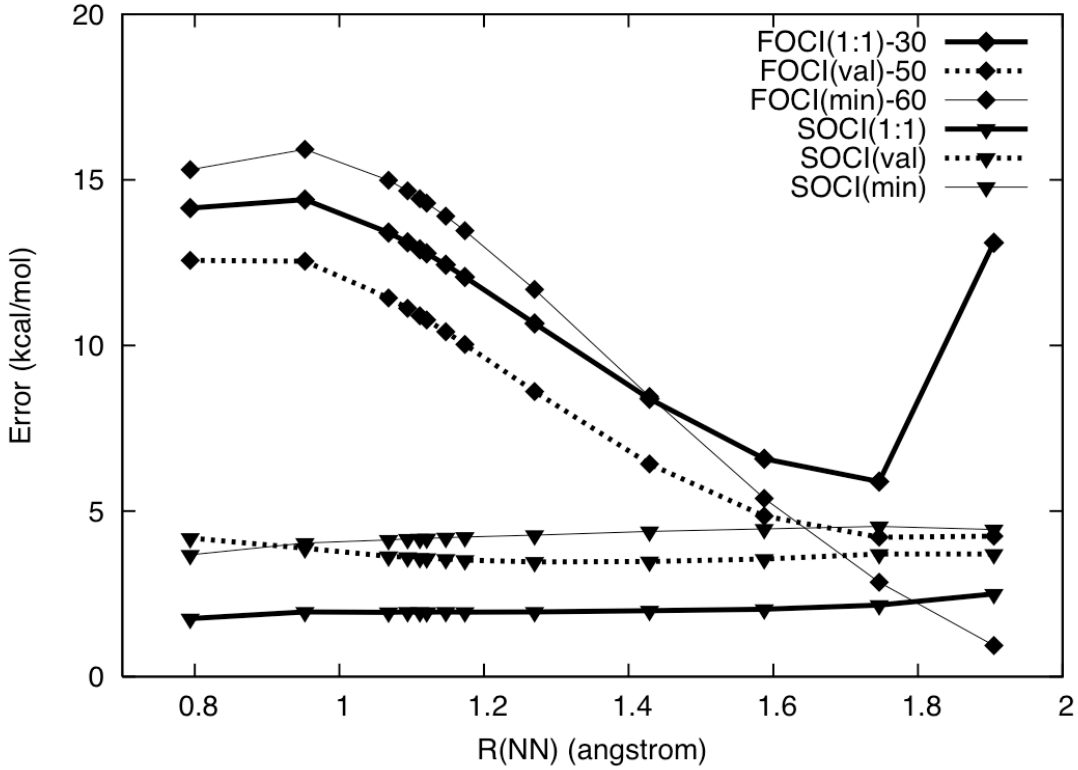

Figure 22. MRCI errors vs. full CI for dissociation of N_2 with a cc-pVDZ basis.

The double dissociation of H_2O may be considered one of the simplest examples of a reaction breaking multiple bonds. From Table 10 one observes that, for the CASSCF method, the larger (1:1) reference outperforms the smaller references. As was observed for HF, the valence and minimal reference space CASSCF results are almost identical because the active spaces are very similar: the valence active space only adds two occupied lone-pair orbitals. As shown in Figure 17, this provides only a small gain in dynamical correlation near equilibrium and gives indistinguishable results near dissociation. This small advantage is erased when dynamical correlation is more fully included via MRPT or MRCI, and NPEs for the minimal active space drop below those for the valence active space. CASPT2 gives NPEs of 4.03 and 3.55 kcal mol^{-1} for the valence and minimal active spaces respectively. CASPT3 reduces these values to 2.30 and 2.09 kcal mol^{-1}. SOCI again appears to be a more robust approach for the inclusion of dynamical correlation, giving NPEs of 2.16 and 1.50 kcal mol^{-1} for the valence and minimal active spaces.

Although the minimal active space results slightly outperform those using a valence active space, they do not perform quite as well as the results with the much larger one-to-one reference. CASPT2, CASPT3 and SOCI give NPEs of 1.83, 0.99, and 0.78 kcal mol^{-1} when using the 1:1 reference. However, from these values it is clear that the exceedingly large increase in computational cost has only resulted in modest improvements in the NPEs. Again, we observe that the inclusion of singles through FOCI

introduces a large imbalance for the one-to-one reference space. Although the double-dissociation of H_2O is only slightly difficult for multireference approaches, this system becomes much more challenging if one relies upon the standard single reference methods. CASPT2, CASPT3 and SOCI with the minimal active space all outperform both CI with five-fold excitations (CISDTQP) and coupled-cluster with full triples (CCSDT) [96].

N_2 is an extremely difficult case for electronic structure theory due to strong dynamical and nondynamical correlation effects. Indeed, CCSDT and CCSDTQ, scaling as n^8 and n^{10} respectively, give nonnegligible NPEs of 6.47 and 1.63 kcal mol^{-1} for this system [103]. The errors versus full CI for the multireference methods considered here are plotted in Figure 20, Figure 21, and Figure 22. Table 11 reports the maximum error, minimum error and NPEs for each of the methods. From the table one can observe large NPEs (>14 kcal mol^{-1}) for all of the CASSCF approaches, a result of the much larger degree of dynamical correlation. However, it is interesting to note that the minimal active space gives a slightly smaller NPE than the larger active spaces. When dynamical correlation is included via CASPT2, the larger active spaces are somewhat better, with NPEs of 1.88 (1:1), 3.56 (valence) and 5.20 kcal mol^{-1} (minimal). Except for the largest, 1:1 active space, these NPEs are significantly larger than for the previous test cases and it appears that the large dynamical correlation in this triply-bonded system is difficult to recover through a second-order MRPT approach. Upon going to third order via CASPT3, NPEs are generally reduced, but they remain over 1 kcal mol^{-1} except for the valence active space.

On the other hand, SOCI again appears as a robust and highly accurate approach for the incorporation of both non-dynamical and dynamical electron correlation effects for

small molecules. SOCI gives NPEs for this system that are less than 1 kcal mol^{-1} for all of the choices in reference (0.75, 0.72 and 0.86 kcal mol^{-1}). Although the larger SOCI calculations perform marginally better than those with the minimal active space, the minimal active space adequately incorporates the strong non-dynamical correlation effects at a fraction of the cost when compared to the larger active space methods. The large 1:1 reference spaces consist of 1332 and 8190 variational parameters for H_2O and N_2 respectively. In comparison, the minimal reference spaces comprise 65 and 92 variational parameters for each of these systems. Furthermore, the minimal SOCI spaces are roughly 10% the size of the corresponding space with a 1:1 reference.

A Generalized RASSCF Approach

The previous results indicate that the minimal CASSCF approaches successfully recover the static correlation effects for the case of both single and multiple bond breaking processes. However, even the minimal CASSCF may become a computationally prohibitive task if one wishes to consider potential energy surfaces consisting of many degrees of freedom. Ignoring spatial symmetry, the minimal active space for N_2 contains 400 determinants. Owing to the high spatial symmetry of the system, this can be reduced to the 56 determinants in the D_{2h} computational subgroup. For large systems, which typically lack the spatial symmetry of this problem, such a reduction would not be possible. Although the minimal CASSCF for N_2 is trivial to compute, the underlying full CI scaling will quickly become insurmountable if reaction channels involving additional active orbitals must be considered simultaneously. Indeed, if one would like to consider a system for which nine bonds may become stretched, such as three N_2 molecules, the

minimal CASSCF reference would consist of more than 2 billion determinants. There is clearly a need to further reduce the size of the reference. We will consider an alternative formulation of the reference here that greatly reduces the size of this expansion. Furthermore, one of the benefits of the full CI expansion in the minimal CASSCF is the size extensivity of the reference. When reducing this expansion, we should hope to maintain this property. Here we will consider an approximation to the minimal CAS, constructed as a generalization of the restricted active-space self-consistent field (RASSCF) wavefunction, that both reduces the scaling of the CI expansion and maintains the size extensivity of the reference.

The original RASSCF approach [102] was constructed by dividing the orbitals into three subspaces. The determinants in the CI expansion were generated by allowing a maximum of q electrons in RAS III and a maximum of p holes in RAS I. RAS II had no restrictions placed upon it and constituted a full CI expansion of the electrons within that space. A CASSCF can be considered a special case of a RASSCF where the active orbitals are all placed in RAS II and $p = q = 0$. Here we consider a generalized RASSCF approximation to the minimal CASSCF which uses an arbitrary number of disjoint 'RAS II' type subspaces. The space of inactive, doubly-occupied orbitals and the space of inactive virtual orbitals remains the same as the minimal CASSCF. The space of bonding and anti-bonding orbitals, which comprise the active, FCI space in the CASSCF, are divided into subspaces of bonding/ anti-bonding pairs. Each of these two-orbital spaces is restricted to contain two electrons for the RASSCF reference, and the overall wavefunction is given as a direct product of these 2×2 subspaces. Because the approach

merely defines configurations and orbitals that are specific for a particular bond or set of bonds, we will refer to this reference as a bond-specific active space (BSAS). Dynamical correlation can be incorporated either through MRPT (BSAS-PT2 and BSAS-PT3) or through MRCI (BSAS-CIS or BSAS-CISD). It should be pointed out that the BSAS reference is similar in spirit to the generalized valence bond (GVB) approach of Goddard and co-workers [110-112] and the quasi-complete active space self-consistent-field (QCAS-SCF) approach of Nakano and Hirao [113]. It is a specific example of the constrained CAS (CCAS) space discussed by Roos [86] and the occupation-restricted multiple-active-space self-consistent-field (ORMAS-SCF) approach of Ivanic [114, 115]. The QCAS space is similar to the CCAS reference space in which additional spin-coupling constraints are placed upon each space. This formulation is identical to the minimal CASSCF for the case of a single bond and those results will not be repeated here. However, where the scaling of the minimal CASSCF is factorial in the number of bonds to be broken, the scaling of BSAS-SCF is exponential in the number of bonds to be broken.

All calculations incorporating a BSAS reference were performed within MOLPRO [28]. The maximum error, minimum error and NPE for BSAS approaches are given in Table 12 for H_2O and Table 13 for N_2. As these approaches are attempts to approximate the minimal CASSCF results, we have plotted the difference between the BSAS methods and their minimal CAS analogues in Figure 23 and Figure 24. From Figure 23 we see that the error introduced at the MCSCF level is greatest near equilibrium and probably results from dynamical correlation effects partially recovered by the CASSCF. When dynamical correlation is included via MRPT and MRCI, there is

very little difference between results using the BSAS or CASSCF references. Indeed, the MRPT results are slightly improved with the BSAS reference, although by a seemingly negligible amount.

Table 12. Maximum, minimum, and non-parallelity error (kcal mol^{-1}) with BSAS methods for H_2O with a cc-pVDZ basis.

Method	Max error	Min error	NPE
BSASSCF	105.78(1.0R_e)	78.21(3.0R_e)	27.57
BSASPT2	10.01(1.0R_e)	6.27(3.0R_e)	3.75
BSASPT3	4.08(1.5R_e)	2.05(3.0R_e)	2.03
BSASCIS	74.78(1.0R_e)	67.92(3.0R_e)	6.86
BSASCISD	4.62(1.5R_e)	2.75(3.0R_e)	1.88

Table 13. Maximum, minimum, and non-parallelity error (kcal mol^{-1}) with BSAS methods for N_2 with a cc-pVDZ basis.

Method	Max error	Min error	NPE
BSASSCF	125.11(1.5875)	110.10(0.7938)	15.01
BSASPT2	14.33(1.2700)	9.17(1.9050)	5.16
BSASPT3	4.88(1.5875)	3.36(0.7938)	1.53
BSASCIS	90.12(1.1473)	86.67(1.9050)	3.45
BSASCISD	5.95(1.5875)	4.32(0.7938)	1.63
BSASCISDT	2.13(1.4288)	1.84(1.9050)	0.29

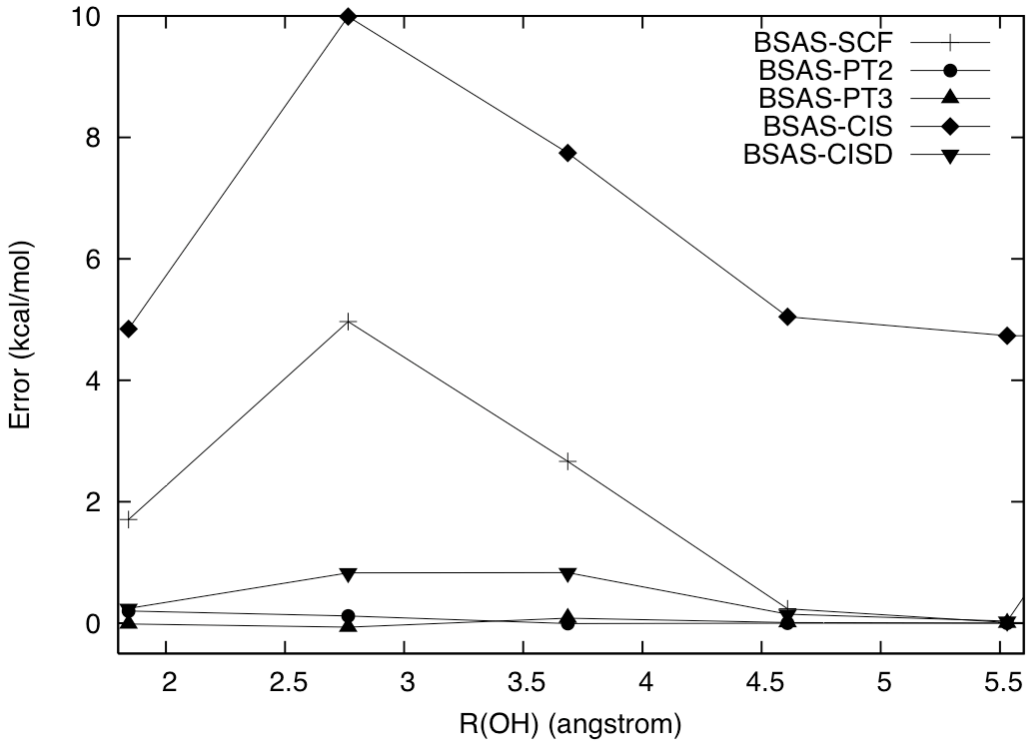

Figure 23. Difference between BSAS methods and their minimal CAS analogues for symmetric dissociation of H_2O with a cc-pVDZ basis.

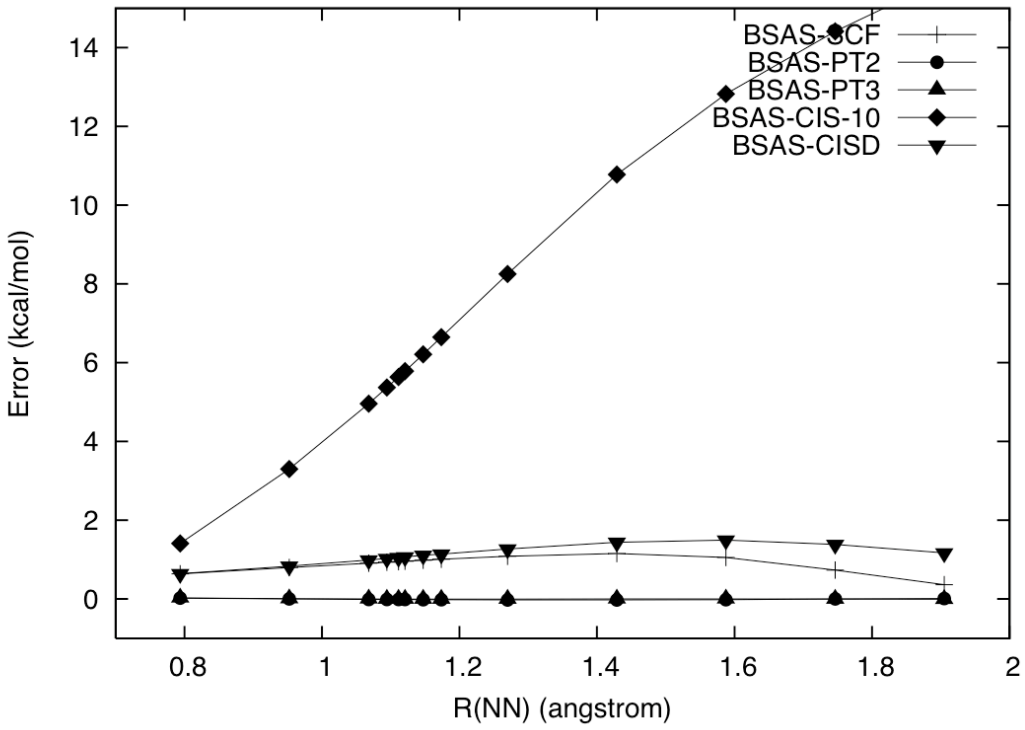

Figure 24. Difference between BSAS methods and their minimal CAS analogues for dissociation of N_2 with a cc-pVDZ basis.

The results for the challenging N_2 molecule, presented in Table 13, are generally similar to those for H_2O, and the MRPT based approaches again are rather insensitive to the choice of reference. BSAS-PT2 and BSAS-PT3 give NPEs of 5.16 and 1.53 kcal mol^{-1} respectively, which compare very favourably to values of 5.20 and 1.55 kcal mol^{-1} for the minimal active space. Recall that even for the large 1:1 active space, the MRPT NPEs are 1.88 and 2.23 kcal mol^{-1}. The large (greater than 10 kcal mol^{-1}) difference between the BSAS-CIS and the minimal FOCI for this system is consistent with the very poor overall performance of FOCI for this system; the BSAS reference itself, without the addition of singles into the virtual space via FOCI, provides a more balanced description of the PES. The BSAS-CISD approach gives a NPE of 1.63 kcal mol^{-1}, compared to 0.86 kcal mol^{-1}

with the minimal SOCI. Due to the similarity between BSAS-SCF and the corresponding minimal CASSCF for this system, this difference is most likely due to dynamical correlation effects. Indeed, if one includes triple excitations with BSAS-CISDT, the NPE is reduced to 0.29 kcal mol^{-1}. Even the BSAS-CISDT wavefunction is still drastically smaller than the SOCI expansion with the 1:1 reference space for this particular case.

Conclusions

We have presented a systematic investigation of the ability of minimal reference spaces to describe strong non-dynamical correlation effects in multi-reference computations of reactions breaking single or multiple bonds. This is the first comparative evaluation of multireference methods across the entire potential energy surface for several different bond-breaking reactions, and it extends previous work that focused specifically on a single molecule [96, 103] or only on singly-bonded molecules [104]. Such a critical analysis is only made possible by the determination of demanding full configuration interaction benchmarks [96, 103, 104].

CASSCF using any of the active spaces considered here effectively captures the strong non-dynamical correlation effects and gives qualitatively correct potential energy curves for any of the bond-breaking reactions considered. When improved by treatments of dynamical electron correlation via multi-reference perturbation theory (e.g. CASPTn) or multi-reference configuration interaction singles and doubles (e.g. second-order CI), potential energy curves achieve quantitative accuracy with non-parallelity errors of a few kcal mol^{-1} or less. The CASPTn approach is an extremely useful method for efficiently adding dynamical correlation effects to the CASSCF reference, but at second or third

orders, it appears incapable of providing spectroscopically accurate potential energy surfaces. Indeed, significant errors remained in CASPT2 or CASPT3 descriptions of the challenging N_2 molecule. However, the multi-reference perturbation theory approaches appeared slightly less sensitive to the choice of reference than the configuration interaction approaches. Second-order CI results, even with the minimal CAS reference, provide high-accuracy surfaces for all of the systems studied.

We considered three different threshold-free criteria for choosing active spaces, which we label minimal, valence and 1:1. The minimal active space consists only of the orbitals for the bonds to be broken and their antibonding counterparts. The non-parallelity errors (NPEs) do not necessarily improve as one goes to the larger active spaces in the CASSCF procedure. Perhaps surprisingly, in the CASPTn or second-order CI computations, the minimal active space often gives NPEs which are as good as or only slightly worse than those with much larger active spaces, at a fraction of the computational cost.

A generalized restricted-active-space definition of the reference space for bond-breaking reactions, the 'bond-specific active space' (BSAS) was presented as a size-extensive approximation to the minimal CAS approaches. Drastically reducing the size of the CI expansion in the reference, the BSAS results offer a very balanced description across the entire potential energy surface. The systematic addition of dynamical correlations, either through MRPT or MRCI, provides increasingly better descriptions across the PES. The balance afforded by the BSAS reference warrants further investigation of its applicabilty to describe complex PESs. Furthermore, the reduced

scaling of the BSAS methods should allow their application to much larger systems than can be afforded using conventional CASSCF based approaches.

CHAPTER 5

NON-DYNAMICAL CORRELATION AND METAL-SALEN CATALYSTS

This chapter will summarize the importance and origins of non-dynamical correlation in metal-ligand systems and provide a brief introduction to a particularly important class of metal-ligand systems: the metal-salens. Metal complexes of salen and salen-like ligands have emerged as quite probably the most important class of homogenous catalysts in the field of asymmetric catalysis [116]. The demand for enantiomerically pure compounds by the pharmaceuticals and fine chemicals industries continues to grow [117], driven by the often superior performance of the pure enantiomers [118] in combination with the tightening regulatory requirements of the Food and Drug Administration. The field of asymmetric molecular catalysis has progressed rapidly over the previous two decades, having been extensively covered in recent reviews [117, 118]. The awarding of the 2001 Nobel Prize in chemistry recognized the importance of the field and highlighted advances in the catalysis of asymmetric epoxidation reactions, one of the most important synthetic tools developed in the past 30 years for the pharmaceuticals and specialty chemicals industries [117]. The development and optimization of highly efficient and selective catalysts for asymmetric catalysis is an often-tedious process that can greatly benefit from knowledge of the underlying catalytic mechanism and the electronic and steric properties of the catalyst. However, the unraveling of a catalytic mechanism is technically challenging [119-121] and a clear picture of the complete catalytic cycle often remains elusive [122]. Theoretical methods, when they produce reliable results, are capable of providing a highly detailed picture of

the electronic properties of a particular catalyst system and a clear picture of the various steps in a proposed catalytic cycle.

Since the pioneering work of Kohn and Sham [123], density functional theory (DFT) has emerged as an invaluable tool in computational chemistry for exploring the ground-state properties of molecular systems. DFT approaches, over the past decade, have almost become the *de facto* method of choice for exploring structures and reaction mechanisms in organometallic catalysts [124-129]. However, the electron density is represented by a single Slater determinant in the Kohn-Sham formulation. Such implementations of DFT should not be expected to be accurately applied to systems that are inherently multi-configurational. Becke has commented that nondynamical correlation effects are at best accidentally captured by LSDA, GGA, and "hybrid" DFT functionals [130]. Although the problems associated with applying current formalisms of DFT to multi-configurational states have long been recognized [131, 132], the extension of DFT to the description of such states remains an active area of research [133-136].

DFT results can be sensitive to the choice of functional (and this is particularly true for some metal-salen systems [137]). Indeed, numerous functionals have been developed for vastly different applications. Of these, the hybrid B3LYP is probably the most widely applied [138], although its applicability should certainly not be considered universal. B3LYP has been shown to give rather poor estimates for spin-state splittings of many first-row transition metal dimers [139]. Indeed, a detailed analysis of the low-spin/high-spin splittings in a series of first-row transition metal dimers demonstrates the strong dependence upon the amount of "exact" exchange and supports decreasing the a_0 parameter to 0.15 [140]. However, other authors have supported increasing the same

parameter to as much as 0.50 to achieve improved performance for energy barriers [141]. When experimental data are scarce, one must rely upon high-level *ab-initio* results to verify the applicability of DFT to a particular class of systems. The remainder of this chapter will discuss the general role of nondynamical correlation in transition-metal catalysts and the importance of the metal-salen catalysts to the homogeneous catalysis community. Of central importance to the catalysis community and the topic of the remaining chapters within is the applicability of DFT to examining structures and mechanisms in metal-salen catalyzed chemistry.

Non-dynamical correlation and transition-metal systems

As was discussed above, single-reference methods tend to break down as bonds are stretched far from equilibrium. The need to treat multiple "nearly degenerate" electronic configurations on an equal footing, both $(\sigma)^2$ and $(\sigma^*)^2$ for the case of stretching a single bond, results in inconsistent and often times unphysical results for methods based upon a HF reference. However, the nondynamical correlation problem is not restricted to geometries far from equilibrium. While the simple diatomic and small polyatomic systems examined above tend to be strongly single-reference at their respective equilibrium geometries, other systems can exhibit strong nondynamical effects even at equilibrium. Such is quite often the case for systems consisting of one or more transition metal atoms, especially for first transition row metals. The partial filling of the spatially and energetically proximal metal d-orbitals gives rise to several low-lying electronic configurations. The problem is compounded for the 3d metals. The spatial proximity of the 3*s*, 3*p*, and 3*d* orbitals gives rise to destabilizing effects for metal-ligand interactions that result in poor overlap between the 3*d* and ligand orbitals. This gives rise

to orbital near degeneracies and a considerable amount of nondynamical correlation [142]. The ability of post-HF and density functional theory (DFT) based approaches to adequately describe these long-range correlation effects remains an open question. It has been generally accepted that separation of the *nd* orbitals from the *ns* and *np* orbitals in 4*d* and 5*d* systems results in reduced nondynamical correlation effects and improved performance for standard theoretical approaches, where relativistic effects are easily incorporated using effective core potentials. This chapter will briefly review the current state of understanding surrounding the nondynamical correlation problem as it pertains to transition metal systems. The discussion will primarily be concerned with "large" transition metal systems consisting of a single metal atom, i.e. systems where the metal center is surrounded by at least four ligands. The distinction is extremely significant. The first one or two ligands to bind a transition metal center will find the latter in an extremely hybridized state consisting of $d^n s^2$, $d^{n+1} s^1$, and $d^{n+2} s^0$ character. As the ligand sphere becomes more heavily saturated, the $(n+1)s$ orbitals will be pushed significantly higher in energy. Furthermore, these large transition metal systems hold a special importance in molecular catalysis. So, while much has been done to explore homo-[139, 143] and hetero-[144, 145] transition metal diatomic species, such work will not be discussed here. Systems consisting of multiple metal centers will also not be covered here [146].

While the "spin-flip" approaches discussed above, and their spin-complete analogues, are capable of effectively recovering much of the static correlation for the bond-breaking problems presented, the definition of an appropriate high-spin reference is much clearer for that problem than it is for the transition-metal systems currently under consideration here. Thus, the applicability of the SF and other "modified" single-reference methods to the case of strong near-degeneracies present in metal ligand systems remains unclear. However, true multi-reference approaches (especially those based upon

a CASSCF/RASSCF reference) are ideally suited to the problem. Indeed, transition metal atoms and molecules have received a considerable amount of attention from researchers developing such methods. On the other hand, it is also true that the widespread use of multireference methods in this domain (as well as in other domains of chemistry) has been hindered by the difficulties in applying such methods. At least at this time, there are no *black-box* multireference approaches. It is clear that, for the foreseeable future, the application of multireference methods to such systems will best be handled by experienced users of such methods. The appropriate selection of the reference space, which can strongly influence the reliability and feasibility of such computations, requires a certain amount of "chemical insight" and experience.

The nature of the nondynamical correlation effects in metal-ligand systems has been shown by Pierloot [147] to be strongly dependent upon the nature of the metal-ligand bonding. Through a series of large RASSCF computations on a set of octahedral Cr compounds, Pierloot has demonstrated the interplay between the nondynamical correlation effects and the degree of metal-ligand covalency. In the case of weakly covalent metal-ligand bonding (predominantly ionic bonding), the nondynamical correlation effects are largely a consequence of the metal d orbitals. This holds great promise for the applicability of relatively small active spaces for such systems. As was demonstrated above, small active spaces (when combined with treatments for dynamical correlation) provide a well-balanced and affordable description of systems exhibiting nondynamical correlation effects. While the ionic picture of metal-ligand bonding lends itself to concepts such as the "formal oxidation state" of the metal and the "formal d orbital occupation," as the degree of metal-ligand covalency increases the ionic picture

becomes smeared. In such cases, the mixing of the metal and ligand orbitals leads to extremely large nondynamical correlation effects. In such instances, the accurate treatment of nondynamical correlation effects will likely extend beyond the metal d-orbitals to include those ligand orbitals that mix most strongly with the metal d-orbitals.

Another important effect (although truly a dynamical one) often attributed to systems containing transition metals is the *3d-double shell effect* [147-151]. For 3d-transition metals with a more than half-filled 3d shell, electron-electron repulsion effects between the closely-held 3d electrons gives rise to extremely strong dynamical correlation effects. The double shell effect is most obvious when considering the relative energies of states containing different d-orbital occupation numbers, i.e., the relative energies of the $(3d)^n(4s)^0$, $(3d)^{n-1}(4s)^1$, and $(3d)^{n-2}(4s)^2$ states of 3d atoms. The 3d double shell effect leads to large errors for the relative energies of these states from CASSCF calculations including only the metal $3d$ and $4s$ orbitals [CASSCF(n/6)]. When the active space is enlarged to include a second, more-diffuse $3d$-shell [CASSCF(n/11)] the errors are greatly reduced. This has been demonstrated, for instance, in CASSCF/CASPT2 calculations on Ti^+, Co^+, and Rh^+ by Pierloot [147]. It is the opinion of this author that such "dynamical" correlation effects are best treated by multireference correlated methods of electronic structure, such as multi-reference perturbation theory or multi-reference CI, built on top of a CASSCF or RASSCF reference designed to describe the dominant nondynamical correlation effects. As pointed out by Roos [152], "The CASSCF model has not been developed for treating dynamical correlation effects, but to provide a good starting point for such studies." This opinion is further supported both by our previous work on bond-breaking [87] and by a careful

observation of Pierloot's CASSCF/CASPT2 results for Co^+ [147]. In our minimal active space studies of bond-breaking potentials, correlated methods built upon a minimal CASSCF (or RASSCF in the case of BSAS methods) performed as well as or better than their analogues employing much larger reference spaces [87]. Furthermore, the results based upon a minimal reference space systematically approach the FCI limit as higher levels of dynamical correlation are included. Going back to the results of Pierloot for Co^+, the CASPT2(8/6) errors in the relative energies are typically less than 0.10 eV from the errors in the CASPT2(8/11) relative energies (when compared to experimental excitation energies) at a fraction of the computational cost [147]. Although not included in the Pierloot study, it is anticipated the CASPT3 or SOCI energies based upon the CASSCF(8/6) reference will be much closer to the experimental excitation energies (or at least to accurate theoretical excitation energies for the given one-particle basis).

While the strong dynamical and non-dynamical correlation effects present in metal-ligand systems combined with the difficulties of selecting appropriate references (either through general MCSCF or active-space CASSCF or RASSCF expansions) make the application of multi-reference methods extremely challenging for many metal-ligand systems, the single-reference formalisms described above cannot be expected to provide reliable results for such systems. This is not to say that single-reference methods will necessarily not work for metal-ligand systems. The increasingly popular DFT approaches have provided reliable results for many metal-ligand systems [128, 139, 143, 144, 152-155], although there are certainly many exceptions to this as well [139, 143, 144, 152, 156-158]. In reality, great care must be taken to ensure that the functional employed provides reliable results for a particular system when DFT is going to be

employed for theoretical studies. This can be done either against reliable experimental data or, in the absence of experimental results, against results from reliable *ab initio* calculations. If DFT does indeed provide such results, the application of DFT to metal-ligand catalyzed reactions can provide a great deal of chemical insight and understanding.

Metal-Salens in Catalysis

The term "salen" refers to a class of [O, N, N, O] tetradentate Schiff base complexes formed by the condensation of an aldehyde with the appropriate ketone. The first salen ligand and its complex with Cu was discovered by Combes in 1889 [159]. It was more than 75 years later when the first application of a well-defined chiral transition-metal complex [a Cu(II)-salen] in asymmetric catalysis was realized [160]. Since this initial discovery, numerous metal-salen systems have been developed for applications in enantioselective chemical transformations [116, 122, 161-167]. A major breakthrough in asymmetric catalysis was observed with the development of the chiral manganese-salen catalysts by the groups of Jacobsen [168] and Katsuki [169], in particular for the asymmetric epoxidation of alkenes. The Jacobsen-Katsuki reaction remains the most highly versatile and widely employed approach for olefin epoxidation [162]. The same ligand, when combined with chromium or cobalt, has proven highly efficient as a catalyst for epoxide ring opening reactions [170, 171]. The tetradentate binding motif of the metal salens is reminiscent of the porphyrins in the heme-based oxidative enzymes [172-176]. Indeed, Mn(III)-salens have been targeted as models for the heme-based porphyrins of the catalase enzymes [177]. However, the salen ligands are more easily prepared than their porphyrin analogues and are more easily modified to induce chirality at the metal center. The salen ligand has proven to be extremely robust and versatile; being easily

prepared and derivatized [178], capable of stabilizing numerous metals in various oxidation states [179], and proficient in transmitting a high degree of enantiomeric specificity [116, 122, 162, 166, 180-183]. As such, the salen ligands have been targeted as an attractive manifold for the development of both bifunctional catalyst systems [184, 185] and recoverable immobilized molecular catalysts [116, 186-189]. Judging by recent reviews [122, 161, 162, 180, 182], the interest in and the discovery of new transformations catalyzed by metal-salen complexes shows no signs of slowing down.

The tremendous interest in metal-salen systems for catalysis has sparked several previous theoretical studies [169, 190-217], although no particular metal-salen system has been as extensively studied by theoretical methods as the Mn(salen) systems employed for asymmetric epoxidation chemistry [169, 203-217]. In order to undertake such studies the authors employ some model system that they expect to mimic the properties of the real system; some of the most common model systems are depicted in Figure 25. The relative scarcity of theoretical work on other metal-salen systems may be a consequence of the difficulty in interpreting the results provided; complicated by the near-degeneracy of the electronic states, the proximity of the low-lying electronic states, and the discrepancies that exist in previous theoretical results. It has been demonstrated by Cavallo and Jacobsen that there exist major qualitative discrepancies in the description of the Mn(salen) catalyzed epoxidation reaction provided by two of the most popular density functionals, BP86 and B3LYP [212]. Concomitant with the discrepancy in theoretical results and the difficulties of nondynamical correlation effects, systems containing 3*d* metals can feature several low-lying excited states of various multiplicities which give rise to surface crossing effects. The effect of intersystem crossings on

chemical reactions involving heavier elements, where spin-orbit coupling effects may be large, has long been a matter of debate. Such reactions are often referred to as "spin-forbidden" processes because at zeroth-order spin-state changes are not allowed. However, it has been well demonstrated that such a view is too simplistic [218]. Indeed, extremely fast reactions may occur in transition metal containing systems despite being spin forbidden in nature. A detailed understanding of the energies and geometries of reactants, products, intermediates, and minimum energy crossing points is often required to account for chemical reactivity and selectivity. Such a detailed picture for metal-salen catalyzed reactions has yet to be presented.

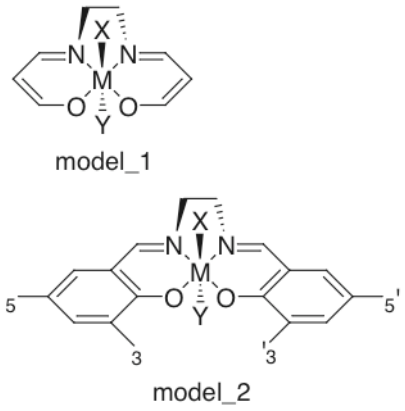

Figure 25. Two of the most common model systems for metal-salen catalysts.

CHAPTER 6

THE CASE OF OXO-MN(SALEN)

Numerous theoretical studies over the past decade have sought to elucidate the electronic properties that give rise to the stereochemical control afforded by the Mn(salen) system [115, 203-217, 219]. Despite a large number of theoretical studies, however, extracting definitive conclusions from theory has proven challenging. For example, it has been noted that there exist major qualitative discrepancies in the description of the epoxidation reaction catalyzed by this system when comparing the two most commonly used density functionals [212]. Manganese is one of the 3*d* metals, which (as discussed above) have proven to be extremely challenging for electronic structure theory [220]. Indeed, both the Mn-dimer [139] and the cationic MnO^+ (Ref. [221]) are particularly difficult for standard theoretical methods, displaying a large degree of nondynamical correlation [142]. Despite a number of theoretical studies, such a detailed picture of Mn(salen) catalyzed olefin epoxidation reactions remains elusive, primarily due to a lack of high-level benchmark calculations. Although this has been attempted for Mn(salen) systems with high-level CC studies [213], the results have been highly disputed [222, 223]. The only remaining high-level theoretical results have been the CASSCF and multireference perturbation theory [207] (MRMP2) results presented by Ivanic *et al.* [207]. Because the CASSCF method is capable of describing the nondynamical correlation effects in the oxo-Mn(salen) system, and because subsequent dynamical correlation effects have been shown by Ivanic *et al.* to be minor [224], we have pursued expanded CASSCF studies here in an attempt to obtain a definitive ordering of the lowest singlet, triplet, and quintet states of the system. The sensitivity of

the CASSCF results to the basis set has been examined along with a possible truncation of the active space from the study of Ivanic *et al.* Additionally, CASSCF wave functions are used to explore low-lying excited singlet and triplet states which have not previously been considered

Finally, we explore the possibility of multiple solutions to the HF and Kohn-Sham DFT equations. In such self-consistent-field (SCF) based approaches a solution is iteratively sought such that the energy functional is stationary with respect to variation of the spin-orbitals. However, convergence to even a local minimum is not ensured by establishing zero first-order variation in the energy functional [225, 226]. A necessary criterion for ensuring convergence to a local minimum is the positive definiteness of the orbital Hessian, the second-order changes of the energy functional with respect to infinitesimal variations of the orbitals. When there exists one or more negative eigenvalues of the orbital Hessian, the SCF solution is unstable with respect to variations of the spin-orbitals. This implies that there exists a lower-energy solution to the SCF equations, although this may not necessarily be the desired solution. The orbital instabilities can be classified into various types, some of which may result in solutions which break some of the employed constraints on the wave function [227]. The orbital-instability problems give rise to symmetry breaking for many simple molecular systems [207]. Ensuring convergence to a global minimum is extremely challenging even for the smallest of systems [228, 229]. In this study, we have examined the existence of multiple solutions and wave function orbital instabilities for several commonly used SCF approaches as an attempt to understand some of the apparent discrepancies in the literature.

Theoretical Methods

The model system and geometry were taken from previous work by Ivanic *et al.*[230]. A 6-31G* basis [231, 232] was employed for most of the computations. Additionally, some CASSCF wave functions were obtained using a larger basis which consisted of the 6-311G*basis [233, 234] for all atoms except Mn, for which the augmented triple-zeta atomic natural orbital basis of Widmark *et al.* was employed [235]. These two choices of basis will be referred to as 6-31G* and 6-311G*, resulting in 273 and 423 contracted Gaussian functions, respectively

Wave function stability analysis was performed within the computational chemistry package QCHEM 2.1 [236, 237]. Along with Hartree-Fock methods, several combinations of popular exchange [28] and correlation [207] functionals were employed. In order to examine the existence of multiple solutions and orbital instabilities, three separate calculations were performed for each spin state, each with a different set of initial guess orbitals. Initial guesses were generated using the core Hamiltonian, using a superposition of atomic densities, and using the generalized Wolfsberg-Helmholtz (GWH) procedure [238]. In all cases, the SCF orbital optimization was performed using geometric direct minimization (GDM) [239]. Although GDM is slightly more expensive than Pulay's direct inversion of the iterative subspace (DIIS) [207], the ability to take nonlinear steps in orbital rotation space provides more stable convergence for difficult systems. Convergence of a solution was assumed when the rms orbital gradient was less than 10^{-8}. The stability of each converged wave function was checked by diagonalization of the molecular orbital Hessian, and the type of instability present was analyzed. Hessian

eigenvalues were assumed to be converged when the maximum deviation was less than 10^{-6}.

State-averaged complete-active-space self-consistent field [101] (SA-CASSCF) calculations were performed with MOLPRO [207]. Two choices of active space were employed and will be discussed further below. Although previous results have indicated that the relativistic effects are likely quite small [240], their impact has been explored by employing the perturbational Cowan-Griffin (CG) operator [241]. The CG relativistic corrections were computed at the SA-CASSCF level of theory in the 6-31G* basis.

Results and Discussion

CASSCF Computations and Electronic State Ordering

SA-CASSCF/6-31G* wave functions were obtained both with a 12 electron in 11 orbital active space as well as an 8 electron in 7 orbital active space. The former has been advocated by previous authors [242, 243] and the latter was chosen after an examination of UHF natural orbital (NO) occupation numbers [244]. The smaller active space consists of the $d_{xy}(\mathrm{Mn})$, $\sigma(\mathrm{Mn\text{-}O_{ax}})$, $\pi_1(\mathrm{Mn\text{-}O_{ax}})$, and $\pi_2(\mathrm{Mn\text{-}O_{ax}})$ occupied molecular orbitals along with the correlating orbitals $\sigma^*(\mathrm{Mn\text{-}O_{ax}})$, $\pi_1^*(\mathrm{Mn\text{-}O_{ax}})$, and $\pi_2^*(\mathrm{Mn\text{-}O_{ax}})$. The larger active space is formed from the smaller by the addition of the two three-center–two-electron C–C–C-type π orbitals from the salen ligand $R\pi_1$ and $R\pi_2$ along with the corresponding correlating orbitals $R\pi_1^*$ and $R\pi_2^*$. All of these orbitals are depicted in Figure 26 from a CASSCF/6-31G*(12/11) calculation of the 1^5A state.

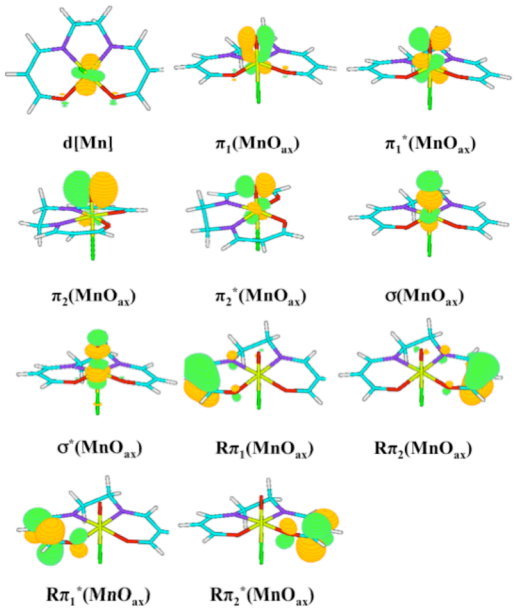

Figure 26. CASSCF/6-31G*natural orbitals for the 1^5A state of oxo-Mn(salen).

In the study of Ivanic *et al.* [207], a triplet ground state is predicted for the oxo-Mn(salen) model system. The singlet was predicted to be a few kcal mol^{-1} higher in energy followed by the quintet at approximately 40 kcal mol^{-1}. However, the authors were unable to converge the CASSCF(12/11) wave function for the singlet state. The problem stemmed from a weakly occupied $d_{xy}(\mathrm{Mn})$ orbital in the active space that rotated with a chlorine core orbital. This led the authors to place the *d* orbital into the restricted space, performing a CASSCF(10/10) calculation. To allow for a comparison of relative energies after the orbitals were converged, the authors then performed an Edminston-Ruedenberg [245] (ER) localization of the restricted-space orbitals and placed the *d* orbital back into the active space, performing a CAS-CI(12/11) computation. The study of Ivanic *et al.* employed modified virtual orbitals [207] from a HF calculation as initial guess orbitals for the CASSCF. Here, the starting orbitals were the natural orbitals from a

CASSCF(12/11) calculation in a STO-3G basis [140]. In turn, the CASSCF/STO-3G computations used the natural orbitals of a CI singles and doubles computation as a guess. Using this procedure, we were able to converge the CASSCF(12/11) calculations for the singlet state while avoiding the rotation of the *d* orbital out of the active space. The resulting CASSCF(12/11) total and relative energies for the 1^1A, 1^3A, and 1^5A states are presented in Table 14 along with the CAS-CI energy of Ivanic *et al.* As can be seen from the table, the energy of the 1^1A drops below that of the 1^3A state when using a converged CASSCF solution. The converged CASSCF energy of the 1^1A state lies a little more than 3 kcal mol^{-1} lower than the CAS-CI energy of Ivanic *et al.* From these calculations, the singlet and triplet states are predicted to be essentially degenerate, with a singlet ground state followed by the triplet less than 0.5 kcal mol^{-1} higher in energy. The quintet remains around 40 kcal mol^{-1} higher in energy. The approach presented above for generating starting orbitals for the CASSCF calculation was employed for all of the remaining calculations unless otherwise stated.

Table 14. Total (hartree) and relative (kcal mol^{-1}) energies for three electronic states of oxo-Mn(salen).

State	Total energy	Relative energy
$1\ ^1$A CASSCF(12/11)/6-31G*	−2251.430 527[a]	0.00
$1\ ^1$A CAS-CI(12/11)/6-31G*	−2251.425 50[b]	3.15
$1\ ^3$A CASSCF(12/11)/6-31G*	−2251.430 11[b]	0.26
$1\ ^5$A CASSCF(12/11)/6-31G*	−2251.362 20[b]	42.88

[a]This work.
[b]Ivanic *et al*.

One of the major sources of difficulty in computational studies of this system has been the number and proximity of many low-lying excited states. In order to gain an understanding of the qualitative ordering of these states, we initially performed CAS-CI

calculations for several roots on each of the spin manifolds using the converged orbitals from the CASSCF/6-31G*(12/11) calculation of the 1^5A state. These calculations indicate that two triplet states and the closed-shell singlet state are nearly degenerate in energy. Lying slightly higher in energy are two open-shell singlet states followed by the high-spin quintet 1^5A. These six lowest electronic states that are capable of being described by the current active spaces have been studied extensively in this work and will be tentatively labeled 1^1A , 2^1A , 3^1A , 1^3A , 2^3A , and 1^5A. Preliminary studies indicate that other states capable of being described with this active space lie higher in energy and were not considered further. It should be noted that only three of these states (the lowest singlet, triplet, and quintet) have been considered previously by other authors and it is unclear at this stage what impact the presence of these low-lying excited states will have on the chemistry of this system.

The SA-CASSCF method has been shown to provide a reliable reference for vertical excitation energies in some systems [207] as it affords a balanced description of the relevant electronic states. However, one important consideration when performing such calculations is how to average over the electronic states. There are inherent advantages and disadvantages both to averaging over more and to averaging over fewer of the states of a given system. The states included in a SA-CASSCF calculation are orthogonal by construction and must be described by a common set of molecular orbitals. Averaging over fewer states in a given calculation will certainly provide more flexibility in the description of the electronic states, but may lead to erroneous root-flipping problems for states that lie close in energy. Averaging over more states will lead to fewer calculations required to obtain the desired excitation energies and fewer root-flipping

problems, but the primary consideration now is whether all of the electronic states can be accurately described by a common set of molecular orbitals. If this is the case, it may be possible to reliably obtain all of the excitation energies of interest from a single calculation.

In the present study, we have obtained SA-CASSCF wave functions using three different averaging schemes. In the most flexible approach considered, SA-CASSCF wave functions were obtained from four separate calculations including (a) the 1^1A state, (b) the 2^1A and 3^1A states, (c) the 1^3A and 2^3A states, and (d) the 1^5A state. This will be conveniently represented with the following notation [$1^1A/2^1A,3^1A/1^3A,2^3A/1^5A$]. The total and relative energies are presented in Table 15. Both sets of calculations predict the ground spin state to be the 1^1A state, in contrast to the triplet state found by Ivanic. Only slightly higher in energy are the nearly degenerate 1^3A and 2^3A states. A nearly degenerate pair of open-shell singlet states, 2^1A and 3^1A, is found around 35 kcal mol^{-1} followed by the 1^5A state above 40 kcal mol^{-1}. Single-state CASSCF calculations attempted on the 3^1A and the 2^3A states resulted in root-flipping problems and could not be converged. It is extremely promising that the results from the two active spaces [(12/11) and (8/7)] are very similar. The relative energies differ by less than 0.5 kcal mol^{-1} for all of the states except the high-lying 1^5A state, for which the difference is only 1.4 kcal mol^{-1}.

Table 15. Total (hartree) and relative (kcal mol^{-1}) SA-CASSCF/6-31G* [1^1A/2^1A,3^1A/1^3A,2^3A/1^5A] energies for the relevant electronic states of oxo-Mn(salen).

	SA-CASSCF(12/11)		SA-CASSCF(8/7)	
State	Total energy	Relative energy	Total energy	Relative energy
1^1A	−2251.430 527	0.00	−2251.401 094	0.00
2^1A	−2251.376 300	34.03	−2251.346 203	34.44
3^1A	−2251.373 073	36.05	−2251.343 313	36.26
1^3A	−2251.427 234	2.07	−2251.397 173	2.46
2^3A	−2251.426 278	2.67	−2251.396 381	2.96
1^5A	−2251.362 197	42.88	−2251.330 493	44.30

The second state-averaging approach, [1^1A,2^1A,3^1A/1^3A,2^3A/1^5A], averages separately over each of the spin manifolds, requiring three separate calculations. The only impact this has on the energies is upon the singlet states, which are now required to be orthogonal and described by a common set of orbitals. The total and relative energies are presented in Table 16. From the results we see that, by averaging over all of the singlet states, we have significantly raised the energy of the 1^1A state. This could either be the result of requiring a common set of molecular orbitals or the result of the imposed orthogonality of the singlet states. A closer examination of the results implies that the effect is most likely the result of the imposed orthogonality. The energies of the 2^1A and 3^1Astates are much less affected by the changes, the increase in total energy being an order of magnitude less for these states than for the 1^1A state.

Table 16. Total (hartree) and relative (kcal mol^{-1}) SA-CASSCF/6-31G* [1^1A,2^1A,3^1A/1^3A,2^3A/1^5A] energies for the relevant electronic states of oxo-Mn(salen).

	SA-CASSCF(12/11)		SA-CASSCF(8/7)	
State	Total energy	Relative energy	Total energy	Relative energy
1^1A	−2251.424 606	1.65	−2251.395 150	1.27
2^1A	−2251.375 485	32.47	−2251.345 394	32.49
3^1A	−2251.372 129	34.58	−2251.342 357	34.40
1^3A	−2251.427 234	0.00	−2251.397 173	0.00
2^3A	−2251.426 278	0.60	−2251.396 381	0.63
1^5A	−2251.362 197	40.81	−2251.330 493	41.84

The final averaging scheme, [1^1A,2^1A,3^1A,1^3A,2^3A,1^5A], attempts six states from a single CASSCF. The total and relative energies are presented in Table 17. This averaging scheme imposes no additional orthogonality constraints on the system as the states of different spin symmetries are orthogonal by construction. As such, the predicted relative energies are changed only slightly in comparison with those from the SA-CASSCF [1^1A,2^1A,3^1A/1^3A,2^3A/1^5A] results presented in Table 16. Both approaches predict the ground state to be characterized by a pair of nearly degenerate triplet states, followed by a low-lying closed-shell singlet state. These results clearly demonstrate that the ordering of the relevant electronic states depends strongly upon the choice of averaging schemes. However, it is indeed promising that the smaller active space gives results consistent with those from the larger active space.

Table 17. Total (hartree) and relative (kcal mol^{-1}) SA-CASSCF/6-31G* [1^1A,2^1A,3^1A,1^3A,2^3A,1^5A] energies for the relevant electronic states of oxo-Mn(salen).

	SA-CASSCF(12/11)		SA-CASSCF(8/7)	
State	Total energy	Relative energy	Total energy	Relative energy
1^1A	−2251.419 298	4.15	−2251.389 802	3.79
2^1A	−2251.374 790	32.08	−2251.344 722	32.08
3^1A	−2251.372 001	33.83	−2251.342 249	33.63
1^3A	−2251.425 905	0.00	−2251.395 843	0.00
2^3A	−2251.424 670	0.78	−2251.394 843	0.63
1^5A	−2251.352 430	46.11	−2251.320 483	47.29

A molecular orbital diagram of the most important orbitals is presented in Figure 27 The ground state of the system, 1^1A (at least according to our most flexible SA-CASSCF averaging scheme) corresponds to the closed-shell configuration $\sigma\left(\text{Mn-O}_{\text{ax}}\right)^2 \pi_1\left(\text{Mn-O}_{\text{ax}}\right)^2 \pi_2\left(\text{Mn-O}_{\text{ax}}\right)^2 d[xy]^2$. The 1^3A and 2^3A states and the open-shell 2^1A and 3^1A states correspond to $d[xy] \rightarrow \pi^*\left(\text{Mn-O}_{\text{ax}}\right)$. It is interesting to note the extent to which the $\pi\left(\text{Mn-O}_{\text{ax}}\right)$ and the $\pi^*\left(\text{Mn-O}_{\text{ax}}\right)$ pairs of molecular orbitals are split. This leads to a slight splitting of the triplet states which is magnified in the pair of open-shell singlet states (approximately 2 kcal mol^{-1}). This is further exemplified by the CI coefficients for the two states. The coefficients for the $d[xy]\alpha\,\pi_1^*\left(\text{Mn-O}_{\text{ax}}\right)\alpha$ and the $d[xy]\alpha\,\pi_2^*\left(\text{Mn-O}_{\text{ax}}\right)\alpha$ configurations are 0.14 and 0.85 for the 1^3A state and 0.85 and −0.14 for the 2^3A state. The 1^5A state corresponds to a $\pi\left(Mn-O_{ax}\right) \rightarrow \pi^*\left(Mn-O_{ax}\right)$ excitation from the triplet states. Again, it is interesting to note that the leading configuration is $\sigma^2\pi_2^2 d^1\pi_1^1\pi_1^{*1}\pi_2^{*1}$ with a weight of 0.96. The corresponding $\sigma^2\pi_1^2 d^1\pi_2^1\pi_1^{*1}\pi_2^{*1}$ configuration has a weight of less than 0.05.

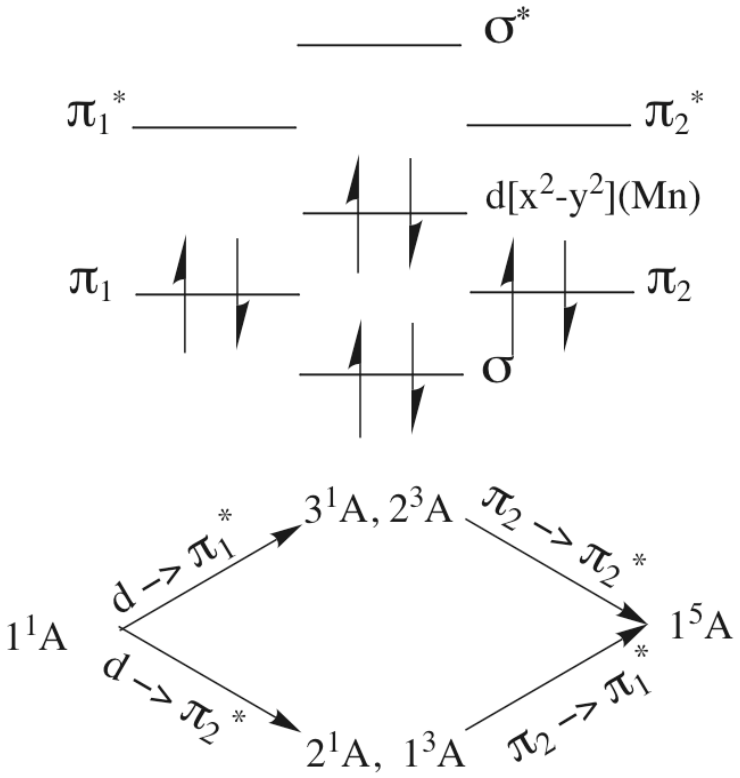

Figure 27. Diagram of the key orbitals in the description of the low-lying electronic states of oxo-Mn(salen). Below these are the dominant excitations that lead to the excited states from the closed-shell 1^1A state.

The largest error in the CASSCF computations might be thought to be the lack of dynamical electron correlation, which is captured only indirectly in CASSCF, but may be included explicitly via CASPT2 or other multi-reference methods. Previous work by Ivanic using the multi-reference MP2 [213] (MRMP2) method indicates that the effect of dynamical correlation is rather small (contributing 0.6 and 5.5 kcal mol^{-1} respectively to the relative energies of the 1^3A and 1^5A states), in both cases increasing the energy relative to the 1^1A state. This is consistent with the observations that closed-shell systems exhibit larger dynamical correlation effects and thus tend to be overestimated energetically at the CASSCF level [213]. The next most important source of error might be the basis set. It is well known that wave function based approaches are typically slower to converge with respect to basis set than DFT based approaches. We have

investigated the basis set convergence of the relative SA-CASSCF energies using a 6-311G*basis set. The SA-CASSCF/6-311G*[1^1A/2^1A,3^1A/1^3A,2^3A/1^5A] and SA-CASSCF/6-311G*[1^1A,2^1A,3^1A,1^3A,2^3A,1^5A] total energies are presented in Table 18 and Table 19, respectively, along with the changes in total and relative energies for the various electronic states. The results indicate that basis set effects may indeed be more important for determining the ground spin state of the system than are the effects of dynamical correlation. In the most flexible averaging scheme, increasing the size of the basis raises the relative energies of all of the triplet and open-shell singlet states by approximately 1.2 kcal mol^{-1}, with the relative energy of the 1^5A state increasing by only 0.39 kcal mol^{-1}. Although the more restrictive, [1^1A,2^1A,3^1A,1^3A,2^3A,1^5A], choice of averaging does not reproduce the proper ordering of the electronic states, the 1^1A and 1^3A states are still stabilized relative to the triplet states upon going to the larger basis. Finally, even though none of the atoms are particularly heavy, one might suppose that relativistic effects could be significant due to the Mn atom. Ivanic *et al.* examined the importance of relativistic effects on the electronic state ordering of this system by comparing all-electron calculations to those employing a relativistic effective core potential [207]. Although the results indicated that the relativistic effects were negligible for determining the electronic state ordering, we have examined the importance of such effects using the Cowan-Griffin relativistic correction to the all-electron calculations. The results are presented in Table 20. From the results one can see that, although the relativistic corrections to the total energies are quite large, the contribution of the relativistic effects to the relative energies is typically less than 0.1 kcal mol^{-1}.

Table 18. Total energies (hartree) at the SA-CASSCF/6-311G* [1^1A/2^1A,3^1A/1^3A,2^3A/1^5A] level of theory and changes in total energies (hartree) and relative energies (kcal mol^{-1}) for the relevant electronic states of oxo-Mn(salen).

	SA-CASSCF(12/11)			SA-CASSCF(8/7)		
State	Total energy	ΔE_{tot}	ΔE_{rel}	Total energy	ΔE_{tot}	ΔE_{rel}
1^1A	−2251.745 514	−0.314 987	0.00	−2251.715 642	−0.314 548	0.00
2^1A	−2251.689 302	−0.313 002	1.24	−2251.658 787	−0.312 584	1.24
3^1A	−2251.686 166	−0.313 094	1.19	−2251.655 956	−0.312 643	1.19
1^3A	−2251.740 367	−0.313 133	1.16	−2251.709 875	−0.312 702	1.16
2^3A	−2251.739 428	−0.313 150	1.15	−2251.709 073	−0.312 692	1.16
1^5A	−2251.676 429	−0.314 231	0.47	−2251.644 424	−0.313 931	0.39

Table 19. Total energies (hartree) at the SA-CASSCF/6-311G* [1^1A,2^1A,3^1A,1^3A,2^3A,1^5A] level of theory and changes in total energies (hartree) and relative energies (kcal mol^{-1}) for the relevant electronic states of oxo-Mn(salen).

	SA-CASSCF(12/11)			SA-CASSCF(8/7)		
State	Total energy	ΔE_{tot}	ΔE_{rel}	Total energy	ΔE_{tot}	ΔE_{rel}
1^1A	−2251.732 704	−0.313 406	−0.23	−2251.732 704	−0.313 406	−0.23
2^1A	−2251.687 477	−0.312 687	0.22	−2251.687 477	−0.312 687	0.22
3^1A	−2251.684 653	−0.312 652	0.24	−2251.684 653	−0.312 652	0.24
1^3A	−2251.738 948	−0.313 043	0.00	−2251.738 948	−0.313 043	0.00
2^3A	−2251.737 650	−0.312 980	0.04	−2251.737 650	−0.312 980	0.04
1^5A	−2251.666 479	−0.314 050	−0.63	−2251.666 479	−0.314 050	−0.63

Table 20. Cowan-Griffin relativistic corrections (hartree) to the energy of the electronic states of oxo-Mn(salen) computed at the SA-CASSCF /6-31G* level of theory and their contribution to the relativer energies (kcal mol^{-1}).

State	E_{rel}	ΔE
1^1A	−9.115 630	0.01
2^1A	−9.115 772	−0.08
3^1A	−9.115 768	−0.08
1^3A	−9.115 645	0.00
2^3A	−9.115 638	0.00
1^5A	−9.116 107	−0.29

Of primary importance when considering the applicability of single-reference based electronic structure theories to the current problem is the multireference nature of the electronic wave function. For each state, Table 21 presents the contribution (CI coefficient) in the CASSCF NO basis for all determinants with a coefficient of 0.15 or

larger. The results show that the triplet states are highly multireference, with the leading determinant in each case capturing only about 72% of the total wave function. A single-determinant description is not expected to be applicable for the open-shell singlet states. However, the leading pair of determinants (the smallest number of determinants capable of describing the open-shell wave function) capture only about 77% of the total wave function for each of these states. This may be contrasted with CASSCF wave functions for the ground state of well-behaved systems. For the H_2O molecule in an aug-ccpVDZ basis set near its equilibrium geometry (R =1.843 45 bohr, Θ=110.60°), the leading closed-shell determinant captures 96% of the CASSCF wave function using a valence active space and a CASSCF-NO basis (the second leading configuration contributes less than 1%). The coefficient of the leading determinant of the closed-shell 1^1A state of our Mn(salen) model system, 0.90, is larger than that for the triplet states but is still smaller than what one might expect for a well-behaved single-reference system. The 1^5A state, with a leading coefficient of 0.96, appears to be the most highly single-reference of the states considered. It is clear from the CI coefficients that the triplet and singlet states are highly multireference in nature. As such, accurate relative energies for these states should not be expected from single-reference approaches.

Table 21. Leading configurations in the description of the low-lying electronic states of oxo-Mn(salen) computed at the SA-CASSCF(8/7)/6-31G* [1^1A/2^1A,3^1A/1^3A,2^3A/1^5A] level of theory.

State	Configuration	Coefficient
1^1A	$(d)^2(\sigma)^2(\pi_1)^2(\pi_2)^2$	0.90
	$(d)^2(\sigma)^2(\pi_1)^2(\pi_2^*)^2$	–0.18
	$(d)^2(\sigma)^2(\pi_2)^2(\pi_1^*)^2$	0.17
2^1A	$(\sigma)^2(\pi_1)^2(\pi_2)^2(d)\alpha(\pi_2^*)\beta$	0.62
	$(\sigma)^2(\pi_1)^2(\pi_2)^2(d)\beta(\pi_2^*)\alpha$	–0.62
	$(\sigma)^2(\pi_2)^2(\pi_1^*)^2(d)\alpha(\pi_2^*)\beta$	–0.15
	$(\sigma)^2(\pi_2)^2(\pi_1^*)^2(d)\beta(\pi_2^*)\alpha$	0.15
3^1A	$(\sigma)^2(\pi_1)^2(\pi_2)^2(d)\alpha(\pi_1^*)\beta$	0.62
	$(\sigma)^2(\pi_1)^2(\pi_2)^2(d)\beta(\pi_1^*)\alpha$	–0.62
	$(\sigma)^2(\pi_1)^2(\pi_2^*)^2(d)\alpha(\pi_1^*)\beta$	–0.15
	$(\sigma)^2(\pi_1)^2(\pi_2^*)^2(d)\beta(\pi_1^*)\alpha$	0.15
1^3A	$(\sigma)^2(\pi_1)^2(\pi_2)^2(d)\alpha(\pi_2^*)\alpha$	0.85
	$(\sigma)^2(\pi_1)^2(\pi_2)^2(d)\alpha(\pi_2^*)\alpha$	–0.24
	$(\sigma)^2(\pi_2)^2(\pi_1^*)^2(d)\alpha(\pi_2^*)\alpha$	–0.22
	$(\sigma)^2(\pi_2)^2(\pi_1^*)^2(d)\alpha(\pi_2^*)\alpha$	0.15
2^3A	$(\sigma)^2(\pi_1)^2(\pi_2)^2(d)\alpha(\pi_1^*)\alpha$	0.85
	$(\sigma)^2(\pi_1)^2(\pi_2)^2(d)\alpha(\pi_1^*)\alpha$	–0.24
	$(\sigma)^2(\pi_1)^2(\pi_2^*)^2(d)\alpha(\pi_1^*)\alpha$	0.22
	$(\sigma)^2(\pi_1)^2(\pi_2^*)^2(d)\alpha(\pi_1^*)\alpha$	–0.15
1^5A	$(\sigma)^2(\pi_2)^2(\pi_1)\alpha(d)\alpha(\pi_1^*)\alpha(\pi_2^*)\alpha$	0.96
	$(\pi_2)^2(\sigma^*)^2(\pi_1)\alpha(d)\alpha(\pi_1^*)\alpha(\pi_2^*)\alpha$	–0.16

The most accurate calculations presented here, employing large basis sets and relativistic corrections, predict the ground state to be the closed-shell 1^1A state. Lying slightly more than 3 kcal mol^{-1} higher in energy is a pair of nearly degenerate triplet states. A pair of open-shell singlet states lies above 30 kcal mol^{-1}, with the 1^5A state at greater than 40 kcal mol^{-1}. It is anticipated that corrections for dynamical correlation and finite basis sets will tend to stabilize the lowest closed-shell singlet state relative to the other states.

Single-Reference Methods

As noted above, there exist major discrepancies in the description of the asymmetric epoxidation reaction catalyzed by oxo-Mn(salen) when using two of the most commonly employed density functionals. In Table 22 we present the relative energies for the various electronic states from several restricted Kohn-Sham (RKS) and restricted open-shell Kohn-Sham (ROKS) approaches as well as restricted and restricted open-shell Hartree-Fock (RHF/ROHF). Comparing BP86 to BLYP and B3P86 to B3LYP, it is obvious that the spin-state splittings are largely insensitive to the choice of correlation functional. Both B3LYP and B3P86 predict the ground state to be the 1^3A state followed by the closed-shell singlet at 2–3 kcal mol^{-1}. The quintet is predicted to be less than 20 kcal mol^{-1} above the triplet. Both BP86 and BLYP predict the closed-shell 1^1A state to be the ground state, with the 1^3A state around 1–2 kcal mol^{-1}. The quintet is predicted to lie a little more than 20 kcal mol^{-1} higher in energy. It is clear from the results that the hybrid functionals (B3LYP and B3P86) stabilize the high-spin states relative to the nonhybrid approaches (BLYP and BP86). There are a few things to note with respect to the RHF/ROHF results. Exchange terms due to the Pauli exclusion principle result in dramatic overstabilization of the high-spin states. The spin-state stability increases with increasing spin multiplicity, predicting the quintet to be the lowest of the three spin states considered, followed by the triplets and then the singlets. Indeed, a ROHF calculation on the septet state predicts this to be even lower than the quintet by almost 30 kcal mol^{-1}. It is also interesting that there exist multiple solutions to the HF equations for each of the spin multiplicities, differing at one point by more than 15 kcal mol^{-1} in energy. It should also be mentioned that all of the RHF/RKS singlet states exhibit large restricted-

unrestricted orbital instabilities, although the negative orbital Hessian eigenvalues are smaller in magnitude for DFT approaches ($|\varepsilon| < 0.05$) than for HF ($|\varepsilon| > 0.25$).Following these instabilities leads to slightly spin-contaminated un-restricted Kohn-Sham (UKS) solutions and a highly spincontaminated UHF solution as discussed below. We are currently unable to perform stability analysis on the ROHF/ ROKS wave functions.

Table 22. Energies (kcal mol^{-1}) relative to the lowest triplet state for restricted single-reference methods using a 6-31G* basis.

Method	State	Energy
B3LYP	Singlet	1.85
	Triplet	0.00
	Quintet	17.65
BP86	Singlet	−1.30
	Triplet	0.00
	Quintet	24.69
BLYP	Singlet	−1.99
	Triplet	0.00
	Quintet	23.65
B3P86	Singlet	2.92
	Triplet	0.00
	Quintet	13.67
B3LYP*	Singlet	0.82
	Triplet	0.00
	Quintet	15.38
HF	Singlet	41.33
	Singlet	41.39
	Triplet	15.31
	Triplet	0.00
	Quintet	−37.94
	Quintet	−38.10

Table 23 presents the relative energies, $\langle \hat{S}^2 \rangle$ values, and orbital Hessian eigenvalues of all stable and unstable solutions obtained using unrestricted single-reference approaches. Like RHF, UHF theory also results in a very unphysical

description of the electronic state ordering. Indeed, the relative energies of the states considered are completely different than our best CASSCF results presented above. Like ROHF, UHF predicts a septet ground state, and it places the lowest quintet state 10 kcal mol^{-1} below the lowest singlet state, in contradiction to our best CASSCF prediction of a singlet ground state. However, the overstabilization of the quintet and septet is significantly reduced compared to the ROHF results. Concomitant with the very poor UHF relative energies, Table 23 indicates that the UHF wave functions are all highly spin contaminated. The UKS DFT solutions also exhibit spin contamination, although to a much smaller degree. Just as for ROKS, the UKS energies are much less sensitive to the choice of correlation functional than to the treatment of exchange. Additionally, the UKS relative energies are very similar to those obtained using ROKS (typically within 1 kcal mol^{-1}), the only exception being the B3LYLP results Table 23 indicates multiple UHF solutions, just as for ROHF. However, while we observed only one RKS/ROKS solution for each of the singlet, triplet, and quintet states, we observe additional high-spin solutions for unrestricted BP86, BLYP, and B3LYP* (which has 15% HF exchange) [246]. For the unrestricted wave functions, we were able to perform a stability analysis, and the lowest eigenvalues of the orbital Hessian are presented in the table. We find that the "extra" solutions found for UKS but not for ROKS all correspond to unstable wave functions (with negative orbital Hessian eigenvalues). Perhaps surprisingly, however, all of the UHF solutions we obtained are stable, indicating that they are local minima in orbital rotation space. One might suppose that the "wrong" UHF solutions would exhibit very small Hessian eigenvalues. However, from Table 23 we see that the smallest eigenvalues for these wrong solutions may be larger than those for the lowest-energy

UHF solution. Given that these solutions are locally stable, it is not immediately clear how one would know whether such a high-lying solution had been obtained (short of a search for multiple solutions as we have done here). Furthermore, none of the procedures employed for generating the initial guess orbitals consistently provides for the correct SCF solution. The core Hamiltonian appears to be a rather poor initial guess for this particular system, and for the optimization procedures we employed, it always results in the UHF solution that is the highest in energy (of those we found) for the given multiplicity. Using a GWH guess would result in the correct singlet, triplet, and quintet UHF wave functions. However, one would land upon the higher septet result. The only guess to result in the correct septet UHF result was the superposition of atomic densities. However, this particular guess results in the wrong solution for all other states.

Table 23. Energies (kcal mol^{-1}) relative to the lowest triplet state and lowest eigenvalues of the orbital Hessian for unrestricted single-reference methods using 6-31G* basis. (All negative eigenvalues of the molecular orbital Hessian included in this table were from UKS-CUKS orbital instabilities).

Method	State	$\langle S^2 \rangle$	Energy	Eigenvalues
B3LYP	^{1}A	0.52	3.53	0.004,0.033
	^{3}A	2.21	0.00	0.003,0.009
	^{5}A	6.04	11.94	0.007,0.013
	^{7}A	12.07	75.32	0.017,0.018
BP86	^{1}A	0.51	−1.87	0.007,0.033
	^{3}A	2.04	0.00	0.005,0.009
	^{5}A	6.02	29.46	−0.010,0.010
	^{5}A	6.02	24.18	0.006,0.011
	^{7}A	12.02	93.15	−0.003,0.005
	^{7}A	12.03	91.03	0.006,0.011
BLYP	^{1}A	0.47	−2.09	0.007,0.033
	^{3}A	2.04	0.00	0.005,0.010
	^{5}A	6.02	28.22	−0.010,0.011
	^{5}A	6.02	23.08	0.006,0.011
	^{7}A	12.02	91.71	−0.002,0.006
	^{7}A	12.03	89.81	0.005,0.013
B3P86	^{1}A	0.57	3.53	0.004,0.032
	^{3}A	2.21	0.00	0.003,0.008
	^{5}A	6.04	13.42	0.008,0.013
	^{7}A	12.07	77.48	0.016,0.017
B3LYP*	^{1}A	0.51	1.75	0.005,0.033
	^{3}A	2.10	0.00	0.004,0.008
	^{5}A	6.03	20.25	−0.011,0.005
	^{5}A	6.04	14.67	0.007,0.012
	^{7}A	12.06	81.09	0.007,0.008
HF	^{1}A	2.91	40.64	0.003,0.044
	^{1}A	2.33	14.92	0.003,0.026
	^{3}A	2.99	39.79	0.001,0.013
	^{3}A	3.28	0.00	0.001,0.013
	^{3}A	3.35	13.50	0.003,0.027
	^{5}A	6.03	27.91	0.001,0.013
	^{5}A	6.53	4.27	0.003,0.016
	^{7}A	13.16	10.20	0.017.0.085
	^{7}A	12.43	−2.32	0.003,0.012

Conclusions

We have examined several electronic states of the oxo- Mn(salen) model system, some of which have not been previously explored, using robust *ab initio* methods. SA-CASSCF/6-311G*calculations predict the closed-shell 1^1A state to be the ground spin state, with the 1^3A and 2^3A states slightly more than 3 kcal mol^{-1} higher in energy. Such a difference is within the potential errors of the calculations. However, it is anticipated that

calculations incorporating larger basis sets and corrections for dynamical correlation will push the singlet state lower in energy relative to the triplets. A pair of nearly degenerate open-shell singlet states, 2^1A and 3^1A, lie around 35 kcal mol^{-1} followed by the high-spin 1^5A state at a little more than 40 kcal mol^{-1}. It is currently unclear what significance the presence of these previously unexplored electronic states may have in understanding the chemistry of this system. The proximity of so many states may result in highly complex potential energy surfaces involving conical intersections and avoided crossing effects. It is evident from this work that even a definitive determination of the ground spin state for this system will require very extensive treatments of electron correlation in conjunction with very large basis sets. As previously described by Ivanic *et al.* [213], in the closed-shell singlet state, we observe triple-bond character between the manganese metal and the axial oxygen atom. Through detailed analysis of the CI expansion from CASSCF calculations, we have demonstrated the multireference character of this system. Much care should be taken when applying single-reference based approaches to such problems.

We have examined the applicability of several single-reference SCF approaches for describing the electronic structure of the current model system, while exploring the existence of multiple SCF solutions and their potential impact on previous theoretical studies. Hartree-Fock theory has been demonstrated to give an extremely poor description of this system and does not provide a reliable starting point for theoretical investigations. The existence of multiple SCF solutions and large spin-contamination effects in UHF based approaches makes the use of HF and even post-HF single-reference theories suspect. If one were to use standard single-reference approaches, such as the coupled-cluster theories employed by Abashkin *et al.* [213], several potential problems could

arise. First of all, there is the possibility that the HF computation would land on a higher-energy solution which would then be employed as a starting point for the post-HF correlation model. Secondly, even the stable HF solutions provide a very unphysical description for the ordering and would require very large electron-correlation corrections.

These considerations may help explain the rather different energetics found by Abashkin *et al.* [213] using CC theory through perturbative triple excitations [CCSD(T)] with a polarized double-zeta basis and a similar model system: 0.0 (singlet), 14.5 (triplet), and 10.9 kcal mol^{-1} (quintet). It is unclear from the CCSD(T) total energies reported by these authors if they might have resulted from the use of higher-lying HF solutions. However, we note that these computations were performed using GAUSSIAN 98 [11], which uses a pseudoextended Huckel guess by default . A very interesting 1999 study by Vacek *et al.* [246] demonstrated that Huckel guess orbitals led to the lowest-energy HF wave function only 14% of the time for a set of 80 organometallic molecules. Hence, in the absence of further information, it is possible that the study by Abashkin *et al.* [213] may have used one of these higher-lying HF reference solutions. Assuming that the lowest-energy HF references were employed, the discrepancy between our CASSCF results and the CCSD(T) results may very well be a consequence of the multireference nature of the singlet and triplet states. Although the quintet state appears to be primarily single reference, the singlet and triplet states are clearly multireference. The lower relative energy of the 1^5A state predicted by CCSD(T) may thus be the result of CC theory predicting too high a total energy for the singlet and triplet states, for which single-reference formalisms may not be applicable.

DFT approaches provide a much more physical description than does HF theory. Although all DFT approaches predict the lowest singlet and triplet states to lie very close in energy, the hybrid functionals stabilize the triplet state relative to the nonhybrid approaches. All functionals explored place the quintet state much lower in energy than predicted by the CASSCF method, with the hybrid functionals again stabilizing the high-spin states relative to the nonhybrid approaches. Again, this may very well be a result of the multireference nature of the singlet and triplet states. Although a few (unstable) SCF solutions were observed with some of the density functionals, we did not find as many DFT solutions as HF solutions. The nonhybrid approaches BP86 and BLYP give results that appear to be in better agreement with the CASSCF results (or with previous coupled-cluster results) [213] than the hybrid DFT approaches, but it would be difficult to advocate their superiority based solely upon the results presented here. It is clear from previous work that the choice of functional provides for qualitatively different results in mechanistic studies involving the current system. A definitive answer as to what functional, if any, is capable of accurately describing the mechanisms of Mn(salen) catalyzed epoxidation reactions remains as yet unanswered.

CHAPTER 7

THE ELECTRONIC STRUCTURE OF 3D0-METAL SALENS

In an effort to ascertain the reliability of DFT for exploring metal-salen chemistry [247], we examine the electronic structure of a series of 3d0 metal-salens [Sc(III), Ti(IV), V(IV), Cr(VI), and Mn(VII)] using high-level *ab initio* methods as benchmarks. Possessing an empty 3d-shell, it is anticipated that the d0-metal salens will be the most well described by single-reference approaches of all the metal-salen systems. The salen ligand is probably the most highly employed synthetic ligand system to date, having earned the title of "privileged catalysts" by Yoon and Jacobsen [170]. Complexes of salen ligands with first- and second-row transition metals have been employed in the catalysis of a plethora of chemical transformations [116, 122, 162, 166, 170, 171, 180-182, 248] ranging from conjugate additions [248-250] and Diels-Alder reactions [251-253] to olefin epoxidations [121, 167, 205, 254, 255] and cyclopropanations [163, 256-258]. Although the goal of this work is to benchmark results from DFT against reliable *ab initio* data and not to directly explore the chemistry of any particular experimentally-employed metal-salen catalysts, it should be noted that many d0-metal salens have been synthesized for metal-salen catalyzed reactions. Sc(III)-salens have been employed as highly efficient catalysts for Diels-Alder reactions [253, 259]. Ti(IV)-salens have seen extensive use as catalysts for asymmetric ring-opening [260-262], while Ti(IV)- and V(V)-salens have been routinely employed as catalysts in cyano-addition reactions [181, 263-268]. The ability of electronic-structure methods to reliably model metal-salen catalyzed chemical transformations will open the doorway to the theoretical exploration and the understanding of varied and numerous catalytic pathways.

Although transition-metal systems have long been of interest to researchers developing and testing multi-reference methods in electronic structure theory [88, 269], the application of such methods to large metal-ligand systems such as these remains far from routine [137]. Multi-reference methods are far less "black box" than traditional approaches of electronic structure theory and their application to the large systems that are often of chemical interest remains challenging even for specialists in the field. The necessity of defining an appropriate active space and the ability to overcome the often-encountered difficulties in the non-linear optimization of such wave functions requires a certain amount of experience and chemical insight. However, multi-reference approaches (when carefully applied) are capable of providing highly reliable theoretical results for systems exhibiting strong non-dynamical correlation effects [88, 152].

In the remainder of this chapter we compare DFT results (geometries and relative energies) to MP2, CCSD(T), CASSCF, CASPT2, and CASPT3 for the lowest singlet, triplet, and quintet states of a series of 3d0-metal salens. For this benchmark study we have employed a reduced model of the salen ligand, model_1[$X = \text{none}$, $Y = \text{none}$, $\text{M} \in \{\text{Sc(III)}, \text{Ti(IV)}, \text{V(V)}, \text{Cr(VI)}, \text{Mn(VII)}\}$] from Figure 25. This is the model of the salen ligand most commonly applied in theoretical studies, having been employed in recent theoretical work by us [137] and others [204, 206, 207]. It is anticipated that the trends observed will guide the future theoretical investigations of metal-salen catalyzed chemistry.

Theoretical Approach

All DFT calculations were performed with Jaguar 5.5 [4]. The computations were performed using three of the most common combinations of exchange and correlation

functionals; the combination of Becke's 1988 exchange functional [232] with Perdew's 1986 [234] functional for correlation referred to as BP86, the combination of Becke's 1988 exchange functional with the Perdew Wang 1991 functional for correlation [270] referred to as BPW91, and the combination of Becke's three-parameter hybrid functional [231] with the correlation functional by Lee, Yang, and Parr [233] referred to as B3LYP. Unless otherwise stated, all DFT computations employed the pseudospectral implementation of DFT [6] and a fine grid as found in Jaguar 5.5, and the Los Alamos basis-sets and corresponding effective core potentials of Hay and Wadt (LANL2DZ) for all transition-metal atoms [271] and a 6-31G* basis for all other atoms [272]. Geometries were completely optimized (RMS gradient 10^{-3}) for the lowest singlet, triplet, and quintet states using each functional. The nature of the stationary points was verified by computing analytic frequencies.

Geometries were also optimized (RMS gradient 10^{-3}) at the MP2 [17] level with ACES II [24] and the CASSCF [51] level with MOLPRO 2006.1 [28]. Unless otherwise stated, the converged BP86 geometries were employed as a starting point for these optimizations. Active spaces for CASSCF computations were chosen by examination of the CI vector from large CAS-CI [36] calculations performed in a CISD [36] natural orbital basis. Starting orbitals for the CASSCF computations were generated from CASSCF natural orbitals computed in the smaller STO-3G [242, 243, 273] basis. The STO-3G CASSCF computations employed a CISD natural orbital guess. Such an approach has been shown to give reliable convergence for CASSCF computations on other metal-salen systems, when more conventional approaches have failed to do so [137]. The active spaces and optimized states for each system will be described in the

discussion, employing the notation from our previous work [137]. Single-point energy calculations were computed at the MP2-optimized geometries using coupled-cluster theory including single and double excitation operators (CCSD) and perturbative triples (CCSD(T)) with MOLPRO 2006.1. Single-point energy calculations were computed at the CASSCF-optimized geometries at the complete active-space second-order and third-order perturbation theory (CASPT2 and CASPT3) with MOLPRO 2006.1. Due to limitations on the number of correlated orbitals in the CASPT3 program, CASPT3 calculations were computed with the lowest σ-orbitals frozen and combined as corrections to the internally contracted CASPT2 calculation. All wavefunction-based computations employed a 6-31G* basis and the frozen-core approximation using a small core, defined as 1s2s2p3s for first transition-row metals.

Optimized geometries were compared and the least root-mean-squared deviations (LRMSD) in molecular geometries were computed using the Visual Molecular Dynamics (VMD) program [274]. Molecular orbital isosurfaces were generated (contour value of 0.05) using MOLEKEL [275]. Numerous diagnostics to ascertain the multi-reference character of the wave function based upon amplitudes from MP2 or CCSD calculations have been developed [276-281]. To assess the multi-reference character of the electronic states in 3d0-metal salens, we report two of the most commonly employed diagnostics; the T1-diagnostic [276] and the D1-diagnostic [281] from the converged CCSD calculations. The T1-diagnositc, based upon the Euclidian norm of the t_1 vector from a CCSD calculation, provides information about the average magnitude of the singles amplitudes while the D1-diagnostic, based upon the 2-norm of the t_1 vector, provides information about the largest singles amplitudes. As suggested by Lee [277], we have

also examined the ratio of the T1-diagnostic and the D1-diagnostic. As Lee points out [277], "the T1/D1 ratio itself does not indicate how well the coupled-cluster approach is performing – it is only a measure of the molecular electronic structure homogeneity." Lee demonstrates that in a completely homogeneous system the ratio (T1/D1) tends to $1/\sqrt{2}$ and that in molecular systems it will deviate from the value by becoming less than $1/\sqrt{2}$. When T1/D1 is small is an indication that there is a large variation in the orbital rotation parameters. Additional information about the multi-reference nature of the electronic states has been provided by examination of the leading determinants (and coefficients) from the CASSCF CI expansions.

Results and Discussion

None of the M(salen) complexes studied contain any symmetry elements, and therefore all calculations were performed in C_1 symmetry. The salen ligand does, however, form a pseudo-square-planar coordination sphere around the central metal atom. The selection of appropriate active spaces for the construction of the CASSCF wave functions requires a certain amount of chemical insight, thus it is useful to consider the important properties of the electronic structure of metal-salen systems before proceeding further. The four coordinating atoms [O,N,N,O] induce a well known splitting of the metal d-orbital energy levels. Two typical d-orbital splitting diagrams for square-planar coordination presented in the literature are displayed in Figure 28. The degenerate (nearly degenerate for the case of nonsymmetrical coordination) d_{xz} and d_{yz} orbitals are typically considered to be the lowest in energy and this is typically true in the weak-field case. The d_{xz} and d_{yz} orbitals are followed closely by the d_{z^2} orbital, and these are

energetically well separated from the d_{xy} and the much higher lying $d_{x^2-y^2}$ orbitals. Strong ligand fields, mixing of the s and d_{z^2} orbitals, or strong metal-ligand covalency have been shown to result in a flipping of the ordering of the d_{xz} and d_{yz} orbitals and the d_{z^2} orbital [282-284]. This splitting will play heavily into the construction and interpretation of the active spaces discussed below, as the metal d-orbitals most likely to contribute to the electronic structure will be the low-lying d_{xz}, d_{yz}, and d_{z^2} orbitals. To ascertain the important electronic effects of the salen ligand and further divulge the chemistry taking place in the metal-salen systems, RHF/6-31G* wave functions were constructed (consisting of 54 doubly occupied molecular orbitals) at the BP86 1^1A optimized geometries and the occupied orbitals were localized via Edmiston-Ruedenberg (ER) localization [240]. The anticipated σ bonds occurring in the salen ligand are observed along with the N and O lone pairs involved in dative bonding with the central metal atom. Each O atom has an additional lone pair that is not involved in any bonding interactions. The most important feature observed for the electronic structure is the presence of six π-type orbitals on the salen ligand; two representing C-O π bonds, two representing C-N π bonds, and two C-C-C (three-center-two-electron) π bonds hereafter referred to as $R\pi_1$ and $R\pi_2$. These are displayed in Figure 29 from the ER localized orbitals of Sc(III)-salen. Given the absence of metal d electrons for the systems studied here (at least in the formal oxidation state picture) it is anticipated that the low-lying electronic states will be dominated by the closed-shell electronic configuration and either ligand $\pi \rightarrow \pi^*$ excitations or $\pi \rightarrow d$ ligand-to-metal excitations, the latter becoming increasingly important as the formal oxidation state of the metal center is increased. The

construction and interpretation of the active spaces for each system and the nature of the low-lying electronic states will be discussed in detail in the following sections.

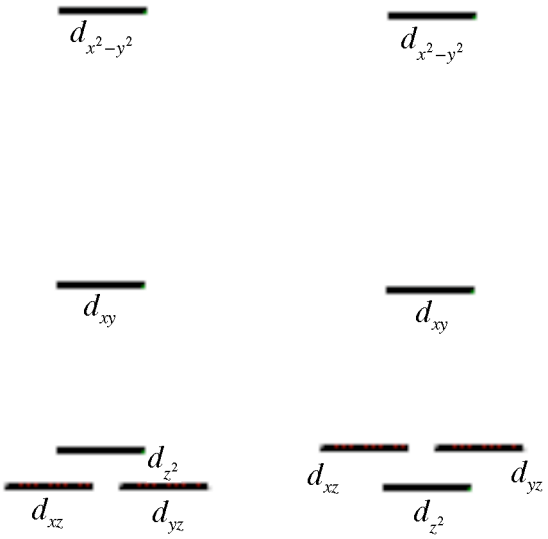

Figure 28. Two commonly presented d-orbital splitting diagrams for a square-planar coordination geometry.

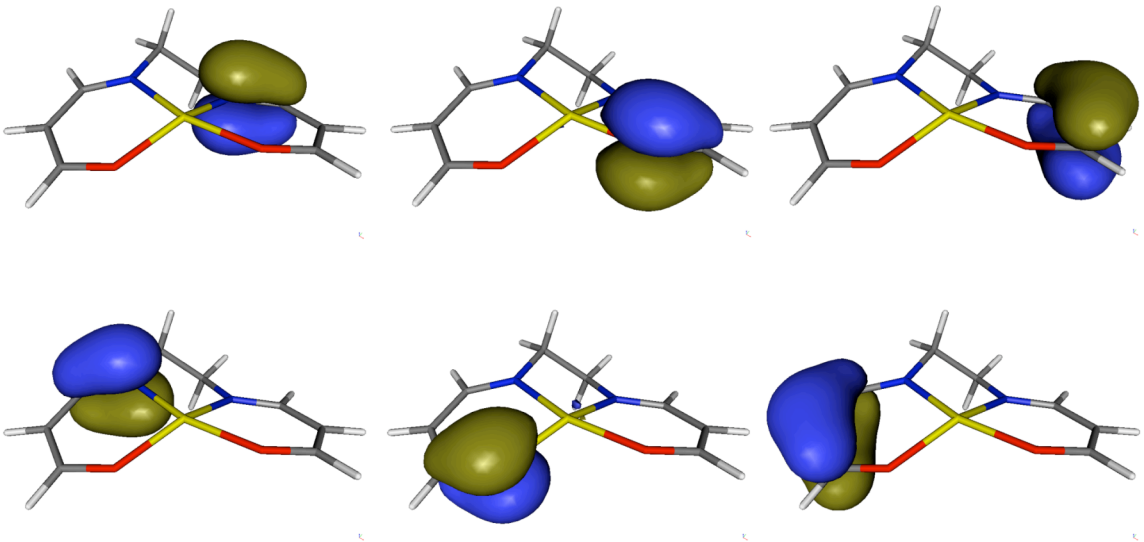

Figure 29. Figure of the Edmiston-Ruedenberg localized C-Nπ (left), C-Oπ (center), and three-center-two-electron Rπ orbitals (right) of the salen ligand from a HF/6-31G* calculation of the singlet state of Sc(III)-salen.

Sc(III)-Salen

For Sc(III)-salen, as anticipated, all DFT calculations predict a closed-shell singlet ground state well separated from the lowest triplet and quintet states. The relative energies from all DFT and *ab initio* calculations are included in Table 24. As has been observed in other metal-salen systems [137], the DFT relative energies are much less sensitive to the choice of correlation functional than to the choice of exchange functional; the results from BP86 and BPW91 are nearly identical. Somewhat surprisingly, B3LYP predicts larger high-spin/low-spin splittings than the non-hybrid approaches. B3LYP (as a consequence of the HF exchange) is known to overstabilize high-spin states in other metal-salen systems when compared to non-hybrid functionals [137]. Overall, all functionals provide a consistent picture of the electronic structure for Sc(III)-salen; a singlet ground state followed by the triplet state at approximately 50 kcal mol^{-1} and the quintet state at slightly more than 100 kcal mol^{-1}.

Table 24. Relative energies (kcal mol^{-1}) for the low-lying electronic states of Sc(III)-salen computed at various levels of theory.

	CASPT3[a]	CASPT2[a]	CASSCF	CCSD(T)[b]	CCSD[b]	MP2	B3LYP	BP86	BPW91
1^1A	0.00	0.00	0.00	0.00	0.00	0.00	0.00	0.00	0.00
1^3A	64.44	58.36	66.17	62.98	62.30	65.13	52.84	48.00	47.91
2^3A	82.23	77.32	66.17	---	---	---	---	---	---
1^5A	129.16	117.56	132.99	126.59	125.19	130.67	109.85	104.78	104.51

a. Relative energies computed at the CASSCF optimized geometries.
b. Relative energies computed at the MP2 optimized geometries.

It is not completely clear a priori, given that Sc(III)-salen is anticipated to be strongly single-reference, whether CCSD(T) or CASPT3 will provide more reliable relative energies. CAS-CI calculations including 12 electrons in 12 molecular orbitals

reveal the closed-shell singlet ground state and two nearly-degenerate (and highly multi-reference) triplet states. All states appear well described by an active space consisting of four electrons in four spatial orbitals. The geometries of these state were optimized at the SA-CASSCF(4/4)/6-31G*[1^1A,1^3A,2^3A,1^5A] level of theory, where the states in brackets are those included in the state averaging. The SA-CASSCF NO's from the optimized 1^3A state are depicted in Figure 30. The relative energies from all *ab initio* calculations are included in Table 24. Both CASPT3 and CCSD(T) predict a closed-shell ground state, with the first triplet state slightly more than 60 kcal mol^{-1} higher in energy. The quintet is observed at slightly less than 130 kcal mol^{-1}. From Table 24 it is clear that all methods provide similar relative energies for the lowest electronic states.

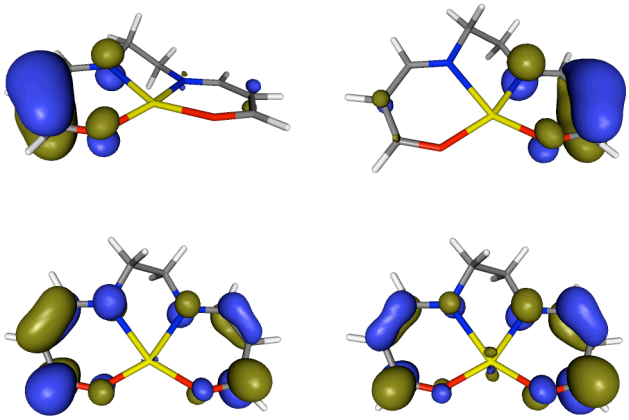

Figure 30. Isosurface plots of the Rπ_1 (upper left), Rπ_2 (upper right), CN/COπ_1^* (lower left), and CN/COπ_2^* (lower right) orbitals that comprise the active space for Sc(III)-salen.

The optimized geometries of the 1^1A, 1^3A, and 1^5A states from DFT, MP2 and CASSCF are overlaid in Figure 31 and the LRMSD's in molecular geometries are tabulated in Table 25. The CASSCF and MP2 geometries are very similar for all states

(LRMSD < 0.1Å). As has been observed with the relative energies above, the geometries from DFT appear highly insensitive to the choice of correlation functional. The geometries from BP86 and BPW91 are nearly indistinguishable (LRMSD < 0.01Å). One noticeable trend in the geometries is that the amount of "exact" exchange appears to have an effect on the out-of-plane puckering of the Sc(III) center. The MP2 and CASSCF geometries predict a nearly planar geometry while the BP86 and BPW91 geometries predict the Sc(III) center to be slightly distorted out of the ring. The B3LYP geometry lies somewhere in between, with the Sc center out of the plane but not to the extent predicted by the non-hybrid functionals. Overall, B3LYP more closely reproduces the *ab initio* geometries with a maximum LRMSD of 0.140Å .

Table 25. LRMSD(Å) in molecular geometries for the 1^1A, 1^3A, and 1^5A states of Sc(III)- and Ti(IV)-salens.

		CASSCF	MP2	B3LYP	BP86	BPW91		
Sc(III)	CASSCF	--- --- ---					CASSCF	Ti(IV)
	MP2	0.049 0.043 0.097	--- --- ---	0.113 0.301 0.343	0.103 0.359 0.279	0.125 0.358 0.287	MP2	
	B3LYP	0.140 0.093 0.125	0.130 0.122 0.131	--- --- ---	0.037 0.081 0.079	0.027 0.086 0.070	B3LYP	
	BP86	0.246 0.184 0.172	0.247 0.211 0.176	0.125 0.099 0.051	--- --- ---	0.028 0.025 0.011	BP86	
	BPW91	0.246 0.188 0.169	0.245 0.214 0.172	0.123 0.103 0.047	0.004 0.006 0.009	--- --- ---	BPW91	

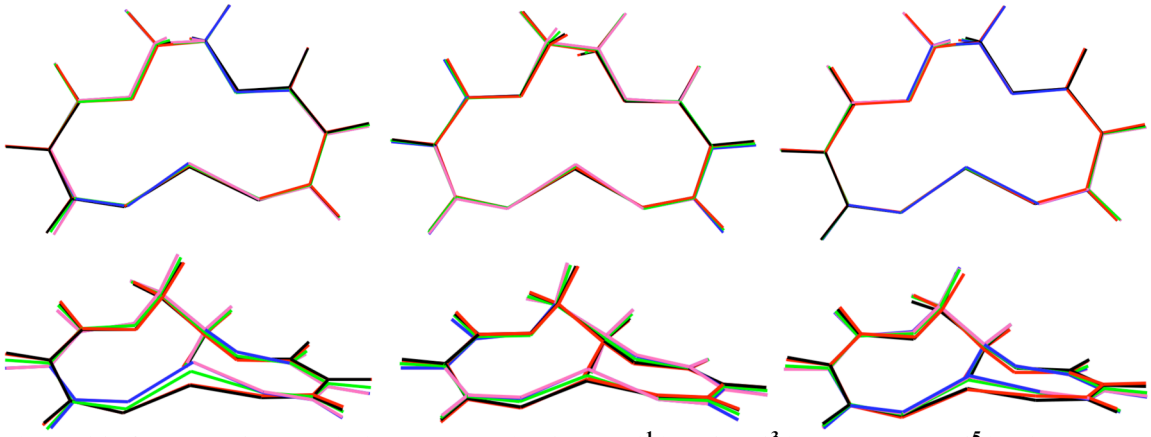

Figure 31. Overlay of the optimized geometries for the 1^1A (left), 1^3A (center), and 1^5A (right) states of Sc(III)-Salen from different levels of theory. The theoretical methods include CASSCF (black), MP2 (red), B3LYP (green), BP86 (blue), and BPW91 (mauve).

One of the central concerns related to the applicability of DFT to these systems is the multi-reference nature of the electronic states. The diagnostics from CCSD calculations are tabulated in Table 26 and the leading determinants in the CASSCF description of the electronic states are tabulated in Table 27. From Table 26 we observe that the T1 diagnostics are slightly larger than typically accepted cut-off values (0.020 and 0.025 for closed- and open-shell systems respectively [276, 279, 281]) although it should be noted these cut-offs are based upon previous studies of small diatomic and polyatomic systems of first- and second-row atoms [276-281]. There have been limited applications of the T1- and D1-diagnostics to large transition-metal containing systems and the values observed from Table 26 for Sc(III)-salen are smaller than those observed in other transition-metal systems where CCSD(T) has been shown to provide reliable results [285, 286]. On the other hand, the D1 diagnostics from Table 26 are considerably larger than the suggested cut-offs, indicating potential problems with the single-reference approximation. However, the small T1/D1 ratios indicate that the non-dynamical effects may be well described by a relatively small active space (such as the four electron in four orbitals active space employed here). The leading determinants from the SA-CASSCF calculations presented in Table 27 clearly demonstrate the multi-reference nature of the electronic states. The leading coefficients for the triplet states (0.783 and 0.778 respectively) are both extremely small and the leading coefficient for the singlet state (at 0.968) is still much smaller than what would be expected for a well-behaved single-reference system.

Table 26. Coupled-cluster diagnostics from CCSD calculations on the 1^1A (top), 1^3A (middle), and 1^5A (bottom) states of 3D0-metal salens.

	T1(CCSD)	D1(CCSD)	T1/D1
	0.0202	0.0785	0.2573
Sc(III)	0.0402	0.2880	0.1396
	0.0369	0.2131	0.1732
	0.0295	0.1318	0.2238
Ti(IV)	0.0394	0.1870	0.2107
	0.0426	0.2642	0.1612
	0.1044	0.8323	0.1254
V(V)	0.0473	0.3227	0.1467
	0.0381	0.2039	0.1867
	0.0738	0.4484	0.1646
Cr(VI)	0.0450	0.2058	0.2185
	0.0746	0.4840	0.1541
	0.0881	0.6620	0.1331
Mn(VII)	0.0404	0.2143	0.1885
	0.0629	0.3597	0.1749

Table 27. Leading determinants from CASSCF calculations on the low-lying electronic states of Sc(III)-salen.

State	Determinant	Coefficient
1^1A	$(R\pi_1)^2(R\pi_2)^2$	0.968
1^3A	$(R\pi_1)^2(R\pi_2)\alpha(\mathrm{CN/CO}\pi_1^*)\alpha$	0.783
	$(R\pi_1)^2(R\pi_2)\alpha(\mathrm{CN/CO}\pi_2^*)\alpha$	0.544
	$(R\pi_2)^2(R\pi_1)\alpha(\mathrm{CN/CO}\pi_1^*)\alpha$	0.197
2^3A	$(R\pi_2)^2(R\pi_1)\alpha(\mathrm{CN/CO}\pi_2^*)\alpha$	0.778
	$(R\pi_2)^2(R\pi_1)\alpha(\mathrm{CN/CO}\pi_1^*)\alpha$	-0.544
	$(R\pi_1)^2(R\pi_2)\alpha(\mathrm{CN/CO}\pi_2^*)\alpha$	-0.210
1^5A	$(R\pi_1)\alpha(R\pi_2)\alpha(\mathrm{CN/CO}\pi_1^*)\alpha(\mathrm{CN/CO}\pi_2^*)\alpha$	1.000

Ti(IV)-Salen

The relative energies for Ti(IV)-salen are included in Table 28. The definition of an appropriate active space for accurately describing the low-lying electronic states of Ti(IV)-salen turned out to be considerably more challenging than for the other systems presented here. The increased formal oxidation state at the metal center results in the expected increased contribution of the metal d-orbitals. However, large CAS-CI computations at the BP86 1^1A geometry predict an electronic structure and active-space requirements very similar to that of Sc(III)-salen presented above. During the geometry optimization at the SA-CASSCF(4/4)/6-31G* [1^1A, 1^3A, 2^3A, 1^5A] level, the CASSCF computations becomes highly unstable as the CN/COπ^* begin to rotate in and out of the active space with the low-lying Ti(IV) d-orbitals. CAS-CI computations at this geometry reveal an increased contribution of the d_{z^2}, d_{xz}, and d_{yz} orbitals as well as an increased number of low-lying electronic states. However geometry optimizations at the SA-CASSCF(4/7)/6-31G* [1^1A, 2^1A, 3^1A, 1^3A, 2^3A, 3^3A, 1^5A, 2^5A] level were unsuccessfull. Thus, the SA-CASSCF results for Ti(IV)-salen are not presented here.

Table 28. Relative energies (kcal mol^{-1}) for the low-lying electronic states of Ti(IV)-salen computed at various levels of theory.

	CCSD(T)[a]	CCSD[a]	MP2	B3LYP	BP86	BPW91
1^1A	0.00	0.00	344.93	0.00	0.00	0.00
1^3A	72.15	71.86	0.00	17.05	24.36	24.08
1^5A	107.82	99.21	82.17	51.68	66.57	65.80

a. Relative energies computed at the MP2 optimized geometries.

All density functionals provide a qualitatively similar description of the electronic state ordering, being similar to that for Sc(III)-salen above with relatively smaller high-spin/low-spin splittings. The inclusion of HF exchange in the hybrid

functional stabilizes the high-spin states slightly in comparison to BP86 and BPW91. Surprisingly, MP2 provides a highly unphysical description of the electronic state splittings, placing the 1^1A state extremely high in energy. This is dramatically corrected at the coupled-cluster level, with CCSD and CCSD(T) providing similar results. However, even the CCSD(T) results are qualitatively very different from the DFT results. The large errors at the MP2 level require further investigation that will be discussed below. The results from DFT are in overall very good agreement with each other but they are very different from the CCSD(T) and the highly unphysical MP2 results. Overall, the BP86 and BPW91 results appear to give relative energies closer to CCSD(T), our best results for this system.

The T1 and D1 diagnostics from the CCSD computations on the 1^3A and 1^5A states of Ti(IV)-salen (see Table 26) are generally comparable to those from Sc(III)-salen discussed previously. However, the T1 and D1 diagnostics for the 1^1A state are significantly larger (46% and 68% respectively) than the corresponding values for the Sc(III) system. While this signifies potentially larger non-dynamical correlation effects, the smaller T1/D1 ratio indicates these may be well described by a relatively small active space. Returning to the results from single-reference approaches, the large errors from MP2 theory warrant further attention. Perturbation theory corrections for dynamical correlation are well known to provide divergent results for certain chemical systems, especially as bonds are stretched far from equilibrium and small denominators arise from orbital near degeneracies. However, such effects are not typically observed for well-behaved systems at equilibrium geometries. Further examination reveals that the potential divergence of the perturbation correction is not the only source of the large errors

provided by MP2 theory. The perturbation corrections are all of similar magnitude (-2.121269, -2.202915, and -2.297344 hartree for the 1^1A, 1^3A, and 1^5A states respectively) and contribute to not more than 20% of the observed state splittings. The largest contributor to the errors in the spin-state splittings at the MP2 level in actuality is the HF energies. The RHF relative energies at the MP2 optimized geometries are highly unphysical: 1^1A 293.70 kcal mol^{-1}, 1^3A 0.0 kcal mol^{-1}, 1^5A 141.43 kcal mol^{-1}. Such effects have recently been observed, although to a slightly smaller extent, in other metal-salen systems. The oxo-Mn(salen) system has been demonstrated to possess multiple stable and unstable solutions to the self-consistent-field (SCF) equations, with HF theory providing highly unphysical splittings and being more susceptible to such solutions than DFT approaches. In an effort to investigate such effects in Ti(IV)-salen, wave-function stability analysis was performed on the 1^1A RHF solution at the MP2 optimized geometry using QChem 2.1 and an identical procedure as was employed in our previous work. The closed-shell RHF reference solution is reproduced by all three choices of starting orbitals (core Hamiltonian, superposition of atomic densities, and Generalized Wolfgang-Helmholtz) and furthermore, the ^{1}A solution is shown to exhibit no RHF-RHF or RHF-UHF orbital instabilities. The smallest eigenvalue of the molecular orbital Hessian is found to be 0.0023, corresponding to a spatial symmetry breaking of the α and β molecular orbitals. The smallest RHF-RHF Hessian eigenvalue is found to be 0.1311. While this does not definitively rule out the existence of a stable RHF solution that is lower in energy, such an investigation is beyond the scope of current electronic-structure approaches. We are currently unable to perform stability analysis of the ROHF solutions for the 1^3A and 1^5A states and the existence of instabilities for these states would only

serve to further exacerbate the highly unphysical description of the electronic state orderings at the HF-SCF level for Ti(IV)-salen.

The optimized geometries for Ti(IV)-salen are presented in Figure 32 and the LRMSD values are included in Table 25. While the geometries of the 1^1A state are all very similar, the methods provide visibly different geometries for the 1^3A and 1^5A states. This is also clear from the LRMSD values in Table 25, where the LRMSD are more than twice as large for the 1^3A and 1^5A states. It is interesting to note the difference in the 1^3A and 1^5A geometries. For the 1^3A state, the MP2 geometry is much more planar than those from the DFT approaches. In contrast, the MP2 geometry for the 1^5A state exhibits significant out-of-plane puckering. Furthermore, the DFT geometries are much more planr for the 1^5A state than is observed in the 1^3A state. Overall, all of the DFT approaches perform similarly for the geometries of Ti(IV)-salen.

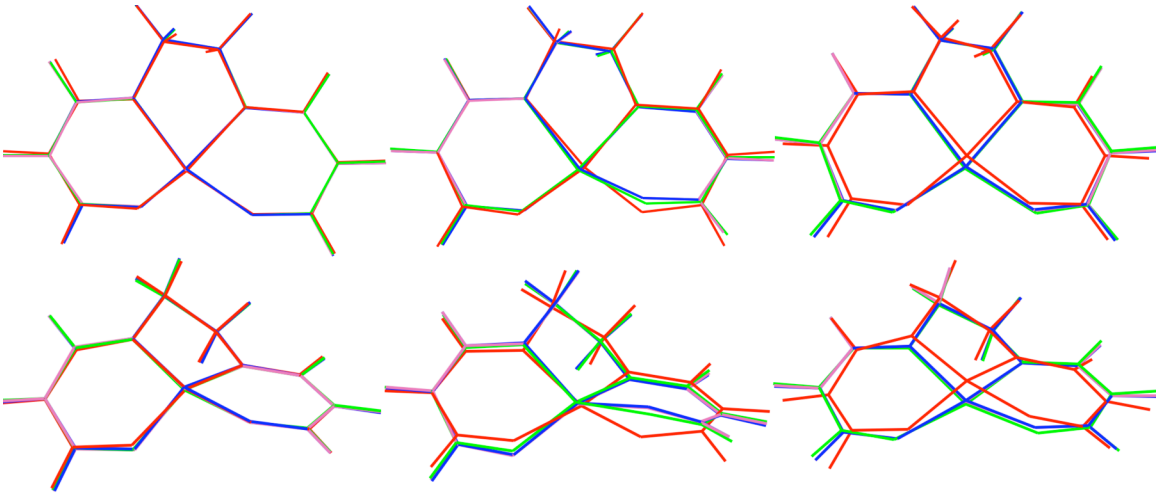

Figure 32. Overlay of the optimized geometries for the 1^1A (left), 1^3A (center), and 1^5A (right) states of Ti(IV)-Salen from different levels of theory. The theoretical methods include MP2 (red), B3LYP (green), BP86 (blue), and BPW91 (mauve).

V(V)-Salen

In V(V)-salen the increased formal oxidation state at the metal center results in a larger d-orbital splitting that places the lowest d-orbitals energetically lower than the π^* orbitals of the salen ligand. The lowest electronic states are dominated by $R\pi \rightarrow$ d excitations and appear to be adequately described by an active space consisting of the two $R\pi$ orbitals along with the d_{z^2}, d_{xz}, and d_{yz} orbitals from the V(V) center, depicted in Figure 33. The SA-CASSCF(4/5)/6-31G*[1^1A,2^1A,1^3A,2^3A,1^5A] relative energies are presented in Table 29. The CASPT3, CASPT2, and CASSCF results provide a consistent picture of the electronic structure for this system. As can be observed from the leading determinants in Table 30, the 1^1A ground state and the low-lying 2^1A state are open-shell singlet states with strong contributions from the metal d-orbitals. The lowest triplet state is predicted to lie less than 2 kcal mol^{-1} above the ground state, with the 1^5A state around 4.5 kcal mol^{-1}. Unlike in the previous systems, for V(V)-salen the density functionals provide a qualitatively different ordering of the low-lying electronic states (see Table 29). Unsurprisingly perhaps, B3LYP predicts a high-spin ^{5}A ground state while the GGA approaches accurately describe the ^{1}A ground state. However, even the description provided from the BP86 and BPW91 functionals is qualitatively very different than that from our most accurate results, with both functionals placing the 1^5A state considerably higher than the 4.6 kcal mol^{-1} predicted at the CASPT3 level. The single-reference wavefunction-based approaches do not fare any better than the DFT results. As was observed for Ti(IV)-salen above, the HF reference dramatically over-stabilizes the high-spin states and provides an extremely challenging starting point from which to accurately describe the energetics of the system. The MP2 results predict the entirely wrong order of

the electronic states and with spin-state splittings that are unphysical and dramatically larger than the CASPT3 results, placing the 1^1A state at 700.80 kcal mol^{-1} relative to the 1^5A state. Even coupled-cluster theory is unable to alleviate the large discrepancies in the HF reference energies, placing the 1^1A state 35.36 and 3.34 kcal mol^{-1} above the 1^5A state at the CCSD and CCSD(T) levels respectively.

Table 29. Relative energies (kcal mol^{-1}) for the low-lying electronic states of V(V)-salen computed at various levels of theory.

	CASPT3[a]	CASPT2[a]	CASSCF	CCSD(T)[b]	CCSD[b]	MP2	B3LYP	BP86	BPW91
1^1A	0.00	0.00	0.00	3.34	35.36	700.80	9.67	0.00	0.00
2^1A	3.73	2.21	2.42	---	---	---	---	---	---
1^3A	1.75	2.63	0.98	0.00	11.76	141.56	2.32	6.21	5.76
2^3A	3.12	4.97	2.07	---	---	---	---	---	---
1^5A	4.61	7.24	2.89	11.52	0.00	0.00	0.00	22.38	20.82

a. Relative energies computed at the CASSCF optimized geometries.
b. Relative energies computed at the MP2 optimized geometries.

Table 30. Leading determinants in the natural orbital basis from SA-CASSCF calculations on the low-lying electronic states of V(V)-salen computed at their optimized geometries.

State	Determinant	Coefficient
1^1A	$(R\pi_1)^2(R\pi_2)\alpha(d_{yz})\beta$	0.4913
	$(R\pi_1)^2(R\pi_2)\beta(d_{yz})\alpha$	-0.4913
	$(d_{xz})^2(R\pi_2)\alpha(d_{yz})\beta$	-0.3663
	$(d_{xz})^2(R\pi_2)\beta(d_{yz})\alpha$	0.3663
2^1A	$(R\pi_1)^2(R\pi_2)\alpha(d_{z^2})\beta$	0.4962
	$(R\pi_1)^2(R\pi_2)\beta(d_{z^2})\alpha$	-0.4962
	$(d_{xz})^2(R\pi_2)\alpha(d_{z^2})\beta$	-0.3669
	$(d_{xz})^2(R\pi_2)\beta(d_{z^2})\alpha$	0.3669
1^3A	$(R\pi_1)^2(R\pi_2)\alpha(d_{yz})\alpha$	0.5774
	$(R\pi_1)^2(R\pi_2)\beta(d_{xz})\alpha(d_{yz})\alpha$	-0.4557
	$(R\pi_1)^2(R\pi_2)\alpha(d_{xz})\alpha(d_{yz})\beta$	0.4436
	$(d_{xz})^2(R\pi_1)\alpha(d_{yz})\alpha$	-0.4368
2^3A	$(R\pi_2)^2(R\pi_1)\alpha(d_{yz})\alpha$	0.5410
	$(R\pi_1)^2(d_{xz})\alpha(d_{yz})\alpha$	-0.5163
	$(R\pi_2)^2(d_{xz})\alpha(d_{yz})\alpha$	-0.4643
	$(d_{xz})^2(R\pi_1)\alpha(d_{yz})\alpha$	-0.4624
1^5A	$(R\pi_1)\alpha(R\pi_2)\alpha(d_{xz})\alpha(d_{yz})\alpha$	0.9998

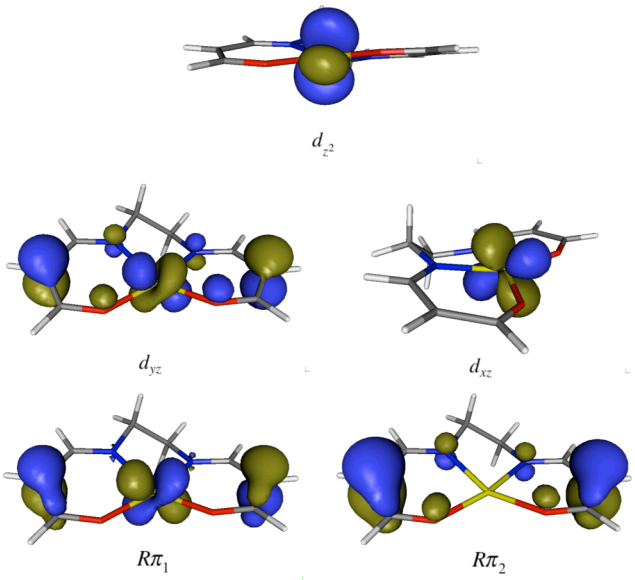

Figure 33. Isosurface plots of the $R\pi$ (bottom), d_{yz} (middle-left), d_{xz} (middle-right), and d_{z^2} (top) orbitals that comprise the active space for V(V)-salen.

The overall very poor performance of the single-reference approaches for V(V)-salen is not at all surprising given the weights of the leading determinants presented in Table 30 and the magnitude of the coupled-cluster diagnostics from Table 26. Both the singlet and triplet states are demonstrated to be highly multi-reference, with leading coefficients of 0.4913 and 0.4992 for the 1^1A and 2^1A states and 0.5774 and 0.5410 for thr 1^3A and 2^3A states. The 1^5A state appears to be strongly single-reference (C_0 = 0.9998) and this effect likely contributes to the dramatic over-stabilization of the 1^5A state by HF-based approaches. The coupled-cluster diagnostics paint a similar picture, with T1's that are nearly twice the recommended cutoff values and D1's that are much larger than those from the previous systems. However, the T1/D1 ratios are actually smaller than those of Ti(IV)-salen and are vary similar to those for the Sc(III) system. This bodes well for the applicability of similar-sized active spaces, being potentially smaller than those anticipated for the Ti(IV) system. Overall, both the coupled-cluster

diagnostics and the CI vectors from the SA-CASSCF computations paint a similar picture of highly multi-reference 1^1A and 1^3A states and a single-reference 1^5A state that are capable of being described by a small to modest active space.

Disappointingly, although it is probably of no surprise, the poor performance for relative energies by all single-reference approaches occurs simultaneously with decreased overall performance for molecular geometries. The LRMSD values relative to the CASSCF geometries presented in Table 31 are all several times larger than those observed in the seemingly well-behaved Sc(III)-salen and the geometries (overlaid in Figure 34) are visibly very different. As was observed in previous systems, the CASSCF geometries are much more planar than those from DFT, again with B3LYP geometries being closer to the CASSCF geometries than those from BP86 and BPW91. Contrary to the results observed previously, the MP2 geometries are closer to the B3LYP than to the CASSCF geometries. The LRMSD's for all methods approach 1 Å, being much larger than previously observed values.

Table 31. LRMSD(Å) in molecular geometries for the 1^1A, 1^3A, and 1^5A states of V(V)- and Cr(VI)-salens.

		CASSCF	MP2	B3LYP	BP86	BPW91		
V(V)	CASSCF	--- --- ---	0.398 0.391 0.486	0.421 0.491 0.486	0.429 0.431 0.605	0.427 0.419 0.615	CASSCF	Cr(VI)
	MP2	0.783 0.777 0.769	--- --- ---	0.073 0.234 0.251	0.135 0.180 0.261	0.141 0.174 0.263	MP2	
	B3LYP	0.865 0.889 0.784	0.319 0.298 0.450	--- --- ---	0.085 0.100 0.021	0.092 0.115 0.020	B3LYP	
	BP86	0.878 0.933 0.796	0.335 0.372 0.474	0.037 0.095 0.033	--- --- ---	0.141 0.017 0.005	BP86	
	BPW91	0.878 0.934 0.796	0.336 0.374 0.477	0.033 0.098 0.035	0.008 0.005 0.005	--- --- ---	BPW91	

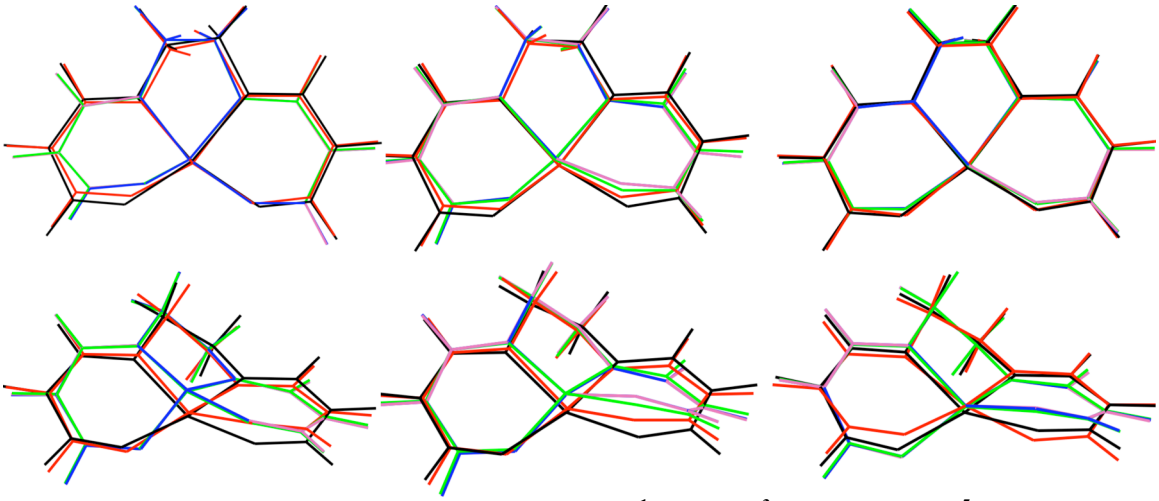

Figure 34. Overlay of the optimized geometries for the 1^1A (left), 1^3A (center), and 1^5A (right) states of V(V)-Salen from different levels of theory. The theoretical methods include CASSCF (black), MP2 (red), B3LYP (green), BP86 (blue), and BPW91 (mauve).

Cr(VI)-Salen

The relative energies for Cr(VI)-salen from all DFT approaches are included in Table 32. All of the functionals predict a 1^5A ground state, with B3LYP predicting much larger splittings than BP86 and BPW91. The predictions from DFT are in stark contrast to those from the multi-reference approaches. CAS-CI computations predict a similar active space (Figure 35) and electronic structure to that of V(V)-salen presented above. The SA-CASSCF(4/5)/6-31G*[1^1A, 1^3A, 2^3A, 1^5A] relative energies are included in Table 32 along with those from CASPT2 and CASPT3. The lowest singlet, triplet, and quintet states are predicted to be nearly degenerate at the CASSCF level, with the 1^5A ground state favored by no more than 0.22 kcal mol^{-1}. The inclusion of dynamical correlation stabilizes the 1^5A state. At the CASPT2 level the 1^5A state is predicted to be the ground state, with the 1^3A and 1^1A states at 10.23 and 8.20 kcal mol^{-1} respectively. At the CASPT3 level these splittings are 8.51 and 11.03 kcal mol^{-1}. The MP2 results again appear highly unphysical, a consequence of the extremely poor description at the RHF level. Although we are currently incapable of performing stability analysis on the ROHF states, stability analysis was performed on the 1^1A RHF solution. The RHF 1^1A energy from ACES II is reproduced with QCHEM for the three sets of starting orbitals. Exhibiting no RHF-RHF orbital instabilities, the lowest eigenvalue of the orbital hessian (-0.0811) corresponds to a RHF-UHF instability. Following the instability leads to a heavily spin-contaminated ($\left\langle \hat{S}^2 \right\rangle$=3.40) UHF solution. The relative energies are dramatically improved at the CCSD and CCSD(T) levels, both being extremely different from the MP2 results. Even with the perturbative triples corrections, the CCSD(T) relative energies are still significantly different from the CASPT3 results. While all

methods accurately predict the 1^5A ground state, the BP86 and BPW91 functionals predict smaller state splittings that are closer to our more reliable CASPT3 results.

Table 32. Relative energies (kcal mol^{-1}) for the low-lying electronic states of Cr(VI)-salen computed at various levels of theory.

	CASPT3[a]	CASPT2[a]	CASSCF	CCSD(T)[b]	CCSD[b]	MP2	B3LYP	BP86	BPW91
1^1A	11.03	8.20	0.22	13.88	4.94	1282.36	31.62	16.81	18.61
1^3A	8.51	10.23	0.16	18.98	16.46	339.54	24.13	6.37	7.40
2^3A	9.93	12.78	1.98	---	---	---	---	---	---
1^5A	0.00	0.00	0.00	0.00	0.00	0.00	0.00	0.00	0.00

a. Relative energies computed at the CASSCF optimized geometries.
b. Relative energies computed at the MP2 optimized geometries.

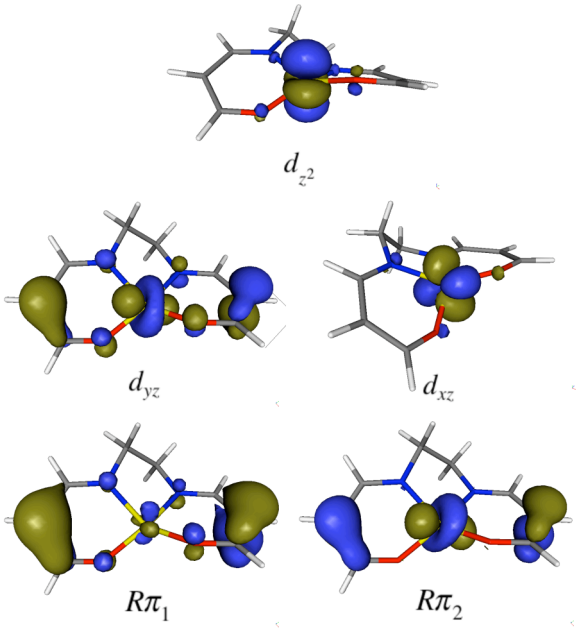

Figure 35. Isosurface plots of the Rπ and Cr(d)-orbitals that comprise the active space for Cr(VI)-salen.

Upon examining the leading determinants from the CASSCF computations presented in Table 33 and considering the results presented previously for V(V)-salen, the rather poor performance of all single-reference approaches for Cr(VI)-salen should come of no surprise. The 1^1A state is strongly open-shell in character and the closed-shell

RHF determinant has a coefficient of only 0.1545. The triplet states are demonstrated to be strongly multi-reference as well, with leading coefficients of 0.5310 and 0.5020 for the 1^3A and 2^3A states respectively. In contrast to the singlet and triplet states, the 1^5A appears strongly single-reference. The diagnostics from the CCSD computations (Table 26) are again much larger than what would be expected for well-behaved systems. Even CCSD(T) is incapable of overcoming the strong near-degeneracy effects present in Cr(VI)-salen.

Table 33. Leading determinants from CASSCF calculations on the low-lying electronic states of Cr(VI)-salen.

State	Determinant	Coefficient
1^1A	$(R\pi_1)^2(R\pi_2)\beta(d_{xz})\alpha$	0.4713
	$(R\pi_1)^2(R\pi_2)\alpha(d_{xz})\beta$	-0.4713
	$(d_{yz})^2(R\pi_2)\alpha(d_{xz})\beta$	0.3577
	$(d_{yz})^2(R\pi_2)\beta(d_{xz})\alpha$	-0.3577
	$(R\pi_1)\beta(R\pi_2)\alpha(d_{yz})\beta(d_{xz})\alpha$	-0.2745
	$(R\pi_1)\alpha(R\pi_2)\beta(d_{yz})\alpha(d_{xz})\beta$	-0.2745
	$(R\pi_1)^2(R\pi_2)^2$	0.1545
1^3A	$(R\pi_1)^2(R\pi_2)\alpha(d_{xz})\alpha$	0.5310
	$(d_{yz})^2(R\pi_2)\alpha(d_{xz})\alpha$	-0.4362
	$(R\pi_1)\alpha(R\pi_2)\alpha(d_{yz})\alpha(d_{xz})\beta$	-0.3441
	$(R\pi_1)^2(d_{yz})\alpha(d_{xz})\alpha$	0.3028
	$(R\pi_2)^2(d_{yz})\alpha(d_{xz})\alpha$	-0.2800
	$(R\pi_2)^2(R\pi_1)\alpha(d_{xz})\alpha$	-0.2362
	$(d_{yz})^2(R\pi_1)\alpha(d_{xz})\alpha$	0.2095
	$(R\pi_1)^2(R\pi_2)\alpha(d_{yz})\alpha$	0.1855
2^3A	$(R\pi_2)^2(R\pi_1)\alpha(d_{xz})\alpha$	0.5020
	$(R\pi_1)^2(d_{yz})\alpha(d_{xz})\alpha$	-0.4904
	$(R\pi_2)^2(d_{yz})\alpha(d_{xz})\alpha$	0.4459
	$(d_{yz})^2(R\pi_1)\alpha(d_{xz})\alpha$	-0.4340
	$(R\pi_1)^2(R\pi_2)\alpha(d_{xz})\alpha$	0.1683
1^5A	$(R\pi_1)\alpha(R\pi_2)\alpha(d_{yz})\alpha(d_{xz})\alpha$	1.0000

The LRMSD in molecular geometries from all methods are presented in Table 31 and the optimized structures are overlaid in Figure 36. While the geometries are visibly

very different, the LRMSD values from Table 31 are smaller than the corresponding values for V(V)-salen presented above. All of the DFT geometries are very similar, with a maximum LRMSD of 0.141 Å occuring between the BP86 and BPW91 1^1A geometries. The LRMSD values with respect to the CASSCF geometries are considerably larger, approaching 0.5 Å for all cases. The B3LYP geometries are overall somewhat closer to those from CASSCF than are the BP86 and BPW91 geometries, while the performance for relative energies is significantly better for the BP86 and BPW91 functionals.

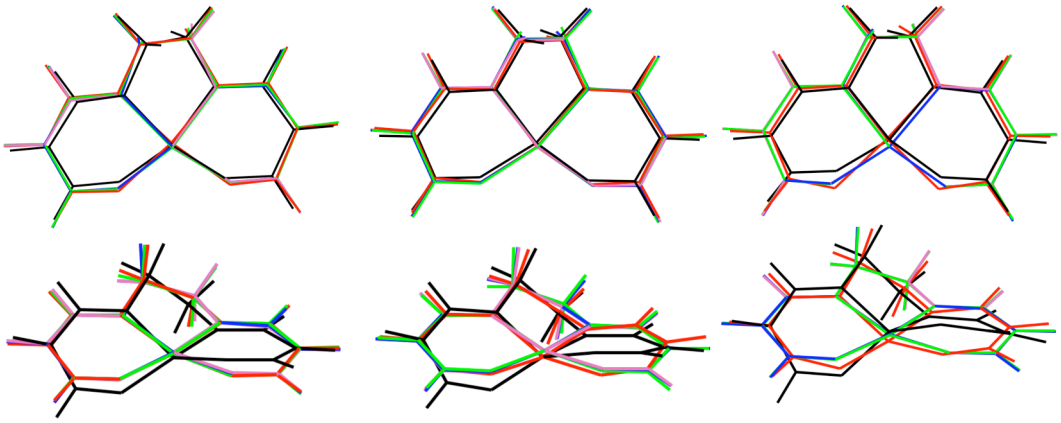

Figure 36. Overlay of the optimized geometries for the 1^1A (left), 1^3A (center), and 1^5A (right) states of Cr(VI)-Salen from different levels of theory. The theoretical methods include CASSCF (black), MP2 (red), B3LYP (green), BP86 (blue), and BPW91 (mauve).

Mn(VII)-Salen

For Mn(VII)-salen, the increased formal oxidation state at the metal center results in the four lowest-lying d-orbitals being energetically much lower than the salen $R\pi$ orbitals. Large CAS-CI computations indicate very little contribution from these orbitals to the low-lying electronic states. The 3 lowest electronic states were optimized at the SA-CASSCF(4/4)/6-31G*[1^1A, 1^3A, 1^5A] level using the active space depicted in Figure 37. The relative energies from all methods are included in Table 34. The DFT

results are all very similar, with the anticipated stabilization of the high-spin 1^5A state by B3LYP relative to BP86 and BPW91. The MP2 results are again completely unphysical. This is a consequesnce of the poor RHF description of the electronic structure of Mn(VII)-salen, although stability analysis of the RHF 1^1A again confirms the lack of an RHF-RHF instability (there is a large RHF-UHF instability). As has been observed in the previous systems, CCSD dramatically improves upon the extremely poor MP2 results. However, it should be noted that the CCSD amplitude equations prove challenging to converge for many of the systems here. Often requiring hundreds iterations and fairly large level shifts, the amplitudes converge very slowly. Even with more than 300 iterations of the amplitude equations, the amplitudes failed to converge to the prescribed convergence criteria for the 1^3A CCSD computation of Mn(VIII)-salen. The amplitudes in this case were converged to 10^{-7} which is slightly larger than the convergence criteria of 10^{-10}. For this reason, the CCSD(T) energy for the 1^3A state is omitted from Table 34. The CASSCF, CASPT2, and CASPT3 results provide a consistent picture of the electronic state ordering in this system and are qualitatively very different from the CCSD and CCSD(T) results. Our best results place the 1^1A and 1^3A states at 91.39 and 64.18 kcal mol-1 respectively relative to the 1^5A ground state. The DFT relative energies provide reasonable (at least qualitative) agreement with the CASPT3 results, being dramatically better than the MP2 and CC results. Overall, the B3LYP relative energies are much closer to those from CASPT3 than are the other methods explored here.

Table 34. Relative energies (kcal mol^{-1}) for the low-lying electronic states of Mn(VII)-salen computed at various levels of theory.

	CASPT3[a]	CASPT2[a]	CASSCF	CCSD(T)[b]	CCSD[b]	MP2	B3LYP	BP86	BPW91
1^1A	91.39	95.71	96.47	0.00	0.00	1709.09	54.35	33.83	37.33
1^3A	64.18	67.78	67.61	---	10.52	598.78	35.73	16.35	18.77
1^5A	0.00	0.00	0.00	8.55	23.72	0.00	0.00	0.00	0.00

a. Relative energies computed at the CASSCF optimized geometries.
b. Relative energies computed at the MP2 optimized geometries.

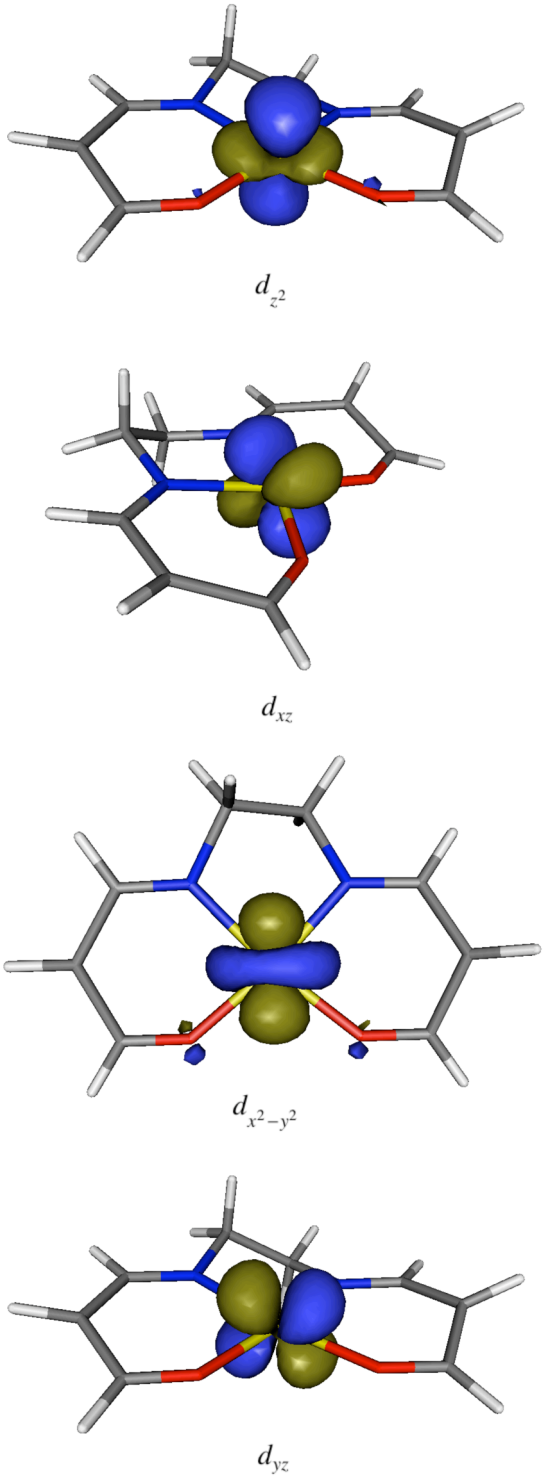

Figure 37. Isosurface plots of the Mn d-orbitals that comprise the active space for Mn(VII)-salen.

The molecular geometries from all methods are overlaid in Figure 38 and the corresponding LRMSD values are presented in Table 35. While the DFT geometries

agree very well with each other (LRMSD < 0.072 Å), the agreement with the CASSCF geometries is considerably worse (LRMSD > 0.313 Å). Despite the extremely poor performance of MP2 for the relative energies, the geometries from MP2 are closer to the CASSCF geometries than are the DFT geometries. However, with LRMSD values in excess of 0.149 Å, the geometries from MP2 and CASSCF remain noticeably different.

Table 35. LRMSD(Å) in molecular geometries for the 1^1A, 1^3A, and 1^5A states of Mn(VII)- and Tc(VII)-salens.

		CASSCF	MP2	B3LYP	BP86	BPW91
Mn(VII)	CASSCF	--- --- ---				
	MP2	0.149 0.314 0.245	--- --- ---			
	B3LYP	0.321 0.313 0.316	0.349 0.483 0.356	--- --- ---		
	BP86	0.333 0.327 0.362	0.358 0.495 0.410	0.026 0.030 0.060	--- --- ---	
	BPW91	0.339 0.326 0.371	0.364 0.493 0.420	0.030 0.028 0.072	0.010 0.006 0.014	--- --- ---

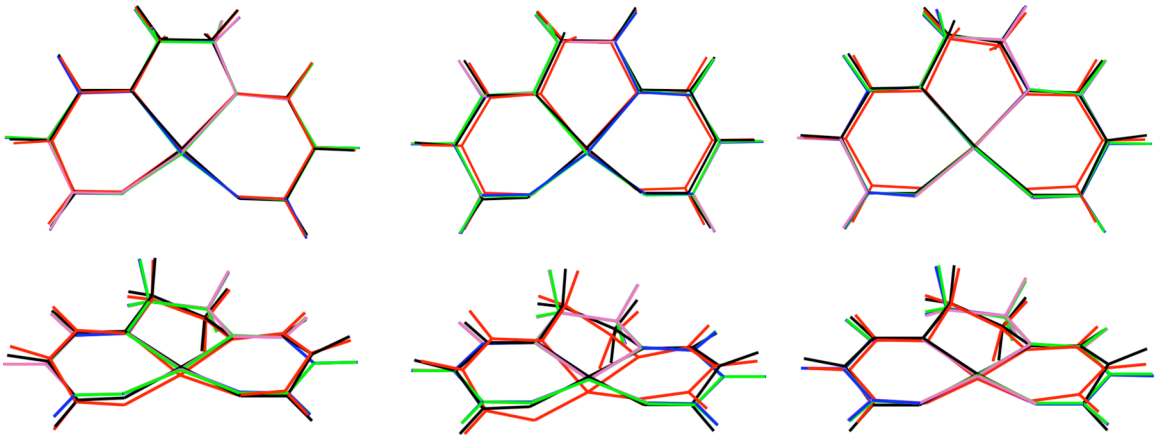

Figure 38. Overlay of the optimized geometries for the 1^1A (left), 1^3A (center), and 1^5A (right) states of Mn(VII)-Salen from different levels of theory. The theoretical methods include CASSCF (black), MP2 (red), B3LYP (green), BP86 (blue), and BPW91 (mauve).

The leading determinants from the SA-CASSCF computations are presented in Table 36. The leading determinants for the 1^1A and 1^3A states are both extremely small (0.5977 and 0.8652 respectively), much smaller than would be expected for a single-reference system. It should be noted that, just as in the case of Sc(III)-salen, the 1^5A state with this active space is a single determinantal wavefunction. The CC diagnostics from Table 26 reveal the same general trend, with the diagnostics being largest for the highly multi-reference 1^1A state. The coefficients from the CASSCF computations and the CC diagnostics both demonstrate the incredibly strong multi-reference character of Mn(VIII)-salen. Surprisingly, the DFT approaches examined here outperform even CCSD(T) for this challenging system. The B3LYP results provide the closest agreement of the three functionals employed.

Table 36. Leading determinants in the natural orbital basis from SA-CASSCF calculations on the low-lying electronic states of Mn(VII)-salen computed at their optimized geometries.

State	Determinant	Coefficient
1^1A	$\left(d_{yz}\right)^2\left(d_{x^2-y^2}\right)^2$	0.5977
	$\left(d_{xz}\right)^2\left(d_{x^2-y^2}\right)^2$	-0.3816
	$\left(d_{xz}\right)^2\left(d_{z^2}\right)^2$	0.3038
	$\left(d_{x^2-y^2}\right)^2\left(d_{z^2}\right)^2$	-0.3009
	$\left(d_{yz}\right)\beta\left(d_{x^2-y^2}\right)\beta\left(d_{xz}\right)\alpha\left(d_{z^2}\right)\alpha$	-0.2795
	$\left(d_{yz}\right)\alpha\left(d_{x^2-y^2}\right)\alpha\left(d_{xz}\right)\beta\left(d_{z^2}\right)\beta$	-0.2795
	$\left(d_{yz}\right)\beta\left(d_{x^2-y^2}\right)\alpha\left(d_{xz}\right)\beta\left(d_{z^2}\right)\alpha$	0.2436
	$\left(d_{yz}\right)\alpha\left(d_{x^2-y^2}\right)\beta\left(d_{xz}\right)\alpha\left(d_{z^2}\right)\beta$	0.2436
1^3A	$\left(d_{x^2-y^2}\right)^2\left(d_{yz}\right)\alpha\left(d_{xz}\right)\alpha$	0.8652
	$\left(d_{z^2}\right)^2\left(d_{yz}\right)\alpha\left(d_{xz}\right)\alpha$	-0.4485
1^5A	$\left(d_{z^2}\right)\alpha\left(d_{x^2-y^2}\right)\alpha\left(d_{yz}\right)\alpha\left(d_{xz}\right)\alpha$	1.0000

Conclusions

Employing compact CASSCF reference spaces in conjunction with corrections for dynamical electron correlation at the CASPT3 level of theory, accurate relative energies and geometries have been obtained for the lowest electronic states of several 3d0-metal salen systems. The results presented clearly demonstrate the strong mult-reference character of the 3d0-metal salen systems explored. The T1 and D1 diagnostics from the CCSD computations (Table 26) are some of the largest values ever observed in a molecular system near its respective equilibrium geometry. The leading determinants from the SA-CASSCF computations serve to further validate this observation.

The DFT geometries and relative energies provide reasonable agreement with the benchmark results for two of the systems explored in this work: Sc(III) and Mn(VII). Interestingly, these are the systems possessing the smallest amount of mixing in the ligand $R\pi$ and the metal d-orbitals. For the case of Sc(III)-salen the electronic states are localized largely on the salen ligand. On the other hand, the electronic states are localized entirely on the metal center for the case of Mn(VIII)-salen. For the systems lying between these two extremes the DFT results perform significantly worse. In these systems, the SA-CASSCF natural orbitals and determinants reveal a strong mixture of ligand $R\pi$ and metal d-orbital character in the lowest electronic states. Describing this appears to be a challenge for DFT approaches as the performance both for molecular geometries and for relative energies is degraded. However, it should be noted that all of the functionals examined perform approximately as well as the expensive CCSD(T) approach for these systems. While the hybrid functional does outperform BP86 and BPW91 for at least a couple of the cases examined, B3LYP is the only functional providing results in strong qualitative disagreement with any of the CASPT3 results. This is the case of V(V)-salen, where B3LYP fails to predict the 1^1A ground state of the system. Given the strong multi-reference character of these systems, the overall reasonable performance of the DFT approaches is surprising.

CHAPTER 8

THE ELECTRONIC STRUCTURE OF D2-METAL SALENS

This work [287] extends our previous efforts [137, 247] to systematically examine the ability of DFT to describe the electronic structure of metal-salen systems to the D2 metals: Ti(II), V(III), Cr(IV), Zr(II), Nb(III), and Mo(IV). The geometries and relative energies from DFT are benchmarked against those from high-level *ab initio* methods capable of accurately treating the multi-reference nature of the systems. Although the purpose of this work is to assess the applicability of DFT to these challenging systems and not to examine the chemical properties of any particular system that has been employed experimentally; several of the metals examined have been employed in metal-salen catalyzed chemical transformations. V(III)-salens have potential application as molecular batteries[288] and have been employed as catalysts in the electroreduction of molecular oxygen [289-291]. Bakac and Guzei have studied hydrogen atom transfer reactions in mixed Cr(IV)-/Cr(V)-salen systems [292]. Metal-salen complexes of Zr(II) have been employed as highly efficient and enantioselective catalysts for Baeyer-Villiger oxidation reactions [293, 294]. Chiral Nb(III)-salen complexes have recently been employed in asymmetric sulfoxidation reactions [295] with promising results and Mo(IV)-salens have been employed as catalysts in asymmetric olefin epoxidations [296].

Theoretical Approach

The theoretical approach is similar to that of our previous studies of metal-salen systems [137, 247]. All DFT calculations were performed with Jaguar 5.5 [4]. The calculations were performed using three of the most common combinations of exchange and correlation functionals: the combination of Becke's 1988 exchange functional [232]

with Perdew's 1986 [234] functional for correlation referred to as BP86, the combination of Becke's 1988 exchange functional with the Perdew Wang 1991 functional for correlation [270] referred to as BPW91, and the combination of Becke's three-parameter hybrid functional [231] with the correlation functional by Lee, Yang, and Parr [233] referred to as B3LYP. Unless otherwise stated, all DFT calculations employed the pseudospectral implementation of DFT [6] and a fine grid as found in Jaguar 5.5, the Los Alamos basis-sets and corresponding effective core potentials of Hay and Wadt (LANL2DZ) for all transition-metal atoms [271], and a 6-31G* basis for all other atoms [272]. Geometries were completely optimized (RMS gradient 10^{-3}) for the lowest singlet, triplet, and quintet states using each functional. The nature of the stationary points was verified by computing analytic vibrational frequencies.

Geometries were also optimized (RMS gradient 10^{-3}) at the CASSCF [51] level with MOLPRO 2006.1 [28]. Unless otherwise stated, the converged BP86 geometries were employed as a starting point for these optimizations. Active spaces for CASSCF calculations were chosen by examination of the CI vector from large CAS-CI [36] calculations performed in a CISD [36] natural orbital basis. Starting orbitals for the CASSCF calculations were generated from CASSCF natural orbitals computed in the smaller STO-3G [242, 243, 273] basis. The STO-3G CASSCF calculations employed a CISD natural orbital guess. Such an approach has been shown to give reliable convergence for CASSCF calculations on other metal-salen systems, when more conventional approaches have failed to do so [137]. The active spaces and optimized states for each system will be described in the discussion, employing the notation from our previous work [137]. Single-point energy calculations were computed at the

CASSCF-optimized geometries using complete active-space second-order and third-order perturbation theory (CASPT2 and CASPT3) with MOLPRO 2006.1. Due to limitations on the number of correlated orbitals in the CASPT3 program, CASPT3 calculations were computed with the lowest σ-orbitals frozen and combined as corrections to the internally contracted CASPT2 calculation. Wavefunction-based calculations employed a LANL2DZ basis for all second transition-row metals and a 6-31G* basis for all other atoms. All single-point calculations employed the frozen-core approximation using a small-core, defined as 1s2s2p3s and 1s2s2p3s3p3d4s for first and second transition-row metals respectively.

Optimized geometries were compared and the least root-mean-squared deviations (LRMSD) in molecular geometries were computed using VMD [274]. Molecular orbital isosurfaces were generated using MOLEKEL [275]. Information about the multi-reference nature of the electronic states has been provided by examination of the leading determinants (and coefficients) from the CASSCF CI expansions.

Results and Discussion

None of the M(salen) complexes studied contain any symmetry elements, and therefore all calculations were performed in C_1 symmetry. The salen ligand does, however, form a pseudo-square-planar coordination sphere around the central metal atom. The definition of appropriate active spaces for the construction of the CASSCF wave functions requires a certain amount of chemical insight, thus it is useful to consider the important properties of the electronic structure of metal-salen systems before proceeding further. The four coordinating atoms [O,N,N,O] induce a well known splitting of the metal d-orbital energy levels. Two typical d-orbital splitting diagrams for square-

planar coordination presented in the literature are displayed in Figure 28. The degenerate (nearly degenerate for the case of nonsymmetrical coordination) d_{xz} and d_{yz} orbitals are typically considered to be the lowest in energy and this is typically true in the weak-field case. The d_{xz} and d_{yz} orbitals are followed closely by the d_{z^2} orbital, and these are energetically well separated from the d_{xy} and the much higher lying $d_{x^2-y^2}$ orbitals. Strong ligand fields, mixing of the s and d_{z^2} orbitals, or strong metal-ligand covalency have been shown to result in a flipping of the ordering of the d_{xz} and d_{yz} orbitals and the d_{z^2} orbital [282-284]. This splitting will play heavily into the construction and interpretation of the active spaces discussed below, as the metal d-orbitals most likely to contribute to the electronic structure will be the low-lying d_{xz}, d_{yz}, and d_{z^2} orbitals. To ascertain the important electronic effects of the salen ligand and further divulge the chemistry taking place in the metal-salen systems, RHF/6-31G* wave functions were constructed (consisting of 55 doubly occupied molecular orbitals) at the BP86 1^1A optimized geometries and the occupied orbitals were localized via Edmiston-Ruedenberg (ER) localization [240]. The anticipated σ bonds occurring in the salen ligand are observed along with the N and O lone pairs involved in dative bonding with the central metal atom. Each O atom has an additional lone pair that is not involved in any bonding interactions. The most important features observed for the electronic structure are the doubly-occupied d_{xz} orbital and the presence of six π-type orbitals on the salen ligand: two representing C-O π bonds, two representing C-N π bonds, and two C-C-C (three-center-two-electron) π bonds hereafter referred to as $R\pi_1$ and $R\pi_2$. These are displayed in

(Figure 39) from the ER localized orbitals of Ti(II)-salen. Given the d2 electronic configuration (at least in the formal oxidation picture) and the expected near-degeneracies of the metal d-orbitals low-lying singlet and triplet states are anticipated arising from different d-orbital occupations. The quintet-states are expected to be higher in energy, arising from mixing of the various d-orbital occupations with either ligand $\pi \rightarrow \pi^*$ excitations or $\pi \rightarrow d$ ligand-to-metal excitations with the latter becoming increasingly important as the formal oxidation state of the metal center is increased. The construction and interpretation of the active spaces for each system and the nature of the low-lying electronic states will be discussed in detail in the following sections.

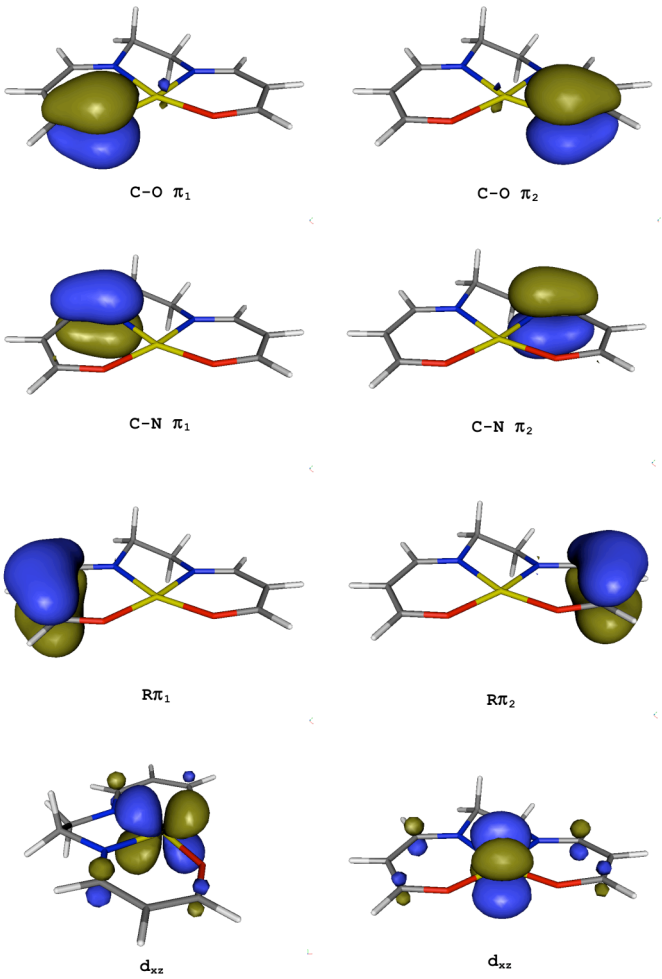

Figure 39. Figure of the localized π orbitals of the salen ligand and the localized Ti(II) d_{xz} orbital from a HF/6-31G* calculation of the singlet state of Ti(II)-salen.

The 3D-Metals

Ti(II)-Salen

The relative energies for Ti(II)-salen from the various density functionals in Table 37 reveal the anticipated near-degeneracy of the lowest singlet and triplet states, with the quintet states considerably higher (> 60 kcal mol^{-1}) in energy. As has been observed in other metal-salen systems [137], the hybrid B3LYP over-stabilizes the high-spin triplet and quintet states relative to "non-hybrid" functionals (BP86 and BPW91). The relative

energies from BP86 and BPW91 are nearly identical (never differing by more than 0.30 kcal mol^{-1}) in consensus with previous observations [137, 247]. CAS-CI computations including up to 14 electrons in 13 orbitals reveal a similar picture of nearly degenerate singlet and triplet states with a much higher-lying quintet state. The three lowest singlet and triplet states appear energetically well separated from remaining electronic states and have been optimized at the SA-CASSCF(2/3)/6-31G* [1^1A,2^1A,3^1A,1^3A,2^3A,3^3A] level of theory, where the states in brackets are those included in the state averaging. All of the states appear to be well described by an active space consisting of two electrons in the three lowest-lying (d_{z^2}, d_{xz}, and d_{yz}) d-orbitals. The active space is depicted in Figure 40 from the SA-CASSCF optimization of the 1^1A state and the relative energies for all states are included in Table 37. The CASSCF results reveal three triplet states below 10 kcal mol^{-1} followed by three low-lying singlet states below 30 kcal mol^{-1}. The inclusion of dynamical correlation reduces the splitting of the lowest singlet and triplet states (23.53 kcal mol^{-1} at the SA-CASSCF level) to 17.76 kcal mol^{-1} at the CASPT2 level and 13.24 kcal mol^{-1} at the CASPT3 level. Overall, a consistent picture of the lowest singlet and triplet states is provided by all methods.

Table 37. Relative energies (kcal mol^{-1}) for the low-lying electronic states of Ti(II)-salen computed at various levels of theory.

	CASPT3	CASPT2	CASSCF	B3LYP	BP86	BPW91
1^1A	13.24	17.76	23.53	10.40	4.27	4.26
2^1A	16.01	18.23	24.24	---	---	---
3^1A	26.65	23.47	27.94	---	---	---
1^3A	0.00	0.00	0.00	0.00	0.00	0.00
2^3A	2.23	4.79	3.28	---	---	---
3^3A	8.18	11.74	9.77	---	---	---
1^5A	---	---	---	68.67	67.15	66.85

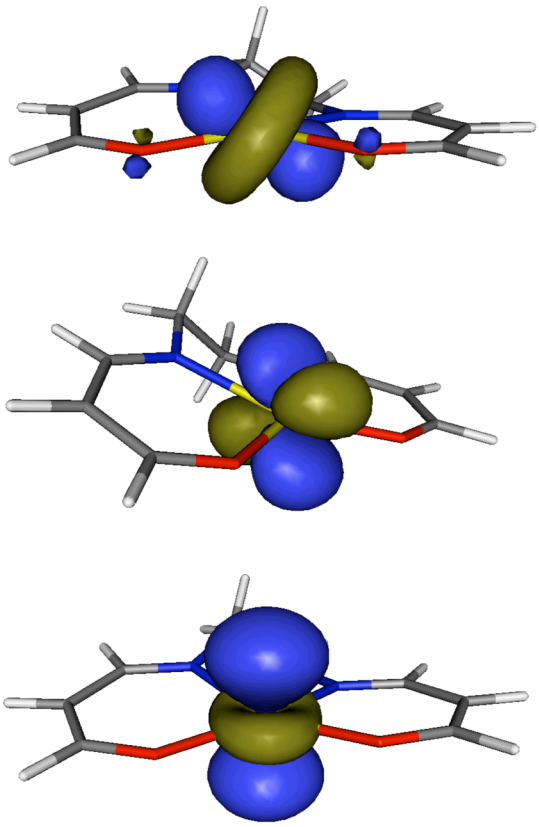

Figure 40. Isosurface plots of the d_{z^2} (lower), d_{xz} (center), and d_{yz} (upper) CASSCF orbitals that comprise the active space for Ti(II)-salen.

The optimized geometries of the 1^1A and 1^3A state from DFT and CASSCF are overlaid in Figure 41. The geometries from all methods are visibly very similar and this is

confirmed by the LRMSD values tabulated in Table 38. The DFT geometries never differ by more than 0.05 Å and are all within 0.2 Å of the CASSCF optimized geometries. In consensus with previous results [247], the geometries from BP86 and BPW91 are nearly indistinguishable. B3LYP provides geometries that are overall closer to the CASSCF geometries, although marginally so.

Table 38. LRMSD(Å) in molecular geometries for the 1^1A and 1^3A states of Ti(II)- and Zr(II)-salens.

		CASSCF	B3LYP	BP86	BPW91		
Ti(II)	CASSCF	--- ---	0.129 0.133	0.147 0.141	0.143 0.138	CASSCF	Zr(II)
	B3LYP	0.159 0.100	--- ---	0.029 0.017	0.025 0.015	B3LYP	
	BP86	0.175 0.116	0.021 0.035	--- ---	0.011 0.004	BP86	
	BPW91	0.173 0.112	0.019 0.035	0.003 0.005	--- ---	BPW91	

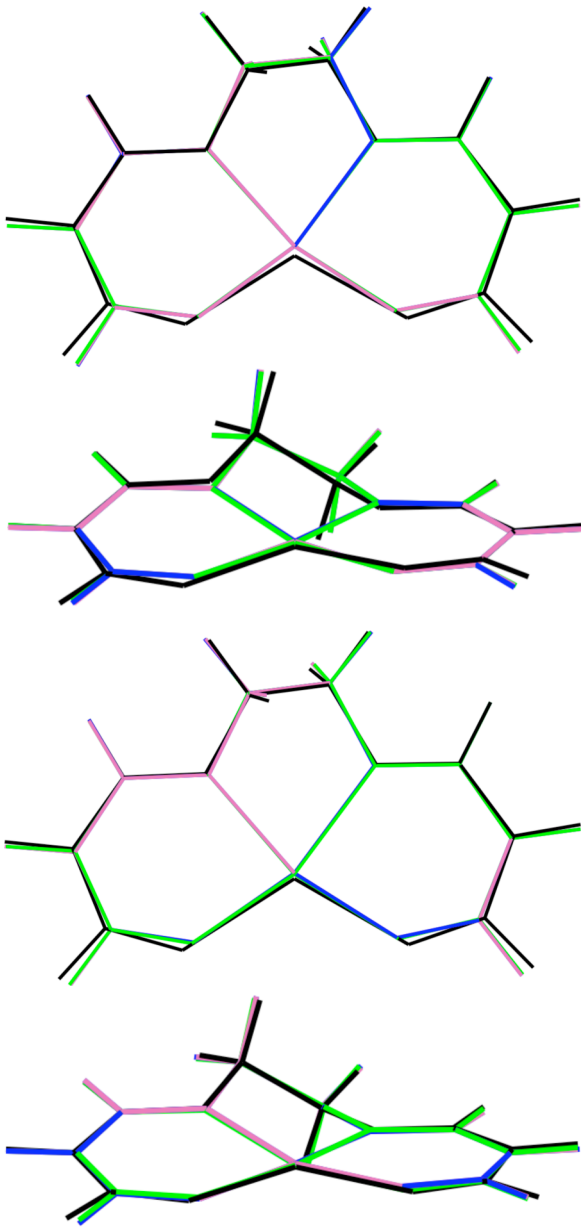

Figure 41. Overlay of the optimized geometries for the 1^1A (top) and 1^3A (bottom) states of Ti(II)-Salen from different levels of theory. The theoretical methods include CASSCF (black), B3LYP (green), BP86 (blue), and BPW91 (mauve).

The multi-reference character of the low-lying electronic states has been explored by examination of the leading determinants from the SA-CASSCF computations. The determinants and coefficients for Ti(II)-salen (included in Table 39) reveal the strong multi-reference nature of the states examined. The ground state is dominated by the

anticipated $\left(d_{z^2}\right)\alpha\left(d_{xz}\right)\alpha$ electronic configuration but with an extremely small leading coefficient of 0.8272 and a large contribution (0.5619) from the $\left(d_{xz}\right)\alpha\left(d_{yz}\right)\alpha$ configuration. With the exception of the 1^1A state, all of the states investigated exhibit stronger non-dynamical effects (smaller leading coefficients) than the 1^3A ground state and the leading coefficient for the 1^1A state (0.9050) is significantly smaller than would be expected for well-behaved single-reference systems. The low-lying singlet states are dominated by the closed-shell $\left(d_{z^2}\right)^2$ and $\left(d_{xz}\right)^2$ configurations with surprisingly little contribution from the complementary $\left(d_{yz}\right)^2$ configuration. Despite the large non-dynamical effects present in Ti(II)-salen, the DFT approaches provide very reasonable agreement with our best results. For this case, B3LYP proved geometries closer to those from CASSCF (LRMSD < 0.159 Å) and relative energies in very good agreement with out CASPT3 results (ΔE_{rel} < 2.84 kcal mol^{-1}).

Table 39. Leading determinants from SA-CASSCF calculations on the low-lying electronic states of Ti(II)-salen.

State	Determinant	Coefficient
1^1A	$\left(d_{z^2}\right)^2$	0.9050
	$\left(d_{xz}\right)^2$	-0.4094
2^1A	$\left(d_{z^2}\right)^2$	0.7071
	$\left(d_{xz}\right)^2$	-0.7071
3^1A	$\left(d_{z^2}\right)\alpha\left(d_{yz}\right)\beta$	0.6022
	$\left(d_{z^2}\right)\beta\left(d_{yz}\right)\alpha$	-0.6022
	$\left(d_{xz}\right)^2$	0.4917
	$\left(d_{yz}\right)^2$	-0.1752
1^3A	$\left(d_{z^2}\right)\alpha\left(d_{xz}\right)\alpha$	0.8272
	$\left(d_{xz}\right)\alpha\left(d_{yz}\right)\alpha$	0.5619
2^3A	$\left(d_{z^2}\right)\alpha\left(d_{yz}\right)\alpha$	0.6811
	$\left(d_{xz}\right)\alpha\left(d_{yz}\right)\alpha$	0.6784
	$\left(d_{z^2}\right)\alpha\left(d_{xz}\right)\alpha$	-0.2753
3^3A	$\left(d_{xz}\right)\alpha\left(d_{yz}\right)\alpha$	0.7077
	$\left(d_{z^2}\right)\alpha\left(d_{yz}\right)\alpha$	-0.7066

V(III)-Salen

CAS-CI computations for V(III)-salen reveal an electronic structure very similar to that for the isoelectronic Ti(II)-salen presented above. The three lowest singlet and triplet states were optimized at the SA-CASSCF(2/3)/6-31G* [1^1A, 2^1A, 3^1A, 1^3A, 2^3A, 3^3A] level of theory employing the active space depicted in Figure 42. The relative energies for these states from all multi-reference computations along with the relative

energies from DFT for the 1^1A, 1^3A, and 1^5A states are included in Table 40. The CASPT3 results predict the anticipated ^{3}A ground state for the system. The singlet state is predicted to lie slightly more than 20 kcal mol^{-1} higher in energy, being in very good agreement with the B3LYP results. Interestingly, the 1^3A and 2^3A states [split by approximately 2 kcal mol^{-1} in Ti(II)-salen] are nearly degenerate in V(III)-salen with the CASPT3 results flipping the state ordering relative to the CASPT2 and CASSCF results. These states are labeled with respect to the ordering observed in the SA-CASSCF computations. All multi-reference approaches place the states within 1 kcal mol^{-1} in relative energies, being within the anticipated error bars for the results. A similar effect is observed for the 1^1A and 2^1A states as well, being separated by only 0.03 kcal mol^{-1} at the CASPT3 level of theory. While BP86 and BPW91 predict the correct ordering of the electronic states, both functionals predict the 1^1A state to be more stable than that observed in our most reliable results. Overall, B3LYP provides superior agreement with CASPT3 for the relative energies in V(III)-salen.

Table 40. Relative energies (kcal mol^{-1}) for the low-lying electronic states of V(III)-salen computed at various levels of theory.

	CASPT3	CASPT2	CASSCF	B3LYP	BP86	BPW91
1^1A	20.71	23.56	30.71	20.29	14.48	14.85
2^1A	20.74	23.06	31.03	---	---	---
3^1A	26.28	28.50	35.84	---	---	---
1^3A	0.85	0.00	0.00	0.00	0.00	0.00
2^3A	0.00	0.44	1.02	---	---	---
3^3A	5.53	7.95	9.24	---	---	---
1^5A	---	---	---	35.34	39.23	38.29

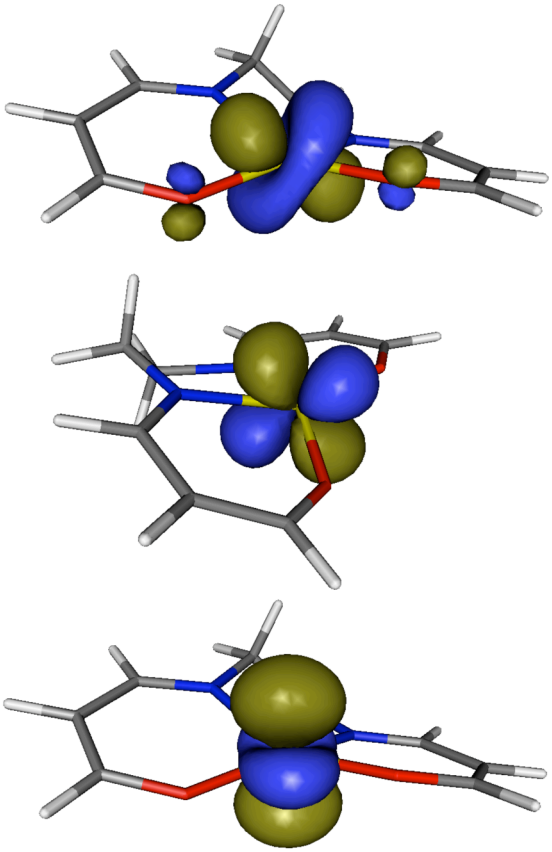

Figure 42. Isosurface plots of the dz2(lower), dxz (center), and dyz (upper) CASSCF orbitals that comprise the active space for V(III)-salen.

The optimized geometries of the 1^1A and 1^3A states of V(III)-salen are overlaid in Figure 43. The DFT geometries for both states are nearly indistinguishable, in both cases being more planar than the corresponding CASSCF geometry. Overall, the differences between the DFT and CASSCF geometries are slightly larger than those observed in Ti(II)-salen. The LRMSDs presented in Table 41 reveal the B3LYP geometries to be somewhat closer to the CASSCF geometries than are BP86 and BPW91, although the difference is clearly negligible. All of the functionals examined perform similarly in comparison to CASSCF for the geometries of both the 1^1A and 1^3A states.

Table 41. LRMSD(Å) in molecular geometries for the 1^1A, 1^3A, and 1^5A states of V(III)- and Nb(III)-salens.

		CASSCF	B3LYP	BP86	BPW91		
V(III)	CASSCF	--- ---	0.326 0.441	0.399 0.067	0.401 0.064	CASSCF	Nb(III)
	B3LYP	0.194 0.200	--- ---	0.093 0.454	0.085 0.457	B3LYP	
	BP86	0.216 0.209	0.034 0.019	--- ---	0.021 0.007	BP86	
	BPW91	0.211 0.207	0.028 0.015	0.008 0.006	--- ---	BPW91	

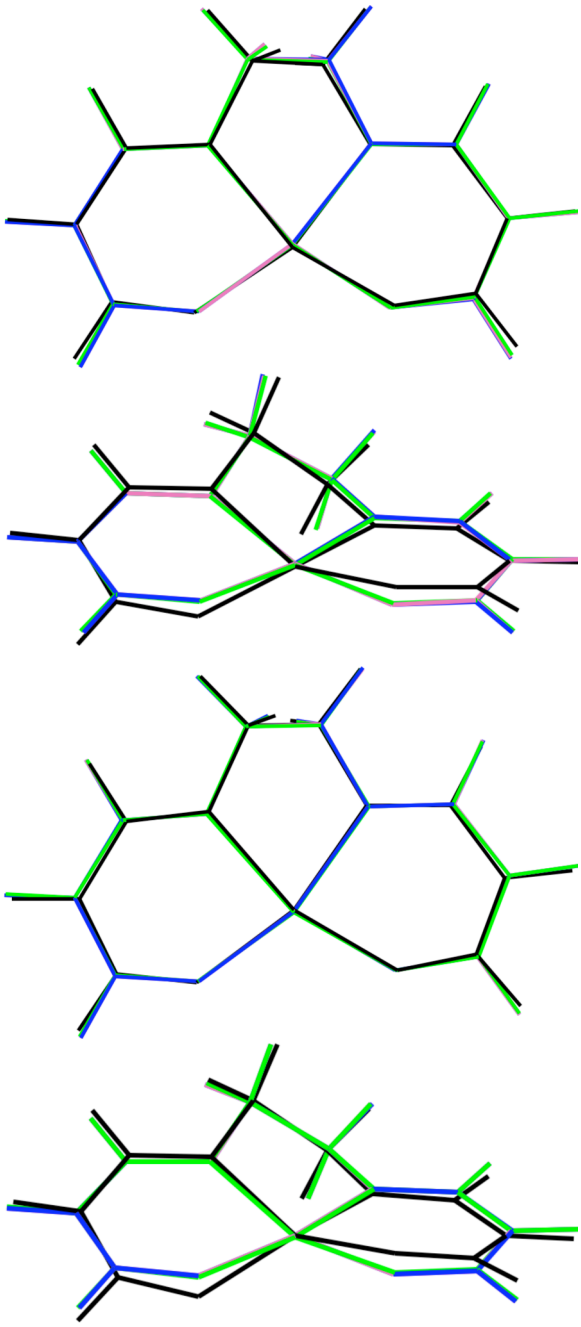

Figure 43. Overlay of the optimized geometries for the 1^1A (top) and 1^3A (bottom) states of V(III)-Salen from different levels of theory. The theoretical methods include CASSCF (black), B3LYP (green), BP86 (blue), and BPW91 (mauve).

The leading determinants from the SA-CASSCF computations are presented in Table 42. The 1^1A and 2^1A states are demonstrated to be qualitatively similar to the corresponding states in Ti(II)-salen, with increased multi-reference character. Relative to

Ti(II)-salen, the weight of the leading determinant is smaller and the weight of the second determinant is larger for both states. This is in contrast to the low-lying triplet states, which become increasingly single-reference with the increased oxidation state. The leading coefficients (0.9694, 1.0000, and 1.0000) are closer to what would be expected for well-behaved single-reference systems. Being very similar to Ti(II)-salen, B3LYP provides geometries and relative energies that are closer to our best results than are the BP86 and BPW91 results (LRMSD < 0.200 Å, ΔE_{rel} < 0.42 kcal mol^{-1}).

Table 42. Leading determinants from SA-CASSCF calculations on the low-lying electronic states of V(III)-salen.

State	Determinant	Coefficient
1^1A	$\left(d_{z^2}\right)^2$	0.8737
	$\left(d_{xz}\right)^2$	-0.4697
2^1A	$\left(d_{z^2}\right)^2$	0.7070
	$\left(d_{xz}\right)^2$	-0.7070
3^1A	$\left(d_{xz}\right)^2$	0.7392
	$\left(d_{yz}\right)^2$	-0.4777
	$\left(d_{z^2}\right)\alpha\left(d_{yz}\right)\beta$	0.3020
	$\left(d_{z^2}\right)\beta\left(d_{yz}\right)\alpha$	-0.3020
	$\left(d_{z^2}\right)^2$	0.2071
1^3A	$\left(d_{xz}\right)\alpha\left(d_{yz}\right)\alpha$	0.9694
	$\left(d_{z^2}\right)\alpha\left(d_{xz}\right)\alpha$	0.2455
2^3A	$\left(d_{z^2}\right)\alpha\left(d_{yz}\right)\alpha$	1.0000
3^3A	$\left(d_{z^2}\right)\alpha\left(d_{xz}\right)\alpha$	1.0000

Cr(IV)-Salen

The increased formal oxidation state in Cr(IV) leads to strong mixing of the metal d-orbitals with the $R\pi$ orbitals of the salen ligand, providing an electronic structure distinctly different from that observed in Ti(II)- and V(III)-salen above. The DFT approaches provide qualitatively different descriptions of the electronic state ordering for this system, as can be observed from the relative energies in Table 43. All functionals predict the 1^5A state to be significantly lower in energy than in the previous systems, and B3LYP even predicts a 1^5A ground state. BP86 and BPW91 again provide a very similar description of the electronic state ordering. CAS-CI computations for Cr(IV)-salen reveal the strong mixing of the metal and ligand orbitals as well as the increased nondynamical correlation effects which result. The three low-lying singlet and triplet states observed in the previous systems are significantly split as a consequence, giving rise to a single low-lying electronic state. The computations further demonstrate the existence of two nearly-degenerate low-lying quintet states. These states were optimized at the SA-CASSCF(6/6)/6-31G* [1^1A, 1^3A, 1^5A, 2^5A] level of theory with an active space consisting of the ligand $R\pi$ orbitals and the four lowest-lying Cr d-orbitals. These are depicted in Figure 44 from the SA-CASSCF computation of the 1^3A state. The SA-CASSCF orbitals clearly reveal the strong mixing of the ligand $R\pi$ and Cr d_{xz} and d_{yz} orbitals. The orbitals have been labeled in the figure based upon the dominant d-orbital character. The CASSCF results reveal nearly degenerate 1^3A, 1^5A, and 2^5A states with small corrections to the relative energies for dynamical electron correlation at the CASPT2 level. The corrections for dynamical correlation are much larger for the high-lying 1^1A state, although the CASPT3 correction is less than 1 kcal mol^{-1} for this state.

The CASPT3 corrections are somewhat larger for the low-lying quintet states (8.29 and 12.40 kcal mol^{-1} respectively). All DFT approaches predict the 1^1A state to be significantly lower in energy than our best results. The B3LYP results are qualitatively very different from all approaches considered, predicting a 1^5A ground state for this system. Depsite overstabilzing the 1^1A state, the BP86 and BPW91 results provide very reasonable agreement with the CASPT3 values for the lowest electronic states.

Table 43. Relative energies (kcal mol^{-1}) for the low-lying electronic states of Cr(IV)-salen computed at various levels of theory.

	CASPT3	CASPT2	CASSCF	B3LYP	BP86	BPW91
1^1A	180.66	181.37	60.25	24.71	19.34	19.87
1^3A	0.00	0.00	0.00	4.31	0.00	0.00
1^5A	8.48	0.19	0.61	0.00	11.52	9.81
2^5A	13.51	1.11	0.88	---	---	---

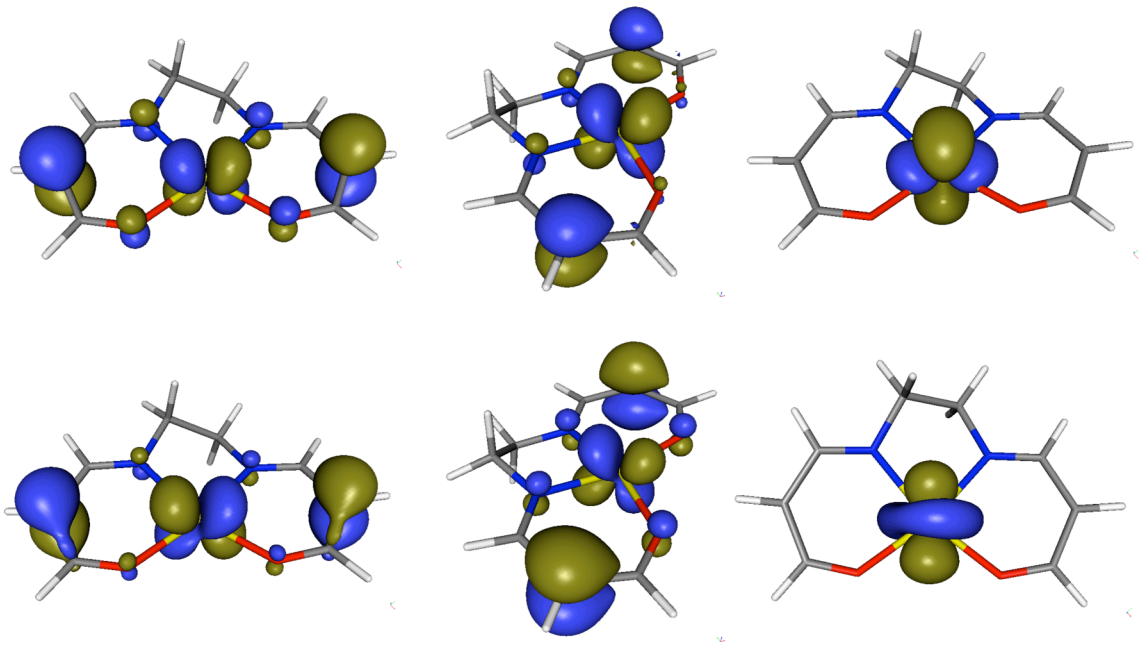

Figure 44. Isosurface plots of the orbitals comprising the active space for Cr(IV)-salen.

While the strong mixing of the $R\pi$ orbitals with the Cr d_{xz} and d_{yz} orbitals is clearly evident from Figure 44, the resulting CI coefficients (included in(Table 44)) reveal the strong multi-reference character of the electronic states. The leading coefficients are never larger than 0.4885 for all of the states explored. Surprisingly, the DFT approaches provide geometries closer to the CASSCF geometries than was observed for Ti(II)- or V(III)-salen. This can be clearly seen from Figure 45 and from the LRMSD values in Table 45. While B3LYP provides geometries that are somewhat closer to CASSCF than are those from BP86 and BPW91, all of the functionals provide similar agreement for the geometries of Cr(IV)-salen.

Table 44. Leading determinants from CASSCF calculations on the low-lying electronic states of Cr(IV)-salen.

State	Determinant	Coefficient
1^1A	$\left(d_{yz}1\right)^2\left(d_{xz}1\right)\alpha\left(d_{xz}2\right)\beta\left(d_{yz}2\right)\beta\left(d_{x^2-y^2}\right)\alpha$	0.3109
	$\left(d_{yz}1\right)^2\left(d_{xz}1\right)\beta\left(d_{xz}2\right)\alpha\left(d_{yz}2\right)\alpha\left(d_{x^2-y^2}\right)\beta$	0.3109
	$\left(d_{z^2}\right)^2\left(d_{xz}1\right)\beta\left(d_{xz}2\right)\alpha\left(d_{yz}2\right)\alpha\left(d_{x^2-y^2}\right)\beta$	-0.2430
	$\left(d_{z^2}\right)^2\left(d_{xz}1\right)\alpha\left(d_{xz}2\right)\beta\left(d_{yz}2\right)\beta\left(d_{x^2-y^2}\right)\alpha$	-0.2430
	$\left(d_{yz}1\right)^2\left(d_{xz}1\right)^2\left(d_{xz}2\right)^2$	-0.2257
	$\left(d_{yz}1\right)^2\left(d_{xz}1\right)^2\left(d_{x^2-y^2}\right)^2$	0.2135
1^3A	$\left(d_{yz}1\right)^2\left(d_{xz}1\right)^2\left(d_{yz}2\right)\alpha\left(d_{xz}2\right)\alpha$	-0.3498
	$\left(d_{yz}1\right)^2\left(d_{x^2-y^2}\right)^2\left(d_{yz}2\right)\alpha\left(d_{xz}2\right)\alpha$	0.3346
	$\left(d_{xz}1\right)^2\left(d_{z^2}\right)^2\left(d_{yz}2\right)\alpha\left(d_{xz}2\right)\alpha$	0.2781
	$\left(d_{yz}1\right)^2\left(d_{xz}1\right)\beta\left(d_{xz}2\right)\alpha\left(d_{yz}2\right)\alpha\left(d_{x^2-y^2}\right)\alpha$	0.2737
	$\left(d_{x^2-y^2}\right)^2\left(d_{z^2}\right)^2\left(d_{yz}2\right)\alpha\left(d_{xz}2\right)\alpha$	-0.2701
	$\left(d_{z^2}\right)^2\left(d_{xz}1\right)\beta\left(d_{xz}2\right)\alpha\left(d_{yz}2\right)\alpha\left(d_{x^2-y^2}\right)\alpha$	-0.2190
1^5A	$\left(d_{yz}1\right)^2\left(d_{yz}2\right)\alpha\left(d_{xz}1\right)\alpha\left(d_{xz}2\right)\alpha\left(d_{x^2-y^2}\right)\alpha$	0.4885
	$\left(d_{xz}1\right)^2\left(d_{xz}2\right)\alpha\left(d_{yz}1\right)\alpha\left(d_{yz}2\right)\alpha\left(d_{z^2}\right)\alpha$	-0.4142
	$\left(d_{x^2-y^2}\right)^2\left(d_{yz}1\right)\alpha\left(d_{yz}2\right)\alpha\left(d_{xz}1\right)\alpha\left(d_{z^2}\right)\alpha$	0.3996
	$\left(d_{z^2}\right)^2\left(d_{xz}1\right)\alpha\left(d_{xz}2\right)\alpha\left(d_{yz}2\right)\alpha\left(d_{x^2-y^2}\right)\alpha$	-0.3920
	$\left(d_{yz}1\right)\alpha\left(d_{yz}2\right)\beta\left(d_{xz}1\right)\alpha\left(d_{xz}2\right)\alpha\left(d_{x^2-y^2}\right)\alpha\left(d_{z^2}\right)\alpha$	-0.2788
	$\left(d_{xz}1\right)\alpha\left(d_{xz}2\right)\beta\left(d_{yz}1\right)\alpha\left(d_{yz}2\right)\alpha\left(d_{x^2-y^2}\right)\alpha\left(d_{z^2}\right)\alpha$	-0.2759
	$\left(d_{xz}2\right)\alpha\left(d_{xz}1\right)\beta\left(d_{yz}1\right)\alpha\left(d_{yz}2\right)\alpha\left(d_{x^2-y^2}\right)\alpha\left(d_{z^2}\right)\alpha$	0.2581
2^5A	$\left(d_{xz}1\right)^2\left(d_{xz}2\right)\alpha\left(d_{yz}1\right)\alpha\left(d_{yz}2\right)\alpha\left(d_{x^2-y^2}\right)\alpha$	0.4377
	$\left(d_{yz}1\right)^2\left(d_{yz}2\right)\alpha\left(d_{xz}2\right)\alpha\left(d_{x^2-y^2}\right)\alpha\left(d_{z^2}\right)\alpha$	-0.4004
	$\left(d_{z^2}\right)^2\left(d_{yz}1\right)\alpha\left(d_{yz}2\right)\alpha\left(d_{xz}2\right)\alpha\left(d_{x^2-y^2}\right)\alpha$	-0.3757

Table 45. LRMSD(Å) in molecular geometries for the 1^1A, 1^3A, and 1^5A states of Cr(IV)- and Mo(IV)-salens.

		CASSCF	B3LYP	BP86	BPW91		
Cr(IV)	CASSCF	--- --- ---	0.150 0.084 ---	0.160 0.097 ---	0.160 0.093 ---	CASSCF	Mo(IV)
	B3LYP	0.131 0.140 0.174	--- --- ---	0.026 0.016 ---	0.023 0.016 ---	B3LYP	
	BP86	0.140 0.134 0.198	0.025 0.023 0.034	--- --- ---	0.006 0.005 ---	BP86	
	BPW91	0.137 0.133 0.183	0.020 0.017 0.030	0.006 0.008 0.018	--- --- ---	BPW91	

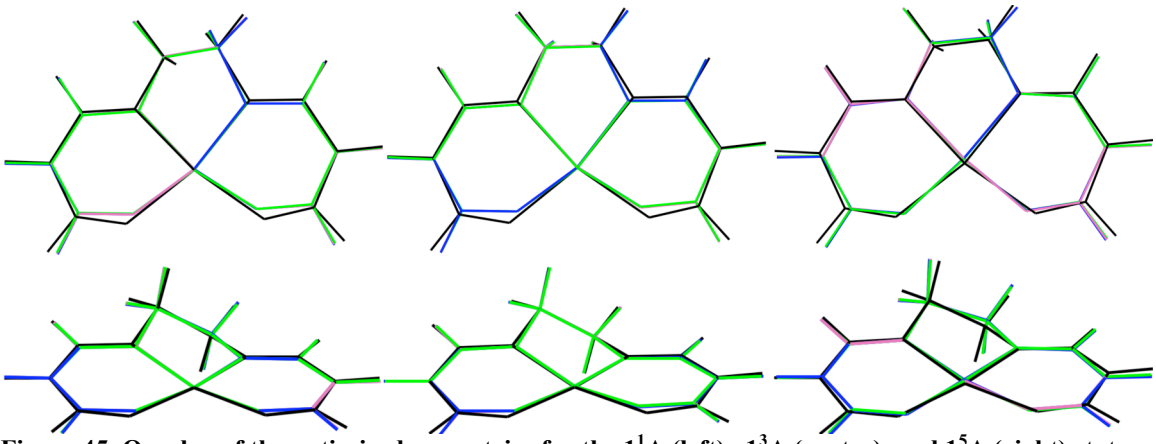

Figure 45. Overlay of the optimized geometries for the 1^1A (left), 1^3A (center), and 1^5A (right) states of Cr(IV)-Salen from different levels of theory. The theoretical methods include CASSCF (black), B3LYP (green), BP86 (blue), and BPW91 (mauve).

The 4D-Metals

Zr(II)-Salen

CAS-CI computations on Zr(II)-salen reveal a similar electronic structure to that of Ti(II)-salen presented above. The relative energies computed at the SA-CASSCF(2/3)/6-31G*[1^1A,2^1A,3^1A,1^3A,2^3A,3^3A] level are included in Table 46 and compared to those from DFT. The active-space orbitals form the SA-CASSCF optimization of the 1^1A state are depicted in Figure 46. It is generally assumed that complexes of 4d metals exhibit smaller non-dynamical correlation effects and larger electronic state splittings. It is interesting to note that, although the splitting of the lowest singlet or triplet states is predicted to be larger in Zr(II)- than in Ti(II)-salen, the splitting of the lowest singlet and triplet states is predicted to be slightly smaller for this system [9.69 kcal mol^{-1} at the CASPT3 level in comparison to 13.24 kcal mol^{-1} for Ti(II)-salen]. Somewhat surprisingly, the singlet-triplet splitting from B3LYP is identical to the CASPT3 result. The "generalized gradient" approaches (BP86 and BPW91) slightly underestimate the stability of the triplet state compared to the B3LYP and the high-level CASPT3 results.

Table 46. Relative energies (kcal mol^{-1}) for the low-lying electronic states of Zr(II)-salen computed at various levels of theory.

	CASPT3	CASPT2	CASSCF	B3LYP	BP86	BPW91
1^1A	9.69	13.59	15.00	9.69	6.48	6.32
2^1A	16.13	17.67	18.70	---	---	---
3^1A	32.65	33.24	28.79	---	---	---
1^3A	0.00	0.00	0.00	0.00	0.00	0.00
2^3A	23.43	26.58	15.52	---	---	---
3^3A	38.54	41.47	25.44	---	---	---
1^5A	---	---	---	68.51	66.45	66.26

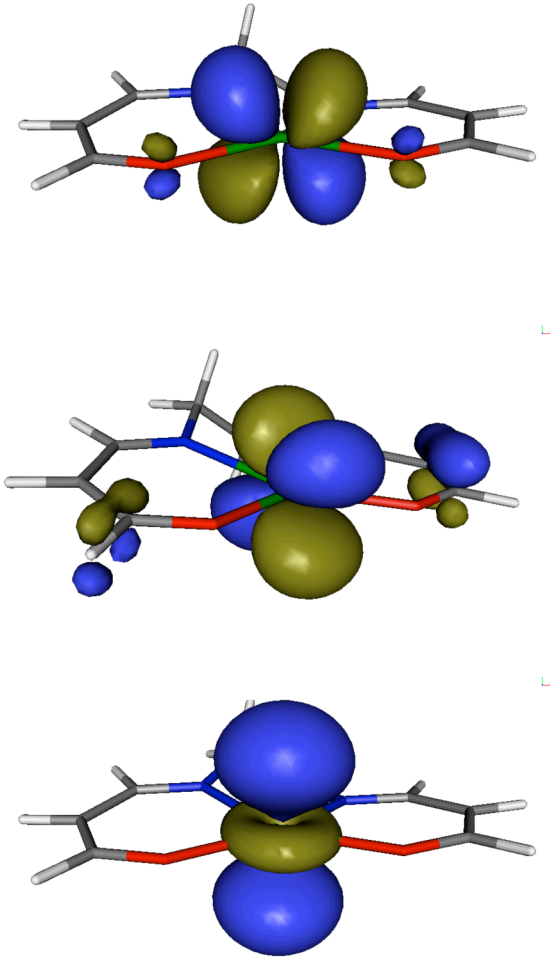

Figure 46. Isosurface plots of the d_{z^2} (lower), d_{xz} (center), and d_{yz} (upper) CASSCF orbitals that comprise the active space for Zr(II)-salen.

The overlays of the optimized 1^1A and 1^3A geometries are displayed in Figure 47. Again, the geometries provided by all functionals agree very well with those from CASSCF. The comparison is similar to that witnessed in Ti(II)-salen as is evident from the LRMSD values in Table 38. As has been observed previously in other metal-salen systems [247], DFT predicts a slightly larger out-of-plane puckering of the central metal atom when compared to the CASSCF results.

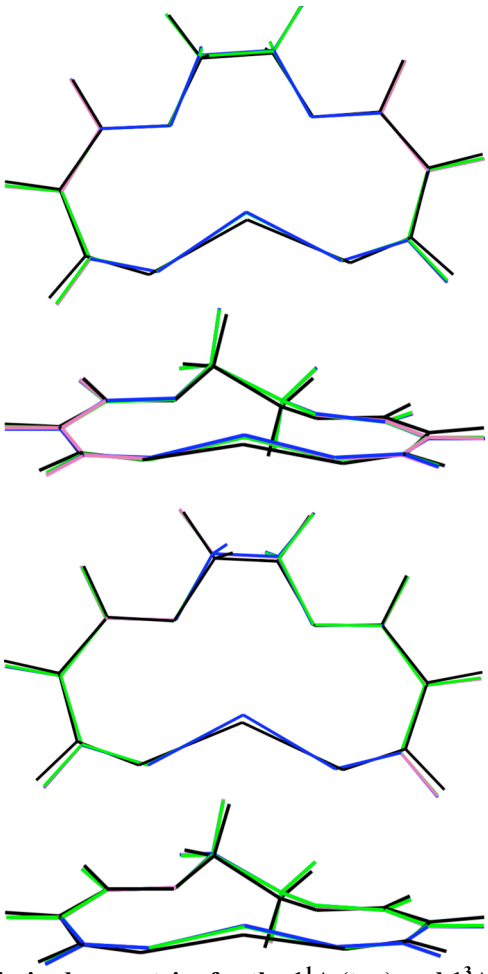

Figure 47. Overlay of the optimized geometries for the 1^1A (top) and 1^3A (bottom) states of Zr(II)-Salen from different levels of theory. The theoretical methods include CASSCF (black), B3LYP (green), BP86 (blue), and BPW91 (mauve).

The leading determinants from the SA-CASSCF computation are presented in Table 47. The triplet state are all predicted to be strongly single-reference (leading coefficients of 0.9992, 1.0000, and 0.9874 respectively). In contrast, the singlet states remain strongly multi-reference and the coefficients are very similar to those observed in Ti(II)-salen above.

Table 47. Leading determinants from SA-CASSCF calculations on the low-lying electronic states of Zr(II)-salen.

State	Determinant	Coefficient
1^1A	$\left(d_{z^2}\right)^2$	0.9093
	$\left(d_{xz}\right)^2$	-0.4077
2^1A	$\left(d_{z^2}\right)^2$	0.7071
	$\left(d_{xz}\right)^2$	-0.7071
3^1A	$\left(d_{z^2}\right)^2$	0.778
	$\left(d_{xz}\right)^2$	-0.544
	$\left(d_{yz}\right)^2$	-0.210
1^3A	$\left(d_{z^2}\right)\alpha\left(d_{xz}\right)\alpha$	0.9922
2^3A	$\left(d_{z^2}\right)\alpha\left(d_{yz}\right)\alpha$	1.0000
3^3A	$\left(d_{xz}\right)\alpha\left(d_{yz}\right)\alpha$	0.9874
	$\left(d_{z^2}\right)\alpha\left(d_{yz}\right)\alpha$	0.1580

Nb(III)-Salen

The relative energies from all methods for the low-lying electronic states of Nb(III)-salen are included in Table 48. While all of the DFT functionals place the 1^5A state significantly higher (approximately 50 kcal mol^{-1}) than the ground state, B3LYP

predicts the 1^1A and 1^3A states (which are revealed to be well separated by both BP86 and BPW91) to be nearly degenerate. CAS-CI computations reveal a very similar electronic structure to Zr(II)-salen above, with three low-lying singlet and triplet states well described by the same 2-in-3 active space (depicted in Figure 48). The SA-CASSCF(2/3)/6-31G*[1^1A, 2^1A, 3^1A, 1^3A, 2^3A, 3^3A] relative energies (included in Table 48) agree well with those from both BP86 and BPW91 and corrections for dynamical correlation both at the CASPT2 and CASPT3 level appear modest. From the leading coefficients (Table 49), all of the singlet states are observed to be strongly multi-reference. While the open-shell 2^1A state is not anticipated to be well described by a single reference function, the leading coefficients for the closed-shell 1^1A and 3^1A states are extremely small (0.8083 and 0.7633 respectively). Overall, the leading determinants for Nb(III)-salen in Table 49 reveal a much stronger multi-reference character than those for the iso-electronic Zr(II)-salen presented in Table 47.While the BP86 and BPW91 results do agree favorably with those from CASPT3, single-reference methods are not expected to provide reliable results for systems with the strong non-dynamical correlation effects observed here for the singlet states of Nb(III)-salen.

Table 48. Relative energies (kcal mol^{-1}) for the low-lying electronic states of Nb(III)-salen computed at various levels of theory.

	CASPT3	CASPT2	CASSCF	B3LYP	BP86	BPW91
1^1A	19.78	19.57	18.30	1.39	13.37	14.00
2^1A	20.71	20.83	18.99	---	---	---
3^1A	29.42	29.50	29.77	---	---	---
1^3A	0.00	0.00	0.00	0.00	0.00	0.00
2^3A	12.75	13.21	9.62	---	---	---
3^3A	25.45	23.63	13.11	---	---	---
1^5A	---	---	---	47.09	57.81	57.07

Table 49. Leading determinants from SA-CASSCF calculations on the low-lying electronic states of Nb(III)-salen.

State	Determinant	Coefficient
1^1A	$\left(d_{z^2}\right)^2$	0.8083
	$\left(d_{xz}\right)^2$	-0.5855
2^1A	$\left(d_{z^2}\right)\alpha\left(d_{xz}\right)\beta$	0.7070
	$\left(d_{z^2}\right)\beta\left(d_{xz}\right)\alpha$	-0.7070
3^1A	$\left(d_{xz}\right)^2$	0.7633
	$\left(d_{z^2}\right)^2$	0.4340
	$\left(d_{yz}\right)^2$	-0.4034
	$\left(d_{z^2}\right)\beta\left(d_{yz}\right)\alpha$	0.1821
	$\left(d_{z^2}\right)\alpha\left(d_{yz}\right)\beta$	-0.1821
1^3A	$\left(d_{z^2}\right)\alpha\left(d_{xz}\right)\alpha$	0.9960
2^3A	$\left(d_{z^2}\right)\alpha\left(d_{yz}\right)\alpha$	
3^3A	$\left(d_{xz}\right)\alpha\left(d_{yz}\right)\alpha$	0.9957

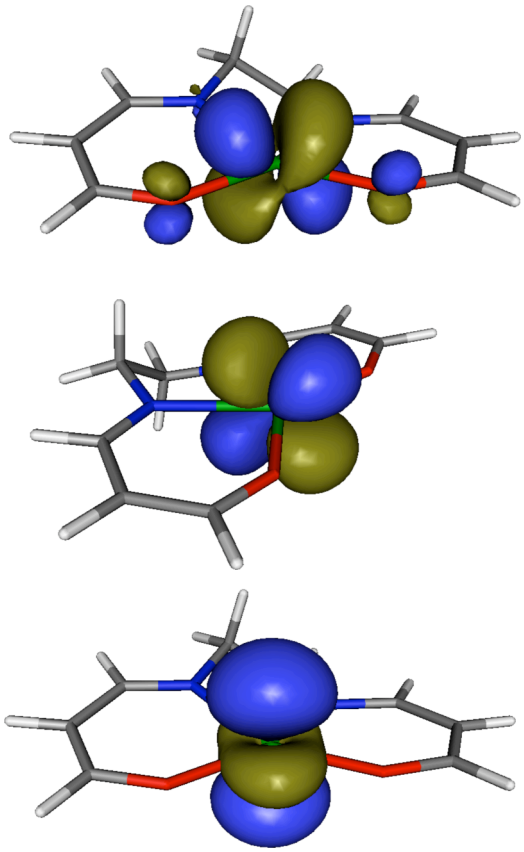

Figure 48. Isosurface plots of the d_{z2}(lower), d_{xz} (center), and d_{yz} (upper) CASSCF orbitals that comprise the active space for Nb(III)-salen.

The optimized geometries for the 1^1A and 1^3A states of Nb(III)-salen are overlaid in Figure 49 and the LRMSD values are tabulated in Table 41. As can be easily observed both by comparing the geometries for Zr(II)-salen in Figure 47 to those in Figure 49 here or by comparing the LRMSD values from Table 38 to those from Table 41, the overall agreement in the molecular geometries is significantly worse for Nb(III)-salen than for Zr(II)-salen. The maximum LRMSD [0.147 Å in the case of Zr(II)-salen] is now 0.457 Å. The geometries from BP86 and BPW91 are nearly identical, being very close (LRMSD < 0.1 Å) to the CASSCF geometry for the 1^3A state. However, none of the functionals employed provide reasonable agreement with the CASSCF geometry for the highly

multi-reference 1^1A state. While the B3LYP 1^1A geometry is closest to that from CASSCF, the LRMSD of 0.326 Å remains quite large. All of the functionals predict the 1^1A state to possess a significant out-of-plane distortion relative to the CASSCF geometry

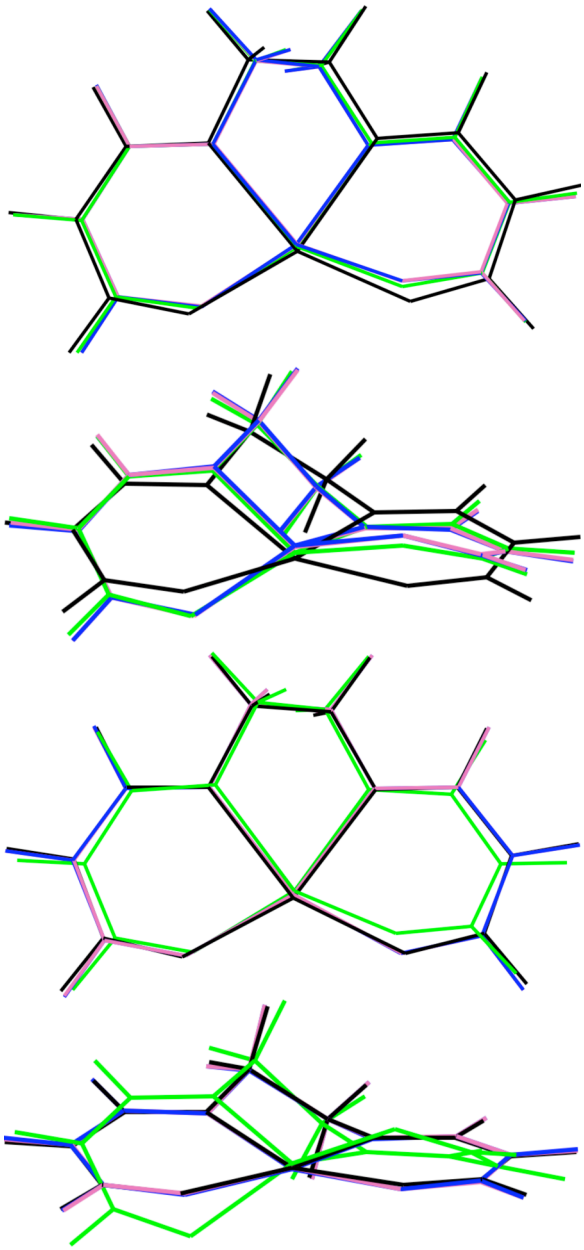

Figure 49. Overlay of the optimized geometries for the 1^1A (top) and 1^3A (bottom) states of Nb(III)-Salen from different levels of theory. The theoretical methods include CASSCF (black), B3LYP (green), BP86 (blue), and BPW91 (mauve).

Mo(IV)-Salen

The relative energies from all methods for Mo(IV)-salen are included in Table 50, being qualitatively similar to those of the iso-electronic Zr(II)- and Nb(III)-salens presented above. All of the density functionals provide very similar descriptions of the electronic state ordering. While all functionals place the 1^5A state much lower in energy than that observed in Zr(II)- and Nb(III)-salen, the DFT approaches along with large CAS-CI computations predict the 1^5A state to be fairly well separated from the low-lying singlet and triplet states. The lowest singlet and triplet states are all seemingly well described by the same three-in-two active-space (see Figure 50) employed for the previous systems and the SA-CASSCF(2/3)/6-31G* [1^1A, 2^1A, 3^1A, 1^3A, 2^3A, 3^3A] relative energies are included in Table 50. The 1^3A-1^1A splitting predicted at the SA-CASSCF level is slightly larger than that observed in Nb(III)-salen as well as that predicted by all of the DFT approaches for this system. Unsurprisingly, the B3LYP functional predicts a slightly larger splitting than the BP86 and BPW91 approaches.

Table 50. Relative energies (kcal mol^{-1}) for the low-lying electronic states of Mo(IV)-salen computed at various levels of theory.

	CASPT3	CASPT2	CASSCF	B3LYP	BP86	BPW91
1^1A	23.21	21.98	19.26	16.47	14.75	14.96
2^1A	22.34	22.80	19.40	---	---	---
3^1A	31.34	30.50	32.72	---	---	---
1^3A	0.00	0.00	0.00	0.00	0.00	0.00
2^3A	7.52	7.99	1.91	---	---	---
3^3A	33.84	35.58	32.72	---	---	---
1^5A	---	---	---	26.12	32.01	31.08

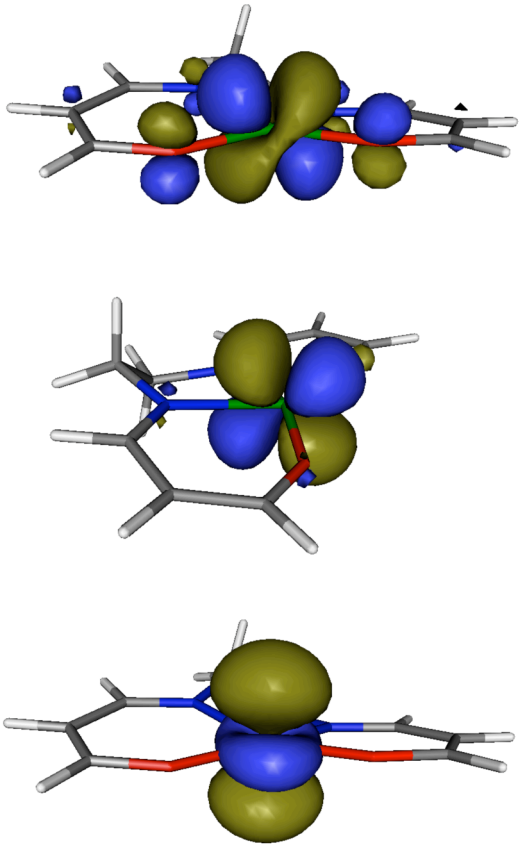

Figure 50. Isosurface plots of the dz2(lower), dxz (center), and dyz (upper) CASSCF orbitals that comprise the active space for Mo(IV)-salen.

The leading determinants from the SA-CASSCF computations are presented in Table 51 for the lowest singlet and triplet states. Just as in Zr(II)- and Nb(III)-salen, the singlet states appear highly multi-reference while the triplet states are all strongly single-reference. The 1^1A state becomes increasingly multi-reference moving from Zr(II)-salen to the present system. The weight of the leading $\left(d_{z^2}\right)^2$ determinant becomes increasingly smaller [being 0.9093, 0.8083, 0.7622 for Zr(II)-, Nb(III)-, and Mo(IV)-salen respectively]. At the same time, the weight of the $\left(d_{xz}\right)^2$ configuration becomes increasingly larger [being -0.4077, -0.5855, and -0.6459 for the same systems].

Table 51. Leading determinants from SA-CASSCF calculations on the low-lying electronic states of Mo(IV)-salen.

State	Determinant	Coefficient
1^1A	$\left(d_{z^2}\right)^2$	0.7622
	$\left(d_{xz}\right)^2$	-0.6459
2^1A	$\left(d_{z^2}\right)\alpha\left(d_{xz}\right)\beta$	0.7071
	$\left(d_{z^2}\right)\beta\left(d_{xz}\right)\alpha$	-0.7071
3^1A	$\left(d_{xz}\right)^2$	0.7601
	$\left(d_{z^2}\right)^2$	0.5542
	$\left(d_{yz}\right)^2$	-0.3182
1^3A	$\left(d_{z^2}\right)\alpha\left(d_{xz}\right)\alpha$	0.9982
2^3A	$\left(d_{z^2}\right)\alpha\left(d_{yz}\right)\alpha$	1.0000
3^3A	$\left(d_{xz}\right)\alpha\left(d_{yz}\right)\alpha$	0.9982

The optimized geometries for the 1^1A and 1^3A states of Mo(IV)-salen from the various levels of theory are depicted in Figure 51 and the computed LRMSD values are presented in Table 45. The CASSCF molecular geometries (especially for the 1^1A state) are noticeably more planar than those from the DFT approaches. As can be observed from the LRMSD values in Table 45, the BP86 and BPW91 geometries are nearly identical and are very similar to those provided by the B3LYP functional. All of the DFT approaches provide geometries that are significantly different from the CASSCF geometries, although less so for the 1^3A state than for the 1^1A state.

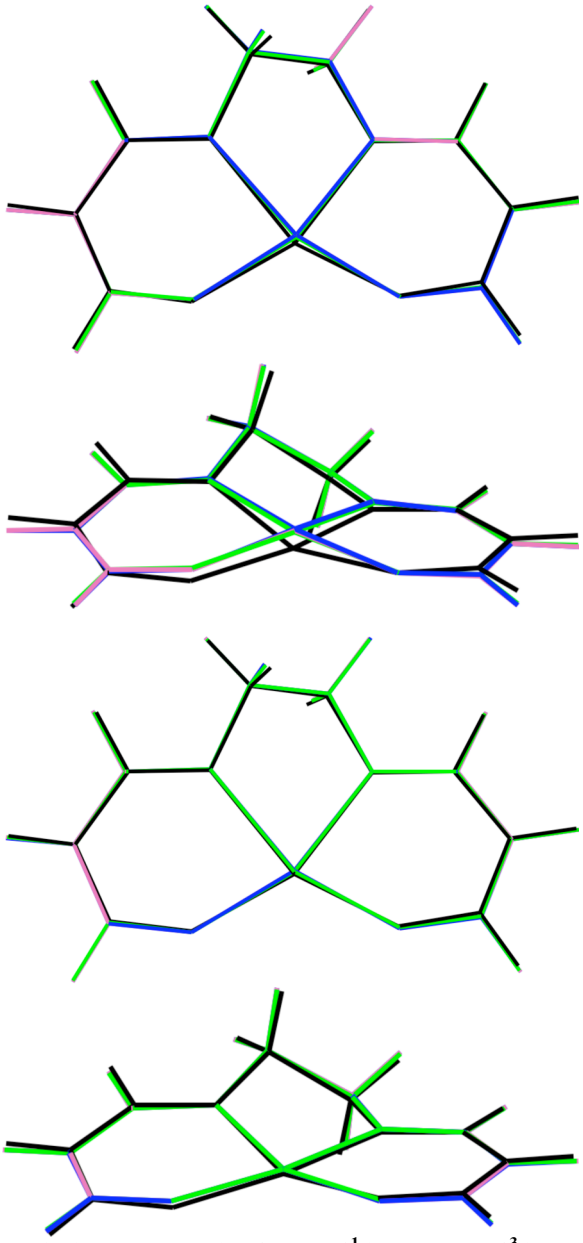

Figure 51. Overlay of the optimized geometries for the 1^1A (top) and 1^3A (bottom) states of Mo(IV)-Salen from different levels of theory. The theoretical methods include CASSCF (black), B3LYP (green), BP86 (blue), and BPW91 (mauve).

Conclusions

The results presented above clearly establish the strong non-dynamical correlation effects in the d2-metal salen systems. With the exception of Cr(IV)-salen, all of the systems examined were found to posses a 1^3A ground state. The 1^1A states were observed to lie 10-30 kcal mol^{-1} higher in energy, with the singlet-triplet splitting

increasing with increasing formal oxidation state at the metal center. The 1^1A states were observed to become increasingly multi-reference with the increasing oxidation state (based both upon a decreasing C_0 and an increasing C_1), in contrast to the 1^3A states become increasingly single-reference. With the exception of Cr(IV)-salen, all of the systems were well described by a relatively small 2-in-3 active space. Interestingly, the 4d metal-salens exhibit similar non-dynaical correlation effects as the corresponding 3d system. The leading coefficients from the SA-CASSCF computations are similar in each.

The results from three commonly-employed density functionals were benchmarked against those from CASSCF and CASPT3. Given the strong multi-reference character of many of the states examined, the overall performance of DFT is surprisingly strong. With the exception of the Nb(III)-salen system, all three functionals provide geometries that are typically within 0.2 Å LRMSD of the corresponding CASSCF geometry. The performance for relative energies was observed to be somewhat worse, with B3LYP providing relative energies closer to the CASPT3 results than BP86 or BPW91 for all systems studied with the exception of Nb(III)-salen. As has been observed in our previous work, the choice of the exchange functional remains the central concern when selecting an appropriate DFT approach for metal-ligand systems such as these. The results from BP86 and BPW91 are nearly identical for all systems. With the exception of Nb(III)-salen, B3LYP was found to provide relative energies superior to the BP86 and BPW91 functionals. Both the BP86 and BPW91 approaches tend to underestimate the relative stability of the high-spin 1^3A states. Although none of the functionals employed provided reliable results for Nb(III)-salen, B3LYP was observed to

provide geometries and relative energies closer to out benchmark values for the remainder of the systems examined.

CHAPTER 9

CONCLUSIONS AND FUTURE WORK

Two seemingly very different problems, the accurate theoretical description of bond-breaking potentials far from equilibrium and the accurate treatement of the equilibrium strucutures of metal-containing catalyst systems, are very closely related within electronic structure theory. As bonds are stretched far from equilibrium, the near-degeneracy of the bonding and anti-bonding orbitals results in a breakdown of the single-reference approximation. In metal-lignand catalysts systems (such as the systems studied here) have been shown to exhibit strong non-dynamical correlation effects resulting from the partial filling of the spatially- and energetically-proximal metal d-orbitals. The work presented here demonstrates that such effects may be significantly stronger in the latter case than in the former.

As near-degeneracy effects arise and the single-reference approximation begins to break down, methods are required that are capable of handling the multi-reference nature of the electronic states. The central theme of the work presented here must certainly be the applicability of small, compact reference functions to reliably treat the multi-refernce nature of the low-lying electronic states. When combined with corrections for dynamical electron correlation, highly accurate results can be obtained employing extremely small reference functions.

The problems associated with the accurate theoretical description of bond-breaking processes were addressed first. The work presented in Chapter 3 demonstrated the importance of spin completeness for the accurate treatment of bond-breaking potentials. The inclusion of the necessary spin-complements reduced the errors in the

original SF-SCF by more than 50%. Given the accuracy of the SF approaches when combined with methods for dynamical correlation, it is anticipated that perturbative corrections to the SC-SF reference function will provide highly accurate results for the description of bond-breaking potentials. In Chapter 4, the choice of an appropriate active space for general CASSCF and RASSCF reference functions was addressed for the bond-breaking problem. The results demonstrated that minimal reference spaces can provide results of similar quality to and at much cheaper computational cost than their larger active space analogues when combined with corrections for dynamical electron correlation. Furthermore, the minimal active space results were demonstrated to systematically approach the correct answer as higher levels of electron correlation are included. This is an important aspect that was not shared with the larger active-space analogues.

In the preceding three chapters, high-level multi-reference approaches were employed to benchmark the performance of more approximate methods for the electronic structure of several metal-salen catalysts. Although there is still a large amount of work to be completed, the results presented are quite revealing. The overall reasonable performance of the DFT approaches is quite surprising, given the strong multi-reference character of the electronic states. MP2 was demonstrated to provide highly unreliable results for these systems. CCSD and CCSD(T) approaches were incapable of completely remedying these discrepancies in most cases, thus all single-reference wavefuntion-based approaches provided highly erroneous results for the vast majority of the systems examined. The choice of which functional should be routinely employed for the study of metal-salen catalyzed chemical transformations remains elusive, as examples were

presented for the successes and failures of all of the functionals explored. Future work will focus upon a more complete examination of the multi-reference effects in metal-salen systems. We will examine additional d-orbital occupations as well as the impact using the full ligand and of counterions. The similarities in the multi-reference character of the 3d and 4d systems were quite surprising. Further investigation of these effects in other metal-containing systems will be required.

Of all the methods employed, CASPT2 likely provides the best balance of accuracy and computation cost. While the ability to employ small reference spaces in such computations extends the range of systems that can be examined, the computations remain extremely demanding. Additional work will examine the possibility of reducing the necessary computational expense by employing additional approximations. We will explore employing geometries from more approximate approaches in conjunction with CASTPT2 single-points for energies, potentially employing geometries from DFT. We will further investigate the ability to employ orbitals other than the CASSCF orbitals for CASPT2 single-point computations, alleviating the need for the orbital optimization.

REFERENCES

1. Moore, G.E., *Cramming more components onto integrated circuits.* Electronics, 1965. **38**(8).

2. Mollick, E., *Establishing Moore's law.* Ieee Annals of the History of Computing, 2006. **28**(3): p. 62-75.

3. Voller, V.R. and F. Porte-Agel, *Moore's law and numerical modeling.* Journal of Computational Physics, 2002. **179**(2): p. 698-703.

4. *Jaguar*. 1991-2003, Schrödinger, L.L.C.: Portland, OR.

5. Case, D.A., et al., *The Amber biomolecular simulation programs.* Journal of Computational Chemistry, 2005. **26**(16): p. 1668-1688.

6. Chasman, D., et al., *Parallel pseudospectral electronic structure: I. Hartree-Fock calculations.* Journal of Computational Chemistry, 1998. **19**(9): p. 1017-1029.

7. Colvin, M.E., et al., *Parallel Direct Scf for Large-Scale Calculations.* Theoretica Chimica Acta, 1993. **84**(4-5): p. 301-314.

8. Crawford, T.D., et al., *PS13: An open-source ab initio electronic structure package.* Journal of Computational Chemistry, 2007. **28**(9): p. 1610-1616.

9. Dachsel, H., et al., *A massively parallel multireference configuration interaction program: The parallel COLUMBUS program.* Journal of Computational Chemistry, 1997. **18**(3): p. 430-448.

10. Ford, A.R., T. Janowski, and P. Pulay, *Array files for computational chemistry: MP2 energies.* Journal of Computational Chemistry, 2007. **28**(7): p. 1215-1220.

11. Frisch, M.J., G.W. Trucks, and H.B. Schlegel, *GAUSSIAN 98*. 1998, Gaussian Inc.: Pittsburgh, PA.

12. Goedecker, S., *Linear scaling electronic structure methods.* Reviews of Modern Physics, 1999. **71**(4): p. 1085-1123.

13. Gomes, A.S.P., A. Merzky, and L. Visscher, *A framework for execution of computational chemistry codes in grid environments*, in *Computational Science - Iccs 2006, Pt 3, Proceedings*. 2006. p. 97-104.

14. Gonze, X., et al., *First-principles computation of material properties: the ABINIT software project.* Computational Materials Science, 2002. **25**(3): p. 478-492.

15. Guest, M.F., et al., *The GAMESS-UK electronic structure package: algorithms, developments and applications.* Molecular Physics, 2005. **103**(6-8): p. 719-747.

16. Guest, M.F., P. Sherwood, and J.H. Vanlenthe, *Parallelism in Computational Chemistry .1. Hypercube-Connected Multicomputers.* Theoretica Chimica Acta, 1993. **84**(4-5): p. 423-441.

17. Headgordon, M., J.A. Pople, and M.J. Frisch, *Mp2 Energy Evaluation by Direct Methods.* Chemical Physics Letters, 1988. **153**(6): p. 503-506.

18. Karlstrom, G., et al., *MOLCAS: a program package for computational chemistry.* Computational Materials Science, 2003. **28**(2): p. 222-239.

19. Kendall, R.A., et al., *High performance computational chemistry: An overview of NWChem a distributed parallel application.* Computer Physics Communications, 2000. **128**(1-2): p. 260-283.

20. Kong, J., et al., *Q-chem 2.0: A high-performance ab initio electronic structure program package.* Journal of Computational Chemistry, 2000. **21**(16): p. 1532-1548.

21. Lischka, H., et al., *Parallel Computing in Quantum-Chemistry - Message-Passing and Beyond for a General Ab-Initio Program System.* Future Generation Computer Systems, 1995. **11**(4-5): p. 445-450.

22. Quiney, H.M. and S. Wilson, *Literate programming in quantum chemistry: a collaborative approach to the development of theory and computer code.* Molecular Physics, 2005. **103**(2-3): p. 389-399.

23. Shao, Y., et al., *Advances in methods and algorithms in a modern quantum chemistry program package.* Physical Chemistry Chemical Physics, 2006. **8**(27): p. 3172-3191.

24. Stanton, J.F., et al., *The Aces-II Program System.* International Journal of Quantum Chemistry, 1992: p. 879-894.

25. Van der Vaart, A., et al., *Linear scaling molecular orbital calculations of biological systems using the semiempirical divide and conquer method.* Journal of Computational Chemistry, 2000. **21**(16): p. 1494-1504.

26. Veryazov, V., et al., *2MOLCAS as a development platform for quantum chemistry software.* International Journal of Quantum Chemistry, 2004. **100**(4): p. 626-635.

27. Von Arnim, M. and R. Ahlrichs, *Performance of parallel TURBOMOLE for density functional calculations.* Journal of Computational Chemistry, 1998. **19**(15): p. 1746-1757.

28. Werner, H.J., et al., *MOLPRO*.

29. Windus, T.L., M.W. Schmidt, and M.S. Gordon, *Parallel Implementation of the Electronic-Structure Code Gamess*, in *Parallel Computing in Computational Chemistry*. 1995. p. 16-28.

30. Yanai, T., et al., *UTChem - A program for ab initio quantum chemistry*, in *Computational Science - Iccs 2003, Pt Iv, Proceedings*. 2003. p. 84-95.

31. Born, M. and R. Oppenheimer, *On the Quantum Theory of Molecules.* Annals de Physik Leipzig, 1927. **84**.

32. Szabo, A. and N.S. Ostlund, *Modern quantum chemistry*. 1989, New York: Dover.

33. Wilson, S., *Electron correlation in molecules*. 1984, Oxford: Clarendon press.

34. Helgaker, T., P. Jørgensen, and J. Olsen, *Molecular Electronic-Structure Theory*. 2000, West Sussex, England: John Wiley $ Sons.

35. Crawford, T.D. and H.F. Schaefer, *An introduction to coupled cluster theory for computational chemists*, in *Reviews in Computational Chemistry, Vol 14*. 2000. p. 33-136.

36. Sherrill, C.D. and H.F. Schaefer, *The configuration interaction method: Advances in highly correlated approaches*, in *Advances in Quantum Chemistry, Vol 34*. 1999. p. 143-269.

37. Brillouin, L., *Perturbation problems and self consistent fields.* Journal De Physique Et Le Radium, 1932. **3**: p. 373-389.

38. Stillinger, F.H., *Moller-Plesset convergence issues in computational quantum chemistry.* Journal of Chemical Physics, 2000. **112**(22): p. 9711-9715.

39. Leininger, M.L., et al., *Is Moller-Plesset perturbation theory a convergent ab initio method?* Journal of Chemical Physics, 2000. **112**(21): p. 9213-9222.

40. Olsen, J., et al., *Surprising cases of divergent behavior in Moller-Plesset perturbation theory.* Journal of Chemical Physics, 1996. **105**(12): p. 5082-5090.

41. Finley, J.P., R.K. Chaudhuri, and K.F. Freed, *Applications of Multireference Perturbation-Theory to Potential-Energy Surfaces by Optimal Partitioning of H - Intruder States Avoidance and Convergence Enhancement.* Journal of Chemical Physics, 1995. **103**(12): p. 4990-5010.

42. Balkova, A. and R.J. Bartlett, *On the Singlet-Triplet Separation in Methylene - a Critical Comparison of Single-Versus 2-Determinant (Generalized Valence-Bond) Coupled-Cluster Theory.* Journal of Chemical Physics, 1995. **102**(18): p. 7116-7123.

43. Zarrabian, S. and J. Paldus, *Applicability of Multireference Many-Body Perturbation-Theory to the Determination of Potential-Energy Surfaces - a Model Study.* International Journal of Quantum Chemistry, 1990. **38**(6): p. 761-778.

44. Wilson, S., K. Jankowski, and J. Paldus, *Applicability of Nondegenerate Many-Body Perturbation-Theory to Quasi-Degenerate Electronic States .2. a 2-State Model.* International Journal of Quantum Chemistry, 1985. **28**(4): p. 525-534.

45. Kaldor, U., *Can Nondegenerate Many-Body Perturbation-Theory Be Applied to Quasidegenerate Electronic States.* International Journal of Quantum Chemistry, 1985. **28**(1): p. 103-108.

46. Iijima, N. and A. Saika, *A Note on the Convergence of Multiconfigurational Many-Body Perturbation-Theory.* International Journal of Quantum Chemistry, 1985. **27**(4): p. 481-493.

47. Wilson, S., K. Jankowski, and J. Paldus, *Applicability of Non-Degenerate Many-Body Perturbation-Theory to Quasidegenerate Electronic States - a Model Study.* International Journal of Quantum Chemistry, 1983. **23**(5): p. 1781-1802.

48. Jankowski, K., et al., *Model study of the impact of orbital choice on the accuracy of coupled-cluster energies. I. Single-reference-state formulation.* International Journal of Quantum Chemistry, 1998. **67**(4): p. 205-219.

49. Mok, D.K.W., R. Neumann, and N.C. Handy, *Dynamical and nondynamical correlation.* Journal of Physical Chemistry, 1996. **100**(15): p. 6225-6230.

50. Wilson, S., *Alternatives to multireference methods for the molecular electronic structure problem.* International Journal of Quantum Chemistry, 2004. **99**(6): p. 925-935.

51. Roos, B.O. and P.R. Taylor, *A Complete Active Space Scf Method (Casscf) Using a Density-Matrix Formulated Super-Ci Approach.* Chemical Physics, 1980. **48**(2): p. 157-173.

52. Krylov, A.I., *Size-consistent wave functions for bond-breaking: the equation-of-motion spin-flip model.* Chemical Physics Letters, 2001. **338**(4-6): p. 375-384.

53. Shao, Y.H., M. Head-Gordon, and A.I. Krylov, *The spin-flip approach within time-dependent density functional theory: Theory and applications to diradicals.* Journal of Chemical Physics, 2003. **118**(11): p. 4807-4818.

54. Krylov, A.I. and C.D. Sherrill, *Perturbative corrections to the equation-of-motion spin-flip self-consistent field model: Application to bond-breaking and equilibrium properties of diradicals.* Journal of Chemical Physics, 2002. **116**(8): p. 3194-3203.

55. Krylov, A.I., *Spin-flip configuration interaction: an electronic structure model that is both variational and size-consistent.* Chemical Physics Letters, 2001. **350**(5-6): p. 522-530.

56. Slipchenko, L.V. and A.I. Krylov, *Singlet-triplet gaps in diradicals by the spin-flip approach: A benchmark study.* Journal of Chemical Physics, 2002. **117**(10): p. 4694-4708.

57. Levchenko, S.V., et al., *Photodissociation dynamics of the NO dimer. I. Theoretical overview of the ultraviolet singlet excited states.* Journal of Chemical Physics, 2006. **125**(8).

58. Wang, T. and A.I. Krylov, *Electronic structure of the two dehydro-meta-xylylene triradicals and their derivatives.* Chemical Physics Letters, 2006. **425**(4-6): p. 196-200.

59. Krylov, A.I., *Spin-flip equation-of-motion coupled-cluster electronic structure method for a description of excited states, bond breaking, diradicals, and triradicals.* Accounts of Chemical Research, 2006. **39**(2): p. 83-91.

60. Slipchenko, L.V. and A.I. Krylov, *Efficient strategies for accurate calculations of electronic excitation and ionization energies: Theory and application to the dehydro-m-xylylene anion.* Journal of Physical Chemistry A, 2006. **110**(1): p. 291-298.

61. Krylov, A.I., *Triradicals.* Journal of Physical Chemistry A, 2005. **109**(47): p. 10638-10645.

62. Wang, T. and A.I. Krylov, *The effect of substituents on electronic states' ordering in meta-xylylene diradicals: Qualitative insights from quantitative studies.* Journal of Chemical Physics, 2005. **123**(10).

63. Slipchenko, L.V. and A.I. Krylov, *Spin-conserving and spin-flipping equation-of-motion coupled-cluster method with triple excitations.* Journal of Chemical Physics, 2005. **123**(8).

64. Cristian, A.M.C., Y. Shao, and A.I. Krylov, *Bonding patterns in benzene triradicals from structural, spectroscopic, and thermochemical perspectives.* Journal of Physical Chemistry A, 2004. **108**(31): p. 6581-6588.

65. Levchenko, S.V. and A.I. Krylov, *Equation-of-motion spin-flip coupled-cluster model with single and double substitutions: Theory and application to cyclobutadiene.* Journal of Chemical Physics, 2004. **120**(1): p. 175-185.

66. Slipchenko, L.V. and A.I. Krylov, *Electronic structure of the trimethylenemethane diradical in its ground and electronically excited states: Bonding, equilibrium geometries, and vibrational frequencies.* Journal of Chemical Physics, 2003. **118**(15): p. 6874-6883.

67. Foresman, J.B., et al., *Toward a Systematic Molecular-Orbital Theory for Excited-States.* Journal of Physical Chemistry, 1992. **96**(1): p. 135-149.

68. Krylov, A.I., *Spin-contamination of coupled-cluster wave functions.* Journal of Chemical Physics, 2000. **113**(15): p. 6052-6062.

69. Sears, J.S., C.D. Sherrill, and A.I. Krylov, *A spin-complete version of the spin-flip approach to bond breaking: What is the impact of obtaining spin eigenfunctions?* Journal of Chemical Physics, 2003. **118**(20): p. 9084-9094.

70. Sherrill, C.D. and H.F. Schaefer, *Compact variational wave functions incorporating limited triple and quadruple substitutions.* Journal of Physical Chemistry, 1996. **100**(15): p. 6069-6075.

71. Olsen, J., et al., *Determinant Based Configuration-Interaction Algorithms for Complete and Restricted Configuration-Interaction Spaces.* Journal of Chemical Physics, 1988. **89**(4): p. 2185-2192.

72. Stanton, J.F., *Separability Properties of Reduced and Effective Density-Matrices in the Equation-of-Motion Coupled-Cluster Method.* Journal of Chemical Physics, 1994. **101**(10): p. 8928-8937.

73. In case of two nonequivalent fragments, such as Be and Ne, or two H2 molecules with one of the bonds being stretched, the lowest energy Hartree-Fock triplet state is naturally localized on Be or on the stretched H2 molecule, respectively. However, in case of two identical frafments in a symmetric configuration, the lowest triplet state cannot be described using a single Slater determinant using symmetry-adapted molecular orbitals. therefore, it is necessary to use a symmetry-broken Hartree-Fock wave function to describe localization in the case of symmetrically arranged, noninteracting equivalent fragments.

74. Koch, H., et al., *Excitation-Energies from the Coupled Cluster Singles and Doubles Linear Response Function (Ccsdlr) - Applications to Be, Ch+, Co, and H2o.* Journal of Chemical Physics, 1990. **93**(5): p. 3345-3350.

75. Since the target states are found by diagonalization of the Hamiltonian matrix, the block-diagonal structure of the latter ensures that the eigenvalues of the subsystems A and B are also eigenvalues of the combined system AB. The total SF energies, whihc are the sum of the high-spin reference energy and the corresponding transition energy, are thus also size-consistent due to size-consistency of the Hartree-Fock model. Note that the matrix of the Hamiltonian in the before-mentioned basis has eigenvalues corresponding to the simultaneous excitations of both fragments or to the charge-transfer states. The interpretation of these roots requires some caution. For example, due to the truncated nature of the excitation operators, the EOM and CI formalisms fail to describe situations when both fragments are excited with the same accuracy as the excitations on individual fragments. Due to similar considerations, the total SF energy of the composite system does not equal the sum of the SF energy of the individual fragments; rather, the total SF energy is equal to the sum of the SF energy for fragment A and Hartree-Fock energy for fragment B.

76. Laidig, W.D., P. Saxe, and R.J. Bartlett, *The Description of N-2 and F2 Potential-Energy Surfaces Using Multireference Coupled Cluster Theory.* Journal of Chemical Physics, 1987. **86**(2): p. 887-907.

77. Huzinaga, S., *Gaussian-Type Functions for Polyatomic Systems .I.* Journal of Chemical Physics, 1965. **42**(4): p. 1293-&.

78. Dunning, T.H., *Gaussian Basis Functions for Use in Molecular Calculations .1. Contraction of (9s5p) Atomic Basis Sets for First-Row Atoms.* Journal of Chemical Physics, 1970. **53**(7): p. 2823-&.

79. Krylov, A.I., et al., *Size-consistent wave functions for nondynamical correlation energy: The valence active space optimized orbital coupled-cluster doubles model.* Journal of Chemical Physics, 1998. **109**(24): p. 10669-10678.

80. Salem, L. and C. Rowland, *Electronic Properties of Diradicals.* Angewandte Chemie-International Edition, 1972. **11**(2): p. 92-&.

81. Li, X.Z. and J. Paldus, *Energy versus amplitude corrected coupled-cluster approaches. I.* Journal of Chemical Physics, 2001. **115**(13): p. 5759-5773.

82. Ruedenberg, K., L.M. Cheung, and S.T. Elbert, *Mcscf Optimization through Combined Use of Natural Orbitals and the Brillouin-Levy-Berthier Theorem.* International Journal of Quantum Chemistry, 1979. **16**(5): p. 1069-1101.

83. Bertonci.Pj, G. Das, and A.C. Wahl, *Theoretical Study of 1sigma+, 3sigma+, 3pi, 1pi States of Nali and 2sigma+ State of Nali+*. Journal of Chemical Physics, 1970. **52**(10): p. 5112-&.

84. Docken, K.K. and J. Hinze, *Lih Potential Curves and Wavefunctions for X1sigma+, A1sigma+, B1pi,3sigma+, and 3pi.* Journal of Chemical Physics, 1972. **57**(11): p. 4928-&.

85. Benioff, P.A., G. Das, and A.C. Wahl, *Abinitio Calculations of Minimum Energy Path in Doublet Surface for Reaction N(4s) + O2(3-Sigma-G)-]No(2-Piu) + O(3p).* Journal of Chemical Physics, 1977. **67**(6): p. 2449-2462.

86. Roos, B., Advances in Chemical Physics, 1987. **67**.

87. Sears, J.S. and C.D. Sherrill, *On the choice of reference in multi-reference electronic structure theory: minimal references for bond breaking.* Molecular Physics, 2005. **103**(6-8): p. 803-814.

88. Pierloot, K., *The CASPT2 method in inorganic electronic spectroscopy: from ionic transition metal to covalent actinide complexes.* Molecular Physics, 2003. **101**(13): p. 2083-2094.

89. Pople, J.A. *Energy, Structure and Reactivity*. in *Boulder Summer Research Conference on Theoretical Chemistry,*. 1972. Boulder, CO: Wiley.

90. Ruedenberg, K., et al., *Are Atoms Intrinsic to Molecular Electronic Wavefunctions .1. the Fors Model.* Chemical Physics, 1982. **71**(1): p. 41-49.

91. Ruedenberg, K., M.W. Schmidt, and M.M. Gilbert, *Are Atoms Intrinsic to Molecular Electronic Wavefunctions .2. Analysis of Fors Orbitals.* Chemical Physics, 1982. **71**(1): p. 51-64.

92. Ruedenberg, K., et al., *Are Atoms Intrinsic to Molecular Electronic Wavefunctions .3. Analysis of Fors Configurations.* Chemical Physics, 1982. **71**(1): p. 65-78.

93. Abrams, M.L. and C.D. Sherrill, *An assessment of the accuracy of multireference configuration interaction (MRCI) and complete-active-space second-order perturbation theory (CASPT2) for breaking bonds to hydrogen.* Journal of Physical Chemistry A, 2003. **107**(29): p. 5611-5616.

94. Abrams, M.L. and C.D. Sherrill, *Natural orbitals as substitutes for optimized orbitals in complete active space wavefunctions.* Chemical Physics Letters, 2004. **395**(4-6): p. 227-232.

95. Voorhis, T.V. and M. Head-Gordon, *A nonorthogonal approach to perfect pairing.* Journal of Chemical Physics, 2000. **112**(13): p. 5633-5638.

96. Olsen, J., et al., *Full configuration-interaction and state of the art correlation calculations on water in a valence double-zeta basis with polarization functions.* Journal of Chemical Physics, 1996. **104**(20): p. 8007-8015.

97. Woon, D.E. and T.H. Dunning, *Benchmark Calculations with Correlated Molecular Wave-Functions .1. Multireference Configuration-Interaction Calculations for the 2nd-Row Diatomic Hydrides.* Journal of Chemical Physics, 1993. **99**(3): p. 1914-1929.

98. Chaban, G., M.W. Schmidt, and M.S. Gordon, *Approximate second order method for orbital optimization of SCF and MCSCF wavefunctions.* Theoretical Chemistry Accounts, 1997. **97**(1-4): p. 88-95.

99. Knowles, P.J. and H.J. Werner, *An Efficient 2nd-Order Mc Scf Method for Long Configuration Expansions.* Chemical Physics Letters, 1985. **115**(3): p. 259-267.

100. Jensen, H.J.A. and H. Agren, *A Direct, Restricted-Step, 2nd-Order Mc Scf Program for Large-Scale Abinitio Calculations.* Chemical Physics, 1986. **104**(2): p. 229-250.

101. Pulay, P. and T.P. Hamilton, *Uhf Natural Orbitals for Defining and Starting Mc-Scf Calculations.* Journal of Chemical Physics, 1988. **88**(8): p. 4926-4933.

102. Malmqvist, P.A., A. Rendell, and B.O. Roos, *The Restricted Active Space Self-Consistent-Field Method, Implemented with a Split Graph Unitary-Group Approach.* Journal of Physical Chemistry, 1990. **94**(14): p. 5477-5482.

103. Larsen, H., et al., *Full configuration interaction benchmarking of coupled-cluster models for the lowest singlet energy surfaces of N-2.* Journal of Chemical Physics, 2000. **113**(16): p. 6677-6686.

104. Dutta, A. and C.D. Sherrill, *Full configuration interaction potential energy curves for breaking bonds to hydrogen: An assessment of single-reference correlation methods.* Journal of Chemical Physics, 2003. **118**(4): p. 1610-1619.

105. Gray, D.L. and A.G. Robiette, *Anharmonic-Force Field and Equilibrium Structure of Methane.* Molecular Physics, 1979. **37**(6): p. 1901-1920.

106. Andersson, K., et al., *2nd-Order Perturbation-Theory with a Casscf Reference Function.* Journal of Physical Chemistry, 1990. **94**(14): p. 5483-5488.

107. Werner, H.J., *Third-order multireference perturbation theory - The CASPT3 method.* Molecular Physics, 1996. **89**(2): p. 645-661.

108. Lengsfield, B.H., et al., *The Binding-Energy of the Ground-State of Be-2.* Journal of Chemical Physics, 1983. **79**(4): p. 1891-1895.

109. Schaefer, H.F., *Configuration interaction wave functions and the properties of atoms and diatomic molecules.* 1969, Stanfrod University: Stanford, CA.

110. Hunt, W.J., P.J. Hay, and W.A. Goddard, *Self-Consistent Procedures for Generalized Valence Bond Wavefunctions - Applications H-3, Bh, H2o, C2h6, and O2.* Journal of Chemical Physics, 1972. **57**(2): p. 738-&.

111. Ladner, R.C. and W.A. Goddard, *Improved Quantum Theory of Many-Electron Systems .V. Spin-Coupling Optimized Gi Method.* Journal of Chemical Physics, 1969. **51**(3): p. 1073-&.

112. Goddard, W.A., *Improved Quantum Theory of Many-Electron Systems .2. Basic Method.* Physical Review, 1967. **157**(1): p. 81-&.

113. Nakano, H. and K. Hirao, *A quasi-complete active space self-consistent field method.* Chemical Physics Letters, 2000. **317**(1-2): p. 90-96.

114. Ivanic, J., *Direct configuration interaction and multiconfigurational self-consistent-field method for multiple active spaces with variable occupations. I. Method.* Journal of Chemical Physics, 2003. **119**(18): p. 9364-9376.

115. Ivanic, J., *Direct configuration interaction and multiconfigurational self-consistent-field method for multiple active spaces with variable occupations. II. Application to oxoMn(salen) and N2O4.* Journal of Chemical Physics, 2003. **119**(18): p. 9377-9385.

116. Canali, L. and D.C. Sherrington, *Utilisation of homogeneous and supported chiral metal(salen) complexes in asymmetric catalysis.* Chemical Society Reviews, 1999. **28**(2): p. 85-93.

117. Noyori, R., *Asymmetric catalysis: Science and opportunities (Nobel lecture 2001).* Advanced Synthesis & Catalysis, 2003. **345**(1-2): p. 15-32.

118. Blaser, H.U., F. Spindler, and A. Studer, *Enantioselective catalysis in fine chemicals production.* Applied Catalysis a-General, 2001. **221**(1-2): p. 119-143.

119. Egami, H., S. Onitsuka, and T. Katsuki, *A reasonable explanation for the mechanism of photo-promoted chemoselective aerobic oxidation of alcohols using (ON)Ru(salen) complex as catalyst.* Tetrahedron Letters, 2005. **46**(36): p. 6049-6052.

120. Chisholm, M.H. and Z.P. Zhou, *Concerning the mechanism of the ring opening of propylene oxide in the copolymerization of propylene oxide and carbon dioxide to give poly(propylene carbonate).* Journal of the American Chemical Society, 2004. **126**(35): p. 11030-11039.

121. Dalton, C.T., et al., *Recent progress towards the understanding of metal-salen catalysed asymmetric alkene epoxidation.* Topics in Catalysis, 1998. **5**(1-4): p. 75-91.

122. Venkataramanan, N.S., G. Kuppuraj, and S. Rajagopal, *Metal-salen complexes as efficient catalysts for the oxygenation of heteroatom containing organic compounds - synthetic and mechanistic aspects.* Coordination Chemistry Reviews, 2005. **249**(11-12): p. 1249-1268.

123. Kohn, W. and L.J. Sham, *Self-Consistent Equations Including Exchange and Correlation Effects.* Physical Review, 1965. **140**(4A): p. 1133-&.

124. Zhao, Y. and D.G. Truhlar, *Comparative assessment of density functional methods for 3d transition-metal chemistry.* Journal of Chemical Physics, 2006. **124**(22).

125. Quintal, M.M., et al., *Benchmark study of DFT functionals for late-transition-metal reactions.* Journal of Physical Chemistry A, 2006. **110**(2): p. 709-716.

126. Schultz, N.E., Y. Zhao, and D.G. Truhlar, *Density functionals for inorganometallic and organometallic chemistry.* Journal of Physical Chemistry A, 2005. **109**(49): p. 11127-11143.

127. Tsipis, C.A., *Adventures of quantum chemistry in the realm of inorganic chemistry.* Comments on Inorganic Chemistry, 2004. **25**(1-2): p. 19-74.

128. Bernardi, F., A. Bottoni, and M. Garavelli, *Exploring organic chemistry with DFT: Radical, organo-metallic, and bio-organic applications.* Quantitative Structure-Activity Relationships, 2002. **21**(2): p. 128-148.

129. Siegbahn, P.E.M., *Modeling aspects of mechanisms for reactions catalyzed by metalloenzymes.* Journal of Computational Chemistry, 2001. **22**(14): p. 1634-1645.

130. Dickson, R.M. and A.D. Becke, *Reaction barrier heights from an exact-exchange-based density-functional correlation model.* Journal of Chemical Physics, 2005. **123**(11).

131. Slater, J.C., et al., *Nonintegral Occupation Numbers in Transition Atoms in Crystals.* Physical Review, 1969. **184**(3): p. 672-&.

132. Ziegler, T., A. Rauk, and E.J. Baerends, *Calculation of Multiplet Energies by Hartree-Fock-Slater Method.* Theoretica Chimica Acta, 1977. **43**(3): p. 261-271.

133. Cremer, D., *Density functional theory: coverage of dynamic and non-dynamic electron correlation effects.* Molecular Physics, 2001. **99**(23): p. 1899-1940.

134. Grafenstein, J. and D. Cremer, *Development of a CAS-DFT method covering non-dynamical and dynamical electron correlation in a balanced way.* Molecular Physics, 2005. **103**(2-3): p. 279-308.

135. Grafenstein, J. and D. Cremer, *Can density functional theory describe multi-reference systems? Investigation of carbenes and organic biradicals.* Physical Chemistry Chemical Physics, 2000. **2**(10): p. 2091-2103.

136. Grafenstein, J. and D. Cremer, *The combination of density functional theory with multi-configuration methods - CAS-DFT.* Chemical Physics Letters, 2000. **316**(5-6): p. 569-577.

137. Sears, J.S. and C.D. Sherrill, *The electronic structure of oxo-Mn(salen): Single-reference and multireference approaches.* Journal of Chemical Physics, 2006. **124**(14).

138. Stephens, P.J., et al., *Ab-Initio Calculation of Vibrational Absorption and Circular-Dichroism Spectra Using Density-Functional Force-Fields.* Journal of Physical Chemistry, 1994. **98**(45): p. 11623-11627.

139. Yanagisawa, S., T. Tsuneda, and K. Hirao, *An investigation of density functionals: The first-row transition metal dimer calculations.* Journal of Chemical Physics, 2000. **112**(2): p. 545-553.

140. Reiher, M., O. Salomon, and B.A. Hess, *Reparameterization of hybrid functionals based on energy differences of states of different multiplicity.* Theoretical Chemistry Accounts, 2001. **107**(1): p. 48-55.

141. Poater, J., et al., *Analysis of the effect of changing the a(0) parameter of the Becke3-LYP hybrid functional on the transition state geometries and energy barriers in a series of prototypical reactions.* Physical Chemistry Chemical Physics, 2002. **4**(5): p. 722-731.

142. Niu, S.Q. and M.B. Hall, *Comparison of Hartree-Fock, density functional, Moller-Plesset perturbation, coupled cluster, and configuration interaction methods for the migratory insertion of nitric oxide into a cobalt-carbon bond.* Journal of Physical Chemistry A, 1997. **101**(7): p. 1360-1365.

143. Barden, C.J., J.C. Rienstra-Kiracofe, and H.F. Schaefer, *Homonuclear 3d transition-metal diatomics: A systematic density functional theory study.* Journal of Chemical Physics, 2000. **113**(2): p. 690-700.

144. Nakao, Y., K. Hirao, and T. Taketsugu, *Theoretical study of first-row transition metal oxide cations.* Journal of Chemical Physics, 2001. **114**(18): p. 7935-7940.

145. Ziegler, T. and J. Li, *Bond-Energies for Cationic Bare Metal-Hydrides of the First Transition Series - a Challenge to Density-Functional Theory.* Canadian Journal of Chemistry-Revue Canadienne De Chimie, 1994. **72**(3): p. 783-789.

146. Cotton, F.A. and X.J. Feng, *Density functional theory study of transition-metal compounds containing metal-metal bonds .1. Molecular structures of dinuclear*

compounds by complete geometry optimization. Journal of the American Chemical Society, 1997. **119**(32): p. 7514-7520.

147. Pierloot, K., *Nondynamic Correlation Effects in Transition Metal Coordination Compounds*, in *Computational Organometallic Chemistry*, T.R. Cundari, Editor. 2001, Marcel Dekker: New York.

148. Andersson, K. and B.O. Roos, *Excitation-Energies in the Nickel Atom Studied with the Complete Active Space Scf Method and 2nd-Order Perturbation-Theory.* Chemical Physics Letters, 1992. **191**(6): p. 507-514.

149. Bauschlicher, C.W., P. Siegbahn, and L.G.M. Pettersson, *The Atomic States of Nickel.* Theoretica Chimica Acta, 1988. **74**(6): p. 479-491.

150. Botch, B.H., T.H. Dunning, and J.F. Harrison, *Valence Correlation in the S2dn, Sdn+1, and Dn+2 States of the 1st-Row Transition-Metal Atoms.* Journal of Chemical Physics, 1981. **75**(7): p. 3466-3476.

151. Carlsson, J., *Configuration-Interaction in the Neutral Copper Atom.* Physical Review A, 1988. **38**(4): p. 1702-1710.

152. Roos, B.O., et al., *Multiconfigurational perturbation theory: Applications in electronic spectroscopy*, in *Advances in Chemical Physics, Vol Xciii*. 1996. p. 219-331.

153. Rulisek, L. and Z. Havlas, *Using DFT methods for the prediction of the structure and energetics of metal-binding sites in metalloproteins.* International Journal of Quantum Chemistry, 2003. **91**(3): p. 504-510.

154. Chermette, H., *Density functional theory - A powerful tool for theoretical studies in coordination chemistry.* Coordination Chemistry Reviews, 1998. **180**: p. 699-721.

155. Glukhovtsev, M.N., R.D. Bach, and C.J. Nagel, *Performance of the B3LYP/ECP DFT calculations of iron-containing compounds.* Journal of Physical Chemistry A, 1997. **101**(3): p. 316-323.

156. Vallet, V., et al., *The electronic spectroscopy of transition metal di-hydrides H2M(CO)(4) (M = Fe,Os): a theoretical study based on CASSCF/MS-CASPT2 and TD-DFT.* Physical Chemistry Chemical Physics, 2003. **5**(14): p. 2948-2953.

157. Meier, R.J., *Are DFT level calculations the answer to real-world molecular systems?* Computational Materials Science, 2003. **27**(1-2): p. 219-223.

158. Cai, Z.L., K. Sendt, and J.R. Reimers, *Failure of density-functional theory and time-dependent density-functional theory for large extended pi systems.* Journal of Chemical Physics, 2002. **117**(12): p. 5543-5549.

159. Combes, A., C. R. Acad. Fr., 1889. **108**: p. 1252.

160. Nozaki, H., et al., *Asymmetric Induction in Carbenoid Reaction by Means of a Dissymmetric Copper Chelate.* Tetrahedron Letters, 1966(43): p. 5239-&.

161. Hilt, G., C. Walter, and P. Bolze, *Iron-salen complexes as efficient catalysts in ring expansion reactions of epoxyalkenes.* Advanced Synthesis & Catalysis, 2006. **348**(10-11): p. 1241-1247.

162. McGarrigle, E.M. and D.G. Gilheany, *Chromium- and manganese-salen promoted epoxidation of alkenes.* Chemical Reviews, 2005. **105**(5): p. 1563-1602.

163. Katsuki, T., *Chiral metallosalen complexes: Structures and catalyst tuning for asymmetric epoxidation and cyclopropanation.* Advanced Synthesis & Catalysis, 2002. **344**(2): p. 131-147.

164. Kim, G.J. and J.H. Shin, *Application of new unsymmetrical chiral Mn(III), Co(II,III) and Ti(IV) salen complexes in enantioselective catalytic reactions.* Catalysis Letters, 1999. **63**(1-2): p. 83-90.

165. Ito, Y.N. and T. Katsuki, *Asymmetric catalysis of new generation chiral metallosalen complexes.* Bulletin of the Chemical Society of Japan, 1999. **72**(4): p. 603-619.

166. Kolb, H.C., M.S. Vannieuwenhze, and K.B. Sharpless, *Catalytic Asymmetric Dihydroxylation.* Chemical Reviews, 1994. **94**(8): p. 2483-2547.

167. Irie, R., *Asymmetric Epoxidation Using Chiral Salen Complexes.* Journal of Synthetic Organic Chemistry Japan, 1993. **51**(5): p. 412-420.

168. Jacobsen, E.N., *Asymmetric catalysis of epoxide ring opening reactions.* Accounts of Chemical Research, 2000. **33**(6): p. 421-431.

169. Katsuki, T., *Mn-salen catalyst, competitor of enzymes, for asymmetric epoxidation.* Journal of Molecular Catalysis a-Chemical, 1996. **113**(1-2): p. 87-107.

170. Yoon, T.P. and E.N. Jacobsen, *Privileged chiral catalysts.* Science, 2003. **299**(5613): p. 1691-1693.

171. Cook, G.R., *Transition metal-mediated kinetic resolution.* Current Organic Chemistry, 2000. **4**(8): p. 869-885.

172. Graca, M. and M.G.H. Vicente, *Porphyrins and derivatives: Synthetic strategies and reactivity profiles.* Current Organic Chemistry, 2000. **4**(2): p. 139-174.

173. Groves, J.T., *High-valent iron in chemical and biological oxidations.* Journal of Inorganic Biochemistry, 2006. **100**(4): p. 434-447.

174. Hlavica, P., *Models and mechanisms of O-O bond activation by cytochrome P450 - A critical assessment of the potential role of multiple active intermediates in oxidative catalysis.* European Journal of Biochemistry, 2004. **271**(22): p. 4335-4360.

175. Maravin, G.B., M.V. Avdeev, and E.I. Bagrii, *Oxidative functionalization of saturated hydrocarbons on porphyrin metal complex catalysts (a review).* Petroleum Chemistry, 2000. **40**(1): p. 1-18.

176. Meunier, B., S.P. de Visser, and S. Shaik, *Mechanism of oxidation reactions catalyzed by cytochrome P450 enzymes.* Chemical Reviews, 2004. **104**(9): p. 3947-3980.

177. Abashkin, Y.G. and S.K. Burt, *(salen)Mn-III compounds as nonpeptidyl mimics of catalase. Mechanism-based tuning of catalase activity: A theoretical study.* Inorganic Chemistry, 2005. **44**(5): p. 1425-1432.

178. Kleij, A.W., et al., *A convenient synthetic route for the preparation of nonsymmetric metallosalphen complexes.* European Journal of Inorganic Chemistry, 2005(22): p. 4626-4634.

179. Sawyer, D.T., *Metal [Fe(II), Cu(I), Co(II), Mn(III)] hydroperoxide-induced activation of dioxygen (center dot O-2 center dot) for the ketonization of hydrocarbons: oxygenated Fenton Chemistry.* Coordination Chemistry Reviews, 1997. **165**: p. 297-313.

180. Katsuki, T., *Catalytic Asymmetric Oxidations Using Optically-Active (Salen)Manganese(Iii) Complexes as Catalysts.* Coordination Chemistry Reviews, 1995. **140**: p. 189-214.

181. Ramon, D.J. and M. Yus, *In the arena of enantioselective synthesis, titanium complexes wear the laurel wreath.* Chemical Reviews, 2006. **106**(6): p. 2126-2208.

182. Lu, G., et al., *Synthesis and application of new chiral catalysts for asymmetric alkynylation reactions.* Coordination Chemistry Reviews, 2005. **249**(17-18): p. 1736-1744.

183. Murzin, D.Y., et al., *Asymmetric heterogeneous catalysis: Science and engineering.* Catalysis Reviews-Science and Engineering, 2005. **47**(2): p. 175-256.

184. Costas, M., et al., *Dioxygen activation at mononuclear nonheme iron active sites: Enzymes, models, and intermediates.* Chemical Reviews, 2004. **104**(2): p. 939-986.

185. DiMauro, E.F., A. Mamai, and M.C. Kozlowski, *Synthesis, characterization, and metal complexes of a salen ligand containing a quinoline base.* Organometallics, 2003. **22**(4): p. 850-855.

186. Sherrington, D.C., *Polymer-supported metal complex alkene epoxidation catalysts.* Catalysis Today, 2000. **57**(1-2): p. 87-104.

187. Zheng, X.L., C.W. Jones, and M. Weck, *Poly(styrene)-supported co-salen complexes as efficient recyclable catalysts for the hydrolytic kinetic resolution of epichlorohydrin.* Chemistry-a European Journal, 2005. **12**(2): p. 576-583.

188. Alvaro, M., et al., *Polymer-bound aluminium salen complex as reusable catalysts for CO2 insertion into epoxides.* Tetrahedron, 2005. **61**(51): p. 12131-12139.

189. Yin, D.Y., et al., *Immobilization of Mn(salen) complex on aluminum-containing mesoporous materials by microwave heating for epoxidation of styrene*, in *Nanoporous Materials Iv*. 2005. p. 851-858.

190. Rigamonti, L., et al., *Copper(II) complexes of salen analogues with two differently substituted (push-pull) salicylaldehyde moieties. A study on the modulation of electronic asymmetry and nonlinear optical properties.* Inorganic Chemistry, 2006. **45**(26): p. 10976-10989.

191. Girichev, G.V., et al., *Molecular structure of NiO2N2C16H14 from gas-phase electron diffraction and quantum chemical data.* Journal of Structural Chemistry, 2005. **46**(5): p. 813-823.

192. Schenk, S., et al., *Carbon dioxide and related heterocumulenes at zinc and lithium cations: bioinspired reactions and principles.* Dalton Transactions, 2006(35): p. 4191-4206.

193. Gao, F., et al., *Spectroscopy, NMR and DFT studies on molecular recognition of crown ether bridged chiral heterotrinuclear salen Zn(II) complex.* Spectrochimica Acta Part a-Molecular and Biomolecular Spectroscopy, 2005. **62**(4-5): p. 886-895.

194. Luinstra, G.A., et al., *On the formation of aliphatic polycarbonates from epoxides with chromium(III) and aluminum(III) metal-salen complexes.* Chemistry-a European Journal, 2005. **11**(21): p. 6298-6314.

195. Yeung, W.F., et al., *Heterometallic (MRu2III)-Ru-II compounds constructed from trans-[Ru(Salen)(CN)(2)](-) and trans-[Ru(AcaC)(2)(CN)(2)](-), synthesis, structures, magnetic properties, and density functional theoretical study.* Inorganic Chemistry, 2005. **44**(19): p. 6579-6590.

196. Barone, G., A. Silvestri, and G. La Manna, *DFT computational study on Fe-III-N,N '-ethylene-bis(salicylideneiminato) derivatives.* Journal of Molecular Structure-Theochem, 2005. **715**(1-3): p. 79-83.

197. Sizova, O.V., et al., *Electronic spectra of ruthenium nitrosyl complexes with macrocyclic ligands.* Russian Journal of General Chemistry, 2004. **74**(4): p. 481-485.

198. Rogachev, A., N. Kuzmina, and A. Nemukhin, *Theoretical modeling of the heterobimetallic complex [La(pta)(3)Cu(salen)] and its precursors.* Journal of Alloys and Compounds, 2004. **374**(1-2): p. 335-338.

199. Tucker, R.J., et al., *An ENDOR and DFT analysis of 'solvatochromic' effects in an oxovanadium (IV) complex.* Chemical Physics Letters, 2003. **380**(5-6): p. 758-766.

200. Takayama, T., T. Sekine, and H. Kudo, *Substituent effect on redox potential of nitrido technetium complexes with Schiff base ligand: Theoretical calculations.* Journal of Radioanalytical and Nuclear Chemistry, 2003. **255**(1): p. 97-99.

201. Brandt, P., et al., *Chromium - Salen-mediated alkene epoxidation: A theoretical and experimental study indicates the importance of spin-surface crossing and the presence of a discrete intermediate.* Chemistry-a European Journal, 2002. **8**(18): p. 4299-4307.

202. Henson, N.J., P.J. Hay, and A. Redondo, *Density functional theory studies of the binding of molecular oxygen with Schiff's base complexes of cobalt.* Inorganic Chemistry, 1999. **38**(7): p. 1618-1626.

203. Khavrutskii, I.V., D.G. Musaev, and K. Morokuma, *Cooperative pull and push effects on the O-O bond cleavage in acylperoxo complexes of [(Salen)(MnL)-L-III]: Ensuring formation of manganese(V) oxo species.* Inorganic Chemistry, 2005. **44**(2): p. 306-315.

204. Jacobsen, H. and L. Cavallo, *Re-evaluation of the Mn(salen) mediated epoxidation of alkenes by means of the B3LYP*density functional.* Physical Chemistry Chemical Physics, 2004. **6**(13): p. 3747-3753.

205. Khavrutskii, I.V., D.G. Musaev, and K. Morokuma, *Epoxidation of unfunctionalized olefins by Mn(salen) catalyst using organic peracids as oxygen source: A theoretical study.* Proceedings of the National Academy of Sciences of the United States of America, 2004. **101**(16): p. 5743-5748.

206. Khavrutskii, I.V., et al., *Axial ligand and solvent effects on the O-O bond activation in acylperoxo complexes of [(Salen)(MnL)-L-III]: Mn-IV versus Mn-V oxo species.* Journal of Physical Chemistry B, 2004. **108**(12): p. 3845-3854.

207. Ivanic, J., J.R. Collins, and S.K. Burt, *Theoretical study of the low lying electronic states of oxoX(salen) (X = Mn, Mn-, Fe, and Cr-) complexes.* Journal of Physical Chemistry A, 2004. **108**(12): p. 2314-2323.

208. Cavallo, L. and H. Jacobsen, *Toward a catalytic cycle for the Mn-salen mediated alkene epoxidation: A computational approach.* Inorganic Chemistry, 2004. **43**(6): p. 2175-2182.

209. Abashkin, Y.G. and S.K. Burt, *(Salen)Mn-catalyzed epoxidation of alkenes: A two-zone process with different spin-state channels as suggested by DFT study.* Organic Letters, 2004. **6**(1): p. 59-62.

210. Khavrutskii, I.V., D.G. Musaev, and K. Morokuma, *Insights into the structure and reactivity of acylperoxo complexes in the Kochi-Jacobsen-Katsuki catalytic system. A density functional study.* Journal of the American Chemical Society, 2003. **125**(45): p. 13879-13889.

211. Cavallo, L. and H. Jacobsen, *Electronic effects in (salen)Mn-based epoxidation catalysts.* Journal of Organic Chemistry, 2003. **68**(16): p. 6202-6207.

212. Cavallo, L. and H. Jacobsen, *Transition metal mediated epoxidation as test case for the performance of different density functionals: A Computational Study.* Journal of Physical Chemistry A, 2003. **107**(28): p. 5466-5471.

213. Abashkin, Y.G., J.R. Collins, and S.K. Burt, *(Salen)Mn(III)-catalyzed epoxidation reaction as a multichannel process with different spin states. Electronic tuning of asymmetric catalysis: A theoretical study.* Inorganic Chemistry, 2001. **40**(16): p. 4040-4048.

214. Jacobsen, H. and L. Cavallo, *A possible mechanism for enantioselectivity in the chiral epoxidation of olefins with [Mn(salen)] catalysts.* Chemistry-a European Journal, 2001. **7**(4): p. 800-807.

215. Strassner, T. and K.N. Houk, *Predictions of geometries and multiplicities of the manganese-oxo intermediates in the Jacobsen epoxidation.* Organic Letters, 1999. **1**(3): p. 419-421.

216. Linde, C., et al., *Timing is critical: Effect of spin changes on the diastereoselectivity in Mn(salen)-catalyzed epoxidation.* Journal of the American Chemical Society, 1999. **121**(21): p. 5083-5084.

217. Linde, C., et al., *Is there a radical intermediate in the (salen)Mn-catalyzed epoxidation of alkenes?* Angewandte Chemie-International Edition in English, 1997. **36**(16): p. 1723-1725.

218. Carreon-Macedo, J.L. and J.N. Harvey, *Do spin state changes matter in organometallic chemistry? A computational study.* Journal of the American Chemical Society, 2004. **126**(18): p. 5789-5797.

219. Cavallo, L. and H. Jacobsen, *Radical intermediates in the Jacobsen-Katsuki epoxidation.* Angewandte Chemie-International Edition, 2000. **39**(3): p. 589-+.

220. Siegbahn, P.E.M., *Electronic structure calculations for molecules containing transition metals*, in *Advances in Chemical Physics, Vol Xciii*. 1996. p. 333-387.

221. Bauschlicher, C.W. and G.L. Gutsev, *MnO+: a challenge for density functional theory methods.* Theoretical Chemistry Accounts, 2002. **107**(5): p. 309-312.

222. Hirao, K., *Multireference Moller-Plesset Method.* Chemical Physics Letters, 1992. **190**(3-4): p. 374-380.

223. Hirao, K., *Multireference Moller-Plesset Perturbation-Theory for High-Spin Open-Shell Systems.* Chemical Physics Letters, 1992. **196**(5): p. 397-403.

224. Seeger, R. and J.A. Pople, *Self-Consistent Molecular-Orbital Methods .18. Constraints and Stability in Hartree-Fock Theory.* Journal of Chemical Physics, 1977. **66**(7): p. 3045-3050.

225. Cizek, J. and J. Paldus, *Stability Conditions for Solutions of Hartree-Fock Equations for Atomic and Molecular Systems . Application to Pi-Electron Model of Cyclic Polyenes.* Journal of Chemical Physics, 1967. **47**(10): p. 3976-&.

226. Adams, W.H., *Stability of Hartree-Fock States.* Physical Review, 1962. **127**(5): p. 1650-&.

227. Kowalski, K. and K. Jankowski, *Towards complete solutions to systems of nonlinear equations of many-electron theories.* Physical Review Letters, 1998. **81**(6): p. 1195-1198.

228. McLean, A.D. and G.S. Chandler, *Contracted Gaussian-Basis Sets for Molecular Calculations .1. 2nd Row Atoms, Z=11-18.* Journal of Chemical Physics, 1980. **72**(10): p. 5639-5648.

229. Krishnan, R., et al., *Self-Consistent Molecular-Orbital Methods .20. Basis Set for Correlated Wave-Functions.* Journal of Chemical Physics, 1980. **72**(1): p. 650-654.

230. Widmark, P.O., et al., *Density-Matrix Averaged Atomic Natural Orbital (Ano) Basis-Sets for Correlated Molecular Wave-Functions .2. 2nd Row Atoms.* Theoretica Chimica Acta, 1991. **79**(6): p. 419-432.

231. Becke, A.D., *Density-Functional Thermochemistry .3. the Role of Exact Exchange.* Journal of Chemical Physics, 1993. **98**(7): p. 5648-5652.

232. Becke, A.D., *Density-Functional Exchange-Energy Approximation with Correct Asymptotic-Behavior.* Physical Review A, 1988. **38**(6): p. 3098-3100.

233. Lee, C.T., W.T. Yang, and R.G. Parr, *Development of the Colle-Salvetti Correlation-Energy Formula into a Functional of the Electron-Density.* Physical Review B, 1988. **37**(2): p. 785-789.

234. Perdew, J.P., *Density-Functional Approximation for the Correlation-Energy of the Inhomogeneous Electron-Gas.* Physical Review B, 1986. **33**(12): p. 8822-8824.

235. Wolfsberg, M. and L. Helmholz, *The Spectra and Electronic Structure of the Tetrahedral Ions Mno4- Cro4--, and Clo4.* Journal of Chemical Physics, 1952. **20**(5): p. 837-843.

236. Pulay, P., *Improved Scf Convergence Acceleration.* Journal of Computational Chemistry, 1982. **3**(4): p. 556-560.

237. Pulay, P., *Convergence Acceleration of Iterative Sequences - the Case of Scf Iteration.* Chemical Physics Letters, 1980. **73**(2): p. 393-398.

238. Cowan, R.D. and D.C. Griffin, *Approximate Relativistic Corrections to Atomic Radial Wave-Functions.* Journal of the Optical Society of America, 1976. **66**(10): p. 1010-1014.

239. Van Voorhis, T. and M. Head-Gordon, *A geometric approach to direct minimization.* Molecular Physics, 2002. **100**(11): p. 1713-1721.

240. Edmiston, C. and K. Ruedenberg, *Localized Atomic and Molecular Orbitals.* Reviews of Modern Physics, 1963. **35**(3): p. 457-&.

241. Bauschlicher, C.W., *Construction of Modified Virtual Orbitals (Mvos) Which Are Suited for Configuration-Interaction Calculations.* Journal of Chemical Physics, 1980. **72**(2): p. 880-885.

242. Hehre, W.J., et al., *Self-Consistent Molecular Orbital Methods .4. Use of Gaussian Expansions of Slater-Type Orbitals - Extension to Second-Row Molecules.* Journal of Chemical Physics, 1970. **52**(5): p. 2769-&.

243. Hehre, W.J., R.F. Stewart, and J.A. Pople, *Self-Consistent Molecular-Orbital Methods .I. Use of Gaussian Expansions of Slater-Type Atomic Orbitals.* Journal of Chemical Physics, 1969. **51**(6): p. 2657-&.

244. Yamaguchi, Y. and H.F. Schaefer, *An ab initio study on the four electronically lowest-lying states of CH2 using the state-averaged complete active space second-order configuration interaction method.* Chemical Physics, 1997. **225**(1-3): p. 23-31.

245. Cramer, C.J., *Essentials of Computational Chemistry*. 2002, England: Wiley.

246. Vacek, G., J.K. Perry, and J.M. Langlois, *Advanced initial-guess algorithm for self-consistent-field calculations on organometallic systems.* Chemical Physics Letters, 1999. **310**(1-2): p. 189-194.

247. Sears, J.S. and C.D. Sherrill, *Assessing the performance of DFT for the electronic structure of metal-salens: The 3d0 metals*. 2007.

248. Hatano, M., T. Miyamoto, and K. Ishihara, *Recent progress in selective additions of organometal reagents to carbonyl compounds.* Current Organic Chemistry, 2007. **11**(2): p. 127-157.

249. Taylor, M.S., et al., *Highly enantioselective conjugate additions to alpha,beta-unsaturated ketones catalyzed by a (Salen)Al complex.* Journal of the American Chemical Society, 2005. **127**(4): p. 1313-1317.

250. Chen, C., et al., *Low ligand loading, highly enantioselective addition of phenylacetylene to aromatic ketones catalyzed by Schiff-base amino alcohols.* Organic Letters, 2006. **8**(11): p. 2277-2280.

251. Berkessel, A. and N. Vogl, *DIANANE-Cr-III-salen complexes as highly enantioselective catalysts for hetero-Diels-Alder reactions of aldehydes with dienes.* European Journal of Organic Chemistry, 2006(22): p. 5029-5035.

252. Chaladaj, W., P. Kwiatkowski, and J. Jurczak, *Sterically modified chiral (salen)Cr(III) complexes - Efficient catalysts for the oxo-Diels-Alder reaction between glyoxylates and cyclohexa-1,3-diene.* Synlett, 2006(19): p. 3263-3266.

253. Fukuzawa, S., et al., *New chiral scandium(III)/bisimine and diol complexes catalyzed asymmetric Diels-Alder reaction.* Tetrahedron Letters, 2003. **44**(18): p. 3671-3674.

254. Nakata, K., et al., *Asymmetric epoxidation with a photoactivated [Ru(salen)] complex.* Chemistry-a European Journal, 2001. **7**(17): p. 3776-3782.

255. Zhou, X.G., et al., *Binaphthyl Schiff base complexes of palladium(II). Structures and reactivities toward alkene epoxidation.* Journal of the Chemical Society-Dalton Transactions, 2000. **7**(7): p. 1075-1080.

256. Uchida, T. and T. Katsuki, *alpha-Diazoacetates as carbene precursors: Metallosalen-catalyzed asymmetric cyclopropanation.* Synthesis-Stuttgart, 2006(10): p. 1715-1723.

257. Li, G.Y., et al., *Enantioselective intramolecular cyclopropanation of cis-alkenes by chiral ruthenium(II) Schiff base catalysts and crystal structures of (Schiff base)ruthenium complexes containing carbene, PPh3, and CO ligands.* Organometallics, 2006. **25**(7): p. 1676-1688.

258. Saha, B., T. Uchida, and T. Katsuki, *Asymmetric intramolecular cyclopropanation of diazo compounds with metallosalen complexes as catalyst: structural tuning of salen ligand.* Tetrahedron-Asymmetry, 2003. **14**(7): p. 823-836.

259. Meermann, C., et al., *Synthesis and structural characterization of scandium SALEN complexes.* Dalton Transactions, 2006(8): p. 1041-1050.

260. Zhou, Z.H., et al., *(Salen)Ti(IV) complex catalyzed asymmetric ring-opening of epoxides using dithiophosphorus acid as the nucleophile.* Journal of Organometallic Chemistry, 2006. **691**(26): p. 5790-5797.

261. Gregson, C.K.A., et al., *Titanium-salen complexes as initiators for the ring opening polymerisation of rac-lactide.* Dalton Transactions, 2006(25): p. 3134-3140.

262. Zhou, Z.H., et al., *(Salen)Ti(IV)-catalyzed asymmetric ring-opening of monosubstituted epoxides with dithiophosphorus acid.* Letters in Organic Chemistry, 2005. **2**(8): p. 752-754.

263. Ilyashenko, G., M. Motevalli, and M. Watkinson, *An alternative model for the asymmetric addition of cyanide to aldehydes catalysed by titanium-salen complexes based on a structurally related iron-salen complex.* Tetrahedron-Asymmetry, 2006. **17**(11): p. 1625-1628.

264. Kim, S.S., *Asymmetric cyanohydrin synthesis from aldehydes and ketones using chiral metal (salen) complex as catalyst.* Pure and Applied Chemistry, 2006. **78**(5): p. 977-983.

265. Belokon, Y.N., et al., *Cyanide ion cocatalysis in Ti(salen) catalysed asymmetric cyanohydrin carbonate synthesis.* Chemical Communications, 2006(16): p. 1775-1777.

266. Belokon, Y.N., et al., *The asymmetric addition of trimethylsilyl cyanide to aldehydes catalyzed by chiral (salen)titanium complexes.* Journal of the American Chemical Society, 1999. **121**(16): p. 3968-3973.

267. Khan, N.U.H., et al., *Asymmetric addition of trimethylsilyl cyanide to aldehydes promoted by chiral polymeric vanadium(V) salen complex as an efficient and recyclable catalyst.* Tetrahedron-Asymmetry, 2006. **17**(18): p. 2659-2666.

268. Blacker, J., et al., *Catalytic, asymmetric Strecker reactions catalysed by titanium(IV) and vanadium(V)(salen) complexes.* Tetrahedron-Asymmetry, 2006. **17**(9): p. 1449-1456.

269. Ambrosek, D., et al., *A multi state-CASPT2 vs. TD-DFT study of the electronic excited states of RCo(CO)(4) (R = H, CH3) organometallic complexes.* Chemical Physics Letters, 2006. **417**(4-6): p. 545-549.

270. Perdew, J.P. and Y. Wang, *Accurate and Simple Analytic Representation of the Electron-Gas Correlation-Energy.* Physical Review B, 1992. **45**(23): p. 13244-13249.

271. Hay, P.J. and W.R. Wadt, *Abinitio Effective Core Potentials for Molecular Calculations - Potentials for the Transition-Metal Atoms Sc to Hg.* Journal of Chemical Physics, 1985. **82**(1): p. 270-283.

272. Francl, M.M., et al., *Self-Consistent Molecular-Orbital Methods .23. a Polarization-Type Basis Set for 2nd-Row Elements.* Journal of Chemical Physics, 1982. **77**(7): p. 3654-3665.

273. Pietro, W.J. and W.J. Hehre, *Molecular-Orbital Theory of the Properties of Inorganic and Organometallic Compounds .3. Sto-3g Basis-Sets for 1st-Row and 2nd-Row Transition-Metals.* Journal of Computational Chemistry, 1983. **4**(2): p. 241-251.

274. Humphrey, W., A. Dalke, and K. Schulten, *VMD: Visual molecular dynamics.* Journal of Molecular Graphics, 1996. **14**(1): p. 33-&.

275. Portmann, S. and H.P. Luthi, *MOLEKEL: An interactive molecular graphics tool.* Chimia, 2000. **54**(12): p. 766-770.

276. Lee, T.J. and P.R. Taylor, *A Diagnostic for Determining the Quality of Single-Reference Electron Correlation Methods.* International Journal of Quantum Chemistry, 1989: p. 199-207.

277. Lee, T.J., *Comparison of the T-1 and D-1 diagnostics for electronic structure theory: a new definition for the open-shell D-1 diagnostic.* Chemical Physics Letters, 2003. **372**(3-4): p. 362-367.

278. Ivanov, V.V., D.I. Lyakhy, and L. Adamowicz, *New indices for describing the multi-configurational nature of the coupled cluster wave function.* Molecular Physics, 2005. **103**(15-16): p. 2131-2139.

279. Leininger, M.L., et al., *A new diagnostic for open-shell coupled-cluster theory.* Chemical Physics Letters, 2000. **328**(4-6): p. 431-436.

280. Nielsen, I.M.B. and C.L. Janssen, *Double-substitution-based diagnostics for coupled-cluster and Moller-Plesset perturbation theory.* Chemical Physics Letters, 1999. **310**(5-6): p. 568-576.

281. Janssen, C.L. and I.M.B. Nielsen, *New diagnostics for coupled-cluster and Moller-Plesset perturbation theory.* Chemical Physics Letters, 1998. **290**(4-6): p. 423-430.

282. Wissing, K. and J. Degen, *Dynamic ligand-field theory for square planar transition metal complexes.* Theochem-Journal of Molecular Structure, 1998. **431**(1-2): p. 97-107.

283. Messmer, R.P., Interran.Lv, and K.H. Johnson, *Electronic-Structure of Square-Planar Transition-Metal Complexes .1. Ptcl42- and Pdcl42- Ions.* Journal of the American Chemical Society, 1974. **96**(12): p. 3847-3854.

284. Rosch, N., R.P. Messmer, and K.H. Johnson, *Electronic-Structure of Square-Planar Transition-Metal Complexes .2. Zeises Anion, [Pt(C2h4)Cl3]-La.* Journal of the American Chemical Society, 1974. **96**(12): p. 3855-3860.

285. Peterson, K.A., et al., *Energy-consistent relativistic pseudopotentials and correlation consistent basis sets for the 4d elements Y-Pd.* Journal of Chemical Physics, 2007. **126**(12).

286. Peterson, K.A., B.C. Shepler, and J.M. Singleton, *The group 12 metal chalcogenides: an accurate multireference configuration interaction and coupled cluster study.* Molecular Physics, 2007. **105**(4): p. 445-461.

287. Sears, J.S. and C.D. Sherrill, *Assessing the performance of DFT for the electronic structure of metal-salens: The d2 metals*. 2007.

288. Franceschi, F., et al., *Molecular batteries based on carbon-carbon bond formation and cleavage in titanium and vanadium Schiff base complexes.* Chemistry-a European Journal, 1999. **5**(2): p. 708-721.

289. Liu, Z.H. and F.C. Anson, *Schiff base complexes of vanadium(III, IV, V) as catalysts for the electroreduction of O-2 to H2O in acetonitrile.* Inorganic Chemistry, 2001. **40**(6): p. 1329-1333.

290. Liu, Z.H. and F.C. Anson, *Electrochemical properties of vanadium(III,IV,V)-salen complexes in acetonitrile. Four-electron reduction of O-2 by V(III)-salen.* Inorganic Chemistry, 2000. **39**(2): p. 274-280.

291. Yamamoto, K., K. Oyaizu, and E. Tsuchida, *Catalytic cycle of a divanadium complex with salen ligands in O-2 reduction: Two-electron redox process of the dinuclear center (salen equals N,N'-ethylenebis(salicylideneamine)).* Journal of the American Chemical Society, 1996. **118**(50): p. 12665-12672.

292. Bakac, A. and I.A. Guzei, *Hydrogen atom and hydride transfer in the reactions of chromium(IV) and chromium(V) complexes with rhodium hydrides. Crystal structure of a superoxorhodium(III) product.* Inorganic Chemistry, 2000. **39**(4): p. 736-740.

293. Watanabe, A., et al., *Zr[bis(salicylidene)ethylenediaminato]-mediated Baeyer-Villiger oxidation: Stereospecific synthesis of abnormal and normal lactones.* Proceedings of the National Academy of Sciences of the United States of America, 2004. **101**(16): p. 5737-5742.

294. Watanabe, A., et al., *Highly enantioselective Baeyer-Villiger oxidation using Zr(salen) complex as catalyst.* Tetrahedron Letters, 2002. **43**(25): p. 4481-4485.

295. Miyazaki, T. and T. Katsuki, *Nb(salen)-catalyzed sulfoxidation.* Synlett, 2003(7): p. 1046-1048.

296. Luts, T., et al., *Epoxidation of olefins catalyzed by novel Mn(III) and Mo(IV) Salen complexes immobilized on mesoporous silica gel Part I. Synthesis and characterization of homogeneous and immobilized Mn(III) and Mo(IV) Salen complexes.* Journal of Molecular Catalysis a-Chemical, 2007. **261**(1): p. 16-23.

VITA

JOHN S. SEARS

John S. Sears was born in Winchester, Tennessee in 1979 to Steve and Donna Sears. He attended public schools in Franklin County, Tennessee prior to entering the freshman class at The University of the South in Sewanee, Tennessee as a Bruce-Greene Fellow and a Welch-Foundation scholar. During his time at Sewanee, he was a member of the Order of Gownsmen, a recipient of the Puckette award for academic excellence, and a recipient of the Robert Hooke prize for achievement in mathematics. John graduated, magna cum laude, from The University of the South in 2002 with a BS and departmental honors in both Chemistry and Mathematics, before coming to Georgia Tech as a Presidential Fellow to pursue a doctorate in Chemistry. When not working on his research, John enjoys spending time with his family, coaching youth athletics, attending services at his church, and volunteering at church and at local Masonic lodges.